Applications of Dynamical Systems with Symmetry

Peter Brian Ashwin

Submitted for PhD examination

University of Warwick
Coventry CV4 7AL, UK

Mathematics Institute

September 1991

Contents

Acknowledgements

I would like to thank British Gas for the support of one of their Research Scholarships in undertaking this work, and the members of high temperature division, heating plant at the Midlands Research Station, Solihull, especially Kevin Howell and Rachel Palmer for introducing me to some real flames.

There are numerous people who have helped me with advice or discussions, including many members of the Nonlinear Systems Laboratory at the Mathematics Institute, University of Warwick. My supervisor Ian Stewart gave me constant help and direction towards interesting (and solvable) problems. I was lucky enough to have a second supervisor, Greg King who gave me a lot more help and attention than I deserved. Special thanks go to Jim Swift for teaching me some of the unwritten rules about what research is and how to do it. The work in this thesis has benefitted immensely from discussions with Klaus Böhmer, Jacques Furter, Gabriela Gomes, Martin Krupa, Robert MacKay, Mark Muldoon, Mei Zhen, Ian Melbourne and Mark Roberts. Thanks are also due to Marty Golubitsky for inspiring work on symmetric chaos and for enabling me to go to Houston in January 1990 to continue work with Jim Swift. Thanks to Barry Joyce and James Stewart for assistance with the electronics. Steve Gaito and Catherine Wattebot provided considerable help with computers.

I would like to thank all my parents, brothers, family, friends and colleagues for being there, and Angela Kelber for deciding to go on holiday in Wales in 1989.

And finally, I would like to thank the most important person right now: YOU, the reader for sparing some of your time to read what I have put together here. I hope you find some of it interesting.

For W.

Declaration

This thesis is the original work of the author, with the exception of sources cited in the text. The sections of chapters 2, 3 and 4 which have appeared in [17, 18] are joint work of the author with Dr. G.P. King and Dr. J.W. Swift.

Peter Brian Ashwin (September 1991).

Summary

This thesis examines the application of symmetric dynamical systems theory to two areas in applied mathematics: weakly coupled oscillators with symmetry, and bifurcations in flame front equations.

After a general introduction in the first chapter, chapter 2 develops a theoretical framework for the study of identical oscillators with arbitrary symmetry group under an assumption of weak coupling. It focusses on networks with 'all to all' $\mathbf{S}_n$ coupling. The structure imposed by the symmetry on the phase space for weakly coupled oscillators with $\mathbf{S}_n$, $\mathbf{Z}_n$ or $\mathbf{D}_n$ symmetries is discussed, and the interaction of internal symmetries and network symmetries is shown to cause decoupling under certain conditions.

Chapter 3 discusses what this implies for generic dynamical behaviour of coupled oscillator systems, and concentrates on application to small numbers of oscillators (three or four). We find strong restrictions on bifurcations, and structurally stable heteroclinic cycles.

Following this, chapter 4 reports on experimental results from electronic oscillator systems and relates it to results in chapter 3. In a forced oscillator system, breakdown of regular motion is observed to occur through break up of tori followed by a symmetric bifurcation of chaotic attractors to fully symmetric chaos.

Chapter 5 discusses reduction of a system of identical coupled oscillators to phase equations in a weakly coupled limit, considering them as weakly dissipative Hamiltonian oscillators with very weakly coupling. This provides a derivation of example phase equations discussed in chapter 2. Applications are shown for two van der Pol-Duffing oscillators in the case of a twin-well potential.

Finally, we turn our attention to the Kuramoto-Sivashinsky equation. Chapter 6 starts by discussing flame front equations in general, and non-linear models in particular. The Kuramoto-Sivashinsky equation on a rectangular domain with simple boundary conditions is found to be an example of a large class of systems whose linear behaviour gives rise to arbitrarily high order mode interactions.

Chapter 7 presents computation of some of these mode interactions using competerised Liapunov-Schmidt reduction onto the kernel of the linearisation, and investigates the bifurcation diagrams in two parameters.

Chapter 1

The Dynamics of Symmetric Systems

This chapter gives a basic introduction to the theory of symmetric dynamics, some motivating examples for its use and points to the applications presented in the other chapters. This material is not original.

1.1 Introduction

There has been a revolution in mathematical applications to the natural sciences in the past thirty years with the widespread appearance of the theory of *nonlinear dynamical systems*. Although the theory of systems that evolve with time has been implicitly studied from the first time that people attempted to describe the universe around them using mathematical notions, the lack of closed form solutions to many problems was only circumvented in the late nineteenth century when Poincaré began to develop the *qualitative theory of ordinary differential equations* (ODEs), realising that such systems can have a very rich structure. Since the beginning of the century, great progress has been made with the discovery of chaos in deterministic systems, and there has been a lot of input from many fields of maths from complex analysis to group theory, but especially topology. In the last few decades, a lot of effort has been applied to understand the mathematics of nonlinear dynamics, and now that many of the problems have been solved, the theory is being applied more to problems in the natural sciences that first motivated its investigation. During the last decade, the importance of symmetry has been realised, and the way it affects possible behaviour of systems, at least on a local level, has been put on firm foundations using *group theory* and *singularity theory*.

This thesis presents the results of investigations into some problems motived by those of combustion; namely coupled oscillating flames and the stability of flame fronts. These problems are applications of dynamical systems theory to finite and infinite dimensional problems respectively.

1.1.1 What is dynamics?

There are two types of dynamical system at the most basic level; those where time flows smoothly (continuous dynamical systems), and those where it jumps in discrete steps (discrete dynamical systems). These two families have many similarities but some subtle differences, although it is always possible to convert between the two types.

The essential ingredients are [13, 61, 108]:

Space (Or in the jargon, the state space or the phase space). The 'real space' where the system we are studying must be described in enough detail that it is unambiguous. For example, the set of all voltages in an electric circuit describe the state of that circuit.

Time As mentioned before, this (like peanut butter) comes in two types, smooth or lumpy. The important thing is that it is a one-dimensional real set and so it allows a cause-and-effect type of law to work, due to the natural well ordering of the real numbers.

Laws These tell us how we change our position in the phase space with the change in time. Given the state of the the system at one instant of time, the laws tell us how to find the state at the next instant in time *uniquely*.

Questions Of course, this is the most essential part of the study of any dynamical system; what do we want to know? If we really want to know everything about a system, the only answer usually is to build it and observe it in great detail. Many questions in the natural sciences are concerned with much less detailed questions, and the one that dynamical systems has examined most is: *What happens eventually?* After a short-lived settling-down has been allowed to happen, what are we left with? This was at one time thought to be synonymous with the question: *What is the stable behaviour of the system?*, but one of the basic achievements of dynamical systems theory is to show that there is a wide gulf between these two questions.

Continuous dynamical systems. These have a continuous passage of time which is taken to be $\mathbf{R}^+$, the positive real numbers, but this can be extended (if the reverse system is uniquely defined) to be $\mathbf{R}$, the real line, and the phase space M. If the system is defined by an ODE, M is typically some finite dimensional manifold or for a partial differential equation (PDE), some function space. The system is described by an evolution operator (which might typically be the solution operator of a differential equation):

$$\begin{aligned} \Phi : M \times \mathbf{R}^+ &\rightarrow M \\ \Phi_t(x(0)) &= x(t) \end{aligned}$$

this advances the system by a time t and has the following properties:

- Φ_0 is the identity on M
- $\Phi_s \circ \Phi_t = \Phi_{(s+t)}$
- Φ is continuous in t and x; moreover we shall assume Φ is jointly of class C^∞ in (x, t).
- Φ is called a *flow* on M

Such a system is induced by the solution of a well-posed problem in ODEs or PDEs, but it also allows evolution to be governed by, for example, non-local (integro-differential) evolution equations in spatially extended problems.

Discrete dynamical systems Here, the evolution of the system with discrete time is defined by a mapping f of the form:

$$\begin{aligned} f : M &\rightarrow M \\ f(x_n) &= x_{n+1} \end{aligned}$$

with the property that $f(x)$ is continuous in $x \in M$. This mapping can be invertible or noninvertible. We assume the mappings are invertible unless specified otherwise.

The above two types of dynamical systems are closely related; from any continuous dynamical system it is possible to define a discrete one by looking at the *time-T map* for a fixed T (i.e. $f \equiv \Phi_T$), or by looking at the intersections of a trajectory with a codimension one plane in the phase space. The latter is known as a Poincaré map. Going the other way is less trivial, but by extending the map to an invertible one it is possible to *suspend* the map in a flow which has the property that the time-1 map is the original map.

Fixed points and periodic orbits The paths of points in phase space which obey the laws of a system are called *orbits* or *solutions* of the system. Out of all possible solutions, there are some we turn our attention to as being dynamically important. These are *fixed points*, which are unvarying with respect to time, and *periodic orbits* which return to their starting point after some fixed time. Whether or not such solutions are observed depends on their stability, discussed shortly.

Homoclinic and heteroclinic orbits One particular type of orbit has been found to play a very important role in dynamical systems, namely the homo- or heteroclinic orbit.

Definition 1.1.1 *An orbit $x(t)$ is said to be* heteroclinic *to two fixed points x_0, y_0 if*

$$x(t) \rightarrow x_0$$

as $t \rightarrow \infty$, and

$$x(t) \rightarrow y_0$$

as $t \rightarrow -\infty$.

An orbit $x(t)$ is said to be homoclinic *to one fixed point x_0, y_0 if*

$$x(t) \rightarrow x_0$$

as $t \rightarrow \pm\infty$.

Solution stability There are a variety of definitions of stability. We use *orbital Liapunov stability* unless otherwise mentioned. An orbit $x(t)$ of the flow Φ_t on M is stable if: $\forall\, \epsilon > 0$, $\exists\, \epsilon > \delta > 0$ such that $|x(0) - y| < \delta \Rightarrow |x(t) - \Phi_t(y)| < \epsilon$ for all $t > 0$. If a flow is linearly stable (the real parts of the eigenvalues of a linearisation of an ODE are less than zero), then it is stable, but the converse may not hold.

For fixed points, we can look at the linearisation of the system, and the eigenvalues or more generally the *spectrum* of this can tell us whether the point is stable to small perturbations or not. If the real part of the spectrum is negative (for the flow) or less than one (for the mapping), then the fixed point is linearly stable. If it is positive, it is unstable, and otherwise (if the real part of the spectrum is bounded away from zero) it is a *saddle* point.

A homoclinic orbit is called a *saddle connection* if it connects two fixed points that are saddles.

The stability of periodic solutions in flows is determined by defining a *section* transverse to the orbit, and examining the stability of the fixed point of the mapping that the periodic orbit induces.

Genericity A very important concept is that of a *generic* system, which we shall define precisely in section 1.2.4, but for the moment think of it as a *typical* system; if we picked a system at 'random', the chances are that it would be generic. We can make some basic assumptions about what does *not* normally happen, on the grounds that if we have a real system, by shaking it a little we should end up with a qualitatively similar system. This corresponds to the idea of *structural stability* which we discuss in greater detail later.

An important idea, recognised implicitly for a long time, is that the appropriate concept of genericity is very different in systems whose laws and state space possess some sort of symmetry. This motivates the study of generic systems only *after* having included any natural symmetries of the problem. The study of bifurcations with symmetry was considerably extended and refined in the two volumes [51, 54], and this thesis uses their approach.

1.1.2 Symmetry in nature

All around us we have symmetry ... well, maybe we don't really, but our love of simplicity and beauty makes us like to think we have; particle physicists would like us to believe it is really there! And so we haved put symmetries into our models from time immemorial. Thus, in order to understand our models, we need to see if symmetry in them affects them. Perhaps in the real world, the concept of broken symmetry is more relevant, but nevertheless it has been shown by many examples that considering the world to have symmetries in it is useful for answering the **Questions** mentioned above, and this justifies its study.

1.1.3 Symmetry breaking

One final concept left to state in this introductory section is the idea of *symmetry breaking*, when symmetric system spontaneously creates asymmetric solutions from symmetric ones. One of the simplest mathematical statements of this is the *Equivariant Branching Lemma* of Cicogna and Vanderbauwhede [35] which says that for a large class of systems we can generically expect to see branches of steady solutions with symmetry lower than that of the system branching from a solution with full symmetry. This means that when changing a parameter in the system, there are circumstances when it would be highly *unusual* to see no steady solutions with broken symmetry. One simple demonstration of this is to be seen in the break-up of a laminar flame propagating vertically down a tube of premixed gas. For many mixtures, instabilities in the flat flame will very quickly form ridges and troughs that break the rotational symmetry of the flame, even if the turbulence is negligible.

1.2 Some mathematical tools of the trade

This thesis assumes the reader has a background in applied mathematics, including differential equations and some basic dynamical systems theory, such as phase portraits.

Refer to Jordan and Smith [75] or Arrowsmith and Place [13] for introductions to non-linear ODEs and qualitative dynamics. More advanced references are those by Arnold [8] and Guckenheimer and Holmes [61] which provide good all-round introductions. We now introduce some useful techniques.

1.2.1 Bifurcation theory

This is a powerful analytical technique for investigating the asymptotic behaviour of a dynamical system. We assume that we have one or more *parameters* of the system that continuously change the differential equations governing the system, i.e. we consider equations of the form:

$$\frac{dx}{dt} = F(x, \lambda) \tag{1.1}$$

where $x \in \mathbf{R}^n$ is an element in the state space and $\lambda \in \mathbf{R}^m$ is an element in the parameter space. To paraphrase Ian Stewart (who was in turn quoting G. Auchmuty), *bifurcation theory is a way of getting interesting solutions from uninteresting ones.* Suppose we know that the *trivial solution* $x = 0$ is a steady state for the above system, i.e.

$$F(0, \lambda) = 0$$

for all λ. Everywhere that the derivative

$$\mathrm{d}F$$

has no eigenvalues with real part zero, the trivial solution is an isolated solution because the flow generated by F is locally conjugate to its linear part. However, if $\mathrm{d}F$ is of corank $d > 0$ say, then in general we have other solutions in the neighbourhood of $(x, \lambda) = (0, 0)$.

Definition 1.2.1 *A* bifurcation point *of the flow $\dot{x} = F(x, \lambda)$ is a value of λ such that dF has an eigenvalue with real part zero.*

A bifurcation point *of the mapping $x_{n+1} = F(x_n, \lambda)$ is a value of λ such that an eigenvalue of dF has modulus equal to one.*

We shall usually work with $m = 1$, i.e. one-parameter bifurcation theory. In this setting it is possible to use *bifurcation diagrams*, which are schematic representations of the solution structure near the bifurcation. On the horizontal axis, the parameter varies, while the vertical axis shows some distinguishing feature of the solutions, for example the L^2 norm, or a projection of the phase space on to one interesting dimension. As an example, figure 1.1 shows a pitchfork bifurcation.

1.2.2 Smooth germs

In most of local bifurcation theory, it is possible to achieve the simplest and most compact notation by introducing the germ of a function, a local definition of a function.

Definition 1.2.2 *A* smooth germ *is an equivalence class of all functions defined in some neighbourhood of the origin under the equivalence relation that if f is defined on a neighbourhood N of the origin and g on M, then there exists a neighbourhood P of the origin on which $f \equiv g$.*

A consequence of this is that two members of the same germ have the same Taylor series to all orders, but due to the existence of non-zero 'flat' germs with all derivatives zero, the converse is not true.

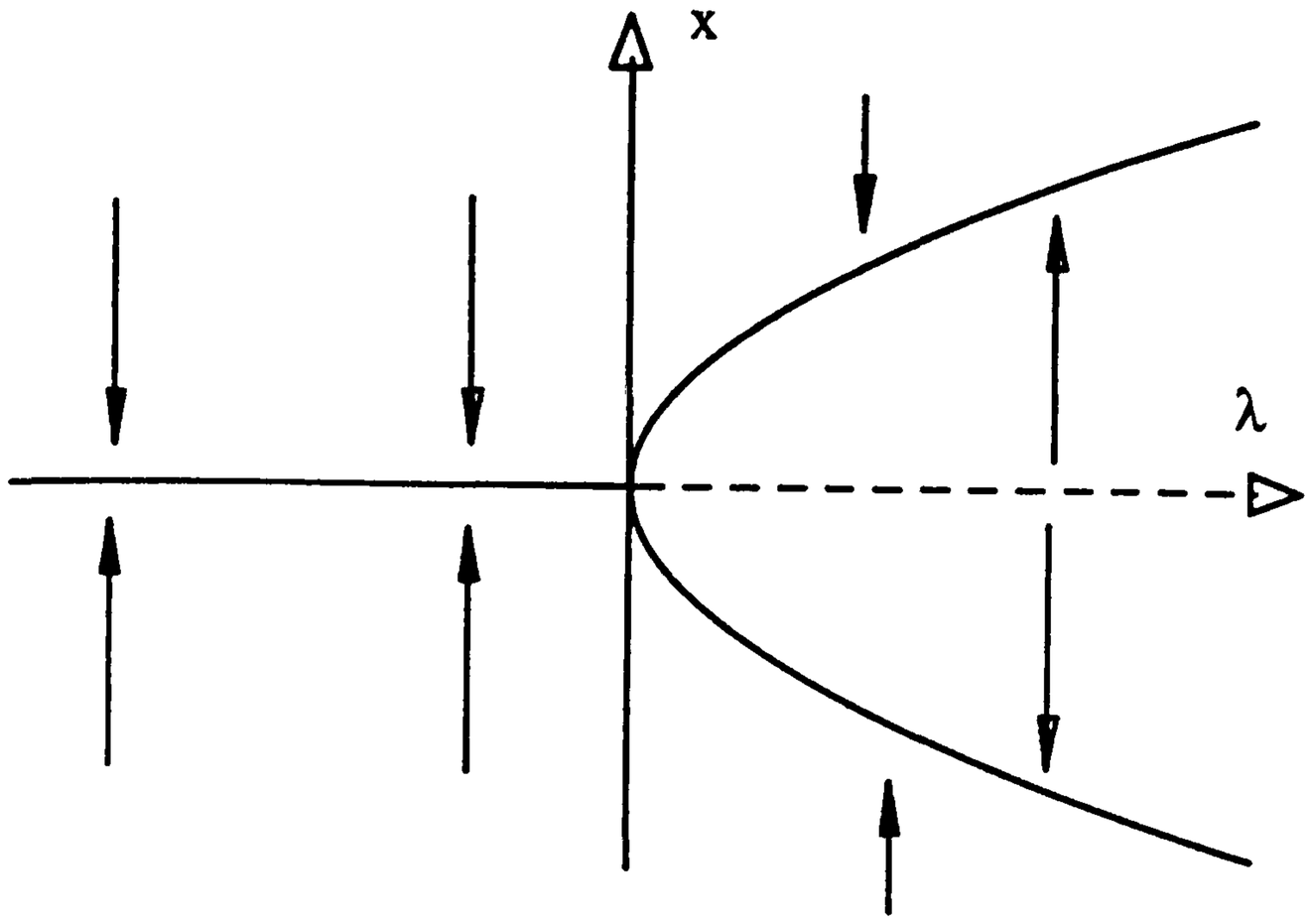

Figure 1.1: A pitchfork bifurcation, the steady solutions of $\dot{x} = x(x^2 - \lambda)$. The parameter λ should be thought of as fixed whilst the dynamics evolve in the x direction. For $\lambda < 0$ there is one stable fixed point which loses stability to create two more stable fixed points for $\lambda > 0$.

1.2.3 Equivalence of systems

If we want to talk about dynamical systems being equivalent, we must introduce some equivalence relation on the class of dynamical systems considered. A broad form of equivalence is *topological equivalence*, which holds between two systems if there is a homeomorphism taking the orbits of one to the orbits of the other preserving their orientation.

A stronger concept of equivalence is a *conjugacy* between two dynamical systems. We define this for discrete dynamical systems on two manifolds; $f : X \to X$ and $g : Y \to Y$. There exists a conjugacy between (f, X) and (g, Y) if and only if there exists a homeomorphism $\pi : X \to Y$ such that the following diagram commutes:

$$\begin{array}{ccc} X & \xrightarrow{f} & X \\ \pi \downarrow & & \downarrow \pi \\ Y & \xrightarrow{g} & Y \end{array}$$

i.e. if $\pi \circ f = g \circ \pi$. If the homeomorphism is C^∞, we say there is the conjugacy is *smooth*. Intuitively, a conjugacy means that the dynamics of one system is a deformation of the dynamics of the other. For example, if f has a periodic orbit of period 74, then so must g. Note that conjugacy ≡ top. equiv. in discrete time

1.2.4 Genericity and structural stability

Consider the following (strong) formulation of genericity [108]. Given a class of mappings/flows on a manifold with the structure of a complete metric space:

Definition 1.2.3 *A property P is* generic *if it holds on an open dense set.*

A more useful definition for smooth germs is given in [54], and in particular for smooth germs with symmetry. Suppose a symmetry group Γ forces some finite set

of equalities, P, involving a finite number of coefficients on the set of coefficients in a Taylor expansion of a singularity. Let the set of smooth germs with this property be denoted by $\mathcal{G}^P$. Suppose we have a finite set of inequalities, Q, involving a finite number of coefficients in a Taylor expansion. Then denote the set of all smooth germs that satisfy both P and Q by $\mathcal{G}^P_Q$. We assume that $\mathcal{G}^P_Q$ is non-empty, i.e. P and Q are not mutually exclusive.

Definition 1.2.4 *A set of smooth germs $\mathcal{S}$ is generic with property P if there exists Q such that $\mathcal{S} = \mathcal{G}^P_Q$.*

Note that symmetry induces a property P, but not all properties P can be induced by a symmetry. Also note that this definition involves not just a countable intersection of open dense sets, but a finite intersection.

Another important concept is *structural stability* of a set of dynamical systems. This means that in some neighbourhood of a system S, all dynamical systems are topologically equivalent to S, i.e. whether the dynamics are merely deformed upon deformation of the system rather than taking on any new qualitative features.

1.2.5 Group representation theory

The language of group theory is the language of symmetry, much of the study of the former being motivated by questions in the latter. In this thesis we shall be concerned with studying problems which have symmetries corresponding to compact Lie groups (continuous groups) acting on $\mathbf{R}^n$ (with the exception of the Euclidean group discussed in parts of chapter 6). Consider a symmetry group Γ, and define equivariance under Γ for a bifurcation problem thus:

Definition 1.2.5 *A bifurcation problem $dx/dt = F(x, \lambda)$ is* Γ-equivariant *if, and only if:*

$$F(\gamma x, \lambda) = \gamma F(x, \lambda)$$

for all $\gamma \in \Gamma$.

Note that implicit in this definition is that the group has an action, or if it is linear a *representation* on the phase space of the problem.

Definition 1.2.6 *A* representation *of the group Γ on a vector space V is a homomorphism into the group $GL(V)$ of linear transformations of V,*

$$\rho : \Gamma \to GL(V)$$

i.e. we can identify elements in the group Γ with invertible matrices in the space of linear maps of V to itself, and thus we write $\gamma(x)$ instead of $\rho_\gamma x$ for elements in V acted on by elements in Γ.

The next two definitions are motivated respectively by the questions: (a) Which points in V have symmetry at least Σ? (b) How much symmetry does a point v have?

Definition 1.2.7 *The* fixed point space *of a subgroup Σ of Γ is the set:*

$$Fix(\Sigma) = \{v \in V : \sigma(v) = v, \forall\, \sigma \in \Sigma\}.$$

Definition 1.2.8 *The* isotropy subgroup *of a point $v \in V$ is the subgroup:*

$$\Sigma_v = \{\sigma \in \Sigma : \sigma(v) = v\}\ .$$

Considering all the isotropy subgroups of a group leads to a partial ordering of them given by inclusion. This is referred to this as the *isotropy lattice* of the action of a group.

1.2.6 Singularity theory and normal forms

For answering questions about generic local bifurcations with symmetry, a useful tool is that of singularity theory [118]. This gives a rigorous way of investigating bifurcations of smooth germs by examining how the presence of a symmetry group affects the structure of the Taylor series of the vector field in the neighbourhood of a bifurcation. This leads us to a systematic way of investigating singularities, called *classification by codimension*, where the codimension of a bifurcation measures how many parameters are needed generically in order to get a singularity. We summarise this procedure in section 1.3.2.

1.3 Bifurcation theory with symmetry

In order to answer the question *What types of changes of behaviour are possible/generic in a system of equations with symmetry* Γ *as we alter a parameter* $\lambda \in \mathbf{R}^m$, we need to consider the structure of nonlinear maps with Γ-equivariance (we shall mostly consider one parameter bifurcation theory, $m = 1$).

1.3.1 Reduction to center manifold

In one parameter problems at a generic bifurcation, the corank of the linearisation $\mathrm{d}F$ is the dimension of one of the irreducible representations of the group Γ, and all the other eigenvectors of $\mathrm{d}F$ are either stable ($\mathrm{Re}(\lambda) < 0$) or unstable ($\mathrm{Re}(\lambda) > 0$). Because of this, it is possible in local bifurcations to reduce any problem to one on a vector space equal to the null space of the linearisation by using either the center manifold theorem [30, 93] or Liapunov-Schmidt Reduction [51]. The former has the advantage that the dynamics are preserved in a neighbourhood of the bifurcation, whereas the latter has the advantage that the reduced equations are still smooth.

1.3.2 Local bifurcations

These are bifurcations where the local topology of the solution sets change. There are two basic types which can be considered with symmetric bifurcation theory as it is: steady state and Hopf bifurcations, which we consider separately.

Classification by codimension This involves two stages; the *classification problem* of an equivariant singularity with a symmetry group Γ, and then the application to a problem becomes a problem of determining a set of coefficients and following a tree diagram to give the bifurcation structure of the singularity in question. The latter stage is known as the *recognition problem*. This procedure, coupled with the idea of *finite determinacy*, gives us a rigorous way of deciding which higher order terms in a Taylor expansion can be ignored and which cannot.

The classification problem starts with looking at an irreducible action on the symmetry group Γ on some vector space V, and finding the set of germs I which are invariant and those E which are equivariant under the group action. Note that E has the structure of a module over the ring I. This construction is fortunately a finite process due to Schwarz's theorem [119]. Constructing a general Taylor expansion of the singularity, we write:

$$f(x, \lambda) = \sum_{v \in E} v f_v(I)$$

where the f_v are smooth functions of the invariants. For every coefficient of any f_v that is zero, we move one higher in codimension, and using this, we can construct a tree diagram of tests on coefficients which will determine the codimension. For each possibility, we can give the topological characteristics of the bifurcation diagram, for example, how many branches come off and in what direction they branch.

The recognition problem then becomes a question of examining the Taylor series of the problem at hand, and following down the tree diagram to determine what codimension the problem is and what the bifurcation diagram will look like.

As an example, consider a laminar flame propagating down a cylindrical tube of premixed gas and air. The plane flame will have circular symmetry ($O(2)$ symmetry in group theory terminology). We can write down a general $O(2)$-equivariant germ of a vector field (with $O(2)$ acting irreducibly) in the form:

$$\dot{z} = zf(z\bar{z})$$

for $z \in \mathbf{C}$ and some arbitrary function f. Expanding this as a Taylor series

$$\dot{z} = a_0 z + a_1 z^2 \bar{z} + a_2 z^3 \bar{z}^2 + \cdots$$

we find the vector field is locally topologically equivalent to $\dot{z} = a_0 z$ if $a_0 \neq 0$ (codimension zero), $\dot{z} = a_1 z^2 \bar{z}$ if $a_0 = 0$ and $a_1 \neq 0$ (codimension one), and so on. This is the classification problem. The recognition problem, or finding an equation that locally describes the behaviour of the flame, becomes a problems of determining the coefficients of the Taylor series; the classification problem gives us a way of knowing when to stop. (N.B. This example is particularly simple, because z is the only equivariant and $z\bar{z}$ is the only invariant of the action of $O(2)$ on $\mathbf{C}$. Usually we wish to do this for *bifurcation equations*, when we need to perform two or more variable Taylor expansions, and the exercise becomes non-trivial [34].)

Steady state bifurcation A steady solution (a solution of $F(x, \lambda) = 0$ for an ODE) becomes unstable and one or more steady solutions may branch off in a neighbourhood of the bifurcation point. There are a few basic techniques which work for all groups, e.g. the *Equivariant Branching Lemmma* which states that there is a branch of solutions for every one dimensional isotropy subgroup of the symmetry group [35]. This has been extended to the case of odd dimensional isotropy subgroups which are maximal (i.e. for which there are no isotropy subgroups between it and the full symmetry group.), and led to the conjecture of Golubitsky that all maximal isotropy subgroups have branches at bifurcation, and all branches correspond to a maximal isotropy subgroup. Both these conjectures have been proved false [47], and this should give us some idea of what we are up against; to a large extent, each group brings its own set of problems and its own quirks, and thus must be dealt with separately. As an example, the formation of steady cellular patterns on a burner with the changing of a combustion parameter can be thought of as a steady state bifurcation from a laminar flame; see chapters 6 and 7.

Hopf bifurcation This is the creation of periodic solutions of small amplitude from a steady solution [93]. In the simplest situation, consider an equation of the form $\dot{x} = F(x, \lambda)$, with $F(0, \lambda) = 0$, $x \in \mathbf{R}^n$ and $\lambda \in \mathbf{R}$. A Hopf bifurcation occurs when a pair of complex conjugate eigenvalues of $\mathrm{d}F(0, \lambda)$ pass through the imaginary axis at $i\omega$ as λ passes through 0, under some generic conditions. For λ on one side of zero or the other, it is possible to show existence of a branch of periodic solutions coming from the bifurcation point with angular frequency near ω.

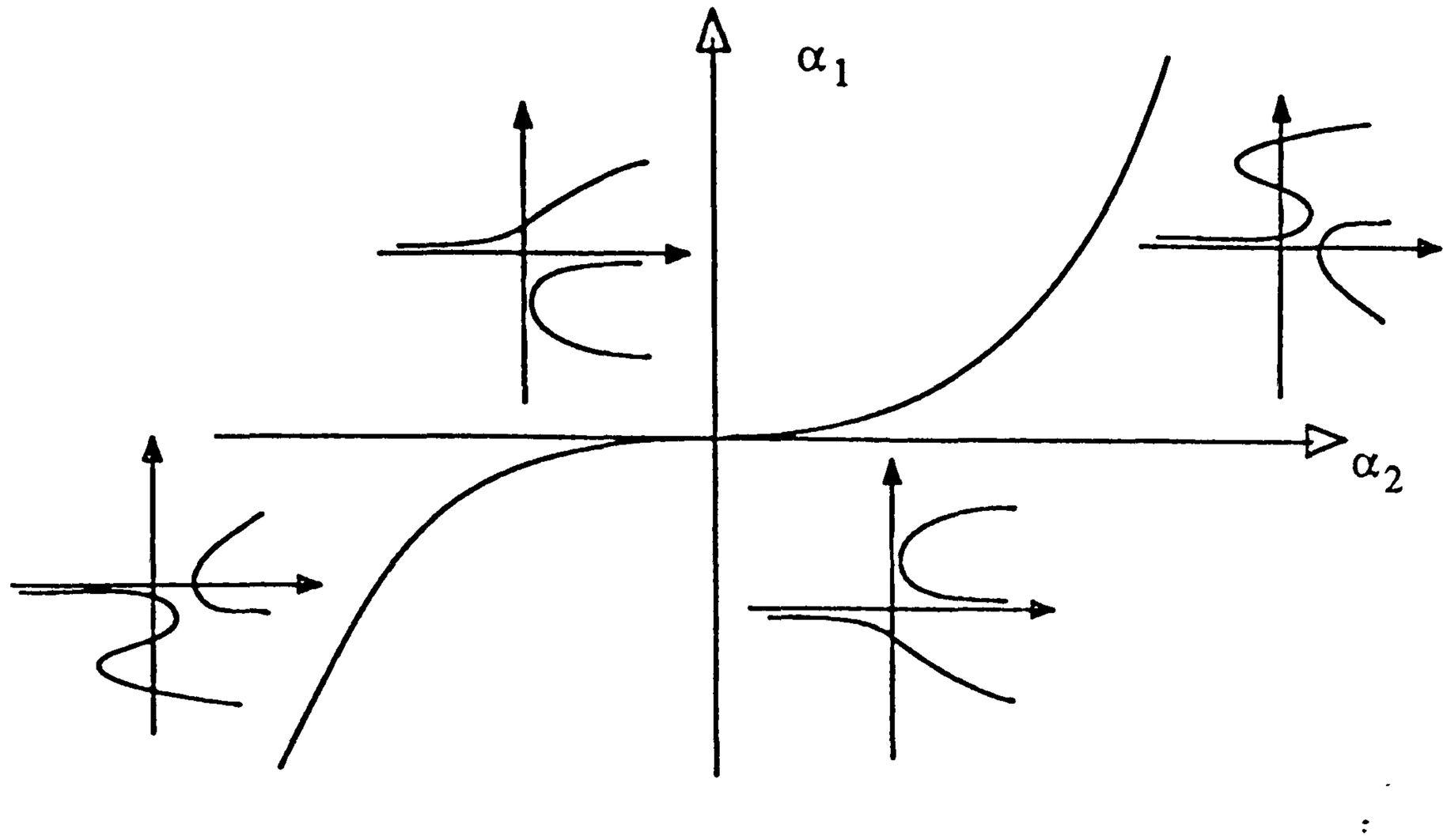

Figure 1.2: The universal unfolding of a pitchfork bifurcation, $\dot{x} = x^3 - \lambda x + \alpha_1 x^2 + \alpha_2$. the α_i terms break the symmetry as well as unfolding the bifurcation. The four regions of the (α_1, α_2) plane show (x, λ) bifurcation diagrams associated with the four possible generic unfoldings of the pitchfork at $(\alpha_1, \alpha_2) = (0, 0)$. The unfolding is universal in that any unfolding cannot locally have any bifurcation diagrams not equivalent to one of those shown here.

Although at first, singularity theory might appear to be only applicable to fixed point bifurcations, [52] develop a method to treat periodic orbit bifurcating from fixed points. By looking for limit cycles at a particular frequency, they define a *Birkhoff normal form* for equivariant Hopf bifurcation with symmetry $\Gamma \times S^1$, where the S^1 symmetry corresponds to the temporal phase shift symmetry of the periodic orbit. This can be thought of as an asymptotic form of the equations which are similar to averaged equations. In fact, only the periodic orbits and fixed points have the S^1 symmetry, but it is easiest to work with a normal form where the whole germ has the S^1 symmetry. They do this by performing a Liapunov-Schmidt reduction from an *infinite* dimensional system to a finite dimensional one which has the extra symmetry. Examples in laminar flame theory are discussed in chapter 6.

Unfolding a singularity For singularities with codimension greater than one, it is possible to add further generic parameters to the problem and *unfold* the problem into a range of codimension one bifurcations. For example, with the pitchfork bifurcation (codimension one with symmetry but codimension three without), by adding two extra parameters, it is possible to break this down into all possible bifurcation diagrams that are close to (i.e. perturbations of) a pitchfork: see figure 1.2. The two dimensions represent the two unfolding parameters, and the bifurcation diagrams are shown in each of the areas of parameter space.

Mode interactions Going the other way from unfoldings, if we add extra bifurcation parameters to a bifurcation problem, genericity can allow a variety of more obscure transitions. When there are two bifurcations that we cause to happen simultaneously by changing a second parameter, we will usually see a picture that is more complex than

just the sum of the two bifurcations. In particular, we may see secondary bifurcations to mixed modes in either steady-state or Hopf bifurcations, and can show the existence of many more solution branches than we can with the simple bifurcation theory. To illustrate the idea, consider a two dimensional parameter space (a, b). Suppose we have a bifurcation A of an equation $F(x, a, b) = 0$ at $a = 0$ and another, B at $b = 0$. At each point $(0, b)$ or $(a, 0)$ with a and b non-zero, we can examine the bifurcations in some neighbourhood of the bifurcation points than will *necessarily exclude* $(0, 0)$. However, if we examine the *mode interaction* at $(0, 0)$, we will get a valid model of the solutions in some neighbourhood of $(0, 0)$ which must also include a description of the simple bifurcations. Matkowsky and others have considered mode interaction between Hopf bifurcation to different patterns in premixed combustion [24], and use the mode interaction to find quasiperiodic states.

1.3.3 Global bifurcations

Some bifurcations are not possible to describe by purely local phenomena. For example, homoclinic bifurcations on a plane, where a limit cycle is created at an infinite period bifurcation. Here it is necessary to look at a neighbourhood of a homoclinic orbit and examine how the topology of the solution curves in this neighbourhood change as it is generically perturbed.

In this case, it is however possible to reduce to a local problem by constructing a return map in the neighbourhood of the fixed point using assumptions of genericity. What is more, it is possible in most cases to treat such bifurcations as local bifurcation by including an extra parameter to shrink the region of interest down to a point. This is done, for example, to find homoclinic connections and saddle-node bifurcations in a codimension two bifurcation, an interaction between a pitchfork bifurcation and a Hopf bifurcation in a two dimensional phase space; a Bogdanov-Takens bifurcation [61] shown in figure 1.3.

1.3.4 Chaos

This is a generic name for an attracting invariant set of a system that has one or more of the following attributes;

- Sensitive dependence on initial conditions and topological transitivity (a dense orbit).
- Ergodicity (equality of space and time averages).
- Positive Liapunov exponents (exponentially diverging trajectories).
- Fractal dimensionality.
- Mixing (weak or strong, metric or topological)
- Positive topological entropy

and can appear from bifurcations in a variety of manners, for example the *Shilnikov* mechanism [50], where perturbations of an orbit homoclinic to a point with two complex attracting eigenvalues and one real repelling one can, in certain circumstances induce a Smale *horseshoe* map [133] which indicates that at least one subsystem has trajectories with sensitive dependence on initial conditions. The study of these differences are in the

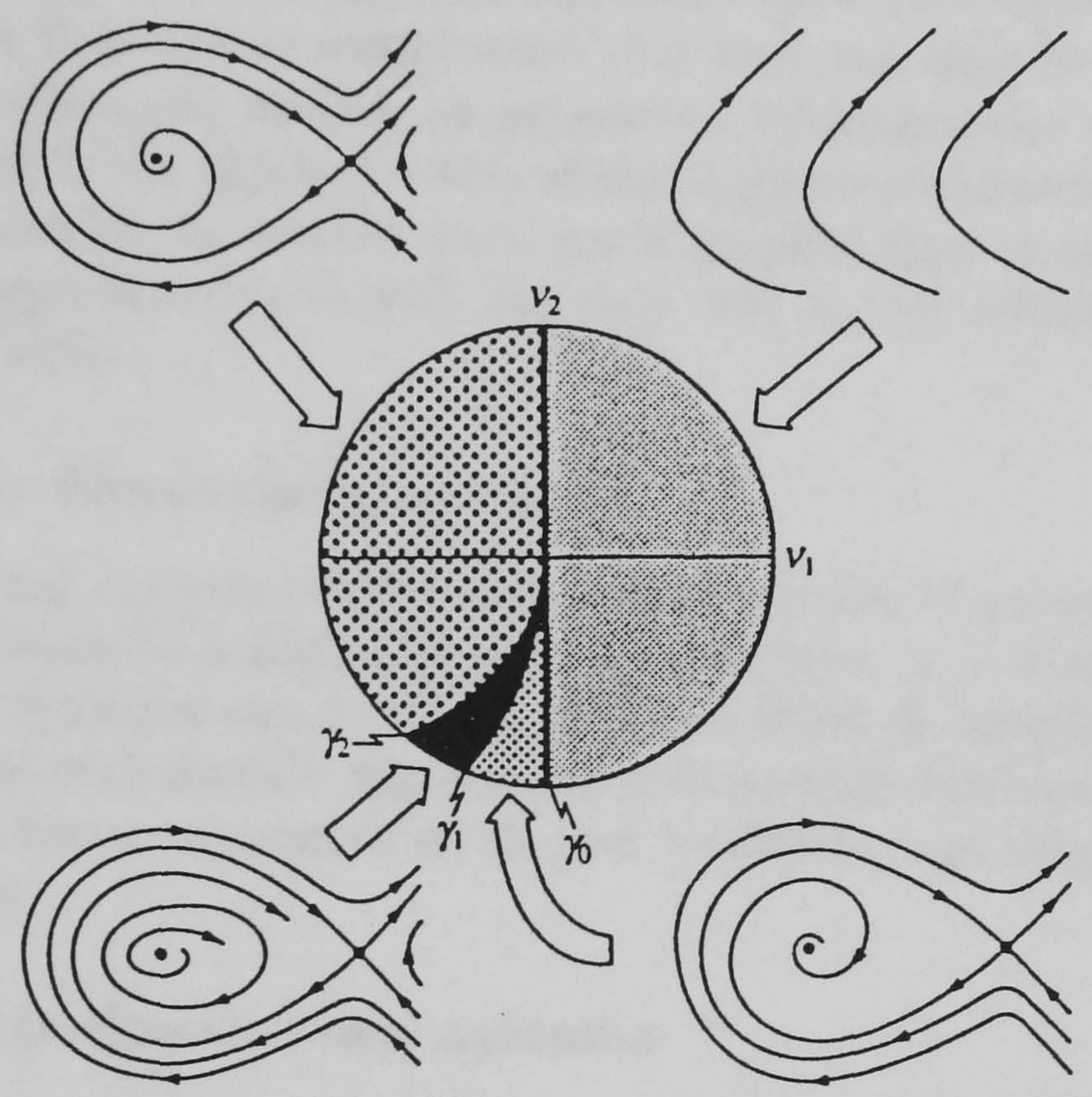

Figure 1.3: The Bogdanov-Takens codimension two bifurcation. This occurs when saddle node and Hopf bifurcations occur simultaneously a the point $(0,0)$.
The two bifurcation parameters (ν_1, ν_2) unfold the phase portraits on the plane as shown in each region. (From Arrowsmith and Place [13].)

domain of *ergodic theory*, the study of measure preserving transformations on measure spaces.

It is possible to get chaotic attractors bifurcating from fixed points of high codimension by using a manner similar to that for global bifurcations, i.e. by shrinking the dynamics down to a point.

1.4 Applications

When applying mathematical theory to the physical world, it is important to try to optimise the model so that it usefully shows much of the behaviour that one is interested in, but it is also as simple as possible to avoid needless effort. While, for example, in combustion theory, the reacting fluid equations have been known for a long time, for many questions they are so complicated that they can only be examined by massive computational effort. By making an asymptotic approximation of delta function flame fronts motivated by the physical reality of the largeness of the nondimensional activation energy, it is possible to restrict to a much smaller class of systems and thus even if numerical approximation is still the only way to get solutions, they require less computational effort.

1.4.1 Finite dimensional systems

Finite dimensional systems require only a finite number of quantities to determine the future of the system to a high degree of accuracy (i.e. it is a *lumped system*), and in most cases the evolution can be described by an ODE. In chapters 2 to 5, we consider a specific class of such models where many systems that have simple periodic dynamics are joined together as a network of coupled oscillators, and discuss some applications of such a theory.

1.4.2 Infinite dimensional systems

Where spatial variations in the state of a system are large, it is not possible to directly argue that we can approximate by a finite dimensional system. Sometimes it is possible to use reduction techniques to reduce to a finite dimensional subsystem that displays behaviour close to the original system for asymptotically large times. What is more, numerical solutions can only be performed to finite accuracy for a finite dimensional system, so it is important to understand if, when and how reduction is possible. Much work has been done on proving the existence of *inertial manifolds* or *global attractors* with finite dimension in PDEs (for example the Navier-Stokes fluid equations [38]), but even this work tends to give dimensions that are very much larger than can be usefully used in analytical work. As the number of actual degrees of freedom becomes larger and larger, it is possible to use such techniques as coherent structures or defect turbulence, and only statistical methods are likely to produce any significant progress in problems which have little coherent structure.

Chapter 2

Coupled Oscillators: Theory

2.1 Introduction

Since the pioneering work of van der Pol [109, 110], the theory of coupled oscillators has become a more or less well defined subject in mathematical modelling. In the following sections, we discuss briefly some of the applications of coupled oscillator models. In this thesis, we are mainly concerned with the development of a theory of symmetrically coupled oscillators, rather than application to physical systems.

2.1.1 Coupled oscillators in combustion theory

In trying to answer questions about real physical systems, it is necessary to strike a balance between the simplicity of the model and the usefulness of the results. What motivated this study was the modelling of coupling between burners in a furnace to understand under what conditions they are likely to break out into oscillation. Fitting together the previous two sentences naturally leads to look at coupled oscillator models, where each burner is represented by a system that has a propensity to oscillate, and there are weaker interactions between them, caused by one of a number of things: for example, acoustic coupling (identified to be important by Rayleigh [115] with many results summarised by Putnam [113]) or fluid-mechanic (incompressible) coupling such as that caused by interaction between vortices.

To a large extent, the original problem has proven to be too difficult in the time to represent in such a simple way. A great deal of effort worldwide in the last twenty or thirty years has been put into understanding the physics and chemistry of combustion but still, owing to the unsolved problems of turbulent flow, there are many properties of flames that are only beginning to be studied (for example, the effect that multi-step chemistry has on a moving flame). Thus, the problems are great enough with the modelling of the physics and chemistry of such a system, and only once these have been surmounted would it be possible to make a model with any confidence, other than by experimental methods.

2.1.2 Coupled oscillators in biological sciences

Some of the earliest motivation to study coupled oscillators came from physiologists making working models of systems such as the heart by van der Pol and van der Mark [111], the gut [87], the spinal cord of the lamprey (references in [102]), the synchronisation of fireflies [135, 137], or one of the most fundamental problems in biology; *morphogenesis*. This is the mechanism for formation of a living organism with head,

feet etc. from something more resembling a blob of jelly, and motivated Turing's seminal work [128]. Work has been done to extend and investigate these systems from simple rings to polyhedral lattices of interacting cells [107], and the work in this chapter examines the case of identical weakly coupled oscillators with arbitrary symmetry. In the mathematical model we imagine an organism to be composed of cells, with rapid diffusion inside and cell walls which only allow slow diffusion through them. Thus we expect the concentrations of chemicals to be more or less constant within each cell, but different between different cells, and this is how Turing justifies going from an infinite dimensional spatially extended system to a finite dimensional one, with the number of cells proportional to the dimension of the system.

General problems of synchronisation between 'biological clocks' were considered by Winfree in [135, 137], and this has been taken further by a number of authors [107, 87, 44, 80]. So-called *central pattern generators* have been studied using these techniques; these are models for the neural arrangements that govern e.g. the locomotion of animals. Modelling each leg as an oscillator with a certain natural frequency, a system of coupled oscillators can provide a minimal mathematical description of the order of footfalls of a quadruped [37] or biped [21]. The recent book by Murray [102] reviews many applications of oscillator techniques to biology.

Three principal techniques have been applied to these problems. Firstly that of weak coupling [44, 80, 135], which we discuss at length in the rest of this chapter. Secondly that of 'phase resetting oscillators', which can be thought of as singular oscillators with very strongly attracting limit cycles that interact only at points when one oscillator goes through zero phase [57, 135]. Thirdly, the use of two or more degree of freedom oscillators to realistically model both phase and amplitude dynamics, whether near Hopf bifurcation [128] or not, such as Fitzhugh-Nagumo or Hodgkin-Huxley equations for nerve fibre impulses. In physical oscillator systems, random variation between oscillator frequencies [121, 135] is important to take into account, but in this thesis we do not consider this.

2.1.3 Coupled oscillators in chemistry

In a similar way to that of biology, chemical reactions occurring in a system that consists of several well-stirred reactors coupled together by links allowing slow diffusion between them can be modelled using coupled equations. This has been done in particular with models for the Belousov-Zhabotinsky reaction [64].

2.1.4 Coupled oscillators in superconductivity

Since the discovery of superconductivity and in particular, *Josephson junctions* (which are also known as *superconductive quantum interference devices* or *SQUIDS*), there has been much effort placed in trying to understand the effects of coupling them together, as one would desire to use them on networks for computing and high frequency detection purposes. The work presented here is closely related to that investigated in [62, 63, 10, 12, 132, 127].

2.1.5 Coupled oscillators in electronics

The study of electronic oscillators has been one of the prime motivators to the study of mathematical oscillators, with much of the theory of oscillators coming from this field. Founding work was done by van der Pol [109, 110], and the spirit of his work was continued in the first half of the century mostly by Russian workers who also examined

the effects of noise in systems of oscillators [4, 101]. An early summary of applications in this field is to be found in the book by Hayashi [68], while later work is to be found in many journals, most notably the IEEE Journal on Circuits and Systems. Networks of electronic van der Pol oscillators have been considered by Linkens [87] and Endo and Mori [42], among others. There are also applications to microwave oscillator theory [106].

The material of the remainder of this chapter has appeared in the pre-print [18], with the exception of section 2.7.1.

2.1.6 Weak coupling

As briefly explained above, many physical systems have the property of having many identical or near identical cells with strong internal dynamics and weak interaction with the other cells. Thinking of this in terms of dynamical systems we describe the whole system as being a perturbation of an uncoupled system; i.e. there is a smooth homotopy between the system and a system that is a product of several dynamical systems. Leaving aside the case of weakly coupling dynamical systems with only stable hyperbolic fixed points (which is a problem in statics, not dynamics!) the simplest non-trivial behaviour that a dissipative dynamical system can have is a stable periodic orbit, and the next four chapters are devoted to studying such systems. We also assume that the oscillators are dissipative so that the periodic orbit is attracting and unique in some neighbourhood.

It would also be of interest to study energy preserving or Hamiltonian systems under a hypothesis of weak coupling, and this might shed some light on the problem of Josephson junctions, but it would involve studying higher dimensional, and thus more complex systems. In the Hamiltonian case, the genericity of systems is very different from that for dissipative systems. For example, there can be Poincaré recurrence (all trajectories return to any neighbourhood of an initial point), many periodic orbits, and tori associated with integrals of the motion.

Weakly coupled systems provide an example of a class of systems which have a clear physical meaning but are non-generic at the limit of no coupling (when the system is a product flow), loosely providing an analogy with the concept of integrability in Hamiltonian systems. Even strongly coupled oscillator systems must have a weakly coupled limit (in a mathematical sense) in order to be able to justify the use of the word 'oscillator'. We examine how the presence of symmetry affects the behaviour of such a system.

It has long been known [44] that in the weak coupling limit, a network of n coupled oscillators can be described by motion on an n-torus for small enough coupling. This corresponds to a robustness of the coordinates where each oscillator is represented by the phase on its own limit cycle, and is rigorously presented as normal hyperbolicity of the n-torus of the uncoupled system. We use this in conjunction with averaging in the style of [20, 44] to present a *normal form* for a system of weakly coupled oscillators which has an artificial circular symmetry from the averaging process, as well that inherited from the symmetry of the network. The circular symmetry can be thought of as a manifestation of the fact that the weak coupling affects the phases on a timescale much longer than the period of the individual oscillators, so there is an asymptotic decoupling between the two timescales. This is comparable with the normal form of Golubitsky and Stewart [52, 53] for Hopf bifurcation with symmetry.

In this normal form we cannot investigate the breakup of the invariant torus which can cause the breakdown of such a system from regular (nonchaotic) motion. In order

to examine questions such as this, we can extend the phase space to incorporate a *radius* coordinate for each oscillator such as Aronson et al. [10] do. Another approach is to examine a return map of the system (i.e. a map on $\mathbf{T}^{n-1}$ transverse to the flow) and examine how it can become non-invertible, as do MacKay and Tresser [89] for general circle maps, and Krupa and Roberts [81] for circle maps with $\mathbf{Z}_n$ symmetry.

2.2 Definitions

We write

$$\mathbf{T}^1 \equiv \{z \in \mathbf{C} : |z| = 1\} \equiv \mathbf{R}/2\pi\mathbf{Z}$$

as the circle group (the 1-torus) and $\mathbf{R}$ as its universal cover. We freely change between two representations of the torus (using exponentiation and taking arguments); we use Greek letters to refer to elements in $\mathbf{R} \bmod 2\pi\mathbf{Z}$ and Roman letters for elements in $\mathbf{C}$ with unit modulus. See appendix A for more notation and conventions.

Definition 2.2.1 *An* oscillator *is a dynamical system governed by an ODE:*

$$\dot{x} = f(x, \lambda) \tag{2.1}$$

where $x \in X$ is the phase space *of the oscillator, $\lambda \in \mathbf{R}$ is a parameter, and the equation has an asymptotically stable limit cycle $\{\gamma(t)\}$ that varies smoothly with λ.*

For convenience, we normalise the period to 2π by rescaling time. The possibilities for the phase space X include $\mathbf{R}^m$ $(m \geq 2)$, $\mathbf{T}^m$ $(m \geq 1)$, and the pendulum phase space $\mathbf{R} \times \mathbf{T}^1$. The results also apply, with some technical assumptions, to oscillators governed by partial differential equations, for which X is a Banach space.

Definition 2.2.2 *A* C^k network of weakly coupled identical oscillators *is a dynamical system governed by an ODE of the form:*

$$\dot{\mathbf{x}} = \mathbf{f}(\mathbf{x}, \lambda, \epsilon) \tag{2.2}$$

where:

- $\mathbf{x} = (x_1, x_2, \cdots, x_n) \in X^n$ is the phase space variable,
- $\lambda \in \mathbf{R}$ is the bifurcation parameter,
- $\epsilon \in \mathbf{R}$ is the coupling strength parameter,

such that the following conditions hold:

- $\mathbf{f}$ is jointly C^k in $\mathbf{x}, \lambda$ and ϵ,
- $\mathbf{f}(\mathbf{x}, \lambda, 0) = (f(x_1, \lambda), \cdots, f(x_n, \lambda))$ for some f on X defining an identical oscillator in each of the n components.

This definition implies that at $\epsilon = 0$, there is an attracting n-torus. There exists an open neighbourhood of initial conditions N of the limit cycle $\gamma \in X$ such that all initial conditions for the vector field $\mathbf{f}$ in N^n are attracted to a limit cycle on the n-torus defined by $\{x_i = \gamma(t + \theta_i) : \Theta \in \mathbf{T}^n\}$.

It is also possible to additionally couple a hyperbolic fixed point without destroying the normal hyperbolicity discussed later.

Definition 2.2.3 *The flow* $\dot{\mathbf{x}} = \mathbf{f}(\mathbf{x}, \lambda, \epsilon)$ *is* equivariant with symmetry group Γ *a subgroup of* $\mathbf{S}_n$ *if it satisfies:*

$$f_i(x_{\sigma(j)}, \lambda, \epsilon) = f_{\sigma(i)}(x_j, \lambda, \epsilon)$$

for all $(i, j) \in 1, \cdots, n$ *and* $\sigma \in \Gamma$.

This is the action induced by having $\mathbf{S}_n$ permute the coordinates of the oscillators. For large n, there can be many such symmetry groups Γ possible, but note that section 2.7.1 shows that restricting the form of the equation to pairwise coupling reduces the number of possible symmetry groups for a network.

2.3 Reduction to normal form

The strong contraction compared to the strength of the coupling in the neighbourhood of the limit cycles enables us to use the normal hyperbolicity of Hirsch et al.[70] to predict persistence of an n-torus which is asymptotically attracting.

Examining the uncoupled system again, all of the orbits (which are periodic orbits due to the oscillators being identical) have n Floquet exponents [61] which are zero because the orbits are neutrally stable to perturbations lying on the n-torus. The rest have negative real part by assumption. For small enough ϵ, this n-torus is preserved by using normal hyperbolicity, as given in Wiggins [133] (theorem 1.3.7), with the torus being the center manifold of the flow.

We shall choose a coordinate system $\Theta \equiv (\theta_1, \ldots, \theta_n)$ for the n-torus that is a deformation of the phases for the uncoupled flow.

In the coordinates on the n-torus, the Γ-equivarant network of coupled oscillators $\dot{\mathbf{x}} = \mathbf{f}(\mathbf{x}, \lambda, \epsilon)$ is conjugated to a flow generated by the ODE:

$$\dot{\Theta} = \mathbf{1} + \epsilon F(\Theta, \lambda) \tag{2.3}$$

for sufficiently small ϵ, where F is a Γ-equivariant and C^k on the n-torus. We have suppressed the dependence of F on ϵ by reparameterisation, as the limit will in general be $O(1)$ in ϵ.

Definition 2.3.1 *The averaged equation 2.3 is defined to be:*

$$\dot{\Theta} = \mathbf{1} + \epsilon G(\Theta, \lambda) \tag{2.4}$$

where the averaged vector field G *of the vector field* F *is:*

$$G(\Theta, \lambda) = \frac{1}{2\pi} \int_0^{2\pi} F(\Theta + t\mathbf{1}, \lambda)\mathbf{dt} \tag{2.5}$$

For $\epsilon \ll 1$, the dynamics of the equation 2.3 can be conjugated to within ϵ of those of equation 2.4 for time $t < O(\epsilon^{-1})$ (see Sanders and Verhulst [117]). Note that it is possible to average the equations to any order in ϵ. The form of averaging we are using is for only one frequency; we do not need to consider quasiperiodic averaging [8].

The averaged vector field defined by equation 2.5 is invariant under the action of $\mathbf{T}^1$ given by:

$$\theta_i \mapsto \theta_i + \phi \text{ for } \phi \in \mathbf{T}^1. \tag{2.6}$$

This averaging is analogous to the reduction of vector fields to Birkhoff normal form, as used for Hopf bifurcation by Golubitsky and Stewart [52].

We have thus reduced the problem to looking at the dynamics of $\Gamma \times \mathbf{T}^1$ equivariant flows on the n-torus, or equivalently Γ equivariant flows on $\mathbf{T}^{n-1}$.

Definition 2.3.2 *We define the* $(n-1)$-torus *for* n *coupled oscillators to be* $\mathbf{T}^{n-1} = \mathbf{T}^n/\mathbf{T}^1(1,\cdots,1)$.

Taking representative points of $\mathbf{T}^{n-1}$, we can write

$$\mathbf{T}^{n-1} = \{\Theta \in \mathbf{T}^n : \sum_{i=1}^{n} \theta_i = 0\}$$

We can think of there being a factorisation of the flow into an average oscillation and a slow drift of phase made explicit through the $\mathbf{T}^1$ symmetry. The $\Gamma \times \mathbf{T}^1$ flow on $\mathbf{T}^n$ is a *normal form* for the weakly coupled case. We investigate the isotropy structure of this normal form in section 2.4.

2.3.1 Relating the normal form to the full equations

For ϵ small enough, hyperbolic periodic orbits in equation 2.3 are detectable as hyperbolic periodic orbits in equation 2.4 as $\epsilon \to 0$. However, periodic orbits with two or more zero Floquet exponents may not imply a periodic orbit in the unaveraged system, and can be destroyed by perturbing by terms which are 'flat' in ϵ. We have to beware of saddle connections, as these do not exist on the limited timescale in which averaging guarantees closeness. Generically, these can give rise to heteroclinic chaos in equation 2.3 as the stable and unstable manifolds may transversely intersect. This is however not the case if the stable and unstable manifolds are coincident with symmetry subspaces as will be discussed in chapter 3.

All the results above are done for the averaged approximation of a weakly coupled oscillator network. In fact, instead of exact $\mathbf{T}^1$ symmetry, we have a symmetry of the equations generated by the semigroup $\mathbf{R}^+$ corresponding to the fact that the equations are *autonomous*.

The $\mathbf{R}^+$ action can be extended into a group action on $\mathbf{R}$ because the θ_i are monotonic for small ϵ and the $\dot{\theta}_i$ are bounded due to the phase space being compact. Thus the equations are defined for all time both forwards and backwards.

By looking at the isotropy spaces for $\Gamma \times \mathbf{R}$, we can get a similar set of results, but the calculations are much harder due to the lack of a concrete temporal action on the phase space; it is easier to work with a Poincaré map in this case and use techniques such as those of Mirollo and Strogatz [100] for existence of rotating wave states.

2.4 The spatio-temporal symmetries of $\mathbf{S}_n \times \mathbf{T}^1$

After discussing the symmetries of networks of identical oscillators, we investigate the isotropy structure of $\mathbf{S}_n \times \mathbf{T}^1$ equivariant flows on $\mathbf{T}^n$. This gives us the isotropy structure of $\Gamma \times \mathbf{T}^1$ flows for any $\Gamma < \mathbf{S}_n$.

There is a trade-off between acting linearly with a non-compact group $\Gamma \times \mathbf{T}^1 \times \mathbf{Z}^n$ on the universal cover of the torus $\mathbf{T}^n$ and acting with the compact group $\Gamma \times \mathbf{T}^1$ on the topologically non-trivial manifold $\mathbf{T}^n$. For the questions considered here, the second route is simpler and gives answers more easily due to less algebra being necessary to take care of the infinite group $\mathbf{Z}^n$.

2.4.1 The symmetries for the phase equations

The flow we are considering is

$$\dot{\Theta}_i = 1 + \epsilon F(\Theta, \lambda) \tag{2.7}$$

This is equivariant under the action of $\Gamma \times \mathbf{T}^1$ on $\mathbf{T}^n$ defined by:

$$[(\sigma, w).\mathbf{z}]_i = w z_{\sigma(i)} \tag{2.8}$$

for $(\sigma, w) \in \Gamma \times \mathbf{T}^1$ (recall $z_j = \exp(i\theta_j)$). This action is reducible since Γ fixes a 1-D subspace of $\mathbf{T}^n$ corresponding to the diagonal $\mathbf{T}^1\mathbf{1}$. Although this group action simple enough that we do not need any theory of group actions on manifolds, there are many features of this action which are different from linear actions of a group on a vector space: There is no point which is fixed by all elements of $\Gamma \times \mathbf{T}^1$, and thus all fixed point subspaces are at least 1-dimensional. Also, there are in general many different 1-dimensional fixed point subspaces, all of which have 'maximal symmetry'.

This can be seen as a linear action of $\Gamma \times \mathbf{T}^1$ on $\mathbf{C}^n$ restricted to $\mathbf{T}^n$. This is what makes the calculations so simple, and in fact the action on $\mathbf{T}^n$ is simpler than the action on $\mathbf{C}^n$ because there are many fixed point subspaces in $\mathbf{C}^n$ which have $z_i = 0$ for at least one i. We do not need to consider these symmetry subspaces because they do not intersect $\mathbf{T}^n$. In our problem, unlike Hopf bifurcation with symmetry, all of the oscillators are oscillating with approximately the same amplitude and frequency.

2.4.2 Indistinguishable oscillator networks

Although the oscillators are identical in the limit of no coupling, we define a network to be *indistinguishable* if any oscillator can do the job of any other oscillator.

That is, the oscillators are indistinguishable if the group is transitive and in this case the system is determined by the equation for just one oscillator. (Recall that transitive means that for all i, j in $\{1 \cdots n\}$, there is an element $\sigma \in \Gamma$ with $i = \sigma(j)$.) Note that $\{(a, a, \cdots, a)\}$ is a symmetry subspace of $\Gamma \times \mathbf{T}^1$ if and only if Γ is transitive. The symmetry groups which give rise to indistinguishable oscillators include the common symmetry groups $\mathbf{S}_n$, $\mathbf{Z}_n$, $\mathbf{D}_n$, and also two or more dimensional lattices such as $\mathbf{D}_k \times \mathbf{Z}_m$ (where $km = n$) etc. for a variety of different structures.

Definition 2.4.1 *The* spatial projection homomorphism *and* temporal projection homomorphisms *are the natural projections of* $\Gamma \times \mathbf{T}^1$ *onto the two factors:*

$$\begin{array}{ccc} & \Gamma \times \mathbf{T}^1 & \\ {\scriptstyle \pi_s}\swarrow & & \searrow{\scriptstyle \pi_t} \\ \Gamma & & \mathbf{T}^1 \end{array}$$

The spatial projection is an *isomorphism* when restricted to any isotropy subgroup $\Sigma < \Gamma \times \mathbf{T}^1$. (See Golubitsky et al. [54] p 300). If two elements of Σ have the same spatial projection, then they are the same element.

The temporal projection must also be a homomorphism, but it need not be an isomorphism. If $\pi_t(\Sigma)$ is non-trivial, we call Σ a *twisted isotropy subgroup*. Because π_s restricted to Σ is an isomorphism, any element of an isotropy subgroup $\Sigma < \Gamma \times \mathbf{T}^1$ can be written as $(\sigma, w(\sigma))$, with $\sigma \in \pi_s(\Sigma)$, where $w(\sigma) = \exp(i\theta(\sigma))$ and $\theta(\sigma)$ is the twist homomorphism in [54], 299.

Lemma 2.4.1 *The image of any isotropy subgroup of* $\Gamma \times \mathbf{T}^1$ *under temporal projection is isomorphic to* $\mathbf{Z}_m$ *for some* m *dividing* n.

Proof Consider the isotropy subgroup of $\Gamma \times \mathbf{T}^1$ corresponding to the isotropy of the point z. Then z is invariant under Σ by definition. Thus

$$z_i = w z_{\sigma(i)}$$

for all $(\sigma, w) \in \Sigma$. Each $\sigma \in \Sigma$ defines a partition of n objects corresponding to the disjoint cycle decomposition of that permutation. Say we have a partition into parts, each of length k_j, $j = 1 \cdots l$. Then for each i in the jth partition, σ^{k_j} acts trivially on the i, and so $w^{k_j} = 1$, because $z_i = w^{k_j} z_{\sigma^{k_j}(i)}$. Thus,

$$w^n = w^{\Sigma k_j} = \Pi w^{k_j} = 1$$

for each $(\sigma, w) \in \Sigma$. This says that any isotropy subgroup of $\Gamma \times \mathbf{T}^1$ is in fact a subgroup of $\Gamma \times \mathbf{Z}_n$, and thus π_t restricted to $\Gamma \times \mathbf{Z}_n$ gives $\pi_t(\Sigma) < \mathbf{Z}_n$. Thus $\pi_t(\Sigma) \equiv \mathbf{Z}_m$ for some m dividing n. □

The previous lemma means that the temporal part of any isotropy subgroup must have order dividing the number of oscillators. What is perhaps more surprising is that this result holds for the isotropy subgroups of any $\Gamma < \mathbf{S}_n$ (see theorem 2.4.2), so for instance six oscillators with five in a ring and one in the centre (an intransitive $\mathbf{D}_5$ symmetry) will not have any isotropy subgroups with temporal order five.

2.4.3 The isotropy subgroups of $\mathbf{S}_n \times \mathbf{T}^1$

We show that conjugacy classes of isotropy subgroups are in one-to-one correspondence with all distinct ways of writing $n = m(k_1 + k_2 + \cdots + k_l)$, where l, m and k_j are all integers, with $k_1 \geq k_2 \geq \cdots \geq k_l \geq 1$. The fixed point subspaces have m blocks of $k = n/m$ oscillators which are 'rotated' by a phase shift of $2\pi/m$. Furthermore, each block is partitioned into l sets of phase-locked oscillators.

Theorem 2.4.1 *The isotropy subgroups of* $\mathbf{S}_n \times \mathbf{T}^1$ *are the elements* Σ *in conjugacy classes of the form:*

$$\Sigma \in \Sigma_{\mathbf{k},m} \equiv (\mathbf{S}_{k_1} \times \cdots \times \mathbf{S}_{k_l})^m \otimes \mathbf{Z}_m$$

where $n = mk$ *and* $k = k_1 + k_2 + \cdots + k_l$. *The dimension (in* $\mathbf{T}^n$*) of fix*$(\Sigma_{\mathbf{k},m})$ *is* l. *The size of the conjugacy class* $\Sigma_{\mathbf{k},m}$ *is* $\frac{n!}{m(k_1!k_2!\cdots k_l!)^m}$.

($G \otimes H$ signifies a semidirect product of the groups G and H.)

Proof. The above lemma gives us the temporal $\mathbf{Z}_m$, m dividing n. Looking at $\pi_s(j)$, this must induce a partition on $\{1 \cdots n\}$ which is respected by $ker(\pi_t)$ and is cyclically permuted by the action of $im(\pi_t) \cong \mathbf{Z}_m$. □

Remarks Any fixed point subspace of a group in $\Sigma_{\mathbf{k},m}$ induces a partition of the oscillators into m blocks, each containing k oscillators. The system is unchanged under a shift in time of $1/m$th of a period, coupled with cyclic permutation of the blocks. (This is the $\mathbf{Z}_m$ symmetry.) Each block is partitioned into sets of k phase-locked oscillators and thus has $\mathbf{S}_{k_1} \times \cdots \mathbf{S}_{k_l}$ symmetry.

name	Γ	fix(Γ)	dim fix	mult.
in-phase	$\mathbf{S}_n$	$(z, \cdots z)$	1	1
rotating waves	$\mathbf{Z}_n$	$(z, z\omega, z\omega^2, \cdots, z\omega^{n-1})$	1	$(n-1)!$
rotating blocks	$(\mathbf{S}_k)^m \otimes \mathbf{Z}_m$	$(z, \cdots, z, z\omega^k, \cdots, z\omega^{-k})$	1	$n!/(mk^m)$
partitioned oscillators	$\mathbf{S}_{k_1} \times \cdots \times \mathbf{S}_{k_l}$	$(z_1, \cdots, z_1, z_2, \cdots, z_l)$	l	$n!/(k_1! \cdots k_l!)$

Table 2.1: Some special fixed point spaces. These include all possible fixed point spaces for n prime or $n < 5$, but in general there will be many more, which we call rotating partitioned blocks.

Example Consider $n = 6$, which incidentally has the smallest n where we get an interesting isotropy subgroup (i.e. m and l both not equal to 1), it can be written as $6 = 2(2+1)$. The two dimensional submanifold of points:

$$(x, y, y, -x, -y, -y) \in \mathbf{T}^6$$

has isotropy

$$(\mathbf{S}_1 \times \mathbf{S}_2)^2 \otimes \mathbf{Z}_2$$

generated by the elements:

$$\{((23), 1), ((14)(25)(36), -1)\} \in \mathbf{S}_6 \times \mathbf{T}^1.$$

We give special names to some of these fixed point subspaces, as shown in table 2.1. Note that the name 'rotating wave' is also called 'ponies on a merry-go-round' (POMs) by Aronson et al. [11] and 'splay phase solutions' by Mirollo, Strogatz, Swift, Tsang and Wiesenfeld [127, 99].

The 1-1 correspondence noted in theorem 2.4.1 enables us to use a simple algorithm to generate the lattice of isotropy subgroups of $\mathbf{S}_n$:

- Note that $\Sigma_{\mathbf{k}',m} < \Sigma_{\mathbf{k},m}$ if $\mathbf{k}'$ is a subpartition of $\mathbf{k}$.
- Furthermore $\Sigma_{\mathbf{k}^p,m} < \Sigma_{\mathbf{k},mp}$ where $\mathbf{k}^p$ is a partition with p copies of $\mathbf{k}$.

These two observations allow us to generate the lattice of isotropy subgroups for any n. This method is shown schematically in figure 2.1, and the lattices for isotropy subgroups for $n = 2$ to 6 are shown in figure 2.2.

2.4.4 The isotropy subgroups of $\Gamma \times \mathbf{T}^1$

Now we are in a position to generate the isotropy lattice for any $\Gamma \times \mathbf{T}^1 < \mathbf{S}_n \times \mathbf{T}^1$, using the following result.

Theorem 2.4.2 *The isotropy subgroups of* $\Gamma \times \mathbf{T}^1$ *are precisely* $(\Gamma \times \mathbf{T}^1) \cap \Sigma$ *where the* Σ *is an element of some conjugacy class* $\Sigma_{\mathbf{k},m}$ *of isotropy subgroups of* $\mathbf{S}_n \times \mathbf{T}^1$.

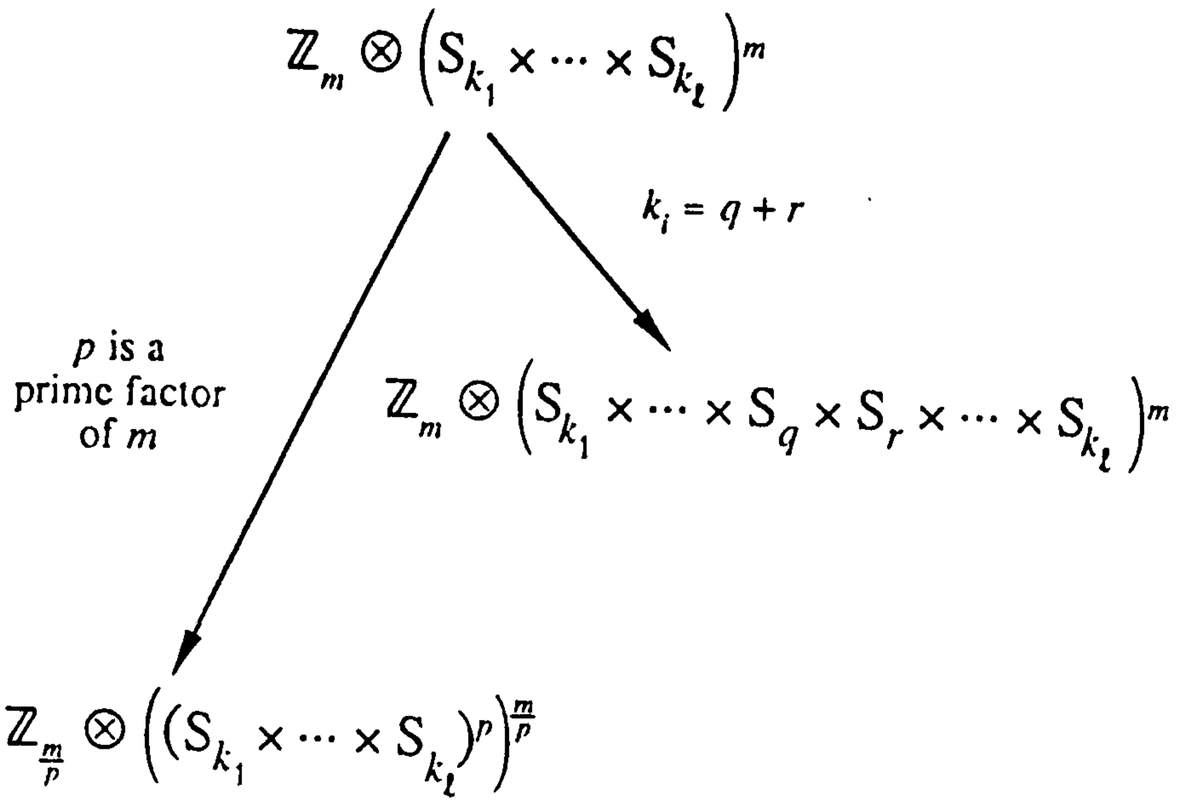

Figure 2.1: The general isotropy subgroup, with the largest isotropy subgroups it contains. The lattice can be generated by repeated applications of these rules.

Proof Consider $z \in \mathbf{T}^n$, with isotropy $\Sigma \in \Sigma_{\mathbf{k},m}$ in $\mathbf{S}_n \times \mathbf{T}^1$. This must have isotropy subgroup $(\Gamma \times \mathbf{T}^1) \cap \Sigma$ in $\Gamma \times \mathbf{T}^1$. □

This theorem is awkward to implement in practice. The intersection of $\Gamma \times \mathbf{T}^1$ with each of the elements in all of the conjugacy classes $\Sigma_{\mathbf{k},m}$ must be computed, which presents a formidable problem (although there are quite probably methods that will give substantial simplifications). This is because taking the intersection with a Γ will split the members of a conjugacy class of subgroups (in $\mathbf{S}_n$) into a variety of conjugacy classes in Σ. However, for small n it is possible to do these calculations by hand, as in the examples below. For groups with easily computable subgroups, it is easier to list all subgroups of Γ in terms of their generators and find the possible twist homomorphisms associated with each of these generators.

2.4.5 Example: $\mathbf{S}_2 \times \mathbf{S}_2$ (i)

If we have a four oscillator system with intransitive $\mathbf{S}_2 \times \mathbf{S}_2$ symmetry group of the elements

$$\{e, (12), (34), (12)(34)\}$$

then for the averaged system, by theorem 2.4.2 there exist isotropy subgroups of the form $\mathbf{S}_2 \times \mathbf{S}_2$, $\mathbf{S}_2$ (twice), $\mathbf{Z}_2$ and 1, corresponding to the spaces (a, a, b, b), (a, a, b, c), (a, b, c, c), $(a, -a, b, -b)$ and (a, b, c, d) respectively on $\mathbf{T}^4$ (where $|a| = |b| = |c| = |d| = 1$). Note there are no in-phase oscillations forced by the symmetry, even for arbitrarily small coupling.

2.4.6 Example: $\mathbf{S}_2 \times \mathbf{S}_2$ (ii)

If we have a four oscillator system with the transitive $\mathbf{S}_2 \times \mathbf{S}_2$ symmetry of

$$\{e, (12)(34), (13)(24), (14)(23)\}$$

(i.e. a different Klein 4-group), then theorem 2.4.2 predicts to existence of isotropy subgroups of the form $\mathbf{S}_2 \times \mathbf{S}_2$, $\mathbf{S}_2$ (three times), $(\mathbf{S}_2 \times \mathbf{Z}_2)$ (three times), $\mathbf{Z}_2$ (three

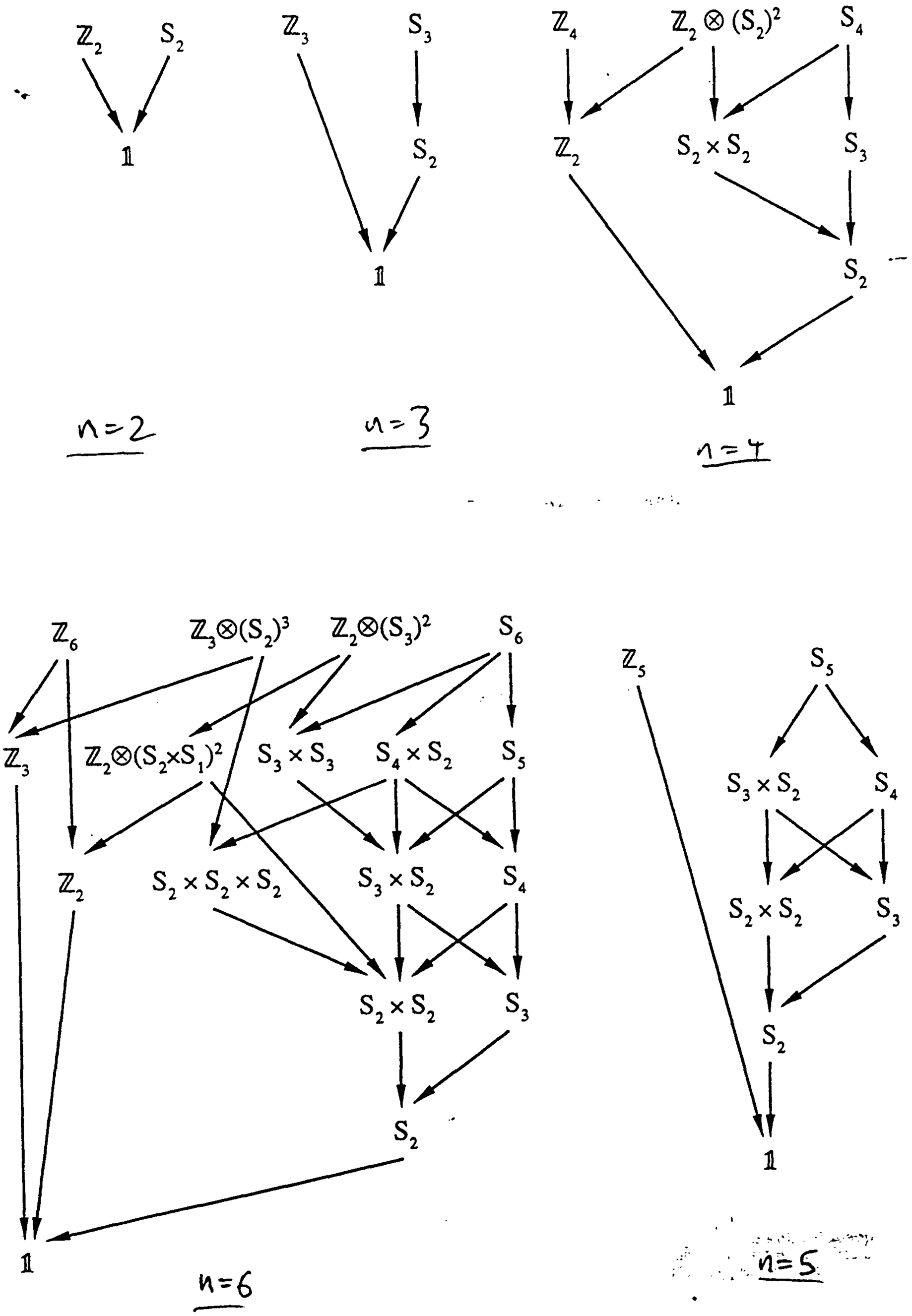

Figure 2.2: The lattice of isotropy subgroups of $\mathbf{S}_n \times \mathbf{T}^1$ for $n = 2, \ldots, 6$.

times), and 1 corresponding to the spaces (a,a,a,a), (a,a,b,b) etc., $(a,-a,a,-a)$ etc., $(a,-a,b,-b)$ etc. and (a,b,c,d) respectively.

The examples $\mathbf{S}_3$ and $\mathbf{S}_4$ are discussed at length in chapter 3.

2.5 The isotropy structure of $\mathbf{Z}_n \times \mathbf{T}^1$ and $\mathbf{D}_n \times \mathbf{T}^1$

In this section we apply similar calculations to those in section 2.4 in order to classify all of the isotropy subgroups of a ring of identical oscillators. This leads us to examine firstly the group of rotations $\mathbf{Z}_n$ and secondly, the dihedral group $\mathbf{D}_n$ (rotations and reflections of the ring) on n identical oscillators, which has also been considered near Hopf bifurcation by Ermentrout [43] and Golubitsky and Stewart [53].

2.5.1 The group $\mathbf{Z}_n \times \mathbf{T}^1$

By labelling the oscillators 1 to n around the ring, we can pick the n cycle $\sigma = (1,\cdots,n)$ as the generator of $\mathbf{Z}_n$. This is applicable when we have a ring of oscillators with a preferred orientation.

Theorem 2.5.1 *The isotropy subgroups are in one-to-one correspondence with pairs of positive integers (m,p) where $n = mk$ and $p \in \{0,1,2,\cdots,m-1\}$. The isotropy subgroups $\mathbf{Z}_m(p)$ are isomorphic to $\mathbf{Z}_m$ under spatial projection, and are generated by:*

$$\{(\sigma^k, \omega^{kp})\}.$$

The fixed point subspaces have dimension k (in $\mathbf{T}^n$) and are:

$$fix(\mathbf{Z}_m(p)) = \{z \in \mathbf{T}^n : z_i = a_i \omega^{ip}\}$$

where $a_i = a_{(j \bmod k)}$.

Proof. Any isotropy subgroup of $\mathbf{Z}_n \times \mathbf{T}^1$ must be isomorphic to $\mathbf{Z}_m$ because the spatial projection of any isotropy subgroup Σ must be a subgroup of $\mathbf{Z}_n$ and thus it can be written as being generated by (σ^k, w) for some w. Looking at the mth power of the generator acting on a point with isotropy Σ, we must have $w^m = 1$, and so we can write $w = \omega^k p$ for some p, with the w distinct for different $p \bmod m$. □

Note that the subgroups with different p are not conjugate in $\mathbf{Z}_n$, and they will have temporal projections which will be $\mathbf{Z}_q$ for all q dividing m. These subgroups are partially ordered in the lattice in the following way:

Theorem 2.5.2 *$\mathbf{Z}_r(s) \leq \mathbf{Z}_m(p)$ if and only if r divides m and $s = p \bmod r$.*

Proof. Let $m = kr$ and $p = s \bmod r$. Then the kth power of the generator of $\mathbf{Z}_m(p)$ is the generator of $\mathbf{Z}_r(s)$. Conversely, if $\mathbf{Z}_r(s) < \mathbf{Z}_m(p)$ (where $mk = rt = n$) we get

$$(\sigma^t, \omega^{ts}) = (\sigma^k, \omega^{kp})^h$$

for some integer h, as they are both cyclic groups. Thus $kh = t$, $nh/m = n/r$, r divides m and $ts = kph \bmod n$ so $s = p \bmod r$. □

As an example, we show the isotropy lattice for $\mathbf{Z}_4 \times \mathbf{T}^1$ in figure 2.3.

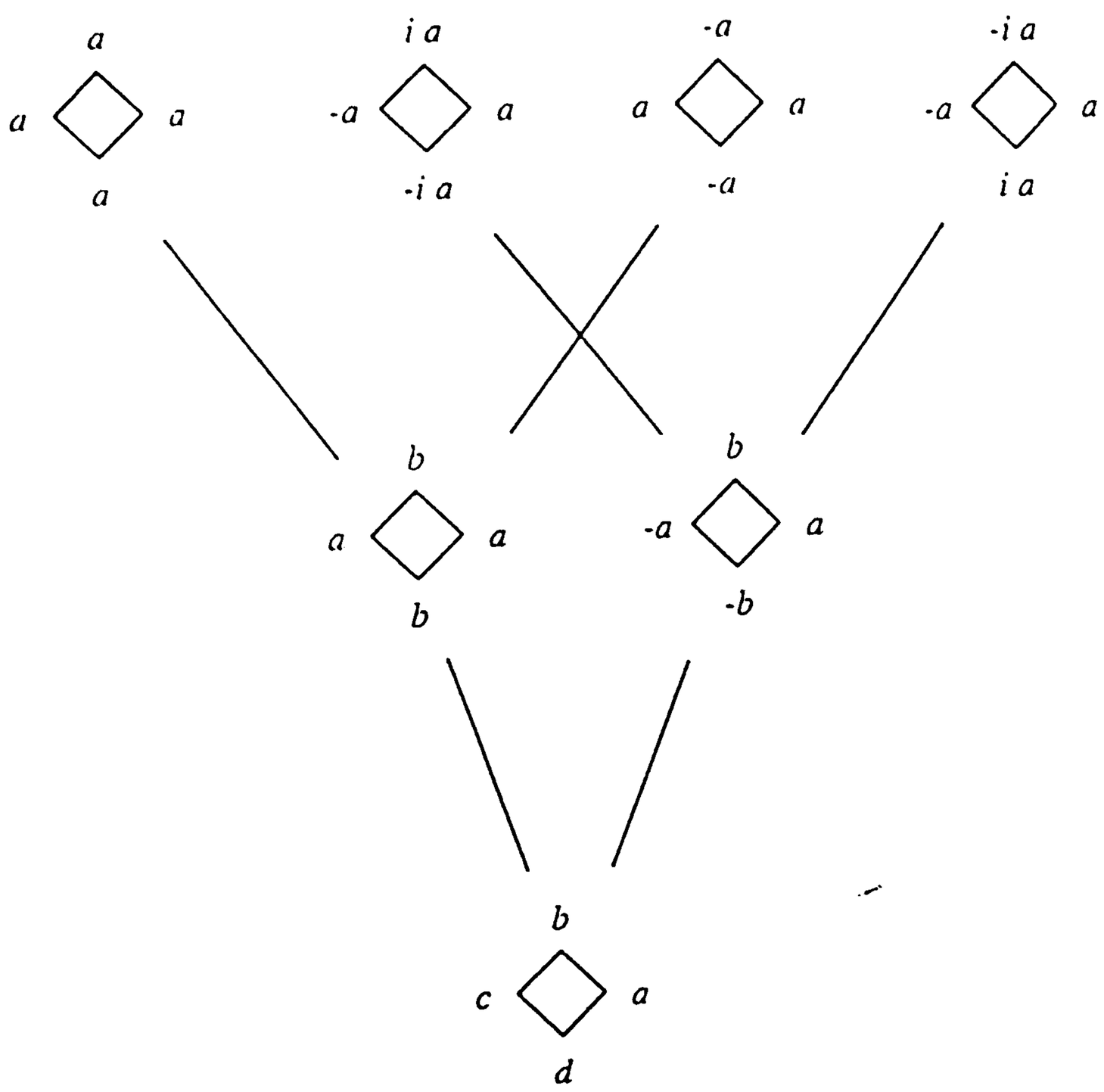

Figure 2.3: The isotropy lattice of symmetry subspaces for $\mathbf{Z}_4 \times \mathbf{T}^1$. The isotropy subgroups are $\mathbf{Z}_4(0)$, $\mathbf{Z}_4(1)$, $\mathbf{Z}_4(2)$, $\mathbf{Z}_4(3)$, $\mathbf{Z}_2(0)$, $\mathbf{Z}_2(1)$ and $\mathbf{Z}_1(0)$.

2.5.2 The group $\mathbf{D}_n \times \mathbf{T}^1$

If the ring of oscillators has no preferred direction, it has the symmetry of an n-sided polygon allowing reflections, $\mathbf{D}_n$.

We define this group:

$$\mathbf{D}_n \equiv < \{\sigma, \kappa\};\ \sigma^n = \kappa^2 = 1, \sigma\kappa\sigma = \kappa > .$$

with

$$\sigma = (1, \cdots, n)$$

and

$$\kappa = (1)(2, n)(3, n-1)\cdots$$

2.5.3 The isotropy lattice for $\mathbf{D}_n$

We now classify all of the isotropy subgroups for the action of $\mathbf{D}_n \times \mathbf{T}^1$. We do this by considering all subgroups of $\mathbf{D}_n$ and then all twisted subgroups of $\mathbf{D}_n$, selecting only those which are isotropy subgroups.

It is well known that all subgroups of $\mathbf{D}_n$ are conjugate to one (or more) of the following:

$$\mathbf{D}_m(\kappa) \equiv < \{\sigma^k, \kappa\} > \equiv < \{\sigma^k\kappa, \kappa\} >$$

$$\mathbf{D}_m(\kappa\sigma) \equiv < \{\sigma^k, \kappa\sigma\} > \equiv < \{\sigma^{k-1}\kappa, \kappa\sigma\} >$$

$$\mathbf{Z}_m \equiv < \{\sigma^k\} >$$

where $mk = n$. For the two $\mathbf{D}_m$ subgroups, we give a set of generating reflections. This is useful when we discuss twisted subgroups below. We refer to the groups named $\mathbf{Z}_2(\kappa)$ and $\mathbf{Z}_2(\kappa\sigma)$ by Golubitsky et al. as $\mathbf{D}_1(\kappa)$ and $\mathbf{D}_1(\kappa\sigma)$ for compactness of notation. $\mathbf{D}_m(\kappa)$ is conjugate to $\mathbf{D}_m(\kappa\sigma)$ when k is odd, since $\sigma^{k-1}\kappa = \sigma^{(k-1)/2}\kappa\sigma^{-(k-1)/2}$ is conjugate to κ. When k is odd we call the group simply $\mathbf{D}_m$.

Lemma 2.5.1 *All twisted isotropy subgroups of* $\mathbf{D}_n \times \mathbf{T}^1$ *are conjugate to one of the following:*

$$\mathbf{D}_m(+-) \equiv < \{(\sigma^{k-1}\kappa, 1), (\kappa\sigma, -1)\} > (m \text{ even })$$

$$\mathbf{D}_m(--) \equiv < \{(\sigma^{k-1}\kappa, -1), (\kappa\sigma, -1)\} > (k \text{ even })$$

$$\mathbf{Z}_m(p) \equiv < \{(\sigma^k, \omega^{pk})\} > \text{ where } p \in \{1, \cdots, [m/2]\}.$$

Proof. We need to consider all possible twists of the generators of the subgroups of $\mathbf{D}_n$, listed above. Let ρ represent any reflection. The only allowed twists of a reflection are $w(\rho) = \pm 1$, since $(\rho, w(\rho))^2 = (1, w(\rho)^2) = (1, 1)$. Furthermore, if ρ fixes an element in $\{1, 2, \cdots, n\}$, and (ρ, w) fixes a point in $\mathbf{T}^n$, then $w = 1$. (To see this, suppose $\rho(1) = 1$. If $(\rho, -1)z = z$, then $z_1 = -z_{\rho(1)} = -z_1 = 0$. This is a contradiction, since $|z_1| = 1$.) Thus if $\Sigma \cong \mathbf{D}_m$ is a twisted isotropy subgroup, then it must contain a reflection conjugate to $(\kappa\sigma, -1)$, and n must be even. There are two classes of twisted dihedral subgroups, depending on twist of the other generating reflection. The group $\mathbf{D}_m(+-)$ has the element $(\sigma^k, -1)$, hence the element $(1, (-1)^m)$. Thus m must be even. The group $\mathbf{D}_m(--)$ has the element $(\sigma^{k-1}\kappa, -1)$. We must have k odd, otherwise the reflection $\sigma^{k-1}\kappa$ fixes the phase of oscillator number $k/2$. The twisted cyclic groups are the same as those for the group $\mathbf{Z}_n \times \mathbf{T}^1$. However, the range of p is restricted because σ^k is conjugate to σ^{-k} within the group $\mathbf{D}_n$, thus $\mathbf{Z}_m(p)$ is conjugate to $\mathbf{Z}_m(m-p)$. Recall that $[m/2]$ denotes the integer part of $m/2$. □

Theorem 2.5.3 *The isotropy subgroups of* $\mathbf{D}_n \times \mathbf{T}^1$ *and their fixed point spaces are as follows: For all factorisations* $n = mk$ *(with* m *and* k *positive integers), find the isotropy subgroups listed in table 2.5.3. The list constructed in this way has no duplications.*

Proof. We go through all the possible subgroups of $\mathbf{D}_n$, first the dihedral ones. The fixed point space has m blocks of k adjacent oscillators. The phases z_1 up to z_k determine the state of the system, and the dimension of the fixed point space is the number of independent phases. We must give special attention to the cases $k = 1$ and $k = 2$ to determine which subgroups are in fact isotropy subgroups.

For $\mathbf{D}_m(\kappa)$, the reflection $\sigma^k\kappa$ permutes the set

$$\{1, 2, \cdots, k\} \text{ to } \{k+1, k, \cdots, 1\}.$$

For k even, dim fix$(\mathbf{D}_m(\kappa)) = k/2 + 1$, since the independent phases are

$$z_1, z_2 = z_k, z_3 = z_{k-1}, \cdots, z_{k/2} = z_{k/2+2}, z_{k/2+1}.$$

For k odd, dim fix$(\mathbf{D}_m(\kappa)) = (k+1)/2$, since the independent phases are

$$z_1, z_2 = z_k, z_3 = z_{k-1}, \cdots, z_{(k+1)/2} = z_{(k+3)/2}.$$

For $\mathbf{D}_m(\kappa\sigma)$, the reflection $\sigma^{k-1}\kappa$ permutes the set

$$\{1, 2, \cdots, k\}$$

to

$$\{k, k-1, \cdots, 1\}.$$

Thus, dim fix$(\mathbf{D}_m(\kappa\sigma)) = k/2$ when k is even, because

$$z_1 = z_k, z_2 = z_{k-1}, \cdots, z_{k/2} = z_{k/2+1}.$$

Similarly, dim fix$(\mathbf{D}_m(\kappa\sigma)) = k/2$ when k is even, because

$$z_1 = z_k, z_2 = z_{k-1}, \cdots, z_{(k-1)/2} = z_{(k+3)/2}.$$

Now consider the twisted subgroups $\Sigma \cong \mathbf{D}_m$. The dimension of the fixed point space is the same as dim fix$(\mathbf{D}_m(\kappa\sigma))$, since the fixed point spaces differ only by the inclusion of some minus signs.

We turn to the subgroups $\mathbf{Z}_m$ of $\mathbf{D}_n$. The phase of each oscillator in the block of k oscillators is arbitrary, thus dim $\text{fix}(\mathbf{Z}_m(p)) = k$.

Finally, we must consider all cases with $k = 1$ and 2 to see if the subgroups are in fact isotropy subgroups. For instance, $\text{fix}(\mathbf{Z}_n) = \{(a, a, \cdots, a)\}$. But $\mathbf{Z}_n$ is not an isotropy subgroup because any point in $\text{fix}(\mathbf{Z}_n)$ has isotropy $\mathbf{D}_n$. We find that $\mathbf{Z}_n, \mathbf{D}_{n/2}(\kappa\sigma), \mathbf{Z}_n(n/2), \mathbf{D}_{n/2}(--)$, and $\mathbf{Z}_n/2$ are not isotropy subgroups, because

$$\text{fix}(\mathbf{Z}_n) = \text{fix}(\mathbf{D}_{n/2}(\kappa\sigma)) = \text{fix}(\mathbf{D}_n) = \{(a, a, \cdots, a)\}$$

$$\text{fix}(\mathbf{Z}_n(n/2)) = \text{fix}(\mathbf{D}_{n/2}(--)) = \text{fix}(\mathbf{D}_n(+-)) = \{(a, -a, \cdots, a, -a)\}$$

$$\text{fix}(\mathbf{Z}_n/2) = \text{fix}(\mathbf{D}_{n/2}(\kappa)) = \{(a, b, \cdots, a, b)\}.$$

□

The lattice of isotropy subgroups of $\mathbf{D}_4 \times \mathbf{T}^1$ is shown in figure 2.4.

Remark. Theorem 2.5.3 can be arrived at by decomposing the action into one on all possible irreducible subspaces and applying the results of Golubitsky and Stewart [53], as they indicate in that paper.

2.6 The canonical invariant region

As we discuss at greater length in chapter 3, for three weakly coupled oscillators with $\mathbf{S}_3 \times \mathbf{T}^1$ symmetry, we can represent the dynamics as an ODE on a two-torus defined by factoring $\mathbf{T}^3$ by the $\mathbf{T}$ symmetry in the $(1, 1, 1)$ direction. The $\mathbf{S}_3$ symmetry manifests itself by dividing each 'unit cell' of the universal cover $\mathbb{R}^2$ into two invariant cells that are equilateral triangles. This section generalizes this to $\mathbf{S}_n$. There are invariant cells (we call 'canonical invariant regions') which are $(n-1)$-dimensional simplices, they only have $\mathbf{Z}_n$ symmetry, so there is a natural projection onto two dimensions given by an irreducible action of $\mathbf{Z}_n$. This projection we call the 'isotropy mandala', and in chapter 3, we use these two notions to help visualise structurally stable heteroclinic cycles and bifurcations in these high dimensional phase spaces.

More precisely, in this section we show that the hyperplanes $\text{fix}(\mathbf{S}_2)$ divide $\mathbf{T}^n$ into $(n-1)!$ disjoint dynamically invariant regions, the closure of which is the whole phase space. We demonstrate how the isotropy structure inside each invariant region relates to the rotational symmetry of an n-sided polygon. Applications of this theory are discussed in chapter 3 Recall that in theorem 2.4.1, we show;

Lemma 2.6.1 *The symmetry subgroups $\Sigma_{(2,1,\cdots,1)}, 1 \cong \mathbf{S}_2$ ($\Sigma_{\mathbf{k},m}$ defined as in theorem 2.4.1) have fixed point subspaces of codimension 1 in $\mathbf{T}^n$ (and therefore $\mathbf{T}^{n-1}$) corresponding to the condition $\theta_i = \theta_j$ for some $i \neq j$. These are the only fixed point subspaces of codimension 1 in $\mathbf{T}^n$.* □

Definition 2.6.1 *The* canonical invariant region *in $\mathbf{T}^n$ is the open set defined by the ordering in the universal cover:*

$$C = \{\Theta : \theta_1 < \theta_2 < \cdots < \theta_n < \theta_1 + 2\pi\}$$

Lemma 2.6.2 *The closure of the canonical invariant region is invariant under the flow.*

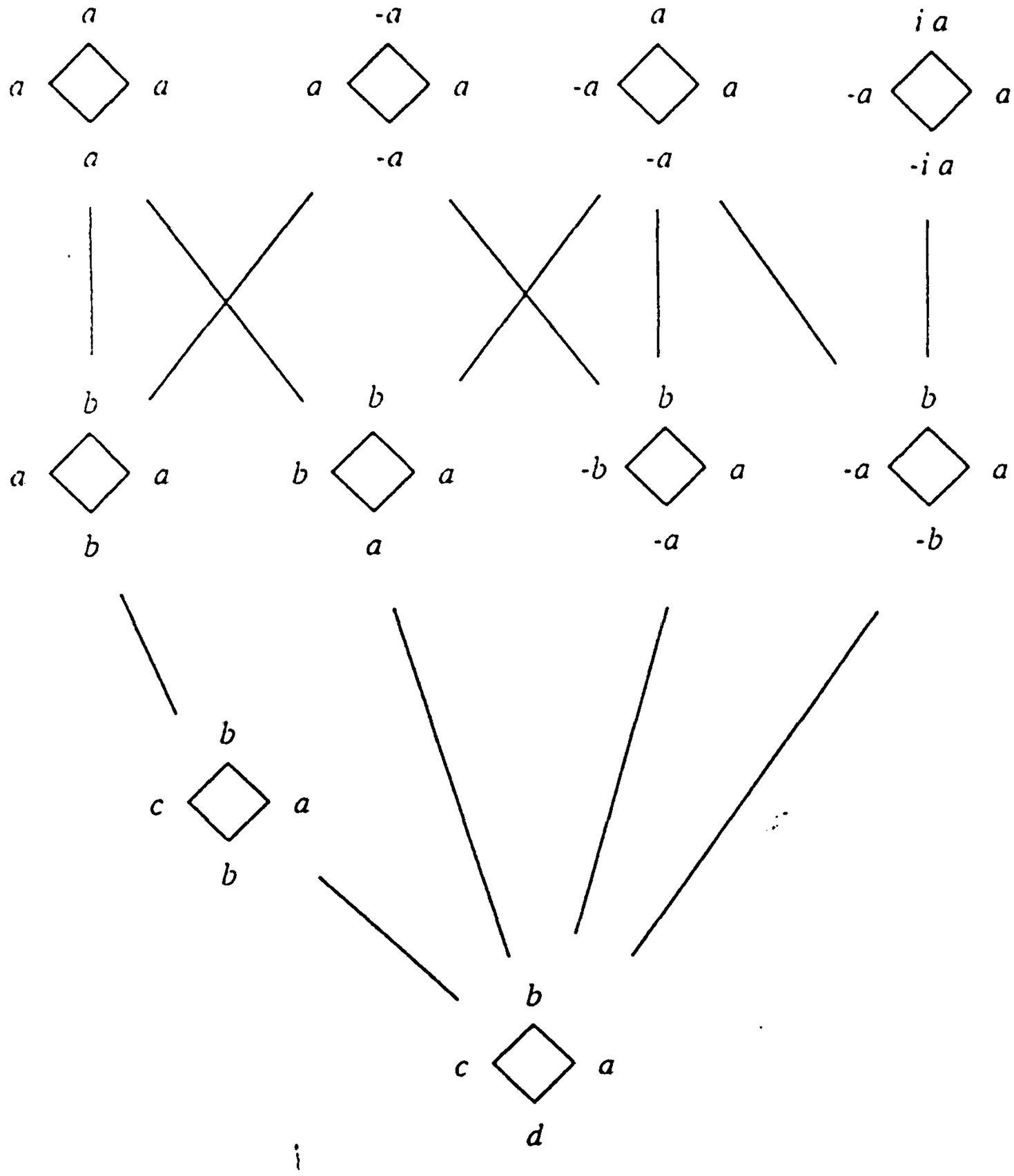

Figure 2.4: The partial ordering of the fixed point subspaces for $\mathbf{D}_4 \times \mathbf{T}^1$. The isotropy subgroups are: (First row) $\mathbf{D}_4$, $\mathbf{D}_4(+-)$, $\mathbf{D}_2(+-)$, $\mathbf{Z}_4(1)$. (Second row) $\mathbf{D}_2(\kappa)$, $\mathbf{D}_1(\kappa\sigma)$, $\mathbf{D}_1(--)$, $\mathbf{Z}_2(1)$. (Third row) $\mathbf{D}_1(\kappa)$. (Fourth row) $\mathbf{Z}_1 = 1$.

Isotropy subgroup	dim fix	example fixed point space
$k = 1$		
$\mathbf{D}_n$	1	$(a, \cdots, a)$
$\mathbf{D}_n(+-) n$ even	1	$(a, -a, a, \cdots, -a)$
$\mathbf{Z}_n(p)$	1	$(a, \omega a, \omega^2 a, \cdots, \omega^{n-1} a)$
$(p \in \{1 \cdots [(n-1)/2]\})$		
$k = 2$		
$\mathbf{D}_{n/2}(+-)(n = 0 \bmod 4)$	1	$(a, a, -a, -a, \cdots a, a, -a, -a)$
$\mathbf{D}_{n/2}(\kappa)$	2	$(a, b, a, b, \cdots a, b)$
$\mathbf{Z}_n/2(p)$	2	$(a, b, \omega^2 a, \omega^2 b, \cdots \omega^{n-2} a, \omega^{n-2} b)$
$(p \in \{1, \cdots, [m/2]\}$		
k odd, $k \neq 1$		
$\mathbf{D}_m$	$(k+1)/2$	$(a, b, c, b, a, \cdots a, b, c, b, a)$
$\mathbf{D}_m(+-)(m$ even$)$	$(k+1)/2$	$(a, b, c, b, a, \cdots - a, -b, -c, -b, -a)$
$\mathbf{Z}_m$	k	$(a, b, c, d, e, \cdots a, b, c, d, e)$
$\mathbf{Z}_m(p)$	k	$(a, b, c, d, e, \omega^5 a, \omega^5 b, \cdots \omega^{n-5} d, \omega^{n-5} e)$
$(p \in \{1, \cdots, [m/2]\}$		
k even, $k \neq 2$		
$\mathbf{D}_m(\kappa)$	$k/2+1$	$(a, b, c, d, c, b, \cdots a, b, c, d, c, b)$
$\mathbf{D}_m(\kappa\sigma)$	$k/2$	$(a, b, c, c, b, a, \cdots a, b, c, c, b, a)$
$\mathbf{D}_m(--)$	$k/2$	$(a, b, c, -c, -b, -a, \cdots a, b, c, -c, -b, -a)$
$\mathbf{D}_m(+-)(m$ even$)$	$k/2$	$(a, b, c, c, b, a, \cdots - a, -b, -c, -c, -b, -a)$
$\mathbf{Z}_m$	k	$(a, b, c, d, \cdots a, b, c, d)$
$\mathbf{Z}_m(p)$	k	$(a, b, c, d, \omega^4 a, \omega^4 b, \cdots \omega^{n-4} c, \omega^{n-4} d)$
$(p \in \{1, \cdots, [m/2]\})$		

Table 2.2: Table of isotropy subgroups of $\mathbf{D}_n \times \mathbf{T}^1$.
There are always m blocks of k adjacent oscillators in the fixed point spaces, where $n = mk$. The case $p = 1$ is shown for the twisted cyclic groups, and $\omega \equiv \exp(i2\pi/n)$.

Proof. As we have defined it, $\partial C = \{\Theta : \theta_i = \theta_j \text{ for some } i - j = 1 \bmod n\}$. Thus ∂C is a union of $\text{fix}(\mathbf{S}_2)$ with $\mathbf{S}_2$ isotropy subgroups of $\mathbf{S}_n \times \mathbf{T}^1$. However, the fixed point subspaces do not permit flow across them, and so the set C and its boundary ∂C must be invariant under the flow. □

In fact, the canonical invariant region and its group orbit under $\mathbf{S}_n$ are the largest possible invariant regions in the sense that they are bounded by codimension one invariant subspaces, and all fixed point spaces inside must be codimension two or higher. Thus, for instance, there exists a dense subset of points in C such that for any two points in it, there exists a vector field with $\mathbf{S}_n \times \mathbf{T}$ symmetry with a trajectory passing through both points.

Lemma 2.6.3 *The fixed point subspaces of the isotropy groups* $\mathbf{S}_2$ *divide the phase space into* $(n-1)!$ *dynamically invariant regions which are the elements in the orbit of the canonical fundamental region under the action of* $\mathbf{S}_{n-1}$. *These elements are disjoint.*

Proof. Any point in the dense set $S = \mathbf{T}^n \cup \text{fix}(\mathbf{S}_2)$ defines an order on the coordinates by the sequence

$$\theta_1 < \theta_{\sigma(2)} < \theta_{\sigma(3)} < \cdots < \theta_{\sigma(n)} < \theta_1 + 2\pi$$

which must be satisfied for some unique $\sigma \in \mathbf{S}\{2, \cdots, n\} \cong \mathbf{S}_{n-1}$. Thus each point in the space S is in the image of the canonical fundamental region under some element of $\mathbf{S}_{n-1}$. There are $(n-1)!$ of them, as they are in 1-1 correspondence with the elements in $\mathbf{S}_{n-1}$. □

The whole canonical invariant region is in fact an n-simplex in the universal cover of $\mathbf{T}^n/\mathbf{T}^1\mathbf{1} \equiv \mathbf{T}^{n-1}$, but it has $\mathbf{Z}_n$ symmetry rather than $\mathbf{S}_n$. At the geometrical centre of each of these invariant regions in the universal cover, there is a rotating wave as defined in section 2.4. For the canonical invariant region, the rotating wave at the centre is that with the ordering $1, \cdots, n$:

$$\mathbf{z} = (a, a\omega, a\omega^2, a\omega^3, \cdots, a\omega^{n-1}).$$

2.6.1 The graph giving the canonical invariant region

In the universal cover $\mathbf{R}^n$, we show that any point in the closure of the canonical invariant region can be obtained by a convex linear combination of the n vectors we call the vertices in $\mathbf{R}^{n-1}$.

Definition 2.6.2 *The* vertices of the canonical invariant region *are the points* Φ_i *on the universal cover of* $\mathbf{T}^{n-1}$ *defined by:*

$$\Phi_1 = (\theta, \theta + 2\pi, \theta + 2\pi, \cdots, \theta + 2\pi)$$

$$\Phi_2 = (\theta, \theta, \theta + 2\pi, \cdots, \theta + 2\pi)$$

$$\cdots$$

$$\Phi_n = (\theta, \theta, \theta, \cdots, \theta).$$

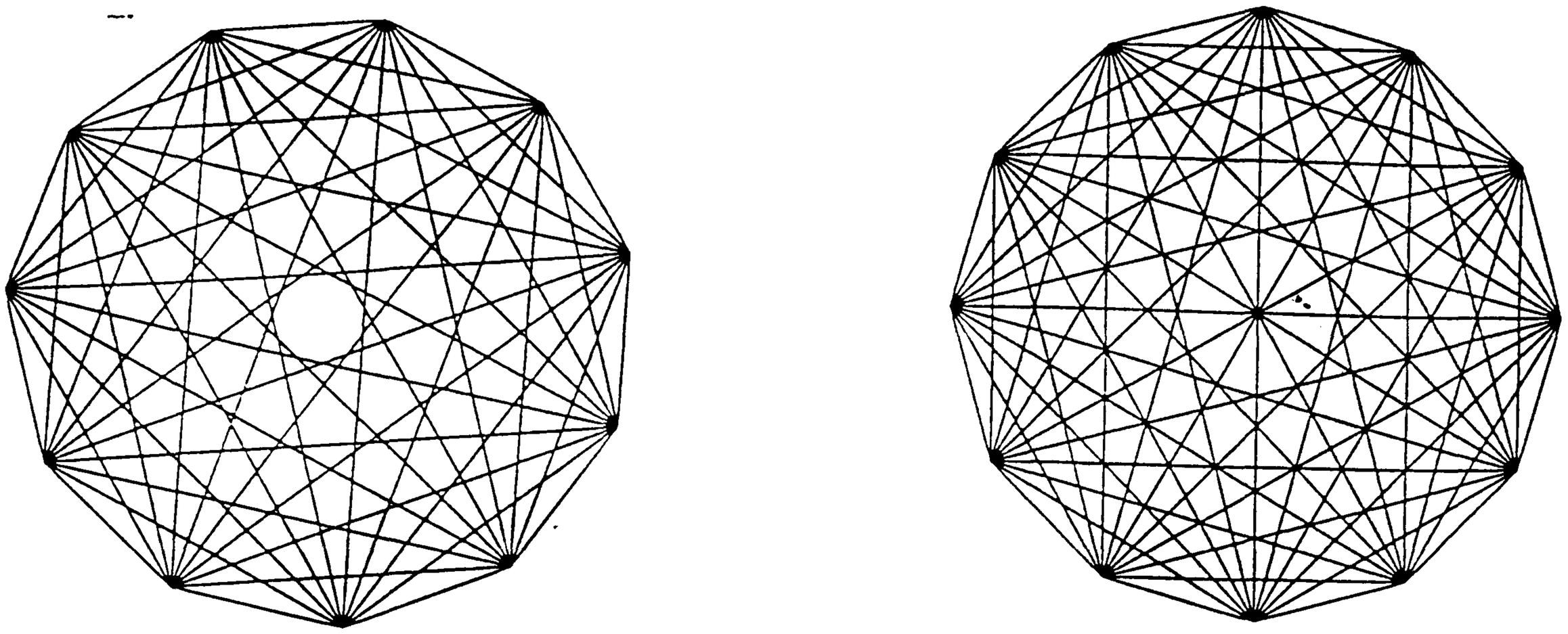

Figure 2.5: The canonical invariant region for $n = 11$ and 12. the complete graphs represent all convex linear combinations of ϕ_1 up to ϕ_n. Each vertex represents an in-phase solution. (The in-phase solution can be approached in n different ways from the interior of the canonical region.) These pictures are the projection of the n-dimensional simplex onto the plane.

The points Φ_j correspond to the n different ways a point can approach the in-phase solution while staying in the interior of the canonical invariant region.

Recall that a convex linear combination of vectors Φ_j is of the form:

$$\Theta = \Sigma\lambda_j\Phi_j, \text{ where } 0 \leq \lambda_j \leq 1 \text{ and } \Sigma\lambda_j = 1.$$

and the convex hull of the vectors Φ_j is the set of all possible convex combinations.

Lemma 2.6.4 *The closure of the canonical invariant region is the convex hull of the points* $\{\Phi_i\}$.

Proof. By construction, the convex combinations Θ of the Φ_i's have the form

$$\{(\theta, \theta + 2\pi\lambda_1, \theta + 2\pi(\lambda_1 + \lambda_2), \cdots, \theta + 2\pi(\lambda_1 + \lambda_2 + \cdots + \lambda_n - 1))\}$$

with all of the $\lambda_i \geq 0$ and $\Sigma\lambda_i = 1$. Thus for any point in the canonical invariant region we can set $2\pi\lambda_i = \theta_i - \theta_{i-1}$ and $2\pi\lambda_n = \theta_1 + 2\pi - \theta_n$. □

These properties allow us to give a graphical method of representing the boundaries of the canonical invariant region.

We draw n points equally spaced around a circle, corresponding to the Φ_j in order and construct the complete (fully connected) graph between these n points. We refer to this as the *isotropy mandala.* See figure 2.5.

Any complete subgraph on $l \leq n$ of these points, say

$$\{\Phi_j : j \in I \text{ a subset of } \{1 \cdots n\}, |I| = l\}$$

represents the fixed point space:

$$\{\Sigma\lambda_j\Phi_j + \theta\mathbf{1} : j \in I, \Lambda \in [0,1]^n, \Sigma\lambda_j = 1, \theta \in \mathbf{T}\}.$$

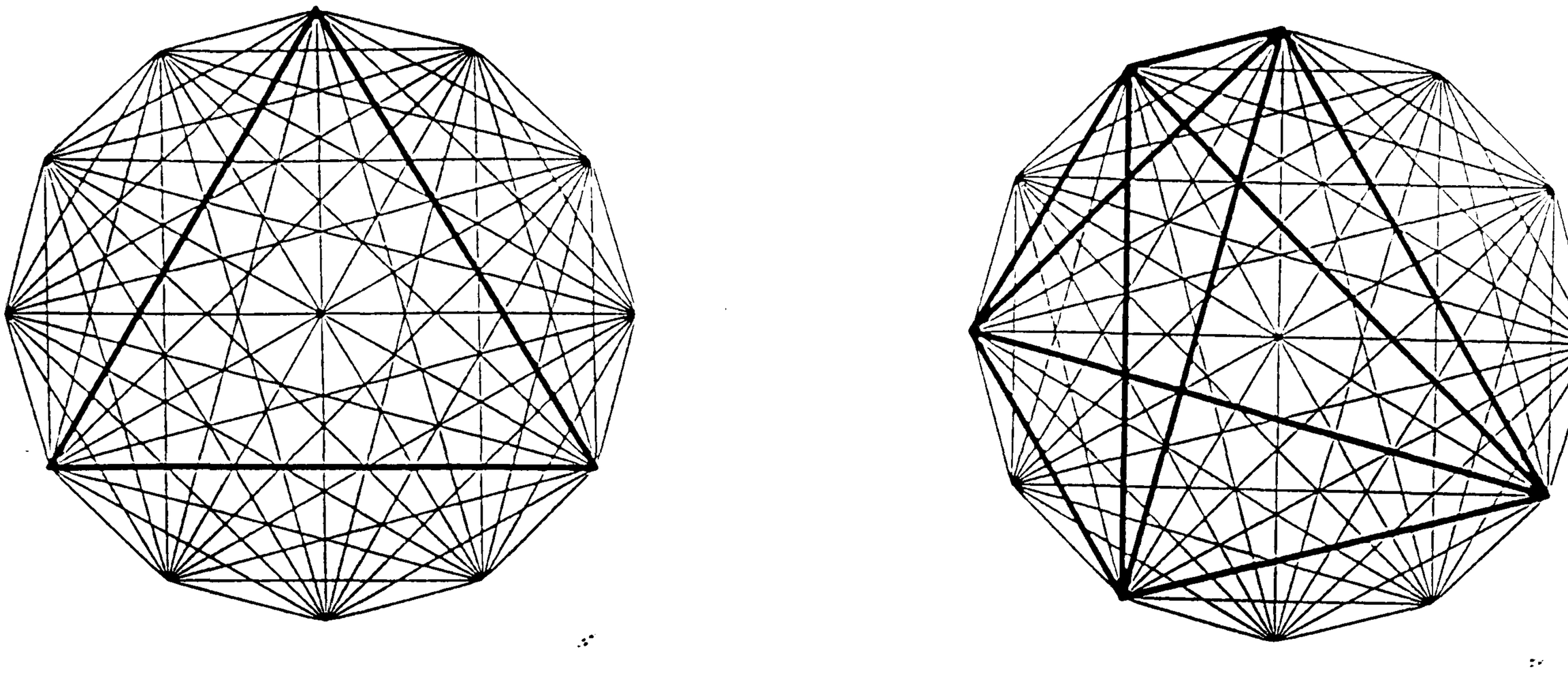

Figure 2.6: The graph representation of fix($(\mathbf{S}_4)^3$) and fix($\mathbf{S}_4 \times \mathbf{S}_3 \times \mathbf{S}_2 \times \mathbf{S}_2 \times \mathbf{S}_1$) for $n = 12$ oscillators. These spaces are given by convex linear combinations of 3 and 5 of the Φ_j, respectively. Thus, there are jumps in the phase around the circle.

Generic points in this convex hull of vectors $\{\Phi_i : i \in I\}$ have isotropy in the conjugacy class $\Sigma_{\mathbf{k},1}$ where the partition $\mathbf{k}$ is at the elements in I.

Examples. A line segment connecting Φ_2 with Φ_5 with $n = 7$ represents the two dimensional space in $\mathbf{T}^n$

$$\{(\theta, \theta, 2\pi\lambda + \theta, 2\pi\lambda + \theta, 2\pi\lambda + \theta, 2\pi + \theta, 2\pi + \theta) : \lambda \in [0, 1]\}$$

corresponding to the isotropy subgroup $\mathbf{S}_4 \times \mathbf{S}_3$. (Note that the last coordinate 'wraps around' to the first on losing 2π from everything.)

Figure 2.6 shows fix($(\mathbf{S}_4)^3$) and fix($\mathbf{S}_4 \times \mathbf{S}_3 \times \mathbf{S}_2 \times \mathbf{S}_2 \times \mathbf{S}_1$) for $n = 12$ oscillators.

Lemma 2.6.5 *If a complete subgraph M of the graph representing the canonical invariant region has symmetry $\mathbf{Z}_m$ for some m (which must divide n), then the region represented by M contains a space of dimension $|M|/m$ with $\mathbf{Z}_m$ temporal symmetry.*

Proof. Suppose that M is a set of pm points $\{\Phi_i : i \in I\}$ invariant under the m-cycle $\sigma = (1, \ldots, n)^k$ ($km = n$, $p \in \{1 \cdots k\}$) acting on the indices of the Φ_i. Then if we set $\lambda_i = \lambda_j$ for $i = j \bmod m$ and also satisfy $\Sigma\lambda_i = 1$, we get that the points

$$\sum_{\Phi \in M} \lambda_j \Phi_j$$

are invariant on $\mathbf{T}^{n-1}$ under σ. This gives us fixed point spaces of dimension p. □

Examples. Let $n = 4$, $m = 2$ and M be the diagonal line from Φ_1 to Φ_3. M corresponds to the space fix($\mathbf{S}_2 \times \mathbf{S}_2$). The midpoint of fix($\mathbf{S}_2 \times \mathbf{S}_2$) is $(\theta, \theta, \pi + \theta, \pi + \theta)$, which has $\Sigma = (\mathbf{S}_2)^2 \times \mathbf{Z}_2$. The $\mathbf{Z}_2$ comes about because of the invariance of the point under the permutation (13)(24) .

With $n = 6$, the triangle connecting Φ_1, Φ_3 and Φ_5 representing the space

$$\{(\theta, \theta, 2\pi\lambda + \theta, 2\pi\lambda + \theta, 2\pi\mu + \theta, 2\pi\mu + \theta) : (\lambda, \mu) \in [0,1]^2\}$$

with isotropy $(\mathbf{S}_2)^3$ has threefold symmetry about the centre of the triangle, and this gives us the $(\mathbf{S}_2)^3 \times \mathbf{Z}_3$ symmetry of its centre:

$$(0, 0, 2\pi/3, 2\pi/3, 4\pi/3, 4\pi/3).$$

2.6.2 The canonical invariant region for symmetry $\Gamma \neq \mathbf{S}_n$

All the above only applies to $\mathbf{S}_n$ (fully symmetric) systems. If we look at oscillator systems with symmetry $\Gamma < \mathbf{S}_n$, we have to look the whole phase space; any invariant regions must be larger than the canonical invariant region, and those isotropy subspaces from the isotropy mandala left distinct from those of higher dimension in which they are embedded, are preserved. Thus we can think of the isotropy structure of the $\Gamma \times \mathbf{T}^1$ equivariant system as a stripped-down version of that for $\mathbf{S}_n \times \mathbf{T}^1$. We formalise this in the following lemma:

Lemma 2.6.6 *The fixed point subspaces in* $\mathbf{T}^n$ *of* $\Sigma \times \mathbf{T}^1$ *correspond to those of* $G \cong \Sigma_{\mathbf{k},m} < \mathbf{S}_n \times \mathbf{T}^1$ *if and only if* $G \cap (\Sigma \times \mathbf{T}^1) \not\cong K \cap (\Sigma \times \mathbf{T}^1)$ *for a proper isotropy subgroups* $K < G$ *of* $\mathbf{S}_n$.

Proof. Using theorem 2.4.2, we know that $G \cap (\Sigma \times \mathbf{T}^1)$ is an isotropy subgroup of $\Sigma \times \mathbf{T}^1$. If it is distinct from all $K \cap (\Sigma \times \mathbf{T}^1)$ with $K < G$ as described above, we have $\mathrm{fix}(G \cap (\Sigma \times \mathbf{T}^1)) = \mathrm{fix}(G)$. □

Remark. The phase space has a symmetry forced in-phase solution if and only if it is symmetric under a transitive subgroup Γ of $\mathbf{S}_n$.

2.7 Pairwise coupling and degenerate decoupling

It has been noted by several authors studying coupled oscillators [2, 45, 123, 3] that with the presence of symmetry in each oscillator, there are seen to be regions in the phase space filled with limit cycles with more than one zero Floquet exponent and where the flow factorises into a product of a flows, even when the coupling is strong. This can result from cases of what we define as 'pairwise coupling' and internal symmetries of the system. We also show that an assumption of pairwise coupling restrict the possible symmetry group allowed in an identical oscillator network.

We find this phenomena in both the averaged system on the n-torus and also in the original system in X^n, but will confine ourselves mostly to the former case.

Definition 2.7.1 *An averaged system of coupled oscillators is* pairwise coupled *if it can be written in the form*

$$\dot{\theta}_j = 1 + \epsilon \sum_{i \neq j} G_j^i(\theta_i - \theta_j, \lambda).$$

This sort of coupling will always arise in the case of diffusive coupling, linear coupling or nearest neighbour coupling, where the phase equations are of the form:

$$\dot{\theta}_i = 1 + \epsilon\{F(\theta_{i+1}, \theta_i) + G(\theta_{i-1}, \theta_i)\}.$$

but is not dependent on this being so.

Example. All $\mathbf{S}_n \times \mathbf{T}^1$ equivariant pairwise coupled vector fields can be written in the form:

$$\dot{\theta}_i = 1 + \epsilon \sum_{i \neq j} G(\theta_j - \theta_i)$$

and thus the dynamics are governed by the function:

$$G : \mathbf{T} \to \mathbf{R}.$$

The only constraint on G is that it must be periodic with period 2π . This allows us to investigate the bifurcation structure of $\mathbf{S}_n \times \mathbf{T}^1$ equivariant vector fields by examining conditions on G.

Definition 2.7.2 *The set* $\{G_j^i : \mathbf{T} \to \mathbf{R}$ *where* $i \neq j\}$ *defined above are called the* pairwise coupling functions *or p.c.f.'s.*

N.B. We can choose the functions G_i^i to be all identically zero by rescaling time. This is because they are only functions of λ. Thus we only need consider the G_j^i where $i \neq j$.

Lemma 2.7.1 *The number of distinct coupling functions is a constant dependent only on the symmetry group* Γ *considered and is equal to the number of orbits in* $\{2, \cdots, n\}$ *under the action of* $Stab_\Gamma(\{1\})$.

Recall that the stabiliser, $Stab_\Gamma(S)$ of a subset S of $\{1, \cdots, n\}$ is the subgroup of Γ that fixes S. □

Examples. $\mathbf{S}_n$ requires only one pairwise coupling function. $\mathbf{Z}_n$ requires $n-1$ p.c.f.s (The maximum number for Γ transitive). $\mathbf{D}_n$ requires $[n/2]$ p.c.f.s.

2.7.1 Allowable symmetries

If Γ is transitive, the number of distinct p.c.f.'s is at most $n-1$, because by knowing the G_j^1, we can find all others by using symmetry.

In some sense, the number of p.c.f.s gives a measure of by how much the group Γ fails to be doubly transitive. (Recall that Γ is doubly transitive if for all $a_1 \neq a_2$ and $b_1 \neq b_2$, there exists a $\sigma \in \Gamma$ such that $\sigma(a_i) = b_i$.)

If the group is doubly transitive and pairwise coupled, it must have just one p.c.f., and must therefore have full $\mathbf{S}_n$ symmetry. Thus, we cannot have some subgroups for symmetry groups of an oscillator network if there is pairwise coupling. For three-way coupling, it is however possible to have doubly transitive groups that are not $\mathbf{S}_n$. (Recall that $\mathbf{A}_n$ is the alternating group of even permutations in $\mathbf{S}_n$; $\mathbf{A}_4$ is the group of symmetries of a tetrahedron excluding reflections.)

Lemma 2.7.2 *The following coupled oscillator system has* $\mathbf{A}_4$ *symmetry of the network*

$$\begin{aligned} \dot{\theta}_1 \;=\; & 1 + f(\theta_2)g(\theta_3) + f(\theta_3)g(\theta_4) + f(\theta_4)g(\theta_2) \\ & - f(\theta_2)g(\theta_4) - f(\theta_4)g(\theta_3) - f(\theta_3)g(\theta_2) \end{aligned} \tag{2.9}$$

for some functions $f \not\equiv g$, *with the other equations generated by the permutations* $(1,2)(3,4)$ *and* $(1,3)(2,4)$.

Proof The system is three-way coupled, and the equation is invariant under all even permutations (in particular, the equation for θ_1 is invariant under the $(2,3,4)$), but not under odd.□

We now show how internal symmetries in the structure of the vector field in this case can lead to degenerate decoupling.

2.7.2 Decoupling from oscillator internal symmetries

Definition 2.7.3 *A periodic function F with (minimal) period T has* m-fold internal symmetry *if*

$$\sum_{k=1}^{m} F(\phi + kT/m) = 0 \text{ for all } \phi \in \mathbf{R}$$

Note that the function $F(\phi) = \sum_{-\infty}^{\infty} c_r e^{ir\phi}$ has m-fold internal symmetry iff $c_n = 0$ for all $n = 0 \bmod m$. Thus, $\sin\phi$ has m-fold internal symmetry for all $m > 1$, and an degree k polynomial in $\cos\phi$ and $\sin\phi$, $F(\phi) = \sum_{-k}^{k} c_n e^{ir\phi}$ will have m-fold internal symmetry at least for m equal to multiples of $\mathrm{lcm}(1,\cdots,k)$.

Definition 2.7.4 *An averaged network of oscillators has* m-fold internal symmetry *if it is pairwise coupled and each coupling function has m-fold internal symmetry.*

Below are examples of some theorems where internal symmetry causes decoupling into groups of oscillators:

Theorem 2.7.1 *If we have an $\mathbf{S}_n \times \mathbf{T}^1$ equivariant pairwise coupled flow on $\mathbf{T}^n$ and the network has m-fold internal symmetry where $mk = n$, then all the fixed point subspaces of the isotropy subgroups $\Sigma_{(1,\cdots,1),m} \cong \mathbf{Z}_m$ will consist purely of limit cycles of identical period.*

Proof. Suppose we have a point in such a fixed point subspace for some $mk = n$. Then $dim(\mathrm{fix}(\Gamma \times \mathbf{Z}_m)) = k$, and we consider the space:

$$\{\theta_1, \theta_1 + 2\pi/m, \cdots, \theta_1 + 2\pi(m-1)/m, \theta_2, \cdots, \cdots, \theta_k, \cdots, \theta_k + 2\pi(m-1)/m\}$$

defined by k phases up to addition of the $\mathbf{T}$ action. Then for any i, j:

$$\begin{aligned}\dot{\theta}_1 &= 1 + \epsilon\{f(2\pi/m) + \cdots + f(2\pi(m-1)/m) \\ &\quad + f(\theta_2 - \theta_1) + \cdots + f(\theta_2 - \theta_1 + 2\pi(m-1)/m) + \cdots\} \\ &= 1 - \epsilon f(0)\end{aligned}$$

by using the definition of m-fold internal symmetry k times. As this is independent of the fact we are looking at θ_1, this implies that $\dot{\theta}_i$ is a constant independent of i, and so there is no change in the relative phases. □

Example. We do an explicit calculation for $\mathbf{S}_4$ with two-fold internal symmetry by considering the $\mathbf{Z}_2$ generated by $((12)(34), -1)$. This has a two dimensional fixed point subspace in $\mathbf{T}^n$:

$$\mathrm{fix}(\mathbf{Z}_2) = \{(\phi, \theta, \phi + \pi, \theta + \pi)\}.$$

Thus:

$$\begin{aligned}(\dot{\phi}-\dot{\theta}) &= 1+\epsilon\{G(\theta-\phi)+G(\phi+\pi-\phi)+G(\theta+\pi-\phi)\} \\ &\quad -1-\epsilon\{G(\phi-\theta)+G(\phi+\pi-\theta)+G(\theta+\pi-\theta)\} \\ &= \epsilon\{G(\theta-\phi)+G(\theta+\phi+\pi)-(G(\phi-\theta)+G(\phi-\theta+\pi))\} \\ &= 0.\end{aligned}$$

because the 2-fold internal symmetry gives us

$$G(\phi)+G(\phi+\pi)=0$$

for all ϕ.

Thus all points in this space have $\theta-\phi$ constant for all time and so are fixed in $\mathbf{T}^{n-1}$. This is investigated experimentally in chapter 4

Theorem 2.7.2 *In the case of* $\mathbf{D}_{4m}$ *system with two-fold internal symmetry and pairwise coupling, the isotropy subgroups* $\mathbf{Z}_{2m}(m)$ *consist only of limit cycles of identical period. This is analogous to the result obtained by Alexander and Auchmuty [2], in the weak coupling limit, but does not require the hypothesis of being close to Hopf bifurcation.*

Proof. A pairwise coupled oscillator system with $\mathbf{D}_{4m}$ can be written in terms of $2m$ PCFs as follows:

$$\dot{\theta}_i = 1+\epsilon\left\{G_0(0)+\sum_{j=1}^{2m-1}[G_j(\theta_{i+j}-\theta_i)+G_j(\theta_{i-j}-\theta_i)]+G_{2m}(\theta_{i+2m}-\theta_i)\right\}$$

where $\theta_i=\theta_j$ if $i=j \pmod{4m}$. If we write the points in the fixed point subspace as

$$(\theta_1,\theta_2,\theta_1+\pi,\theta_2+\pi,\cdots)$$

The ODE restricted to the 2-torus fix($\mathbf{Z}_{2m}(m)$) is

$$\dot{\theta}_1 = 1+\epsilon\left\{\begin{array}{l} G_0(0)+G_1(\theta_2-\theta_1)+G_1(\theta_2+\pi-\theta_1)+G_2(\pi)+G_2(\pi) \\ +G_3(\theta_2+\pi-\theta_1)+G_3(\theta_2-\theta_1)+G_4(0)+G_4(0)+\cdots+G_{2m}(\pi)\end{array}\right\}$$

$$\dot{\theta}_2 = 1+\epsilon\left\{\begin{array}{l} G_0(0)+G_1(\theta_1-\theta_2)+G_1(\theta_1+\pi-\theta_2)+G_2(\pi)+G_2(\pi) \\ +G_3(\theta_1-\theta_2)+G_3(\theta_1+\pi-\theta_2)+G_4(0)+G_4(0)+\cdots+G_{2m}(\pi)\end{array}\right\}$$

The 2-fold internal symmetry of the G_j causes the terms with odd j to cancel, and we are left with

$$\dot{\theta}_1=\dot{\theta}_2 = 1+\epsilon\left[G_0(0)+2G_2(\pi)+2G_4(0)+\cdots+2G_{2m-2}(0)+G_{2m}(\pi)\right]=\text{constant}.$$

Thus the dynamics in this space consists of limit cycles of identical period. □

2.7.3 Pairwise coupling in the full equations

We define the original network to be pairwise coupled if it can be written as:

$$\dot{x}_i = f(x_i) + \epsilon \sum_{i \neq j} g_i^j(x_j, x_i, \lambda, \epsilon)$$

for all $\mathbf{x}, \lambda$ and ϵ (cf. $\mathbf{x} = \mathbf{f}_\epsilon(\mathbf{x}, \lambda)$ in definition 2.2.2).

This is not a general extension of the case $\epsilon = 0$, because we have neglected any terms in the ith equation of the form $x_k x_j$ where $i \neq j \neq k$, etc.

Pairwise coupling of the averaged equations must come from this sort of network, but due to the distortion of the coordinates on the torus for $\epsilon \neq 0$, it is not clear that all networks of this form must give rise to pairwise coupling in the averaged equations, and thus this is a wider definition.

We can recover all the results above in this more general case by allowing m-fold internal symmetry to be some $\mathbf{Z}_m$ symmetry of the equations generated by ρ, a rigid rotation of the phase space X of the individual oscillators (cf Alexander & Fiedler [3]) who look at functions equivariant under some continuous linear transformations of the phase space). If the functions f and g_j^i are equivariant under ρ acting on x_j and x_i and the original hyperbolic limit cycle $\gamma(t)$ of f has this $\mathbf{Z}_m$ symmetry, then the symmetry can only be broken by the n-torus undergoing loss of stability. Thus we can preserve the symmetry of the whole invariant n-torus for small enough ϵ.

We use the fact that $\sum_{k=0}^{m-1} \rho^k(f) = 0$ for any $f : X \to X$ because ρ is a rigid rotation, and thus any state where the system has m-fold phase shifts in one of its symmetry subspaces, we will get decoupling in the same cases as those given above.

As pointed out by Alexander & Fiedler [3], these decoupling phenomena are codimension infinity in the set of vector fields with $\Gamma \times \mathbf{Z}_m$ symmetry, and rely on one picking a vector field with a specific structure of pairwise (which includes linear) coupling.

2.7.4 Other mechanisms for decoupling

Other mechanisms are available to us for providing decoupling, namely time reversibility or Hamiltonian structure in the averaged equations. Note that the original equations cannot be time reversible or Hamiltonian, as we hypothesised the existence of attracting limit cycles. However, it is possible to conceive of examples which display time reversibility in the average in the invariant n-torus, and we would expect these to provide us with decoupling phenomena separate from the above mechanism. For example, in Tsang et al. [127], we see that reversibility gives rise to centre-like behaviour at the rotating waves ('splay states').

Chapter 3

Generic Behaviour of Weakly Coupled Oscillators with $\mathbf{S}_n$ Symmetry

This chapter discusses the application of the theory presented in chapter 2 to study the stability of periodic orbits forced by the symmetry in $\mathbf{S}_n$ networks with weak coupling, and the existence of structurally stable heteroclinic cycles in certain situations. In particular, we focus on small numbers of oscillators (three or four).

Sections of this work have appeared in [18] and [17]. Chapter 4 reports the results of some experiments on electronic oscillators and relates them to the theory in this chapter.

3.1 Generic behaviour for weakly coupled systems

In this section we will apply the results obtained in chapter 2 to gain some insight into the dynamics and bifurcation of systems of n indistinguishable oscillators with full permutation symmetry $\mathbf{S}_n$.

We shall consider the stability of all the fixed points on $\mathbf{T}^{n-1}$ which are forced by the symmetry and exist for all $\mathbf{S}_n$. These have isotropy of the form $(\mathbf{S}_k)^m \times \mathbf{Z}_m$ where $km = n$.

3.1.1 The stability of the in-phase solution ($\mathbf{S}_n$)

The full symmetry of $\mathbf{S}_n$ must commute with any linear part of a vector field around the in-phase solution $(1, \cdots, 1)$. This forces the linear part of the vector field at the point to be simply:

$$\begin{pmatrix} \lambda & & 0 \\ & \ddots & \\ 0 & & \lambda \end{pmatrix}$$

with $\lambda \in \mathbf{R}$, and so this point is a stable ($\lambda < 0$) or unstable ($\lambda > 0$) node. Note that this is equivalent to saying that $\mathbf{S}_n$ acts irreducibly on $\mathbf{T}^{n-1}$.

At bifurcation, there is a degenerate spectrum of $n-1$ identical eigenvalues passing through zero. See Field & Richardson [47] for a detailed discussion of this case. Thus the only codimension one bifurcation of the in-phase solution is the $\mathbf{S}_n$ transcritical bifurcation. On one dimensional subspaces with $\mathbf{Z}_2$ symmetry, this bifurcation will look like a pitchfork, and on those without, it will look like a transcritical bifurcation.

This is because the vector field has a quadratic equivariant which will force the direction of the local branching.

3.1.2 The stability of the rotating waves $\mathbf{Z}_n$

Looking at the rotating waves $\mathbf{Z}_n$, these must have a local vector field which commutes with a subgroup of $\mathbf{S}_n$ corresponding to a cyclic group of order n, and such that the action is given by cyclically permuting the coordinates according to some permutation of the n coordinates.

For the fixed point corresponding to the oscillators firing in the order $1, 2, \cdots, n$, the eigenvalues of this rotation are the set $\{\omega, \omega^2, \cdots, \omega^{n-1}\}$ and this splits the action into $m-1$ different 2-dimensional irreducible rotations where $m = [n/2]$. If n is even, there is also one eigenvalue of -1 corresponding to a 1-dimensional flip (remember there are $n-1$ distinct eigenvalues at most!).

Considering linear parts of the vector field near the rotating wave, because these are forced to commute with the rotation matrix, they will generically have $m-1$ complex conjugate pairs of eigenvalues and if $n = 2m$, one real eigenvalue.

Thus the rotating $\mathbf{Z}_n$ points are generically stable, unstable or saddle spirals with at most one real eigenvalue. We summarise this result by saying that the linear part of the vector field near the rotating wave must be of the form (with suitable choice of basis and n even; if n is odd then disregard the eigenvalue ρ):

$$\begin{pmatrix} \begin{pmatrix} \rho_1 & \omega_1 \\ -\omega_1 & \rho_1 \end{pmatrix} & 0 & \cdots & 0 \\ 0 & \begin{pmatrix} \rho_2 & \omega_2 \\ -\omega_2 & \rho_2 \end{pmatrix} & \cdots & 0 \\ \vdots & \vdots & \ddots & \vdots \\ 0 & 0 & \cdots & \rho \end{pmatrix} \tag{3.1}$$

Codimension one bifurcations of this local vector field will lose stability in only one of the irreducible subspaces, and using this fact, we can see that the rotating wave must generically go unstable via a Hopf bifurcation if n is odd, but may undergo a Hopf or pitchfork bifurcations if n is even. Note that this is obtained by Golubitsky and Stewart [53] for the case of a $\mathbf{Z}_n$ ring of oscillators near Hopf bifurcation; here the natural action of $\mathbf{Z}_n$ on $\mathbf{T}^n$ gives a decomposition including irreducible representations of $\mathbf{Z}_m$ for all m dividing n.

Lemma 3.1.1 *There are* $[(n-1)/2]$ *possible codimension one bifurcations of the* $\mathbf{Z}_n$ *rotating wave in the system of* n *oscillators.* $[n/2]-1$ *of them are Hopf bifurcations and the other one (if* n *is even) is a pitchfork.*

Proof Consider the possible ways the irreducible subspaces of the linear part can go unstable.

□

The linear stability of the rotating waves is as follows: Set $\theta_i = \omega_0 t + 2\pi j/n + \delta\theta_i$. The solution to the linearised equations for the $\delta\theta_i$'s are;

$$\delta\theta_i(t) = \sum_{p=1}^{[n-1]/2} \{r_p \cos(\omega_p t + 2\pi jp/n + \xi_p) \exp(\rho_p t) + r(-1)^j exp(\rho t)\}$$

for the r_p, ξ_p and r constants dependent on the initial conditions. The last term is present if and only if n is even.

The reason that there can be a pitchfork bifurcation for n even is that there is the possibility of the oscillators grouping into two groups which alternate around the rotating wave. The $\mathbf{Z}_2$ symmetry of this arrangement causes the generic bifurcation here to be a pitchfork.

We can generalise this result for all the other one dimensional (in $\mathbf{T}^n$) fixed point subspaces in the following way:

3.1.3 The stability of the rotating blocks

The vector fields near the fixed points (in $\mathbf{T}^{n-1}$) corresponding to the isotropy subgroups $(\mathbf{S}_k)^m \times \mathbf{Z}_m$ have fixed point subspaces of the groups generated by one m-cycle acting by permuting m blocks of m/k oscillators along with all permutations in one block (recall section 2.4.1).

It can be shown that a fixed point with this isotropy has $m(k-1)$ equal real eigenvalues. The other $m-1$ eigenvalues have the same constraints as the $n-1$ eigenvalues of the rotating wave solution (see equation 3.1). Note that this result is consistent with the two special cases: The in-phase solution has $m=1$, $k=n$ and there are $n-1$ equal eigenvalues. The rotating wave has $m=n$, $k=1$.

3.1.4 Stability and pairwise coupling

Using the pairwise coupled systems discussed in section 2.7 allows an explicit derivation of expressions for the eigenvalues giving the stabilities of the periodic orbits above, in terms of properties of the single pairwise coupling function for $\mathbf{S}_n$. This is done in [18]; we omit it here to save space.

3.2 Three oscillators

In this section, we examine what the results from chapter 2 imply for a group of three identical weakly coupled indistinguishable oscillators, coupled such that they are equivariant under the action of $\mathbf{S}_3$.

3.2.1 The reduction to normal form

As discussed in chapter 2, since the flow is nearly linear on $\mathbf{T}^3$, we can construct an $\Gamma \times \mathbf{T}$ normal form, or equivalently, a global Poincaré return map on the two-torus $\mathbf{T}^2$ perpendicular to the $(1,1,1)$ direction in $\mathbf{T}^3$. When the coupling is weak, the Poincaré map is near-identity, and it can be approximated by an ordinary differential equation (ODE) which preserves most of the dynamics of the map. This suspension of the map is in fact the $\mathbf{S}_3 \times \mathbf{T}$ normal form.

We stress that this reduction of the problem to an ODE on $\mathbf{T}^2$ works even for strongly nonlinear relaxation oscillations. It is not necessary to consider the equation of the individual oscillators, other than parametrising them by a phase variable that is a deformation of the uncoupled phases. We parametrise one period of the ith oscillator ($i = 1, 2$ or 3) by the angle θ_i mod 2π, and scale time so that without coupling each oscillator satisfies $d\theta_i/dt = 1$. Weak coupling has the effect of producing an evolution equation for the system:

(3.2)
$$\dot{\theta}_1 = 1 + \epsilon f_1(\theta_1; \theta_2, \theta_3)$$

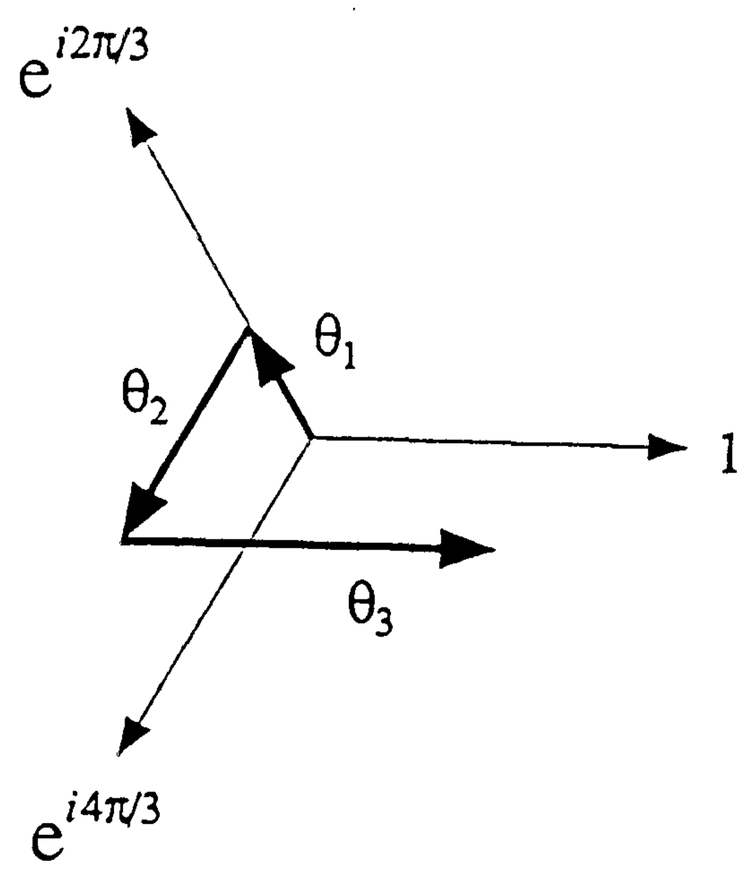

Figure 3.1: The construction of the complex angle representing the state of a three oscillator system on $\mathbf{T}^2 = \mathbf{T}^3/\mathbf{T}(1,1,1)$.

with cyclic permutation of the labels for the other two oscillators, where $f : \mathbf{T} \to \mathbf{R}$. The functions f_i also depends on ϵ , but there is an order-one limit as $\epsilon \to 0$, so we suppress this dependence.

We define

$$\Theta = \frac{1}{3}(\theta_1 + \theta_2 + \theta_3)$$

and

$$\phi = \omega\theta_1 + \omega^2\theta_2 + \theta_3$$

(So that Θ is invariant and ϕ is equivariant under the permutations in Γ.) The general ODE on $\mathbf{T}^3$ can then be written in these coordinates to give:

$$\dot{\Theta} = 1 + \epsilon g(\Theta, \phi), \dot{\phi} = \epsilon h(\Theta, \phi)$$

where g (resp. h) is invariant (resp. equivariant) under the action of Γ on (Θ, ϕ). For small enough ϵ, $d\Theta/dt > 0$ everywhere, and there is a well-defined Poincaré map which gives the change of ϕ as Θ goes from 0 to 1:

$$P : \mathbf{T}^2 \to \mathbf{T}^2 \tag{3.3}$$

This near identity Poincaré map can be approximated, to any power in ϵ , by an ODE [8, 20], which we can obtain by averaging the ODE in $\mathbf{T}^3$ over the angle Θ:

The averaged equation on the two-torus is a global normal form for three weakly coupled oscillators. Being global, there can be no truncation of the normal form, analogous to the Taylor polynomials used in local bifurcations, which controls the dynamics. We expect that a truncation to a few low-order Fourier modes is a good approximation, but we cannot rigorously justify this. (Adding a single Fourier mode with sufficiently large amplitude will change the dynamics qualitatively.)

3.2.2 The action of $\mathbf{S}_3$

Considering possible groups $\Gamma < \mathbf{S}_3$ acting on the three oscillators, the only transitive groups are $\mathbf{Z}_3$ and $\mathbf{D}_3 \cong \mathbf{S}_3$. We shall concentrate purely on the latter group whose

Name	$\mathbf{T}^3$	$\mathbf{T}^2$ Generators	$\mathbf{T}^2$ dim	
in-phase	$\theta_1 = \theta_2\theta_3$	$\phi = 0$	$\mathbf{S}_3 = \{\phi \to \omega\phi, \phi \to \bar{\phi}\}$	0
rotating	$\theta_{i+1}(t) = \theta_i(t + T/3)$	$\phi = \exp(i\pi/6)/\sqrt{3}$	$\mathbf{Z}_3 = \{\phi \to \omega\phi + 1\}$	0
2-in-phase	$\theta_1 = \theta_2 \neq \theta_3$	$\phi \in \mathbf{R}$	$\mathbf{S}_2 = \{\phi \to \bar{\phi}\}$	1

Table 3.1: The symmetries of solutions in $\mathbf{T}^2$ and $\mathbf{T}^3$. Fixed points in $\mathbf{T}^2$ correspond to oscillations in $\mathbf{T}^3$ with period close to 2π. A Hopf bifurcation of the rotating wave gives birth to a torus in $\mathbf{T}^3$ (a limit cycle in $\mathbf{T}^2$), which is taken to itself by the $\mathbf{Z}_3$ symmetry.

only nontrivial irreducible representation is two dimensional, and isomorphic to the symmetries of an equilateral triangle on the plane, allowing reflections. By defining $\mathbf{S}_3$ generated by:

$$\begin{aligned} \kappa &= (12) \\ \rho &= (123). \end{aligned}$$

this induces an action on $\mathbf{C}$, where $\omega = \exp(2i\pi/3)$, of

$$\begin{aligned} \kappa(w) &= \bar{w} \\ \rho(w) &= \omega w. \end{aligned}$$

Because of the symmetry ρ, all the f_i defined above must be identical, say f, and this f satisfies:

$$f(\theta_1; \theta_2, \theta_3) = f(\theta_1; \theta_3, \theta_2)$$

because the permutation $\kappa\rho$ implies that f is symmetric under interchange of the last two arguments. While it is easy to guarantee that such a system on $\mathbf{T}^3$ exists, it is extremely difficult to derive them from the original equations in, say $\mathbf{R}^6$. Alexander and Fiedler [3] have managed to derive the phase equations for 4 oscillators coupled in a ring to second order in ϵ , for a system which is amenable to analysis by averaging.

3.2.3 Isotropy structure for $\mathbf{S}_3$

Figure 3.2 shows the triangular lattice with $\mathbf{S}_3$ symmetry. The isotropy classes are listed in table 3.1 and illustrated in figure 3.2.

The Poincaré map does not satisfy the same symmetry relations as the averaged flow. The $\mathbf{S}_3$ equivariance about $\phi = 0$ holds for P, but the periodicity of the function is different (cf [124] with $\mathbf{Z}_2$ symmetry). The translations are generated by

$$P(\phi) = P(\phi + \omega^2 - 1) = P(\phi + \omega - 1).$$

This is because P is unchanged by those translations in $\mathbf{T}^3$ which leave the section Θ unchanged. These are generated by $(\theta_1, \theta_2, \theta_3) \mapsto (\theta_1 + 1, \theta_2, \theta_3 - 1)$ and $(\theta_1, \theta_2, \theta_3) \mapsto (\theta_1, \theta_2 + 1, \theta_3 - 1)$, which leads to the translational symmetries of P.

3.2.4 The canonical fundamental region

The canonical fundamental region is a triangle bounded by the 2-in-phase lines. On the torus $\mathbf{T}^2$ this corresponds to one half of a generating parallelogram, and the vector field is generated by knowing it in one sixth $(1/|\mathbf{S}_3|)$ of the generating parallelogram and

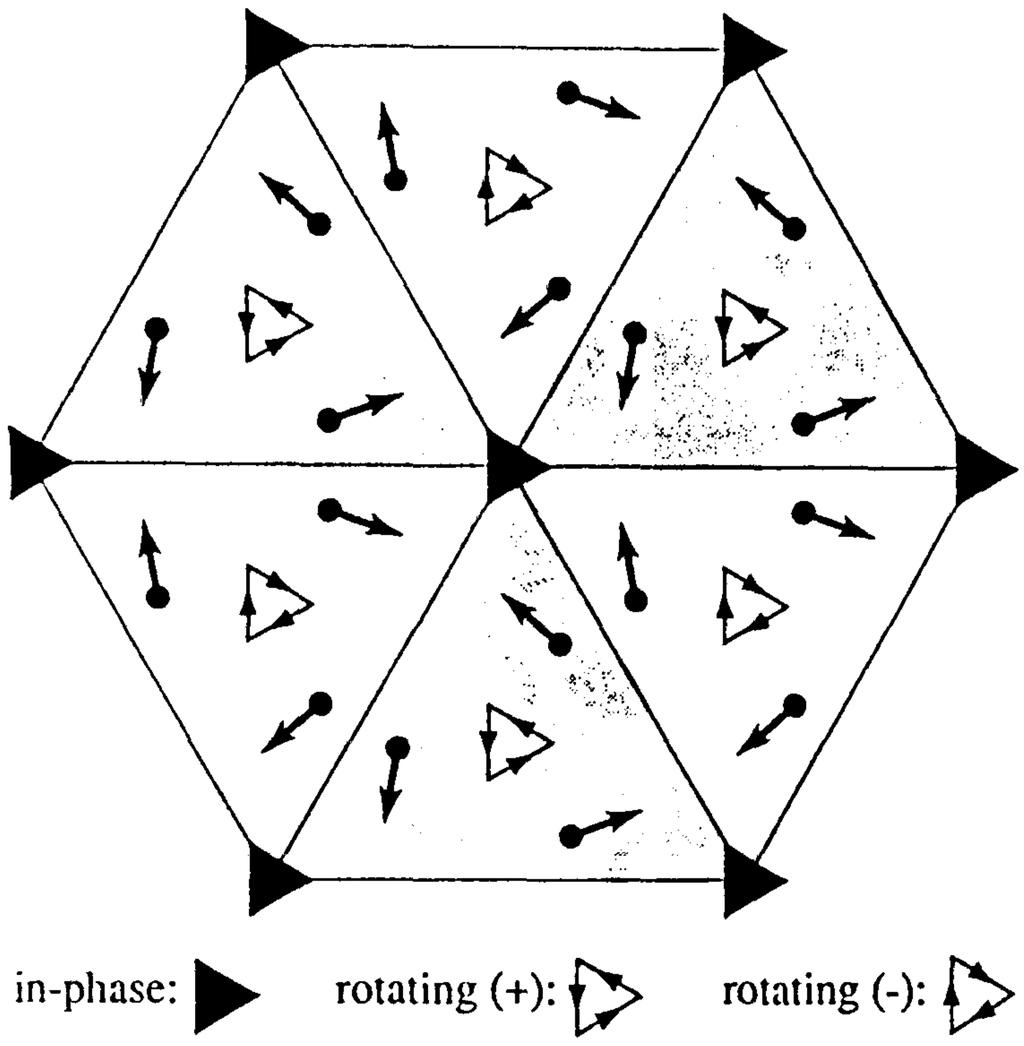

Figure 3.2:
The triangular lattice representation of T^2 in the complex ϕ plane. The in-phase oscillation is indicated by the solid triangle, which is on all lattice points equivalent to $\phi = 0$. The oscillators fire (i.e. reach $\theta = 0$) at equally spaced intervals when the system is in one of the two rotating wave states, indicated by the small triangles with directed edges. Fixed points on the lines of reflectional symmetry are the 2-in-phase oscillations, in which the two oscillators fire together. the circles indicate a typical point and the attached arrows show the drift caused by the coupling of the oscillators. The lines of reflectional symmetry separate the plane into dynamically invariant triangles. The order in which the oscillators fire is ..., 1,2,3,1,2,3,... in the shaded triangles, and ...,3,2,1,3,2,1,... in the white triangles. Two of these invariant triangles form a fundamental region of the torus.

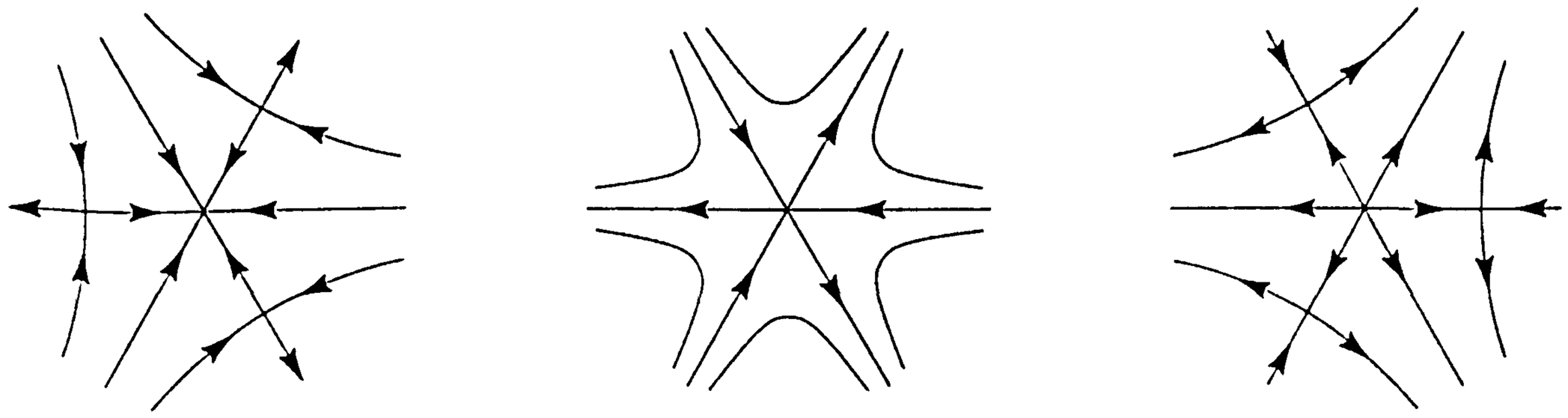

(a) (b) (c)

Figure 3.3:
The $\mathbf{S}_3$ transcritical bifurcation. (a) $\mu < 0$, (b) $\mu = 0$, (c) $\mu > 0$. As μ is varied, three 2-in-phase solutions pass through the in-phase solution. The 2-in-phase solutions are saddles before and after the bifurcation, while the in-phase solution changes from stable to unstable node.

looking at the orbit of the vector field under the action of $\mathbf{S}_3$. As noted in the previous section, there are certain points on the torus $\mathbf{T}^2$ which are forced by the symmetry to be fixed points of the flow F. They are the in-phase solution which is the only point fixed by the whole of $\mathbf{S}_3$, and two rotating wave solutions which are points fixed by $\mathbf{Z}_3$ symmetry. In addition, there is a web of dynamically invariant lines, on which $\theta_i = \theta_j$ for $i \neq j$. A solution to $\phi = 0$ on this line is called a 2-in-phase solution. These features are pictured in figure 3.2, and listed in table 3.1.

3.2.5 A generic bifurcations; the $\mathbf{S}_3$ transcritical

The local bifurcations of each of the solution types are constrained by the symmetry of the solution:

In-phase There are two equal, real, eigenvalues. When they cross through zero there is generically a $\mathbf{S}_3$ ($\sim \mathbf{D}_3$) transcritical bifurcation, [54] with the normal form

$$\dot{\phi} = \mu\phi + \bar{\phi}^2$$

with $\mu \in \mathbf{R}$ and bifurcation at $\mu = 0$. The phase portraits are shown in figure 3.3

Rotating These have two complex conjugate eigenvalues with generically non-zero imaginary parts. Thus the only generic bifurcations from such points are simple Hopf bifurcations.

3.2.6 The $\mathbf{S}_3$THB

There is an interesting global bifurcation shown in figure 3.4 allowed by the topology of the torus. We call this the $\mathbf{S}_3$ transcritical/homoclinic bifurcation ($\mathbf{S}_3$THB). At the bifurcation point there is a connection in the lattice between adjacent in-phase solutions, provided there are no other fixed points of the ODE on the invariant line.

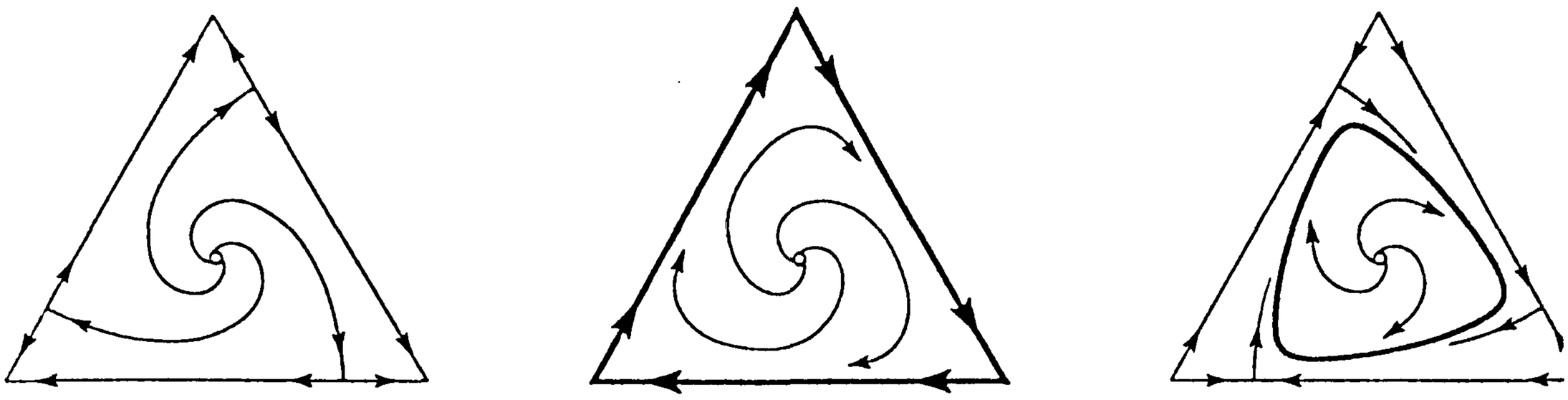

(a) (b) (c)

Figure 3.4:
The $\mathbf{S}_3$ transcritical/homoclinic bifurcation ($\mathbf{S}_3$THB): (a) $\mu < 0$, (b) $\mu = 0$, (c) $\mu > 0$. One dynamically invariant triangle is shown. the local behaviour near an in-phase solution (one of the vertices) is shown in figure 3.3 Simultaneous with the $\mathbf{S}_3$ transcritical bifurcation, there is a triangular heteroclinic connection between the three in-phase solutions. On the torus, the in-phase solutions are identified, thus we call this a homoclinic bifurcation. When the heteroclinic loop at $\mu = 0$ is stable, as shown here, there must be a stable limit cycle very close to the triangle for $0 < \mu \ll 1$.

In the torus, this is a homoclinic orbit, while in the lattice it is a heteroclinic loop. The homoclinic orbit is either attracting or repelling, unless there is a constant of the motion, as in a Hamiltonian system. If it is attracting, then there is a stable limit cycle on the side of the bifurcation where the in-phase solution is unstable. (This situation is shown in figure 3.3.) If, on the other hand, the heteroclinic loop is repelling, then an unstable periodic orbit co-exists with the stable in-phase solution. (This is obtained by time reversal of figure 3.3.)

3.2.7 Transit time near the $\mathbf{S}_3$THB

The stability of this homoclinic connection is very interesting, as unlike homoclinic connections without, or with $\mathbf{Z}_2$ symmetry, the stability is governed by the flow along the invariant sides of the triangle rather than being dominated by the flow near the fixed point.

Without symmetry, the typical homoclinic bifurcation of an ODE in the plane depending on a parameter μ [61]. Assume that when $\mu < 0$ there is a limit cycle which becomes homoclinic and disappears at $\mu = 0$. The ratio of the unstable to the stable eigenvalues, $\delta = \lambda_u/|\lambda_s|$ governs the behaviour. If $\delta < 1$ (resp. $\delta > 1$) then the limit cycle is stable (resp. unstable). The Floquet exponent of the limit cycle approaches the trace of Jacobian matrix of the fixed point, which equals $\lambda_s + \lambda_u$, as $\mu \to 0$, and the period of the limit cycles approaches infinity like μ^{-1}.

The $\mathbf{S}_3$ heteroclinic loop is more subtle than this. From the transcritical normal form it is clear that the in-phase solution has a double eigenvalue of μ, and the trace of the Jacobian matrix is 2μ. Thus the limit cycle is very weakly attracting or repelling,

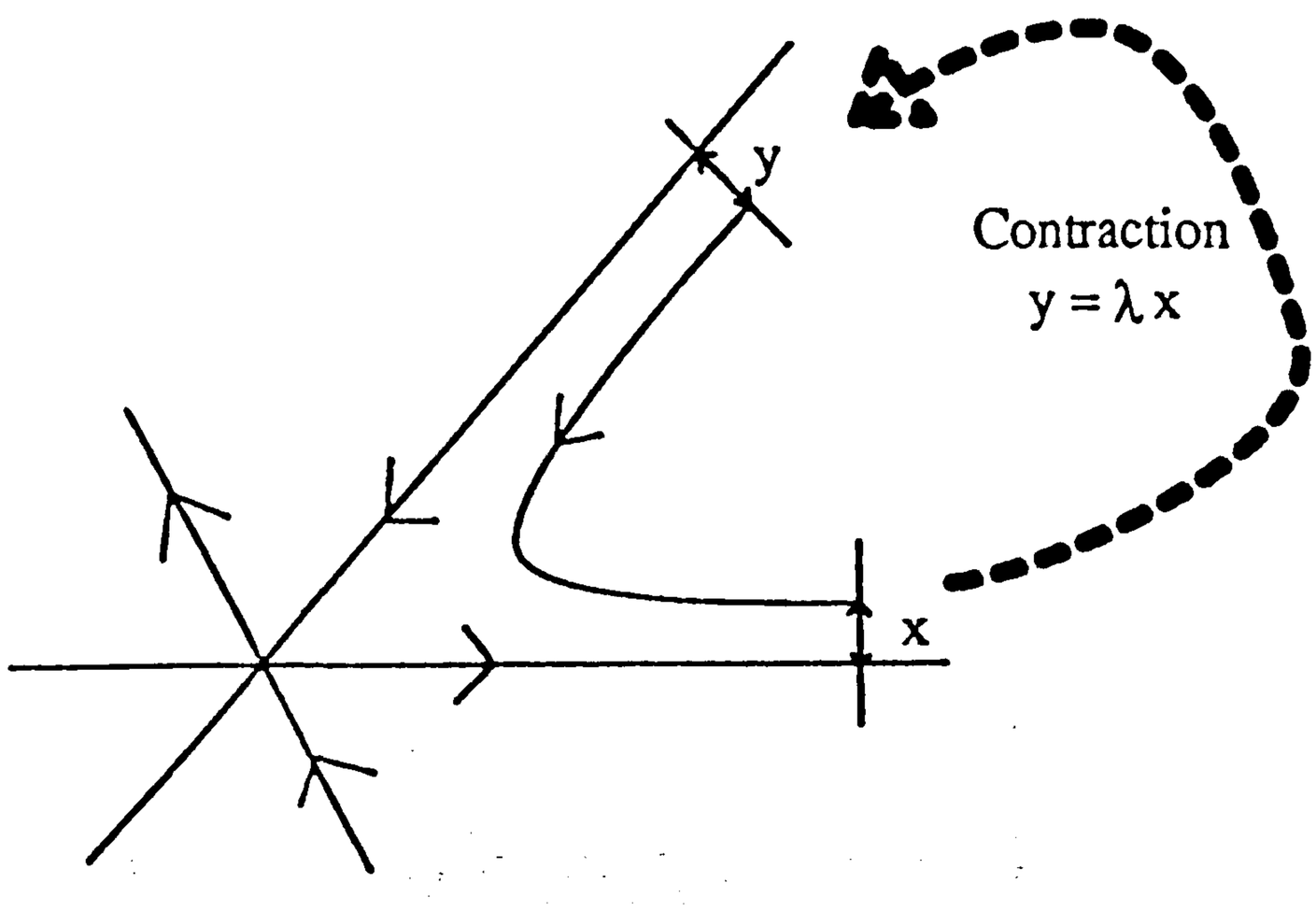

Figure 3.5: Approximating approach to the homoclinic orbit by using a linear contraction along the edges to reinject trajectories back into the corners.

and the stability is not dominated by the fixed point.

At the bifurcation point, the stability is dominated by the flow along the edges of the triangle; if we consider a trajectory approaching a stable $\mathbf{S_3}$THB by reinjecting to a neighbourhood of the fixed point after going through a linear contraction $x \mapsto \lambda x$ with $0 < \lambda < 1$ (see figure 3.5), as the linear part is zero, the local dynamics is symmetric about the line $\theta = \pi/6$, and so the approach to the heteroclinic is asymptotically unaffected by the fixed point, and will go like $x_0\lambda^n$ after n approaches to the fixed point.

Examining the transit time past the fixed point, truncating the equation

$$\dot{z} = -\overline{z}^2 + O(|z|^3)$$

at second order so that in polar coordinates

$$\begin{aligned} \dot{r} &= -r^2 \cos 3\theta \\ \dot{\theta} &= r \sin 3\theta. \end{aligned} \tag{3.4}$$

subject to initial conditions

$$r = 1, \theta = \epsilon$$

at $t = 0$, we get that θ satisfies the second order equation

$$\ddot{\theta} - 2\dot{\theta}^2 \cot 3\theta = 0 \tag{3.5}$$

whence, integrating once and substituting at $t = 0$, we get

$$\ln\left(\frac{\dot{\theta}}{\sin 3\epsilon}\right) = \frac{2}{3}\ln\left(\frac{\sin 3\theta}{\sin 3\epsilon}\right)$$

so that

$$\dot{\theta} = (\sin 3\epsilon)^{1/3}(\sin 3\theta)^{2/3}. \tag{3.6}$$

Now postulating that $\epsilon \ll 1$, expanding $\sin 3\epsilon$ to first order and integrating approximately from $t = 0$ to $t = T$ such that $\theta = \pi/3$, we get that

$$T = K\epsilon^{1/3} + O(1) \tag{3.7}$$

where

$$K = \int_0^{\pi/3} (\sin 3\theta)^{2/3} d\theta.$$

As the reinjection time is constant by hypothesis, we get that the period of successive approaches to the fixed point goes like $K\lambda^{n/3}$. It is interesting that this means the period around the whole loop (three approaches to the fixed point) will go like $K\lambda^n$, as we would get from one approach to a hyperbolic fixed point.

The Poincaré map P cannot have any chaotic dynamics in a small neighbourhood of the $\mathbf{S_3}$THB because its equivariance under the action of $\mathbf{S_3}$ means that its stable and unstable manifolds cannot intersect transversely; they are forced to be coincident with the 2-in-phase spaces. In the case of orbits homoclinic to points other than the in-phase wave, these will generally correspond to transverse homoclinic points in the Poincaré map, and thus we have the possibility of chaos in the map which is not present in the flow.

3.2.8 A global bifurcation scenario

The simplest generic transition from the rotating wave to the in-phase wave (which we observe experimentally by varying the coupling parameter) is:

- The two rotating waves are the only stable solutions.
- There is a supercritical Hopf bifurcation of each of the two rotating waves.
- The only stable solutions are two stable limit cycles, one in each of the invariant triangular regions of the ϕ torus. The limit cycles are 3-fold symmetric. Each one corresponds to an invariant two-torus in the original problem.
- The limit cycles grow until they are destroyed at an $\mathbf{S_3}$ transcritical/homoclinic bifurcation which stabilises the in-phase solution.
- The in-phase oscillation is the only stable solution.

This sequence (as well as the one with time reversed) is the simplest which is consistent with the $\mathbf{S_3}$ symmetry, and is not a special feature of the differential equations governing the system. Figure 3.6(a) shows a bifurcation diagram for this scenario.

In a more general case, but still assuming there are no fixed points other than the minimum necessary (i.e. six in the torus), there will be a global branch of tori starting from the Hopf bifurcation (which is not necessarily supercritical) and ending at the $\mathbf{S_3}$THB, as shown in figure 3.6(b). This branch can fold back on itself several times, creating a sequence of saddle-node bifurcations of tori.

Other modifications of the simplest scenario involve pitchfork or saddle-node bifurcations of the 2-in-phase solutions on the invariant lines. Both of these bifurcations have the possibility of stabilising the 2-in-phase oscillations. In our experiments we have observed the three 2-in-phase solutions to be tristable, but we cannot rule out the possibility that some spurious coupling is causing this.

3.2.9 Breaking the symmetry

Dynamical systems theory provides a framework to understand the effects of imperfect symmetry. The $\mathbf{S_3}$THB is replaced by a sequence of bifurcations which are codimension one in systems without symmetry. The $\mathbf{S_3}$ transcritical bifurcation (fig 3.3) is replaced by several saddle-node bifurcations, and the three saddle connections (fig 3.4) occur

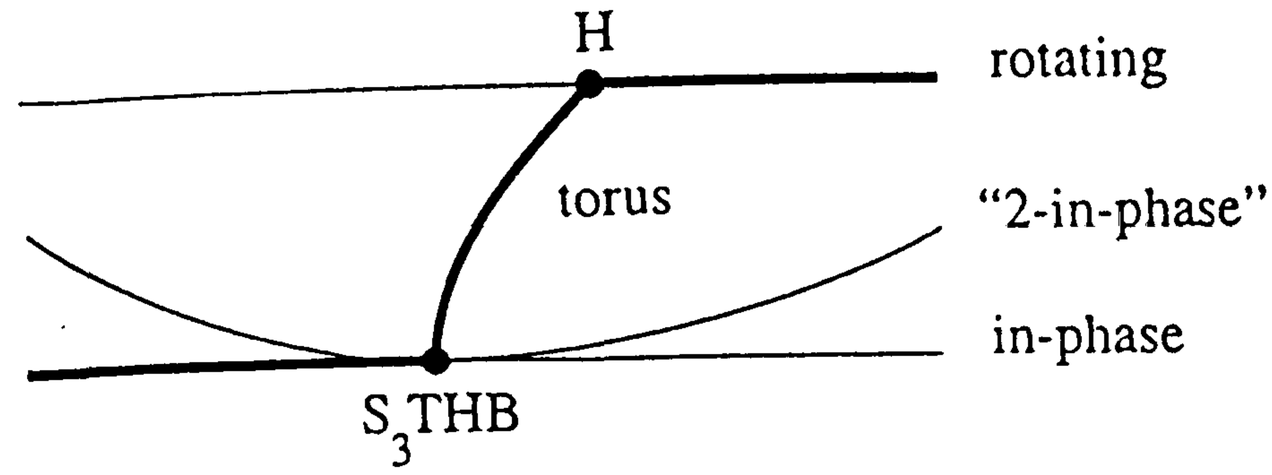

(a)

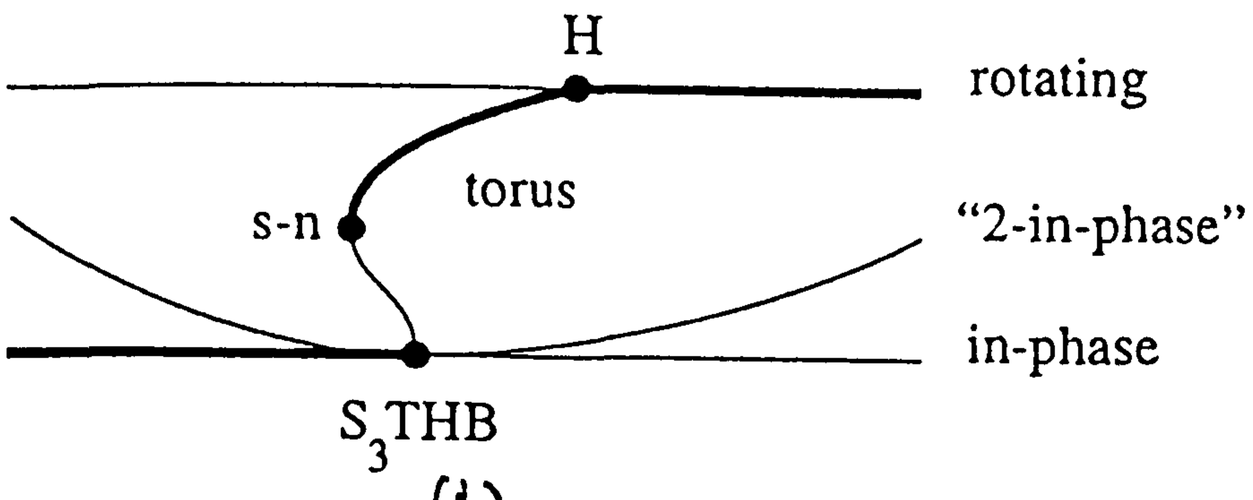

(b)

Figure 3.6:
Some typical bifurcation diagrams. A schematic representation of the solutions is plotted as a function of the parameter. Stable solutions are drawn with a bold curve. The bifurcations are the Hopf (H), saddle node (s-n) and the $\mathbf{S_3}$THB. The simplest scenario (a) is more or less observed in our experiments on oscillators with asymmetric waveforms, and (b) with symmetric waveforms.

separately. When the situation shown in figure 3.4(b) is slightly perturbed, a tubular neighbourhood surrounding the lines connecting the fixed points is stable, although the reflectional symmetry about these lines is lost. The trajectory follows close to the ghosts of the lines of reflectional symmetry and it can drift through the lattice, there being no *a priori* reason why this drift should be periodic in any way. Some of the complexity that can be found in the weakly coupled network without symmetry is discussed in [20, 40, 16].

3.3 The existence of structurally stable heteroclinic connections for an even number of oscillators.

If $n = 2m$ and $m > 1$, we demonstrate a scenario where a vector field with this symmetry can have structurally stable heteroclinic connections.

Referring to the graphical representation of the canonical invariant region described in section 2.6, in the case of n even, we consider an invariant triangle with isotropy $\mathbf{S}_{n/2} \times \mathbf{S}_p \times \mathbf{S}_q$, where $n/2+p+q = n$. The 'hypotenuse' of this triangle, fix$(\mathbf{S}_{n/2} \times \mathbf{S}_{n/2})$, has $\mathbf{Z_2}$ symmetry. It is possible for an equivariant vector field to have a heteroclinic connection between two fixed points on the $(\mathbf{S}_{n/2})^2$ symmetric edges, as shown in figure 3.7. (The two fixed points are related by symmetry, but the eigenvalue pointing into the triangle are different for the two fixed points.) Because of the symmetry there is a heteroclinic cycle, where two heteroclinic connections form a closed curve. This heteroclinic cycle can be stable if the invariant triangle is attracting in the normal direction.

The homoclinic orbit is related to the limit cycle which can bifurcate from points with $(\mathbf{S}_p \times \mathbf{S}_q)^2 \otimes \mathbf{Z}_2$ symmetry for $p + q = n/2$. These points lie in the center of the invariant tetrahedron fix$((\mathbf{S}_p \times \mathbf{S}_q)^2)$. In the case of $p = q$ (so $n = 4k$), the central point has the extra symmetry $(\mathbf{S}_k)^4 \otimes \mathbf{Z}_4$, but it is possible to get such orbits with the

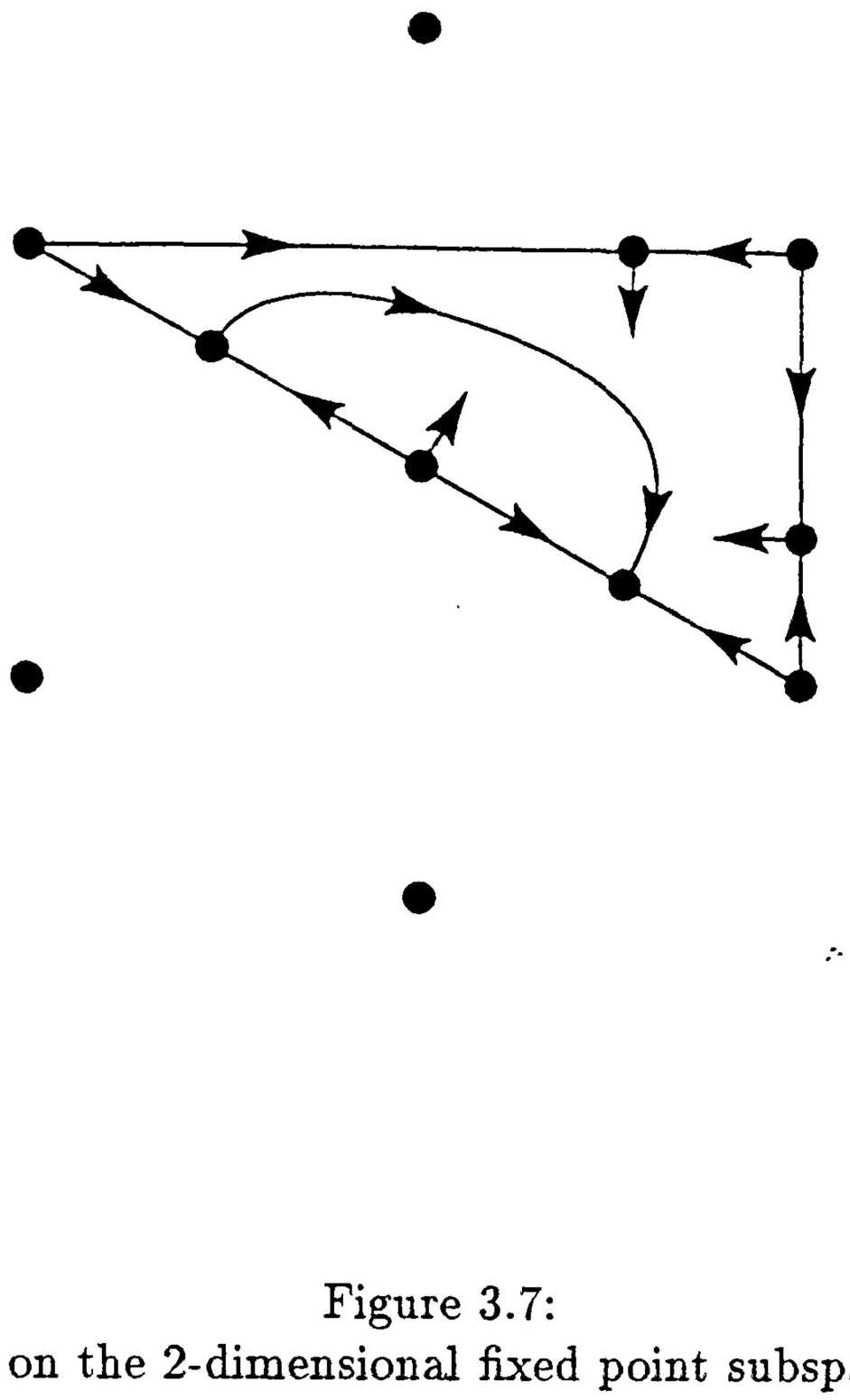

Figure 3.7:
A possible vector field on the 2-dimensional fixed point subspace fix($\mathbf{S}_3 \times \mathbf{S}_2 \times \mathbf{S}_1$) for $n = 6$. The heteroclinic connection between the two solutions with isotropy $(\mathbf{S}_3)^2$ is one segment of a structurally stable heteroclinic cycle.

weaker condition we have presented here.

3.4 Four oscillators

3.4.1 The canonical invariant region

For a group of four oscillators, after factoring out by the action of $\mathbf{T}^1$, we are left with a flow the universal cover which is a 3-dimensional phase space shown in figure 3.8 with symmetries of a crystallographic group related to that of the diamond lattice.

The 2-dimensional fixed point subspaces are a set of planes which cut the space into tetrahedra with four identical edges ($\mathbf{S}_3 \times \mathbf{S}_1$) and two longer edges $(\mathbf{S}_2)^2$. Figure 3.8 shows one of these dynamically invariant tetrahedra.

Each dynamically invariant tetrahedron contains a rotating wave which is on a line fixed by an $\mathbf{Z}_2$ isotropy group and this intersects the long $(\mathbf{S}_2)^2$ edge to give a fixed point with $(\mathbf{S}_2)^2 \times \mathbf{Z}_2$ symmetry.

We can pack $\mathbf{R}^3$ (the universal cover of the 3-torus) by assembling twenty-four of these tetrahedra into a rhombic dodecahedron and then fitting these together (see figure 3.8). We do not take advantage the square symmetry because the dodecahedra have the advantage that they are dynamically invariant, as noted above. The geometry

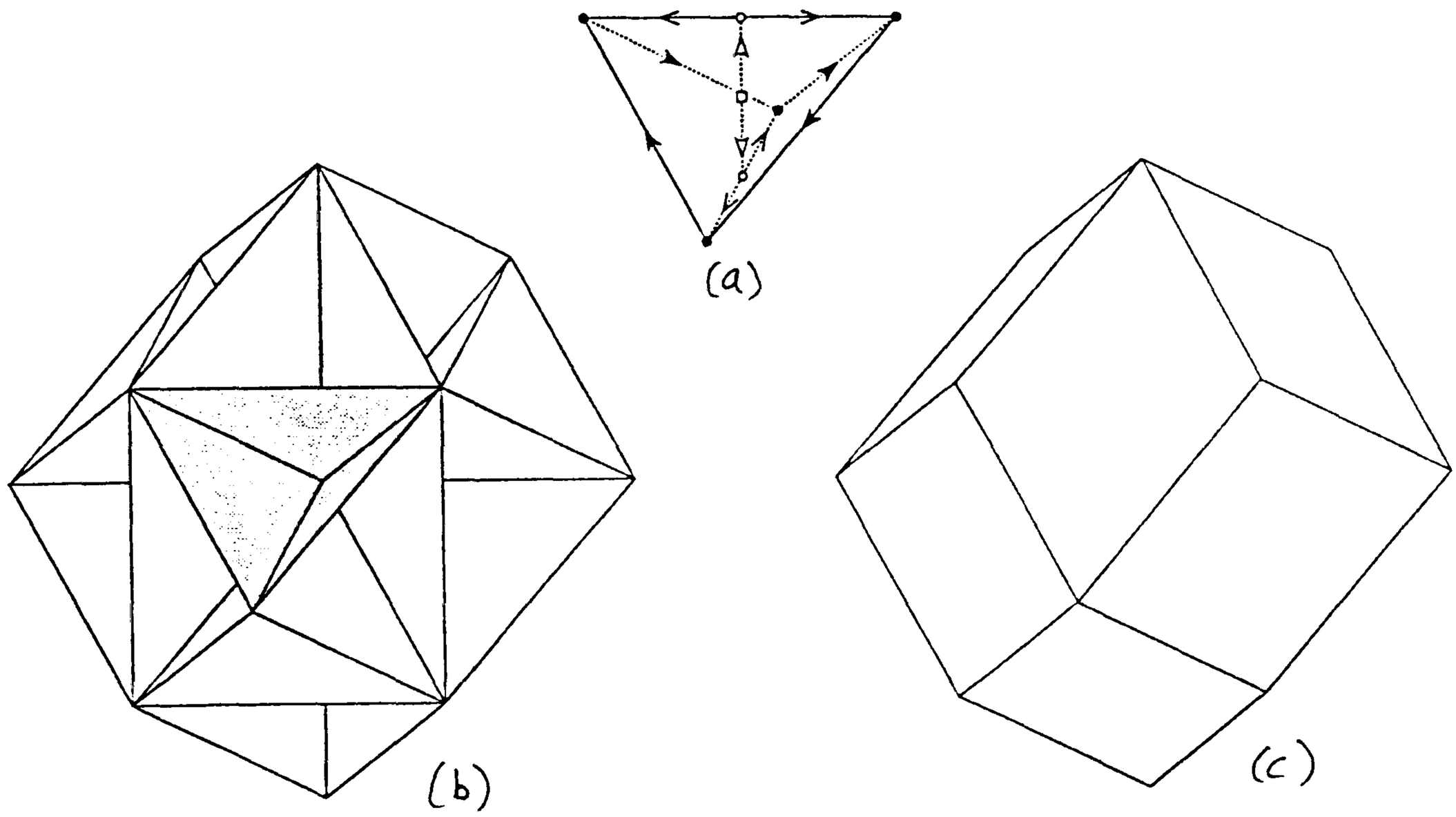

Figure 3.8:
The universal cover of the phase space for $\mathbf{S}_4 \times \mathbf{T}^1$ factored by $\mathbf{T}(1, \cdots, 1)$; (a) shows one invariant tetrahedron. The solid circles are fix($\mathbf{S}_4$), the open circles are fix($(\mathbf{S}_2)^2 \otimes \mathbf{Z}_2$), the square is fix($\mathbf{Z}_4$). the arrows on the line segments indicate which are related by symmetry. The one-dimensional (in $\mathbf{T}^3$) fixed point spaces are fix($\mathbf{S}_3$) - solid arrowheads, fix($\mathbf{Z}_2$) - hollow arrowheads, and fix($\mathbf{S}_2 \times \mathbf{S}_2$) - open arrowheads; (b) and (c) dodecahedron, which is a fundamental domain for the torus and packs 3-space. (In fact only 6 tetrahedra are needed to pack $\mathbf{R}^3$).

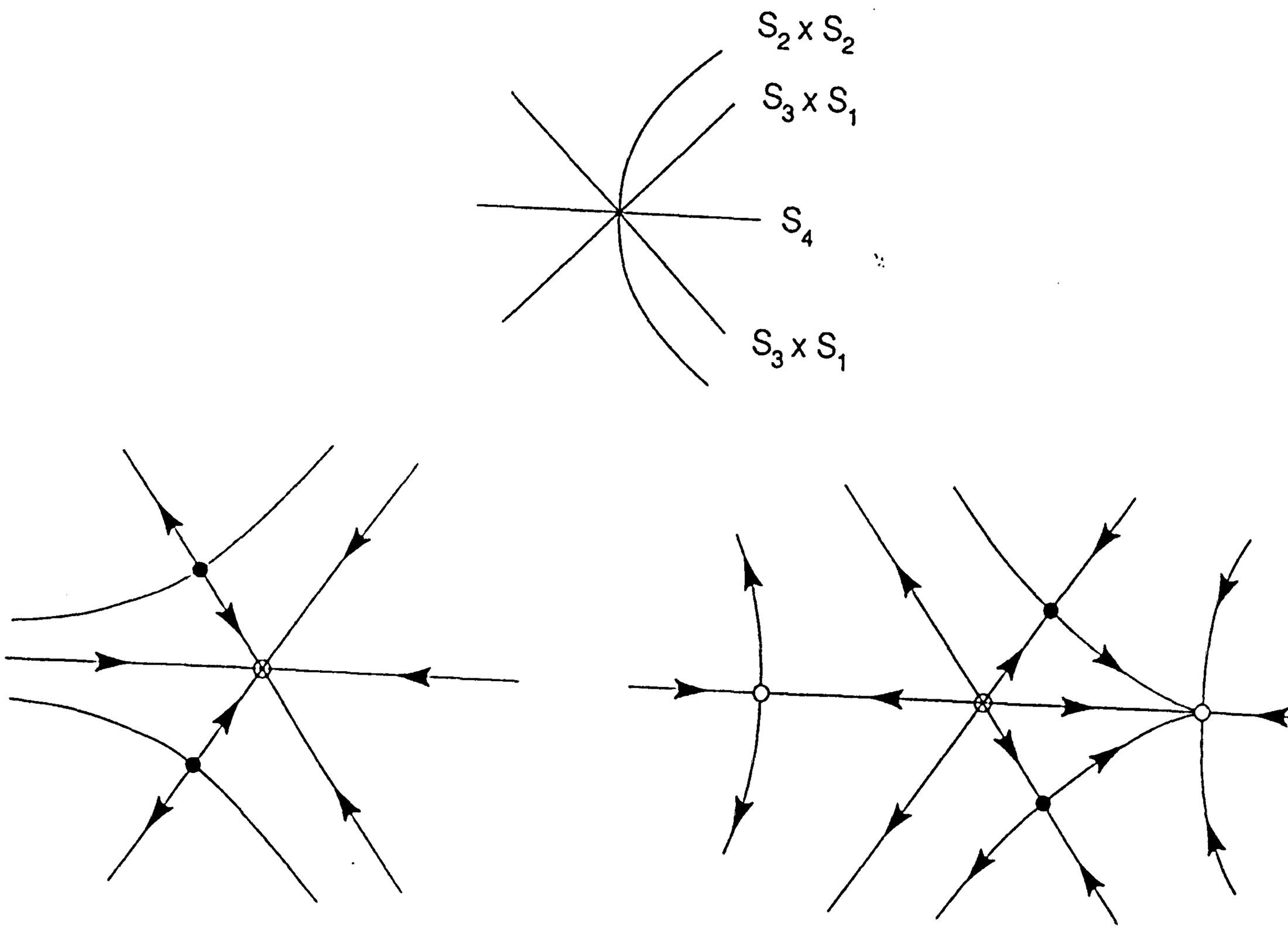

Figure 3.9:
The $\mathbf{S}_4$ transcritical bifurcation. The top figure is a bifurcation diagram which shows the branches of solutions which typically occur as the eigenvalue λ of the in-phase solution goes through zero. The bottom two figures show possible dynamics in the invariant plane fix$((\mathbf{S}_2 \times \mathbf{S}_1 \times \mathbf{S}_1)$, for $\lambda < 0$ (left) and $\lambda > 0$ (right). The in-phase solution, fix$(\mathbf{S}_4)$, is at the centre and the pictures represent a local neighbourhood of the in-phase solution. the solid curves have symmetry $\mathbf{S}_3 \times \mathbf{S}_1$, and the open circles have symmetry $\mathbf{S}_2 \times \mathbf{S}_2$.

of these invariant regions was discussed further in section 2.6.

3.4.2 The $\mathbf{S}_4$THB

The in-phase solution will lose stability typically through the sequence shown in figure 3.9, where four saddles move in along the four invariant lines fix$(\mathbf{S}_3 \times \mathbf{S}_1)$. After bifurcation, in addition to the 4 saddles (which see the whole thing as a transcritical bifurcation), and extra three saddles are formed which go out along the directions fix$(\mathbf{S}_2 \times \mathbf{S}_2)$. If there are no other fixed points in the phase space and the two dimensional surfaces are attracting near the invariant lines, we have a mechanism for the bifurcation directly from the stable in-phase solution to the scenario shown in figure 3.10 for stable heteroclinic cycles, and thus we would expect to see some evidence of this in experiments on such systems.

The rotating wave will generically lose stability either by a pitchfork, forming two fixed points on fix$(\mathbf{Z}_2)$, or by a Hopf bifurcation to a limit cycle winding around this

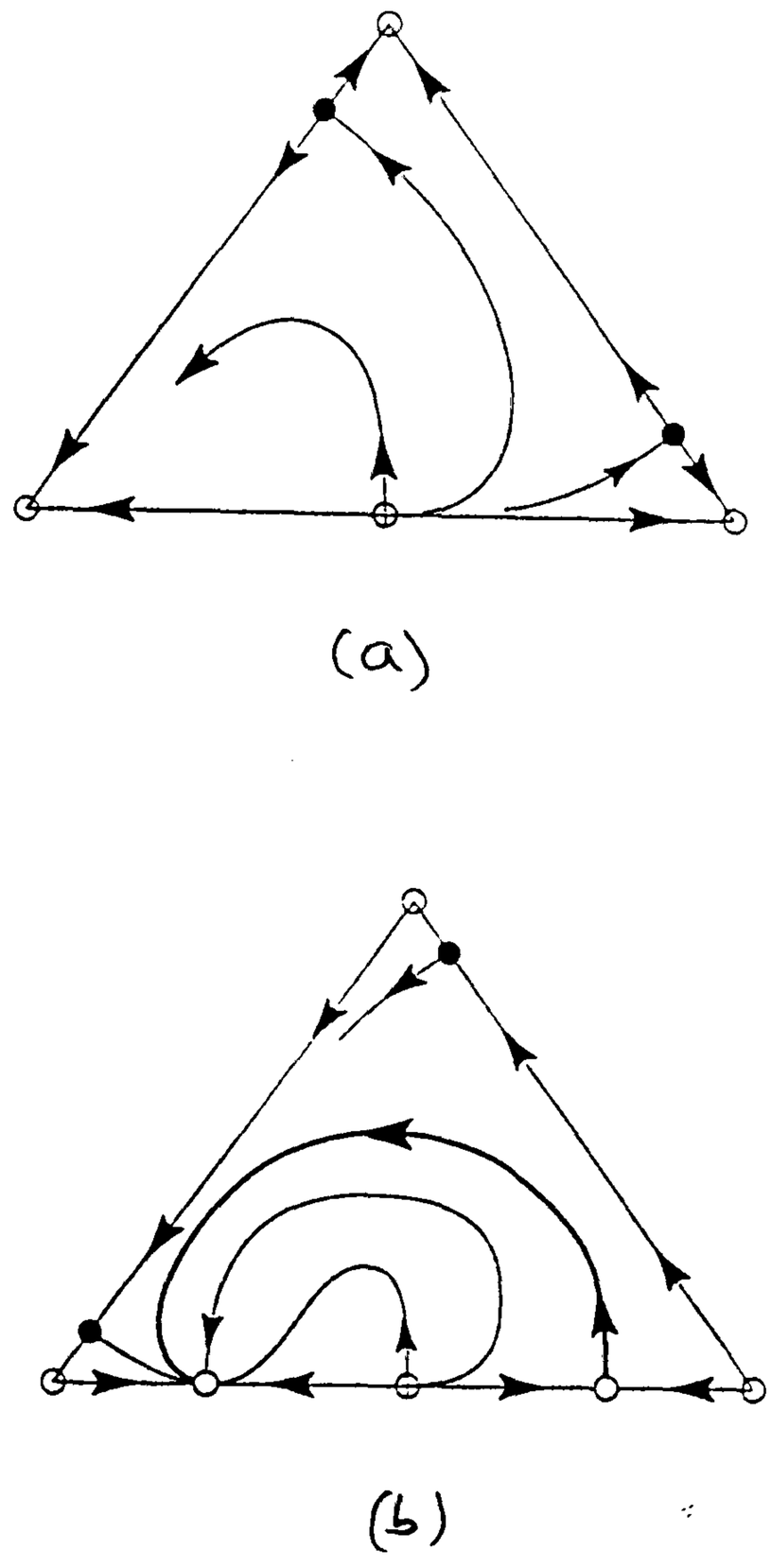

Figure 3.10:
The $\mathbf{S_4}$ transcritical-homoclinic bifurcation. The dynamics on one face of the canonical invariant tetrahedron is shown for (a) $\lambda < 0$ and (b) $\lambda > 0$. this is one possible global phase portrait consistent with the local transcritical bifurcation. each of the four faces of the invariant tetrahedron contains such a connection, so there is a homoclinic cycle which is forced by the symmetry to be structurally stable.

invariant line. This limit cycle is forced by symmetry to lose stability through a saddle-node or a pitchfork of limit cycles; it cannot directly period double, as its Poincaré map is the fourth power of the Poincaré map defined on a quarter of a turn, and thus its Floquet multipliers cannot pass through -1 (Swift & Wiesenfeld [124]).

Chapter 4

Three and four coupled oscillators: experiments

This chapter discusses experimental results from identical electronic oscillator systems with symmetry, using ideas from chapters 2 and 3. Evidence is presented that the $\mathbf{S}_3$THB is observable experimentally and numerically, and that symmetric chaos can appear in forced systems of identical oscillators. Sections of this chapter have appeared in [16, 14, 15].

4.1 Regular behaviour in electronic oscillators

4.1.1 Three oscillators: experiments

To test the theory in chapter 3, in particular to see if it is possible to detect the $\mathbf{S}_3$THB, a system of three coupled van der Pol oscillators was constructed. Each oscillator consists of a parallel inductor-capacitor-resistor (LCR) network. The circuit of one oscillator is shown in figure 4.1. In order to make the oscillators identical, low-tolerance capacitors and wound inductors with ferrite trimmers are used. The nonlinear negative resistor [72] is synthesised using a 741 operational amplifier and an array of diodes (so that the nonlinearity is not determined by saturation of the amplifier). The supply voltages for the operational amplifiers are set at $\pm$12V DC from a laboratory power supply. It was not found necessary to use separate power supplies for each oscillator. A symmetry switch was included to change the individual oscillators between symmetrical and asymmetrical waveforms. Care was taken to minimise the input offset voltage of the operational amplifiers, but as expected this only has a critical effect when the oscillators were used in their symmetrical mode.

In most of this work we find that the stable dynamics of the oscillators is not qualitatively different from that expected from identical ones. However, the system showed extreme sensitivity to any differences between the oscillators near the $\mathbf{S}_3$THB.

The coupling is arranged as shown in figure 4.2. The output from each oscillator is connected via a resistor R to an earthed variable capacitor C. In one sense, it would be more satisfying to use a circuit that did not have the extra degree of freedom in the coupling (i.e. if it is a six rather than a seven degree of freedom system). If all oscillators have a common earth, this could only be done with coupling by parallel LCR circuits, but any alteration to the coupling would have to happen identically in each of the three couplings, and this would be difficult to achieve in practice. A system similar to Hadley's circuit [62, 63], with three van der Pol oscillators connected in a chain with a parallel LCR load, would yield a system with six degrees of freedom. An optional

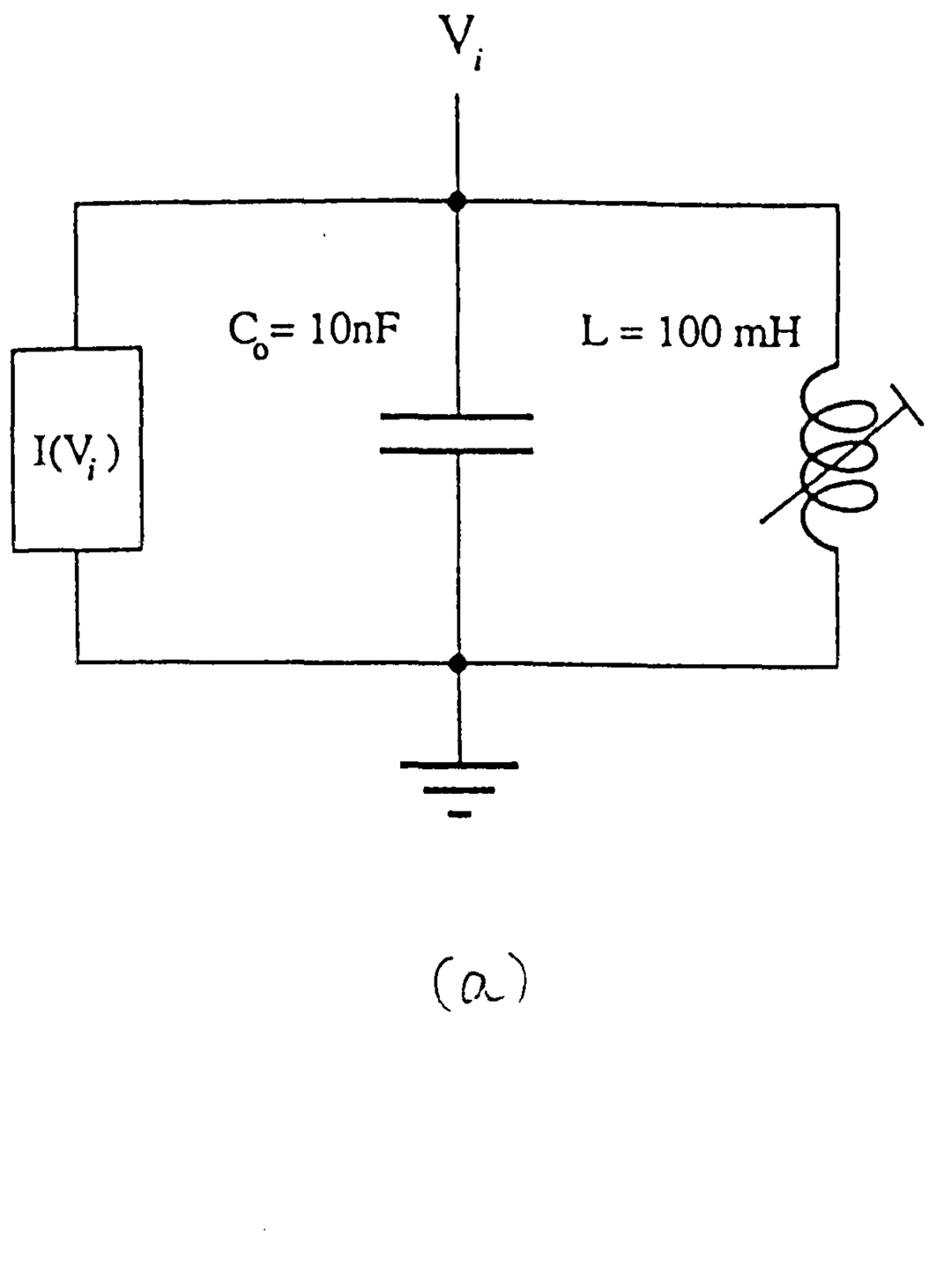

(a)

(b)

Figure 4.1:
(a) The circuit for one van der Pol oscillator. The inductance L is trimmable to enable all the oscillators to be made as close as possible to identical. (b) The nonlinear $I(V)$ characteristic is synthesised by a negative impedance converter and a set of diodes to define the cutoff. The 'symmetry switch' allowed the oscillators to have either symmetric or asymmetric waveforms.

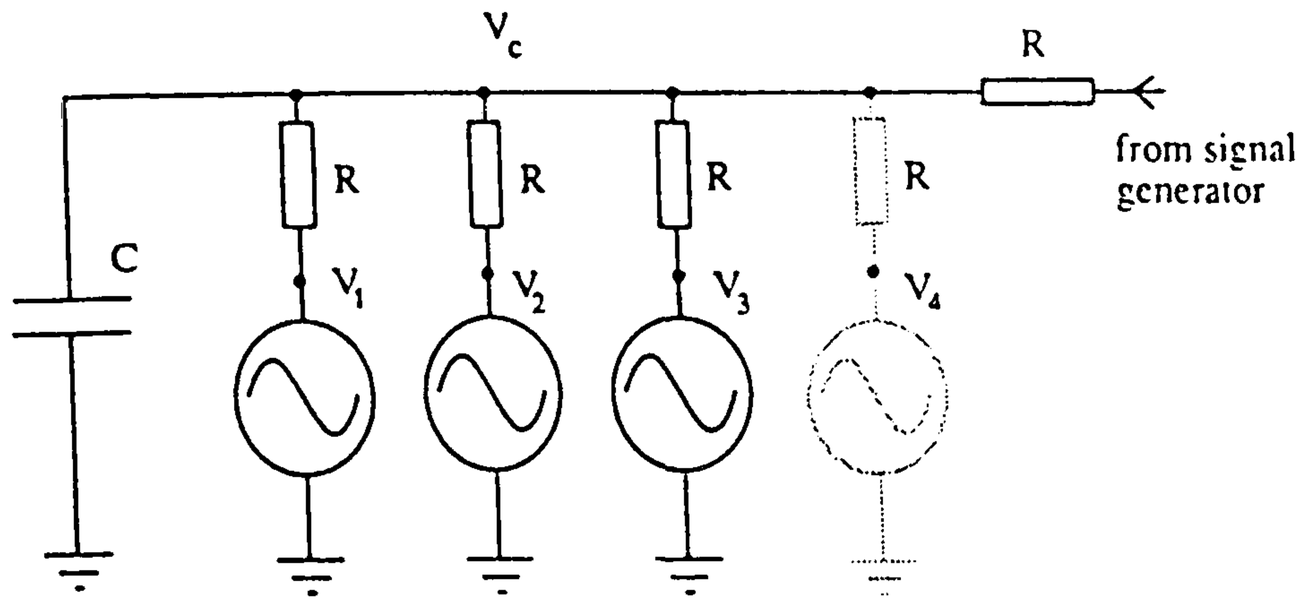

Figure 4.2:
The coupling is achieved through a simple low-pass filter, and the value of C is varied as a bifurcation parameter. The network is symmetric under any interchange of the oscillators. An extra input is provided to allow forcing of the system (discussed in the next section).

input is provided as shown, in order to be able to force the system externally from a signal generator whilst preserving the symmetry of the circuit, but initially this is left unconnected.

4.1.2 Visualisation and results

The output from the three oscillators is visualised on an oscilloscope in two ways: (1) using a multiplexer which allowed the simultaneous display of the waveforms of all three oscillators plus the voltage across the capacitor, and (2) as a phase plot using the voltages:

$$V_x = \frac{1}{2}(-V_1 - V_2 + 2V_3),\ V_y = \frac{\sqrt{3}}{2}(V_1 - V_2)$$

produced by feeding the buffered signals through a network shown in figure 4.4. This is the same projection we use to go from $(\theta_1, \theta_2, \theta_3)$ to the complex angle ϕ, since

$$V_x + iV_y = \omega V_1 + \omega^2 V_2 + V_3$$

This linear combination is an equivariant projection of the three individual voltages onto the plane. A cyclic permutation of the three oscillators gives a rotation by $2\pi/3$ in the $V_x - V_y$ plane, and a permutation of two oscillators gives a reflection.

Experiments were done for various R and C values in the coupling circuit. Results for $R = 10$k, with C treated as the bifurcation parameter, are shown in figs. 4.5- 4.7. Similar results are obtained for R in the range of 5 to 100k, although the details of the bifurcation sequences differed.

Figure 4.5 shows the time series for the in-phase oscillation and rotating wave with both symmetric and asymmetric waveforms.

Figure 4.6 shows the sequence of bifurcations obtained when the individual oscillators have asymmetric waveforms. For large C, the two rotating waves are the only stable solutions. As C is decreased each rotating wave undergoes a supercritical Hopf

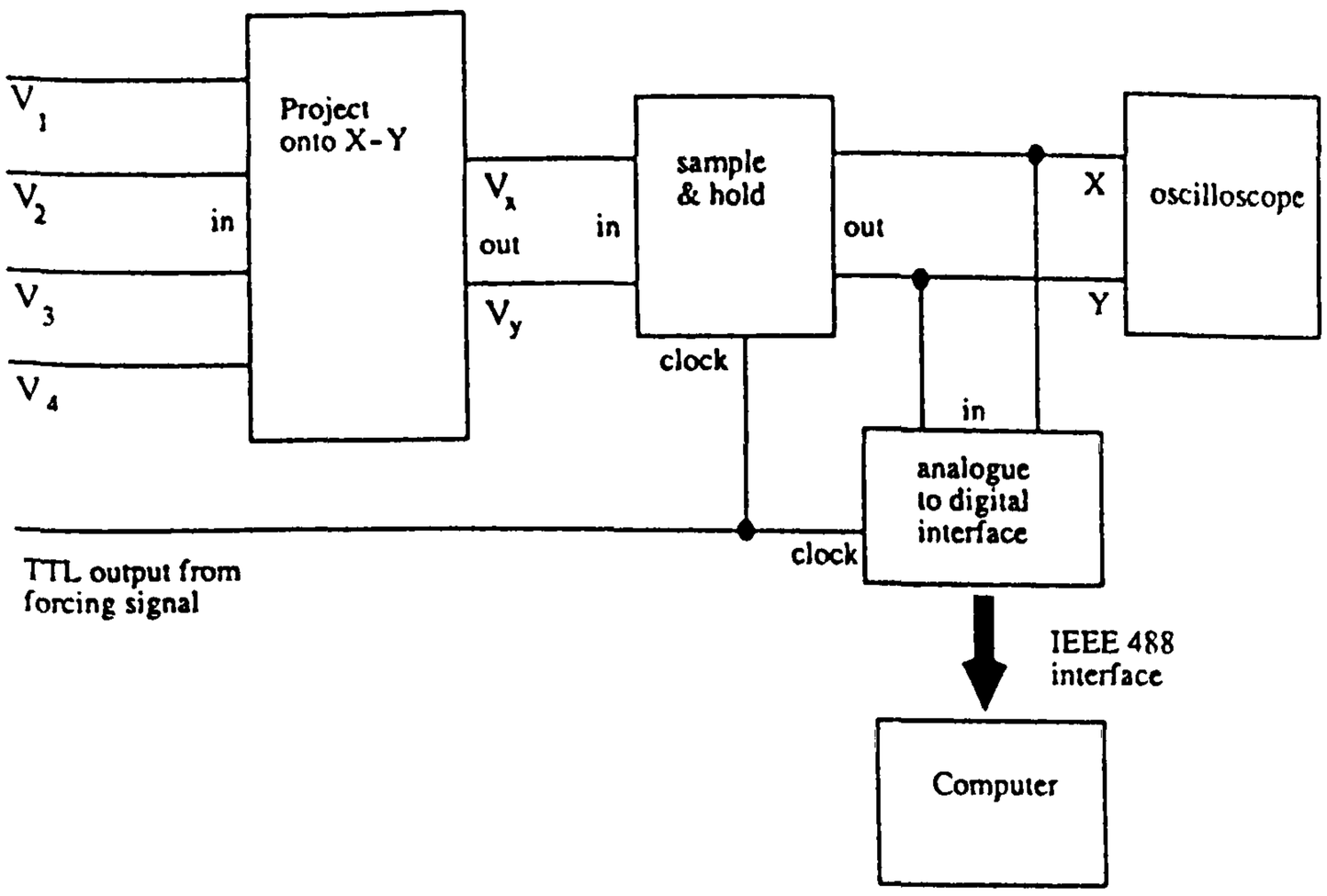

Figure 4.3:
The network used to project the oscillator outputs onto two dimensions and then sample it at the forcing frequency. The projection circuit is detailed in figure 4.4(a).

bifurcation to a stable torus. (In the ϕ plane, this is a normal Hopf bifurcation from a fixed point to a limit cycle, while in $\mathbf{T}^3$ this is a Hopf bifurcation from a periodic orbit to a torus.) This torus grows until it comes very close to the in-phase solution. The theory predicts a direct transition to the in-phase solution, via the $\mathbf{S_3}$THB, as shown in figure 3.6(a). Because the $\mathbf{S_3}$ symmetry is not perfect, the $\mathbf{S_3}$THB is replaced by a sequence of bifurcations, as shown. The in-phase solution is uniquely stable at low C.

The sequence of bifurcations with symmetric waveforms is shown in figure 4.7. The Hopf bifurcation is still supercritical, but the torus (i.e. the limit cycle in the ϕ plane) becomes unstable at a saddle-node bifurcation. It appears that the sequence of bifurcations would be that shown in figure 3.6(b) if the $\mathbf{S_3}$ symmetry were perfect. As in the case with asymmetric waveforms, however, the $\mathbf{S_3}$THB is slightly modified.

The effect of the imperfect symmetry of the system is shown in figure 4.8. In these drifting states, the average frequency of two of the oscillators is the same, while the third has a lightly different frequency. As expected, there is chaos in very small parameter intervals surrounding the homoclinic bifurcations, and this corresponds to breaking the $(1,1,1)$ full mode locking [20].

4.1.3 Four oscillators

(N.B. Experimental results have been omitted to save space.) The setup described in the previous section is also used to investigate the dynamics of four oscillators with $\mathbf{S_4}$ symmetry by altering the projection to give one that is equivariant under the action of some $\mathbf{D_4}$ subgroup of $\mathbf{S_4}$. As the irreducible representations of $\mathbf{S_4}$ are one and three dimensional, we must lose some of the equivariance on projecting to two dimensions. The network in figure 4.4(a) projects the four voltages onto the two

$$\begin{aligned} V_x &= V_1 - V_3 \\ V_y &= V_2 - V_4 \end{aligned}$$

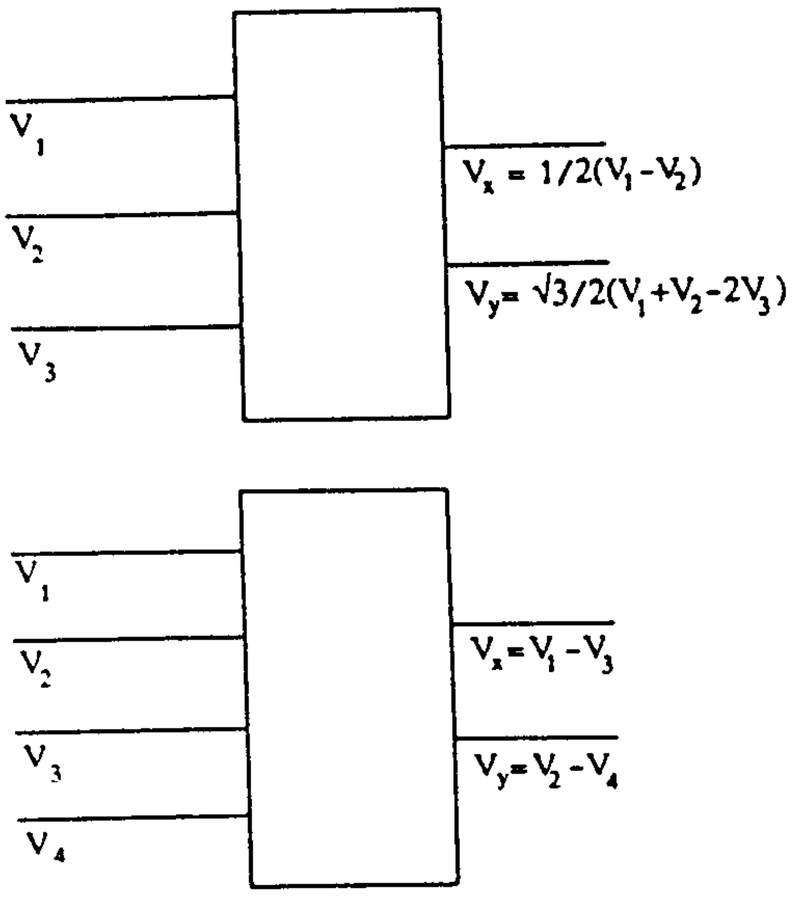

(a)

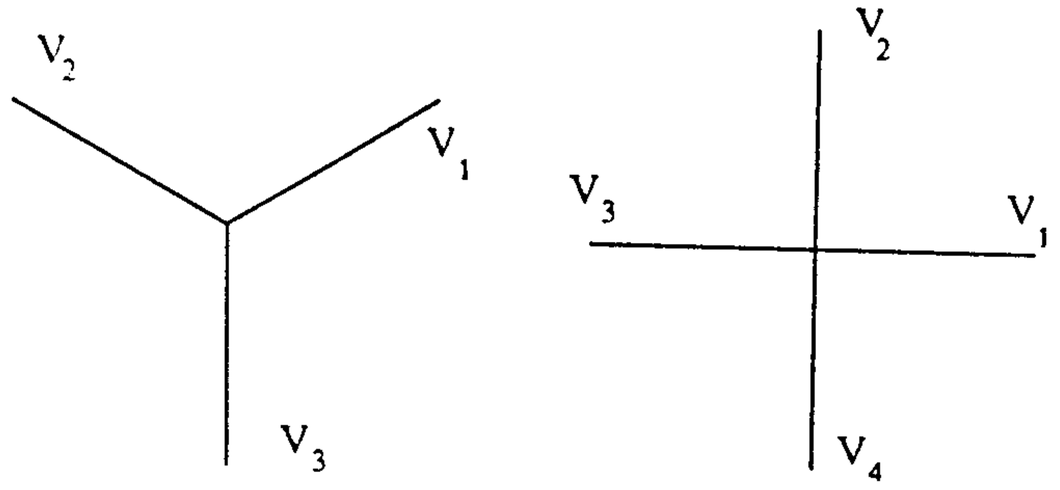

(b)

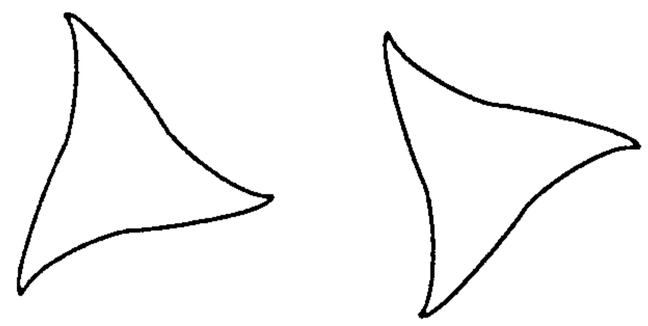

..., 1, 2, 3, ...

..., 1, 3, 2, ...

(c)

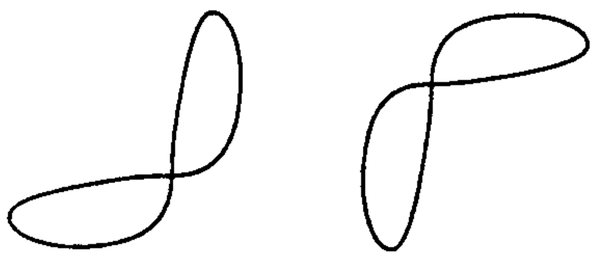

..., 1, 3, 2, 4, ...

..., 1, 4, 2, 3, ...

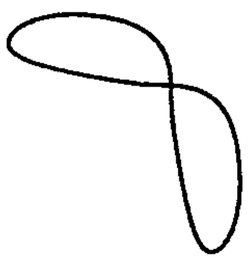

..., 1, 2, 4, 3, ...

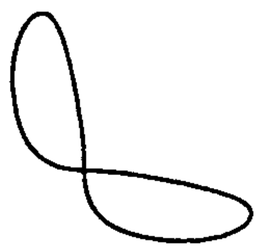

..., 1, 3, 4, 2 ...

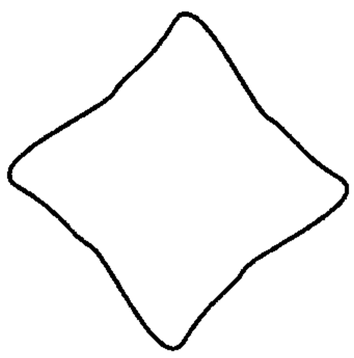

..., 1, 2, 3, 4, ...

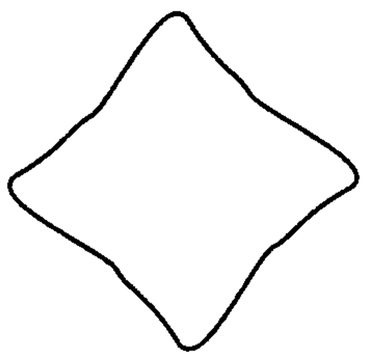

..., 1, 4, 3, 2, ...

(d)

Figure 4.4:
The signals are projected onto the plane preserving at much symmetry as possible. By taking linear combinations as in (a), it is possible to produce a projection (b) that is equivariant under the action of the highest-order polygonal symmetries in the group of symmetries of the network (i.e. $\mathbf{D}_n$ for $\mathbf{S}_n$). For $n = 4$, we lose some of the symmetries. This manifests itself in that only two of the rotating waves have $\mathbf{Z}_4$ symmetry in the projection; the other four having only $\mathbf{Z}_2$ symmetry. (c) shows a drawing of the two possible rotating waves for $n = 3$, and (d) shows the six possible rotating waves for $n = 4$. In general, there are $(n-1)!$ rotating waves given by the possible orders in which the remaining $(n-1)$ oscillators can fire after the first one.

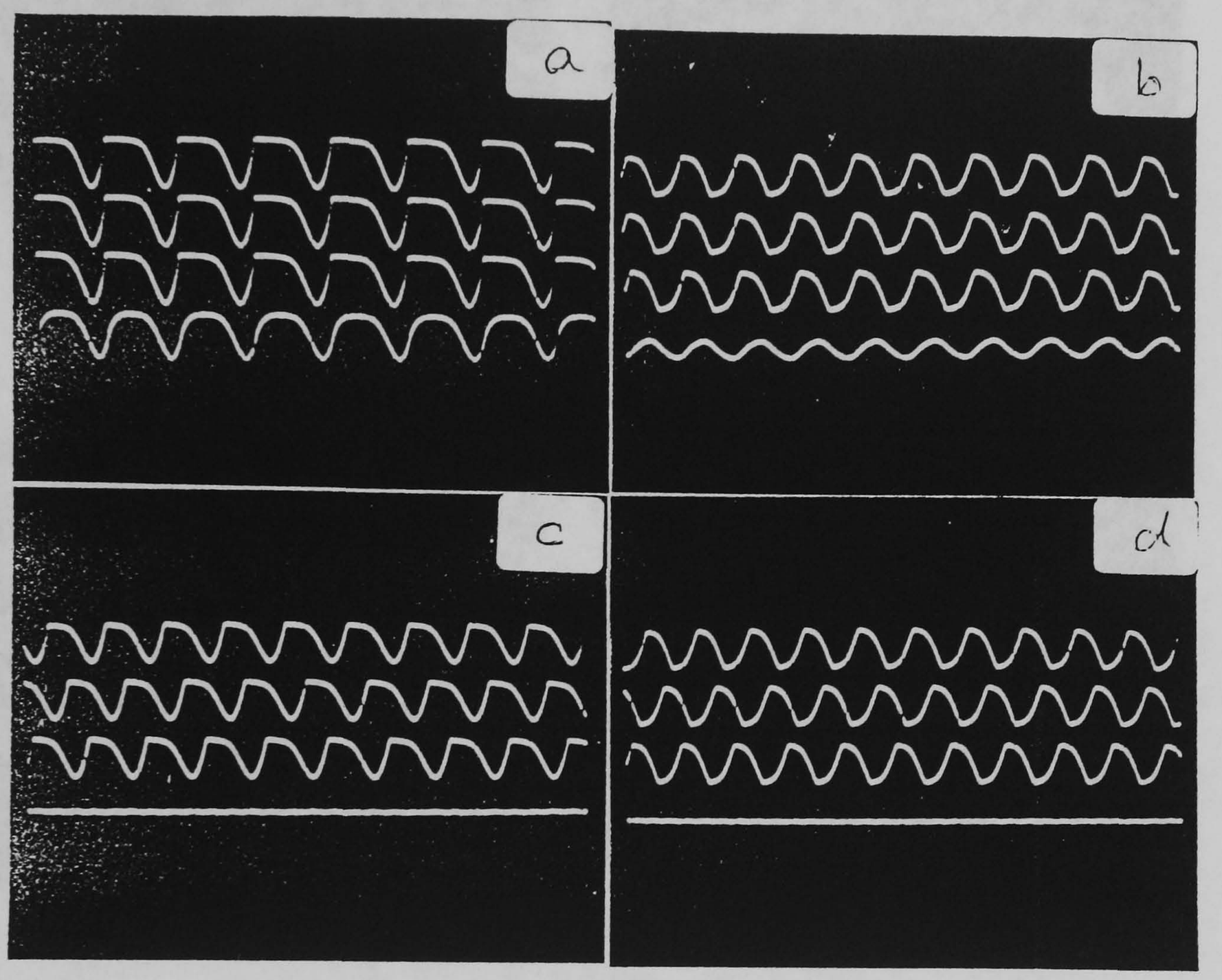

Figure 4.5:
A 2ms interval of the voltages (V_1, V_2, V_3, V_c) from top to bottom, is shown for $R = 10$k and $C =$ (a) 6.69nF (b) 23.60nF (c) 17.00nF (d) 30.00nF. Figures (a) and (b) are in-phase oscillations and (c), (d) are rotating waves. Figures (a) and (c) show asymmetric waveforms, while (b) and (d) show symmetric waveforms. For all values of R and C which we investigated, the frequency is lower for the in-phase oscillation than for the rotating wave.

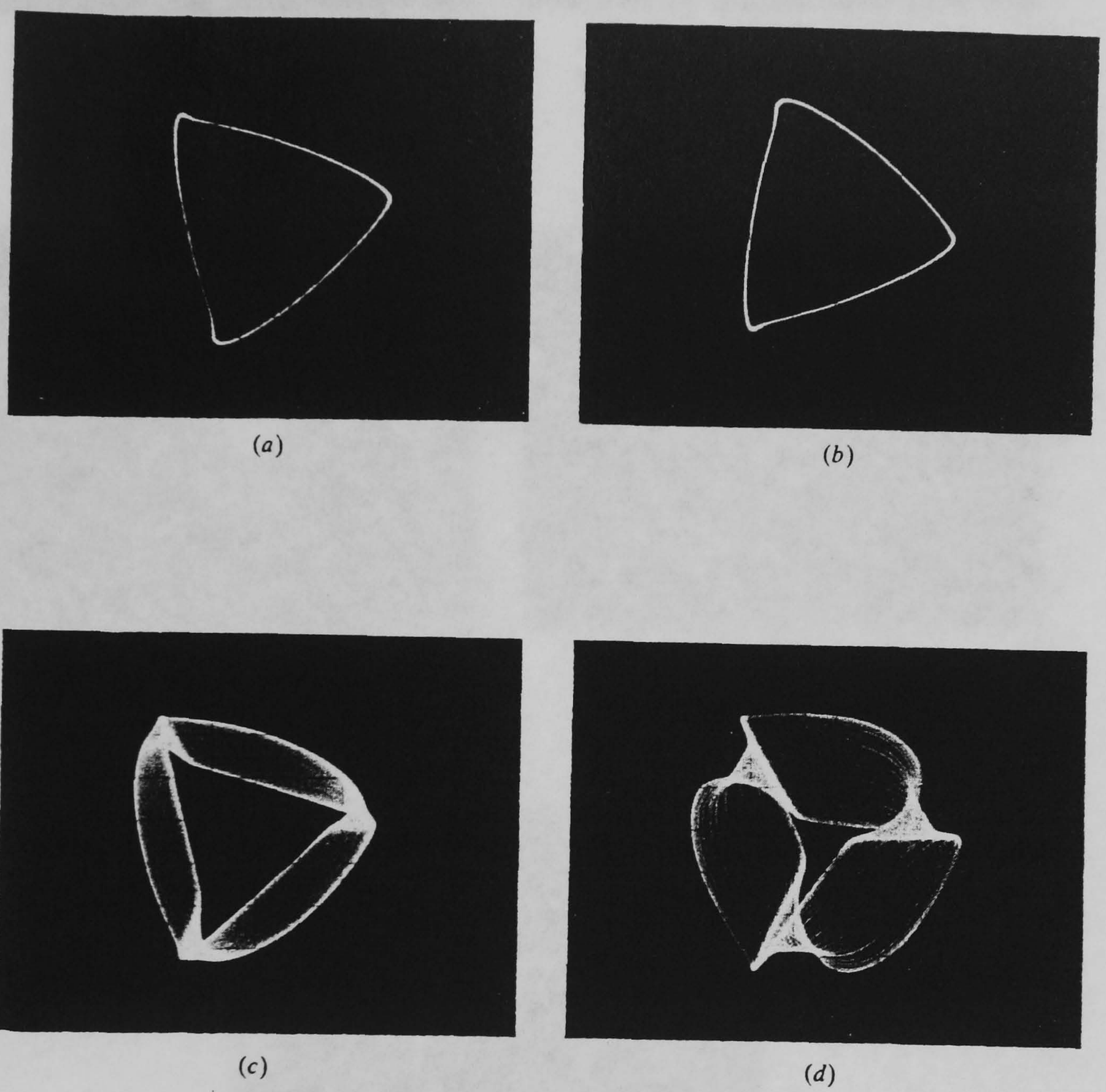

(a) (b) (c) (d)

Figure 4.6:
The equivariant projection (V_x, V_y) showing the details of the transition form the rotating wave (a) to the in-phase oscillation (i) (cf fig. 3.6(a).). The oscillators produced asymmetric waveforms, and the coupling is R = 10k, C =(a) and (b) 17.00nF, (c) 16.10nF, (d) 14.10nF, (e) 13.18nF, (f) 10.30nF, (g) 10.00nF, (h) 7.00nF, (i) 6.00nF. the two orientations of rotating wave are shown in (a) and (b). (continued over)

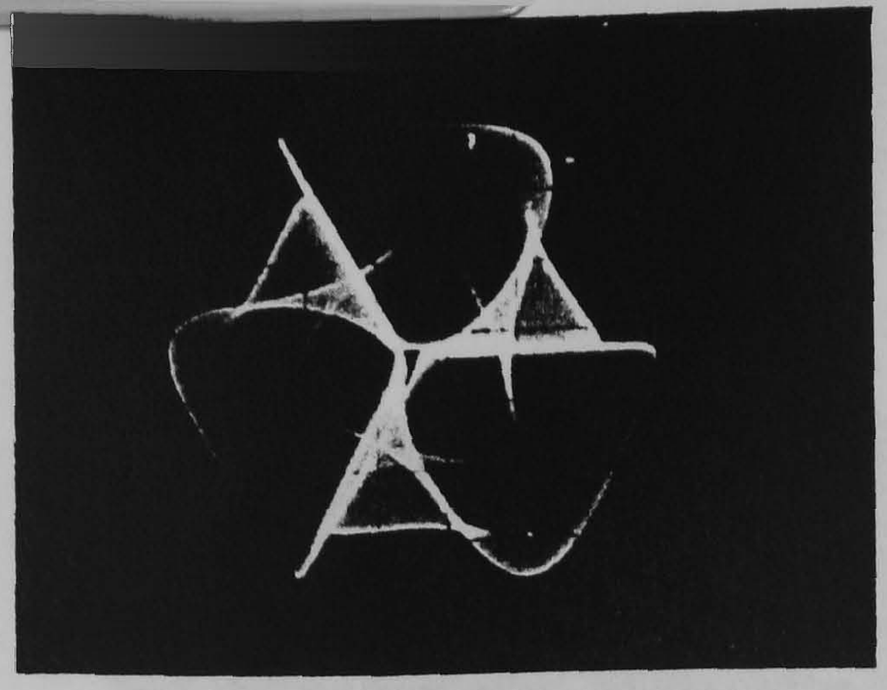

(e)

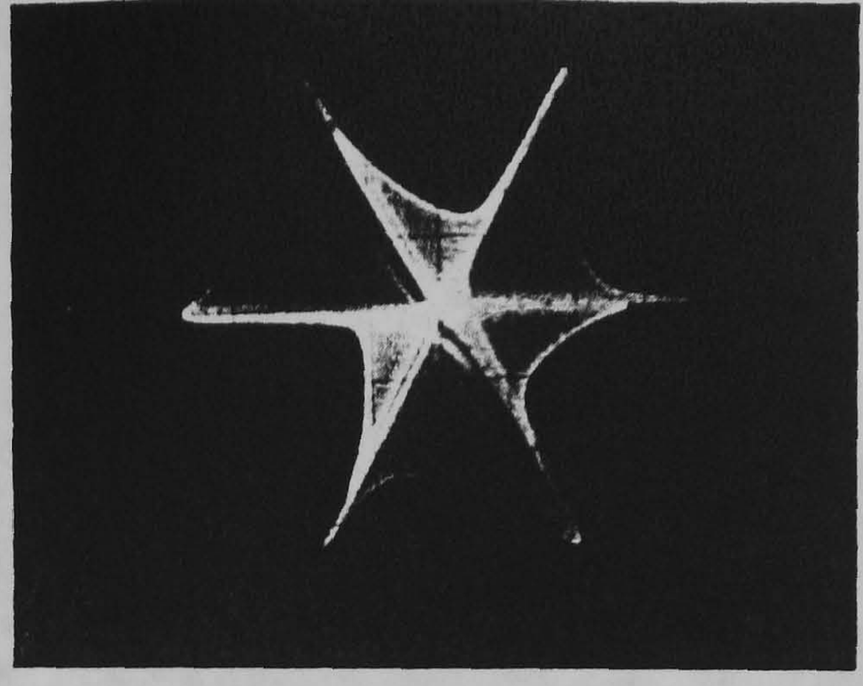

(f)

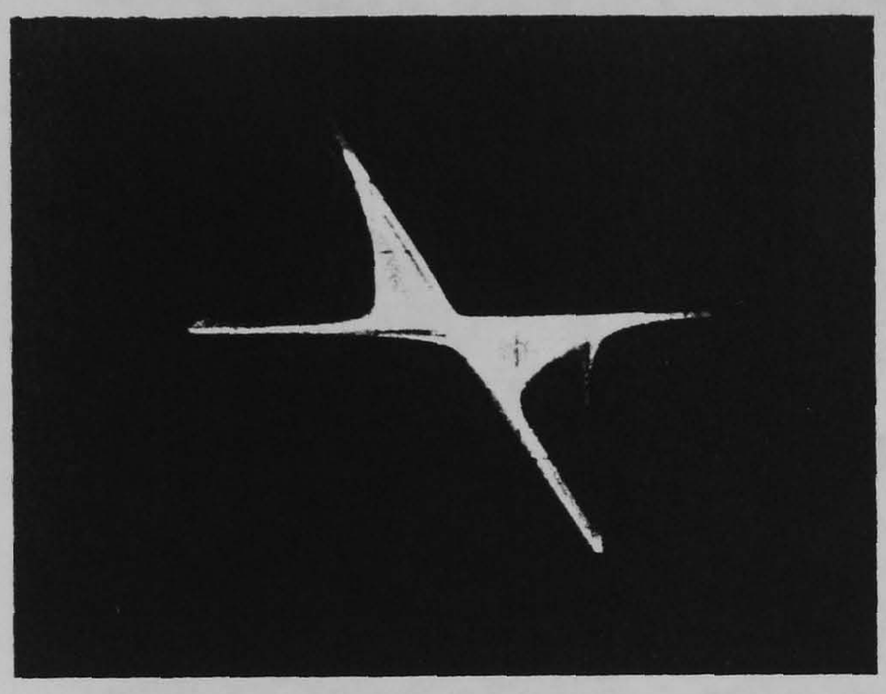

(g)

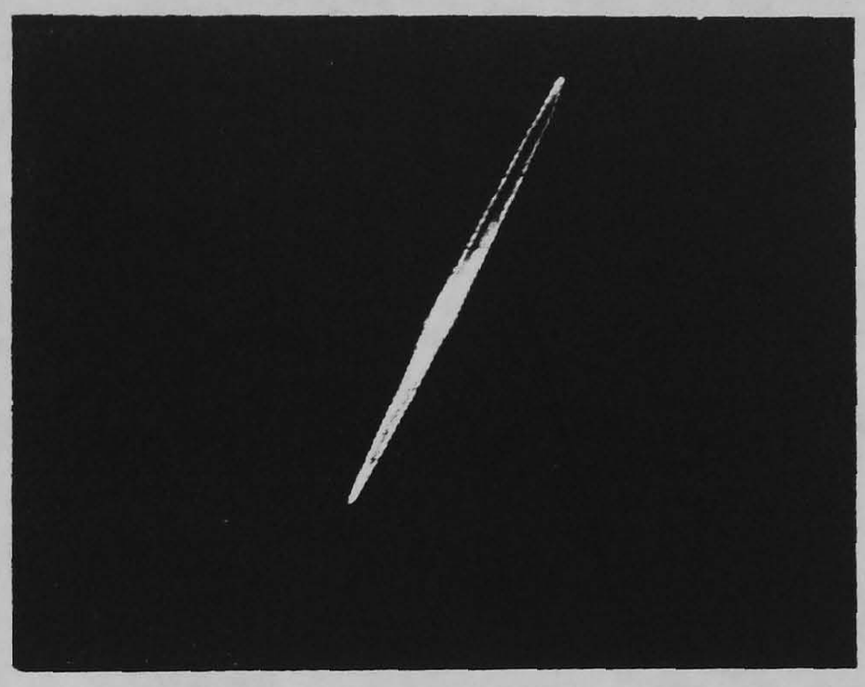

(h)

(i)

(continued) The states (c)-(f) also have twins related by reflection which are not shown. They have $\mathbf{Z}_3$ symmetry because a cyclic permutation of the oscillators leaves the state unchanged. The rotating wave undergoes a supercritical Hopf bifurcation to a torus at $C = 16.90$nF, between (b) and (c). The torus grows until, at (f) it has nearly collided with the in-phase oscillation. In the range 10.07nF$< C <$10.21nF, the states (f) and (g) are both stable. In the range 7.32nF$< C <$7.53nF, the states (g) ansd (h) are both stable. The transition (h) to (i) has no hysteresis. With perfect $\mathbf{S}_3$ symmetry, (g) and (h) would not exist, and the $\mathbf{S}_3$THB would give a transition directly from (f) to (i).

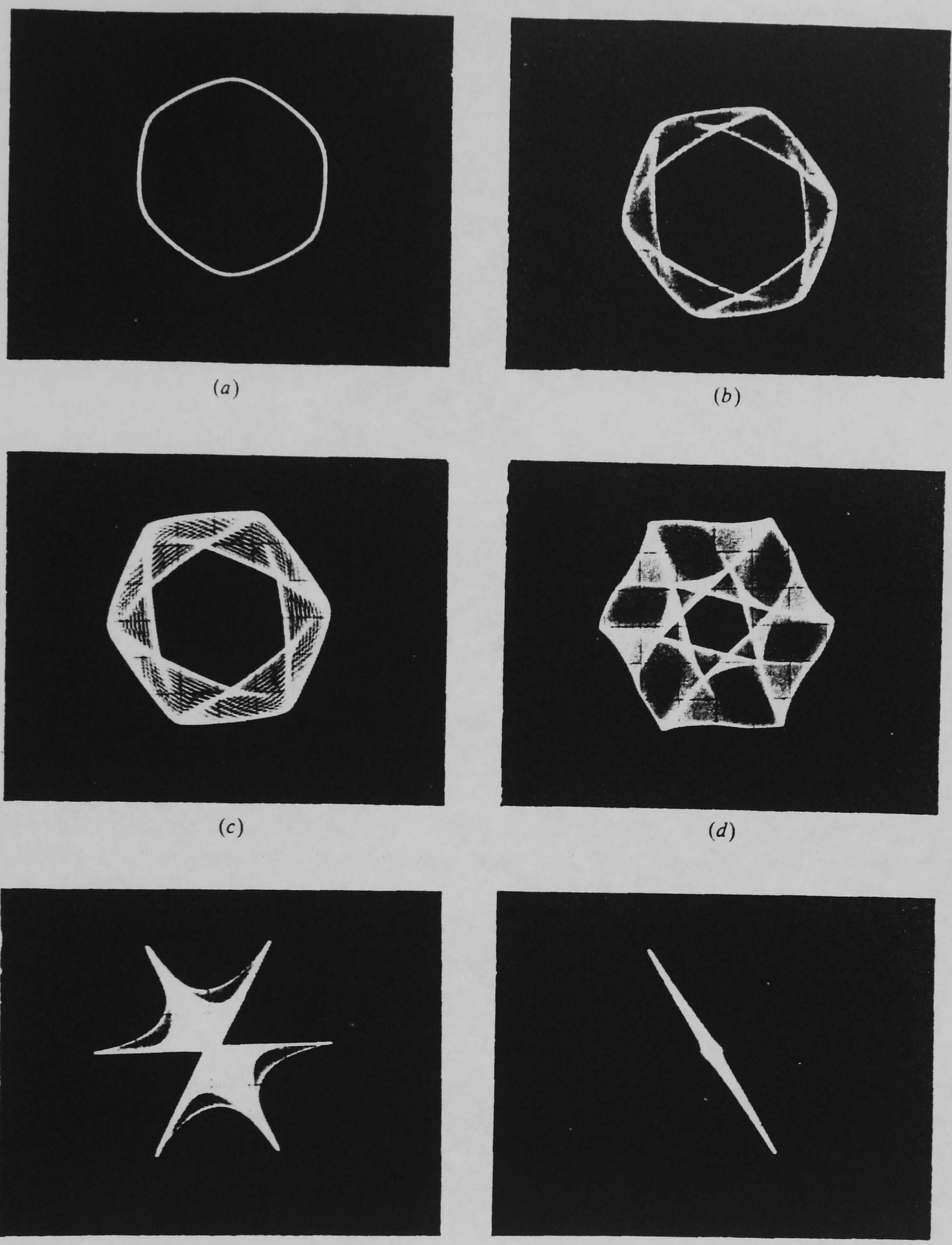

Figure 4.7:
As with the previous figure, but with symmetric waveforms. and C =(a) 30.00nF, (b) 28.94nF, (c) 28.02nF, (d) 25.91nF, (e) 26.00nF, (f) 25.70nF. The figures have $\mathbf{Z}_6$ symmetry because of the $\mathbf{Z}_2$ symmetric waveforms in a $\mathbf{Z}_3$ symmetric state. The rotating wave undergoes supercritical Hopf bifurcation to a torus at $C \sim 29.90$nF. The states shown in (d) and (e) coexist, and the pictures shown are near the limits of bistability. There is a complicated transition (e)-(f) (not shown). With perfect $\mathbf{S}_3$ symmetry, we expect that (e) and (f) would not appear.

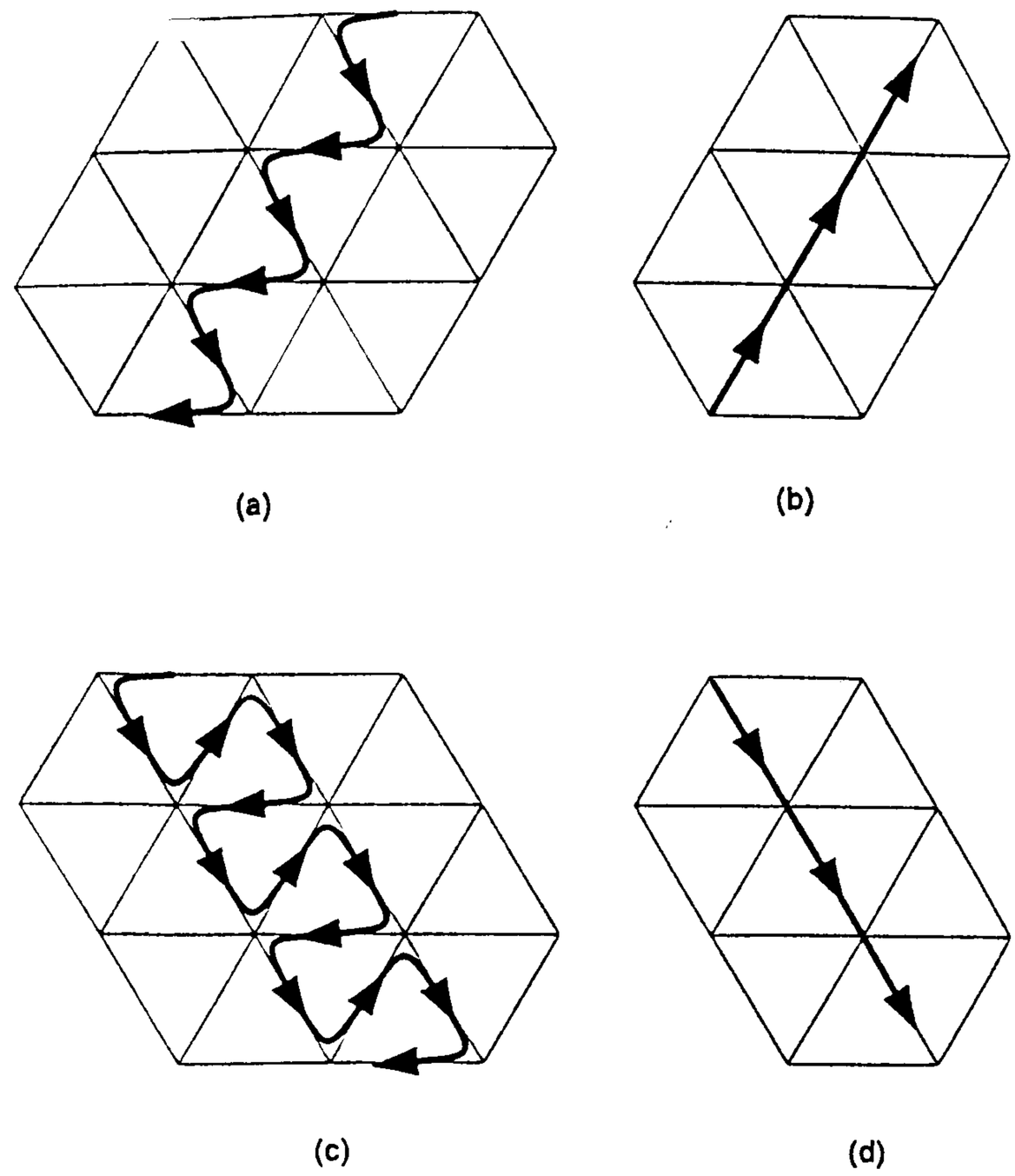

Figure 4.8:
The drift through the ϕ lattice due to lack of perfect symmetry. Near the $\mathbf{S}_3$THB, the system is very sensitive to imperfections. Figure (a), (b), (c) and (d) refer to figure 4.6(g), (h) and figure 4.7 (e) and (f) respectively.

and the six possible rotating waves on the system ordered by the firings of the oscillators are shown in this projection in figure 4.4(d). By changing the coupling capacitance C in the circuit shown in figure 4.2 it is possible to stabilise the in-phase solution for low C and destabilise it for high values of C. When the oscillators are producing asymmetrical waveforms, the rotating solutions are stabilised for large enough C, but it is interesting to note that when the oscillators are producing symmetrical waveforms, the rotating wave solutions drift at a slow timescale related to the imperfections in the system. As the coupling network is linear and the waveforms $v(t)$ with period T have the symmetry

$$v(t + T/2) = -v(t)$$

we have the conditions for decoupling noted in section 2.7.2, and should expect this behaviour. The difficulties in setting up the oscillators to be identical hindered any attempt to find an $\mathbf{S}_4$THB (see section 3.4.2) in the bifurcation diagram. Given a more carefully controlled experiment, this would be an interesting point of departure for further investigation.

4.1.4 The ideal equations

The theory we have presented describes which bifurcations can occur, given the restrictions imposed by symmetry, but to find which bifurcations do occur in a specific system requires an analysis of the equations. In this section we describe the equations which govern the experimental system, and give a physical argument as to why the in-phase oscillation is favoured at low C, while the rotating wave is favoured at large C.

The equations of motion for our system of oscillators may be derived, assuming ideal components, from Kirchoff's current law to yield:

$$C_0 \frac{d^2V_i}{dt^2} + \tilde{\Gamma}(V_i)\frac{dV_i}{dt} + \frac{V_i}{L} = \frac{1}{R}\left[\frac{dV_c}{dt} - \frac{dV_i}{dt}\right] \tag{4.1}$$

$$C\frac{dV_c}{dt} = \frac{1}{R}\left(\sum_{i=1}^{3} V_i - 3V_c + A\cos\omega t\right).$$

where C_0 and L are the capacitances and inductances in each oscillator, and the damping or dissipation function $\tilde{\Gamma}(V) = dI(V)/dV$ is the incremental conductance of the nonlinear element of the circuit. For symmetric oscillators $\tilde{\Gamma}(V) = \tilde{\Gamma}(-V)$. Note that the classical van der Pol equation is obtained using the model $\tilde{\Gamma}(V) = a + bV^2$, with $b > 0$. **In the following section, assume that the forcing term $A\cos\omega t$ is zero.**

By rescaling time so that $dx/dt = \omega_0\dot{x}$, where $\omega_o = (LC_0)^{-1/2}$ is the natural frequency, we obtain the non-dimensional equations:

$$\ddot{V}_i + \Gamma(V_i)\dot{V}_i + V_i = \epsilon(\dot{V}_c - \dot{V}_i) \tag{4.2}$$

$$\dot{V}_c = \delta\sum_{i=1}^{3}(V_i - V_c)$$

with a dimensionless dissipation function $\Gamma(V) = \sqrt{(L/C_0)}\tilde{\Gamma}(V)$. For the classical van der Pol model, scaling V yields $\Gamma(V) = \Gamma(0) + V^2$. There are four time scales in the problem, which leads to three ratios when measured relative to the natural frequency:

$$\Gamma(0) = \frac{a}{\omega_0 C_0} \quad \epsilon = \frac{1}{\omega_0 RC_0} \quad \delta = \frac{1}{\omega_0 RC}$$

For the oscillator components given in figure 4.1, and R = 10k, the numerical values of the dimensionless parameters are $\Gamma(0) = -0.79$, $\epsilon = 0.316$, and $\delta = 0.316C_0/C$.

4.1.5 Modelling the nonlinearity

A simple cubic nonlinearity is found not to model the behaviour of the circuit very well, so it was decided to fit a curve to measurements of the actual system. The current through the nonlinear negative resistor (out of circuit) is measured for a range of voltages in a static situation, we matched them to the following model, as shown in figure 4.9. Note that the negative slope is generated by the negative impedance converter and the saturation of the diodes should go like $I = i_o(\exp(eV/kT) - 1)$, meaning we fit to a sum of exponentials (the Ebers-Moll model [72]).

The measurements of the I-V characteristic of the nonlinearity gave the resulting model:

$$I(V) = -0.475V + 1.752 \times 10^{-5}\sinh(6.025V) \tag{4.3}$$

where I is measured in mA and V is measured in Volts. The model is fitted simply by noting that the steepness of the exponentials meant that at $V = 0$, the linear term is merely the slope of the curve. After removing this linear part, the two factors governing the exponential behaviour are found by fitting to two of the $I(V)$ observations. For the asymmetric oscillator, we us the model, found by assuming the $I(V)$ characteristic for the single diode is the same as that for three diodes in series, but with one third the voltage.

$$I(V) = -0.475V + 8.76 \times 10^{-6}(\exp(6.025V) - \exp(-18.075V)) \tag{4.4}$$

(I measured in mA.) This gives models for $\Gamma(V)$ of the form in the asymmetric case:

$$\Gamma(V) = -0.828 + 1.67 \times 10^{-4}\exp(6.025V) + 5.01 \times 10^{-4}\exp(-18.075V) \tag{4.5}$$

and in the symmetric case:

$$\Gamma(V) = -0.828 + 5.394 \times 10^{-5}\cosh(6.025V). \tag{4.6}$$

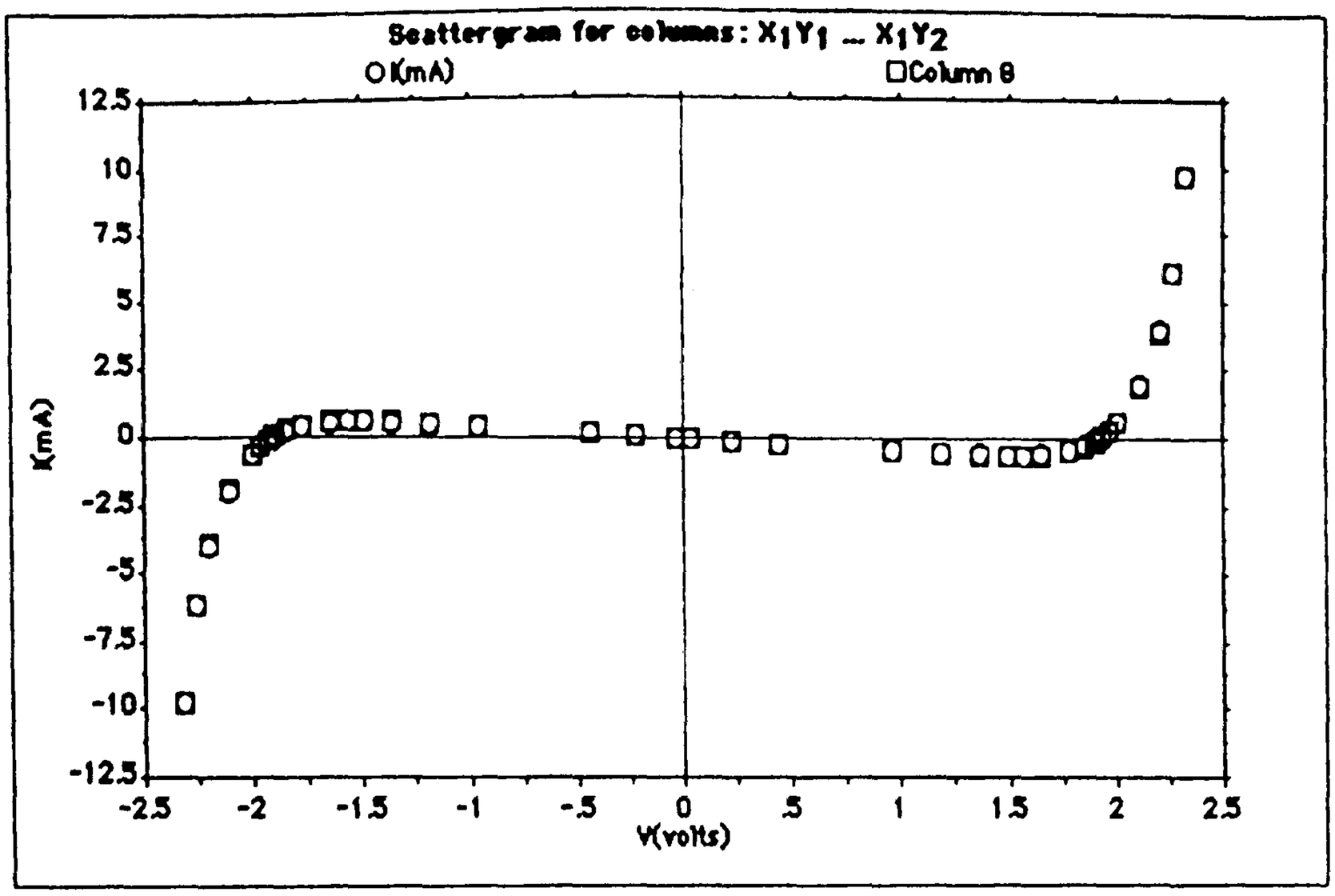

Figure 4.9:
The nonlinear $I(V)$ from the circuit shown in figure 4.1(b) with the symmetry switch open, so that the current I is an odd function of V. The circles represent measured points, while the squares are points on the fitted curve.

Phenomena	Numerical δ	Experimental δ
Asymm. Hopf	0.19	0.17
Asymm. THB	0.32	0.31$\sim$ 0.46
Symm. Hopf	0.10	0.11
Symm. Saddle node	0.13	0.12

Table 4.1: A comparison between the locations of the bifurcations for the numerical and electronic experiments. Note that the experimental location of the THB is approximate due to symmetry imperfections in the circuit.

4.1.6 Numerical experiments

Using the model equations 4.3,4.4, the KAOS interactive dynamical systems package of Guckenheimer and Kim was used to performed some numerical experiments on the equations 4.1 using realistic parameter values. Investigating the asymmetric and symmetric oscillator scenarios, good agreement was found both qualitatively and quantitatively.

The value of $\epsilon = 0.316$ is fixed in all the experiments. In the asymmetric case, there is a Hopf bifurcation at $\delta = 0.19$ giving rise to a stable 2-torus which grew in amplitude until its longest period went to infinity and the system approached the in-phase solution at $\delta = 0.32$. In the symmetric case, The Hopf bifurcation at $\delta = 0.10$ gave rise to a branch of tori which lost stability without the period tending to infinity, at some distance from in-phase solution, at $\delta = 0.13$. Table 4.1 shows that these results compare favourably with those from the electronic experiments.

Figures 4.10- 4.11 compare the appearance of the numerical results in the same projections as that used for the oscilloscope pictures.

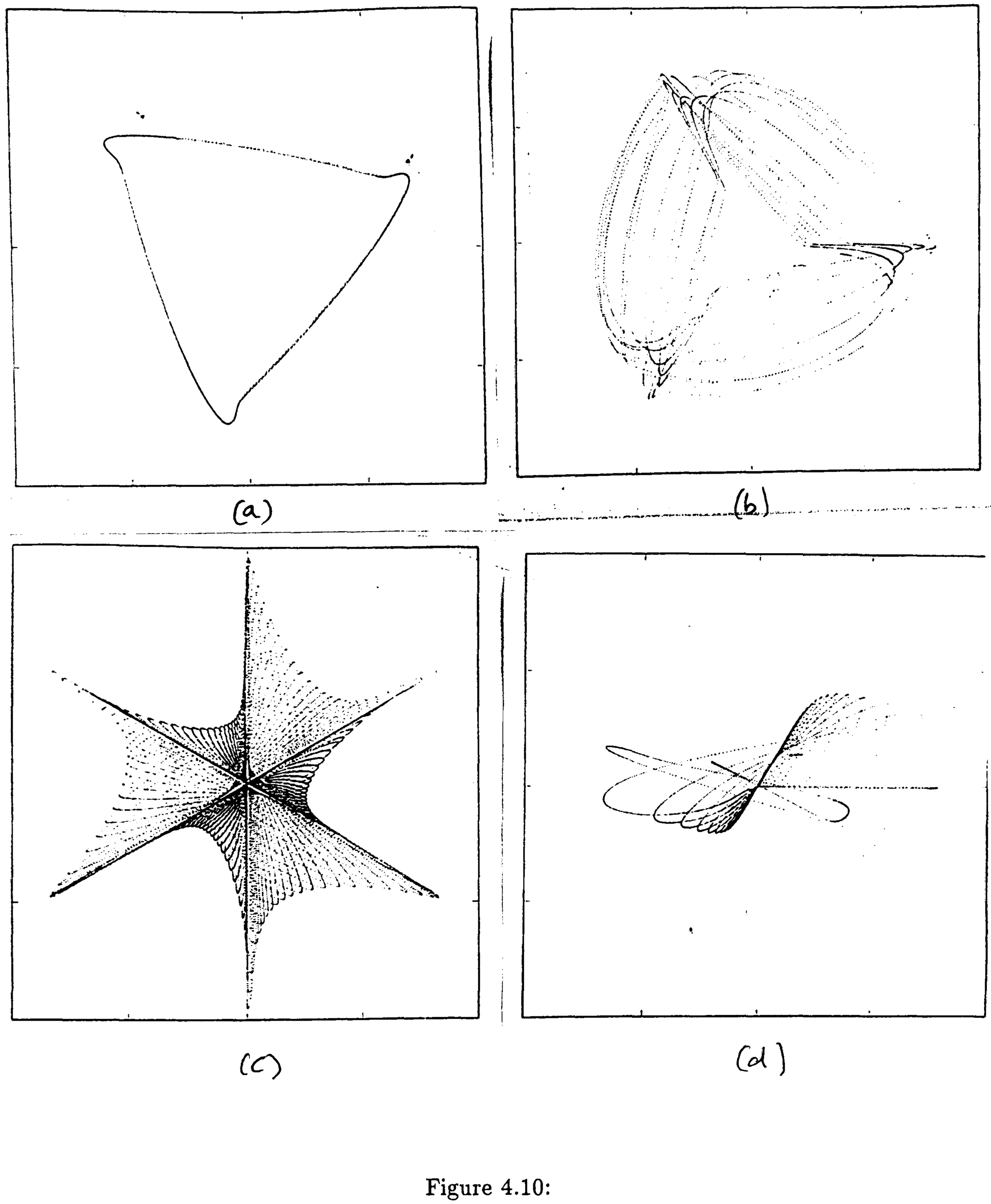

Figure 4.10:
Numerical simulations with asymmetric waveform oscillators. (a) The stable rotating wave, $\delta = .106$ (b) After Hopf bifurcation, $\delta = .2$ (c) Near THB, $\delta = 0.31$ (d) Transient decaying to a stable in-phase solution. Note that it approaches along a 2-in-phase direction. The boxes surrounding the pictures are $4V$ square.

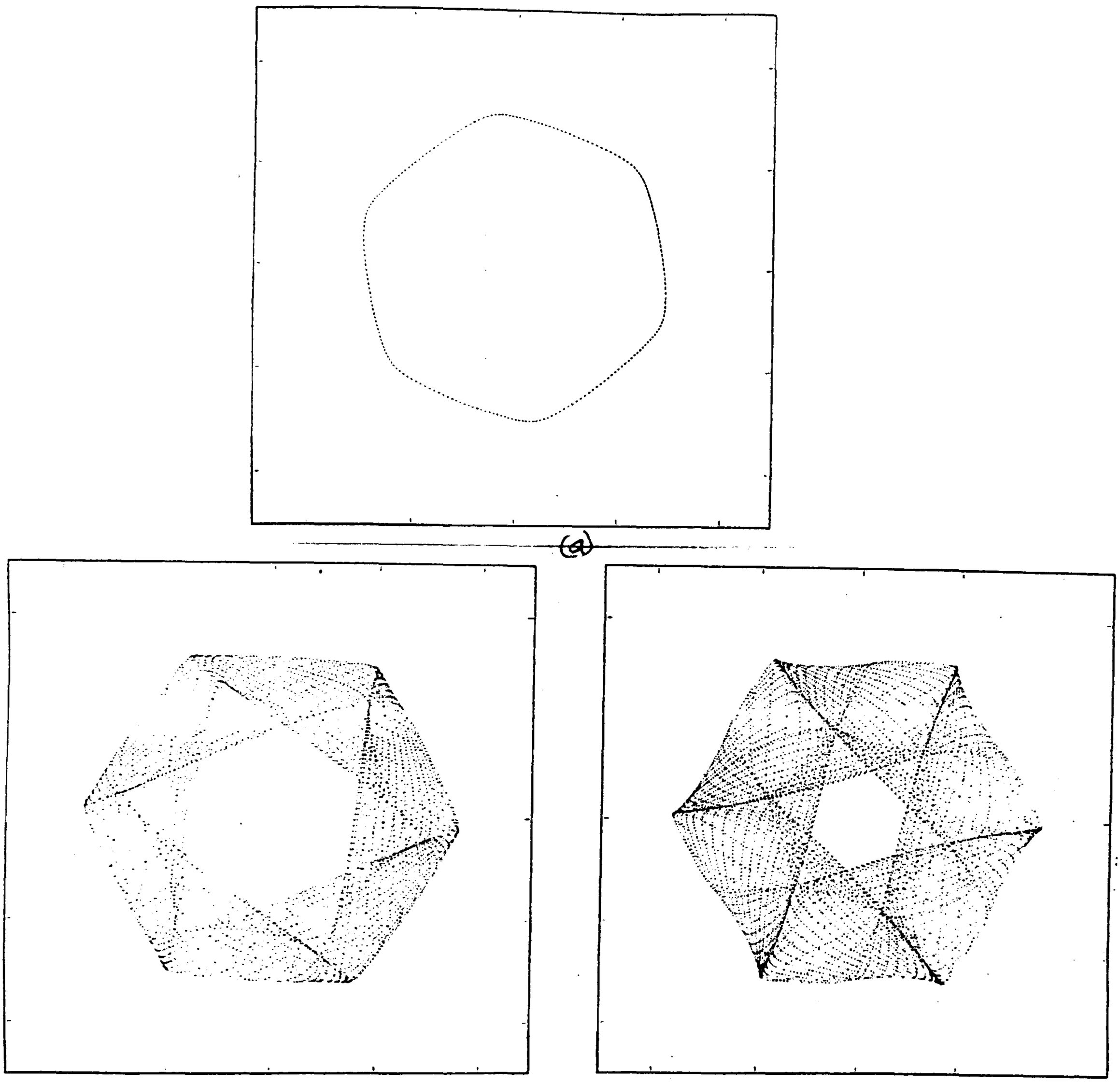

Figure 4.11:
Numerical simulations with symmetric waveform oscillators. (a) The stable rotating wave, $\delta = .05$ (b) After the Hopf bifurcation, $\delta = .12$ (c) Near the saddle node of tori $\delta = .125$. Note that at this loss of stability, the limits of the periods are regular, unlike with the homoclinic where one of them goes off the infinity as the bifurcation is approached. The boxes surrounding the pictures are 10V square.

4.1.7 Results and conclusions

The weak coupling limit is $\epsilon \to 0$, with δ fixed. The finite δ ensures that invariant three-torus in $\mathbf{R}^7$ is normally hyperbolic. The parameter δ can be related to a phase shift between V_c and V_i. When ϵ and δ are varied in the experiments, we observe that δ determines which solutions are stable, while the speed of evolution in the ϕ plane is proportional to $\epsilon\delta$. For instance, with symmetric waveforms, the Hopf bifurcation occurs at $\delta = 0.107$ when $\epsilon = 0.32$ and at $\delta = 0.085$ when $\epsilon = 0.032$. The second frequency introduced by the Hopf bifurcation is roughly proportional to ϵ.

The time scale for charging C_0 by the negative resistor is $C_0/|a|$. The nonzero Floquet exponent of the limit cycle of a single van der Pol oscillator depends on the function $\Gamma(V)$, but it is roughly some positive constant times $\Gamma(0)$ (recall that $\Gamma(0) < 0$). Thus in the limit $\epsilon \to 0$ the Floquet exponents for the three-torus are approximately:

$$(0, 0, 0, \Gamma(0), \Gamma(0), \Gamma(0), -3\delta).$$

The four negative exponents show that trajectories converge exponentially onto the normally hyperbolic invariant three-torus. When the coupling is small the four negative exponents do not change very much, but two of the zero Floquet exponents will become of order $\epsilon\delta$ (with either sign). The two Floquet exponents proportional to $\pm\epsilon\delta$ are the eigenvalues of the linearisation of the dynamics in the ϕ plane. We do not attempt to average the 7th order system to get the ODE in the ϕ plane, so we do not calculate these eigenvalues.

In the experiments we observe that the in-phase solution occurs at larger values of δ than the rotating wave solutions. A simple physical argument explains why this is so. To a first approximation in the weak coupling limit we may regard the van der Pol oscillators as sine wave generators. A simple calculation then yields the transfer function

$$\frac{< V_c^2 >}{< \bar{V}^2 >} = \frac{1}{1 + (3\delta)^{-2}}$$

where the angle brackets represent the time average, and

$$\bar{V} = \frac{1}{3}\sum_{i=1}^{3} V_i$$

The form of the transfer function reveals that our coupling network acts as a low pass filter. For small δ, $V_c \approx 0$ independent of $\bar{V}$, while $V_c \approx V$ for large δ. The rotating wave minimises $< \bar{V}^2 >$, and the in-phase oscillation maximises it, subject to the weak coupling constraint that $< V_i^2 >$ is constant. If the capacitor will not oscillate (δ small), the system prefers not to drive it, and the rotating wave is stable. If the capacitor oscillates easily (δ large) then the system chooses to drive it as hard as possible, and in-phase oscillation is referred.

Thus, we have predicted and observed a new type of bifurcation, the $\mathbf{S_3}$THB, which occurs in systems of three weakly coupled oscillators. We have not considered effects associated with the breakup of the three-dimensional torus which occurs with large coupling. This would require us to work with the Poincaré map rather than the flow, allowing it to become non-invertible as the torus breaks up (in analogy with non-invertible circle maps.) Along these lines, Aronson et al. [12] have studied the period doubling of the in-phase oscillation in $\mathbf{S}_n$ symmetric systems of oscillators. The invariant $\mathbf{T}^n$ is long gone before this period doubling can occur.

4.2 Forced identical oscillators

4.2.1 Symmetric Chaos

The idea of distinguishing between different symmetries of chaotic attractors is not new. Kitano et al. [79] investigate an analogue circuit simulating a delay-differential equation from nonlinear optics. They find that in their $\mathbf{Z}_2$ symmetric system, symmetry that is broken by steady-state bifurcations can be recovered by a crisis in the attractors. The idea of symmetry-forced crises is a natural extension of the ideas expounded in [58], but has mostly been applied to systems with $\mathbf{Z}_2$-symmetry, for example [125] who investigate a $\mathbf{Z}_2$- equivariant map associated with the Lorenz equations.

Motivated by their studies of $\mathbf{D}_n$-equivariant maps of the plane, Chossat and Golubitsky [33] hypothesise the existence of generic symmetry increasing bifurcations of attractors, where a group orbit of attractors can collide to form an attractor of higher symmetry, i.e. there is an increase in the symmetry of the minimal attractor. This parallels the applications of group theory to bifurcations of regular dynamics in symmetric systems; see chapter 1.

In attempting find such phenomena, electronic circuits are convenient systems to work on [130], and forced systems are good candidates for looking for chaotic return maps, the mechanism of how they produce these being well understood, see [61, 56].

The circuit described below can be approximated by integrating a non-autonomous system of ODEs on $\mathbf{R}^7$ or $\mathbf{R}^9$ (for three or four oscillators respectively), giving a Poincaré mapping at a frequency of up to 10kHz which in itself is not especially high for such a circuit, but is very fast compared to computer integration of approximating equations. The circuit should by thought of as a real physical system with noise and broken symmetry, and as such will not show the artifacts of any numerical method used (e.g. rounding errors). Buskirk and Jeffries [130] also present work on chaotic behaviour in networks of electronic oscillators; they use diode resonators operating at high frequency.

4.2.2 The electronic experiment

All the results displayed are generated by the circuit of forced oscillators shown in figure 4.2. Using the network shown in figure 4.3, the resulting stroboscopic map is displayed on an oscilloscope X-Y plot. For producing a high resolution paper copy, the data is sampled using a two channel high resolution (16 bit) analogue to digital interface. The resulting files of X-Y coordinates are plotted using a 1024 by 1024 grid on a laser printer.

The circuit can be though of as a group of symmetrically coupled van der Pol oscillators with an extra forcing oscillator provided by the signal generator.

The oscillators

The oscillators are shown in figure 4.1 and described in section 4.1. In all the subsequent experiment, the oscillators are producing **asymmetric** waveforms, as set by the symmetry switch. The oscillators are coupled together using the phase shift network shown in figure 4.2, but this time using the forcing input, as described below.

The forcing

This is achieved using a signal generator generating a sinusoidal signal at a set amplitude with zero DC offset. For small amplitude forcing, at frequencies far from resonance, we

expect to see two-frequency quasiperiodic motion built up from the frequencies of the oscillators and those of the forcing oscillator. This corresponds to an attracting 2-torus for the dynamics, and would be observable as a limit cycle in the Poincaré section; it can be seen in figure 4.12(a). The most interesting behaviour is found away from the m:1 resonances. Near these, the system usually locked onto a periodic or for all forcing amplitudes above a certain value.

The visualisation of the dynamics

Although one idea of visualising the dynamics might be to plot time series of the signals generated by the circuit, this format gives us information about the dynamics in a very encoded manner. A better idea is to suppress the time dependence and plot one signal against the other, especially if the symmetry of the circuit can be related to the visualisation.

Generalising the equivariant projection given in figure 3.1 to a group of n oscillators, we project the vector in $\mathbf{R}^n$ representing the voltages of the n oscillators onto R^2 by assigning one of n unit vectors (separated by angles of $2\pi/n$) to each oscillator and constructing the vector sum of the voltages along these directions (see figure 4.4(b)). While this cannot show an accurate picture of the phase space for more that three oscillators, the restriction of using two dimensional representations of the results forces this. By using a stroboscopic method to show the trajectories at one of the zero-crossing points of the forcing oscillator [16], we can distinguish between limit cycles, tori and a variety of other behaviour, and also hypothesise links with the results known for dissipative low-dimensional dynamical systems and in particular mappings of the circle and the torus.

In general, these mappings will have to be far from the identity and non-invertible in order to produce the observed results. This is a $\mathbf{D}_n$ equivariant projection of an $\mathbf{S}_n$ equivariant map on $\mathbf{R}^{2n+1}$, and as such there is no objection to attractors having non-empty intersection, unlike mappings on the plane.

Recently, King and Stewart [78] have found numerically that there exist $\mathbf{D}_3$ maps of the plane with chaotic attractors having only $\mathbf{Z}_3$ symmetry.

4.2.3 The equations governing the system

Equation 4.1 easily generalises to n oscillators, describing of motion of the $n+1$ voltages $\{V_1, \ldots, V_n, V_c\}$. Non-dimensionalising the equations, but this time leaving the forcing gives:

$$\begin{aligned} \ddot{V}_i + \Gamma(V_i)\dot{V}_i + V_i &= \epsilon(\dot{V}_c - \dot{V}_i) \\ \dot{V}_c &= \delta\left(\sum_{i=1}^{n} V_i - nV_c + F\cos\nu t\right) \end{aligned} \tag{4.7}$$

In the results presented, $\omega_0 \sim 30 \times 10^3 s^{-1}$, $\epsilon \sim 0.32$ and $\delta \sim 0.15$ so that for $A = 0$, the rotating waves are observed to be stable and there are no other stable dynamics. Since the characteristic (unforced) frequency varies between 4.2kHz ($\delta \sim 0.15$) and 3.4kHz ($\delta \sim 1$), the ratio of this to the forcing frequency, $\nu = (\omega/\omega_0)$, can be calculated and is away from primary resonance in each of the illustrated cases, but note the variation in the unforced frequency means we should be careful about making assumptions about the importance of ν.

Transients The sequences show the coupling capacitor at a value where the rotating wave is marginally stable if no external forcing is applied. For low amplitude forcing at any given frequency, there is a $\mathbf{Z}_n$-symmetric pattern which is a 2-torus for a set of parameter values of almost full measure. As we increase the amplitude at a fixed frequency, the sequences show a variety of breakdowns to full $\mathbf{S}_n$-symmetric chaos.

Figures 4.12- 4.14 are taken after transients had been allowed to die away, as far as is possible to tell. In practice this meant waiting 10 or 20 seconds (approx. 10^5 iterates) to see if the pattern on the oscilloscope had stabilised. All of the sequences shown below are taken following one another using the same tuning of the coils, in order to minimise the effect of drift of parameters within the circuit.

4.3 Symmetric chaos: experimental results

4.3.1 Three oscillators

Figures 4.12 and 4.13 show the three oscillator system with C=21.4nF ($\delta = 0.148$) forced at 6.370kHz ($\nu = 1.5$) and 9.510kHz ($\nu = 2.25$) respectively. Not shown are many intermediate transitions, but the basic route for figure 4.12 is frequency locking via intermittency and a saddle-node bifurcation to a 3:2 periodic orbit. This compares well with mode-locking of a circle map (see e.g. [61]). The periodic orbit then breaks down through period-doubling and Hopf bifurcation to a noisy attractor. All the while, the $\mathbf{Z}_3$ symmetry is preserved until at $A \sim 3.60$V, the two $\mathbf{Z}_3$ attractors collide to form one with $\mathbf{S}_3$ symmetry. Note that as observed in [33], this crisis is associated with the appearance of a large background of points, where the trajectory is changing from the remnants of one $\mathbf{Z}_3$ attractor to the other.

The colour figure 4.13 shows the sampled voltages for the different forcing frequency. This sequence involves a Hopf bifurcation to a 3-torus (not shown), a collision of a 3-torus and the 2-torus shown in (a). Increasing the forcing amplitude further leads to a chaotic attractor with $\mathbf{Z}_3$ symmetry (b), (c) which collides with its conjugate in to give (d) $\mathbf{S}_3$ chaos. The figures are coloured by distance on the plane between successive iterates; for a sampled sequence $\{(x_i, y_i) : i = 1, \cdots, n\}$ of pairs of signed 16 bit numbers from the A-D converter, we colour the ith point according to

$$r = \sqrt{(x_i - x_{i-1})^2 + (y_i - y_{i-1})^2}.$$

taken modulo some m (typically a few hundred). For $r = 0$, we colour the point red, and cycle through the spectrum to violet at $r = m$, using (normalised) red, green and blue levels R, G, B given by

$$\begin{aligned} R &= 1 + \cos(2\pi r/m) \\ G &= 1 + \cos(2\pi(r/m + 1/3)) \\ B &= 1 + \cos(2\pi(r/m + 2/3)). \end{aligned}$$

The extra dimension of colour allows us to examine more closely any apparent intersections between strands of this projection of the attractor. In figure 4.13(b), note that many of the strand of different colours that cross over are disconnected, whereas some of the more 'fuzzy' regions exhibit smooth changes in colour.

4.3.2 Four oscillators

Figure 4.14 shows four forced oscillators coupled by C=25nF ($\delta = 0.126$) with the forcing at 9.500kHz ($\nu = 2.26$). The system is given impulses (by interrupting the

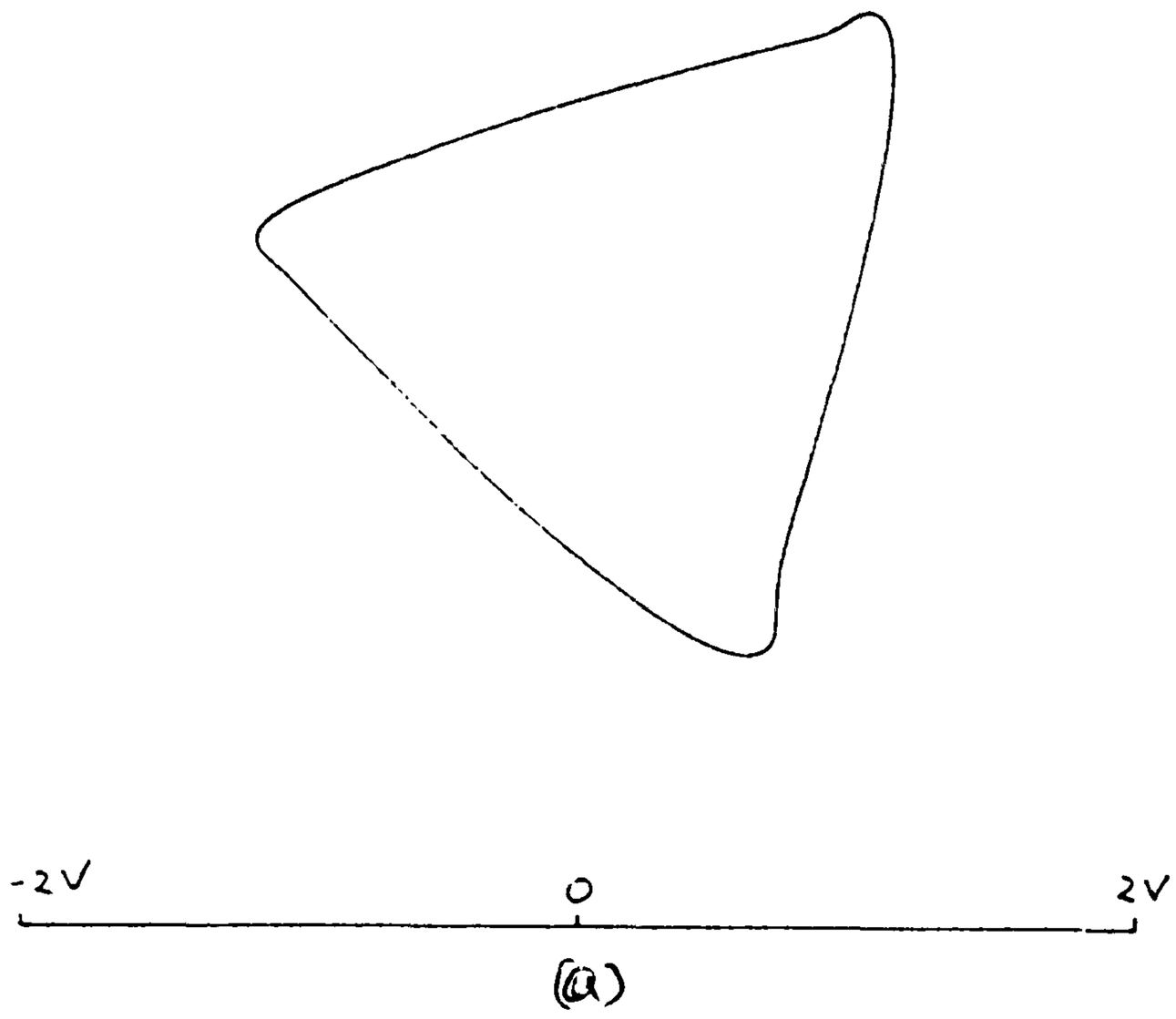

Figure 4.12:
The sequence (a) to (h) (continued on next figure) shows a sequence of plots for samples of the output from three identical oscillators coupled with $\mathbf{S_3}$ symmetry and sinusoidally forced at a frequency of 6.370kHz. The pictures show some of the states observed as the forcing amplitude increases from zero. The transients have died away, leaving just the attracting dynamics. In all of the captions, the forcing amplitude A is given in volts a.c. (rms). All of the pictures in figures 4.12-4.14 are shown to the same scale. (a) Shows the attractor being a 2-torus combining the natural frequency and the forcing frequency. The natural frequency has a stable rotating wave ($2\pi/3$ phase shift between the oscillators), and the $\mathbf{Z_3}$ symmetry of this state is reflected by the $\mathbf{Z_3}$ symmetry of the picture. A=0.8; Iterates=4096. (b) The oscillators have mode-locked into a 3:2 resonance with the forcing frequency. Intermittency is observed just before the appearance of this orbit, suggesting that it appears from a saddle-node bifurcation of limit cycles occurring on the 2-torus. A=1.44; Iterates=8192. (c) A period-doubling bifurcation of the 3:2 resonance gives a 6:4 resonant periodic orbit. A=3.17; Iterates=8192. (d) The period-doubled solution undergoes a Hopf bifurcation to a 2-torus, but still with 6:4 resonance. A=3.37; Iterates=8192.

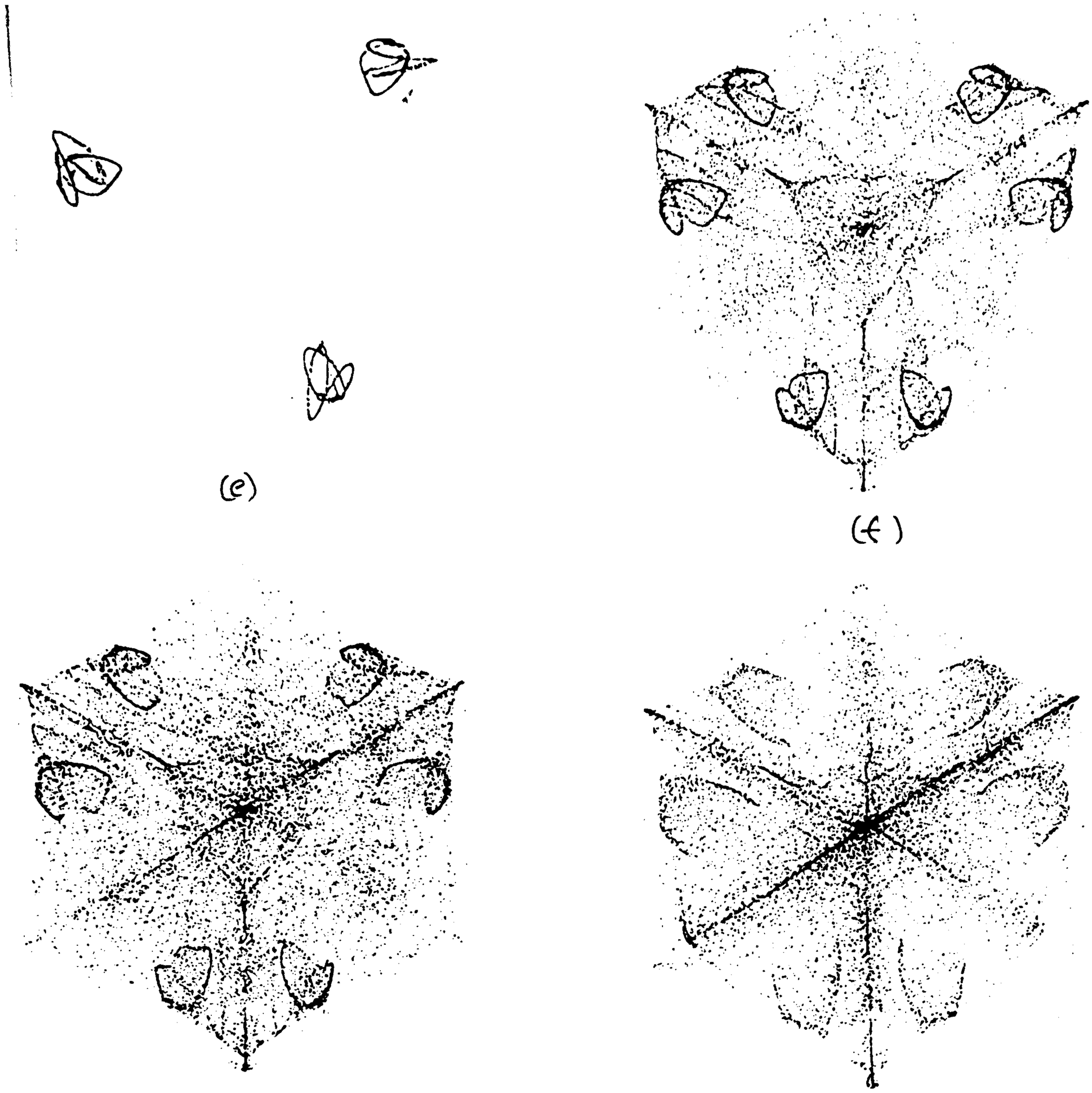

(continued from previous figure) (e) The limit cycle becomes blurred by noise and/or deterministic chaos, whilst retaining its $\mathbf{Z}_3$ symmetry. This manifests itself as a mean phase shift of $2\pi/3$ between the oscillators. A=3.59; Iterates=16384. (f) There is a crisis as the two symmetrically related but unconnected attractors collide to form a chaotic attractor with full S3 symmetry. Noticeable are the remains of the attractors shown in (e), and the trajectory lingers for a long (but irregular) time in one of these two states before switching to the other. A=3.62; Iterates=32768. (g) and (h) show the evolution of the attractor at A=3.66 and 3.92 respectively. The fine structure shown in f) gradually becomes less noticeable and the mean switching time between the remnants of the two $2\pi/3$ attractors becomes shorter. Above A=3.92, the system locks into one particular 3:2 resonance associated with an imperfection in the system. We can see the precursor of this in the form of excessive thickening of the line corresponding to $V_1 = V_3$. This happens on other oscillators dependent on the fine tuning of the system. Iterates=32768 in both pictures.

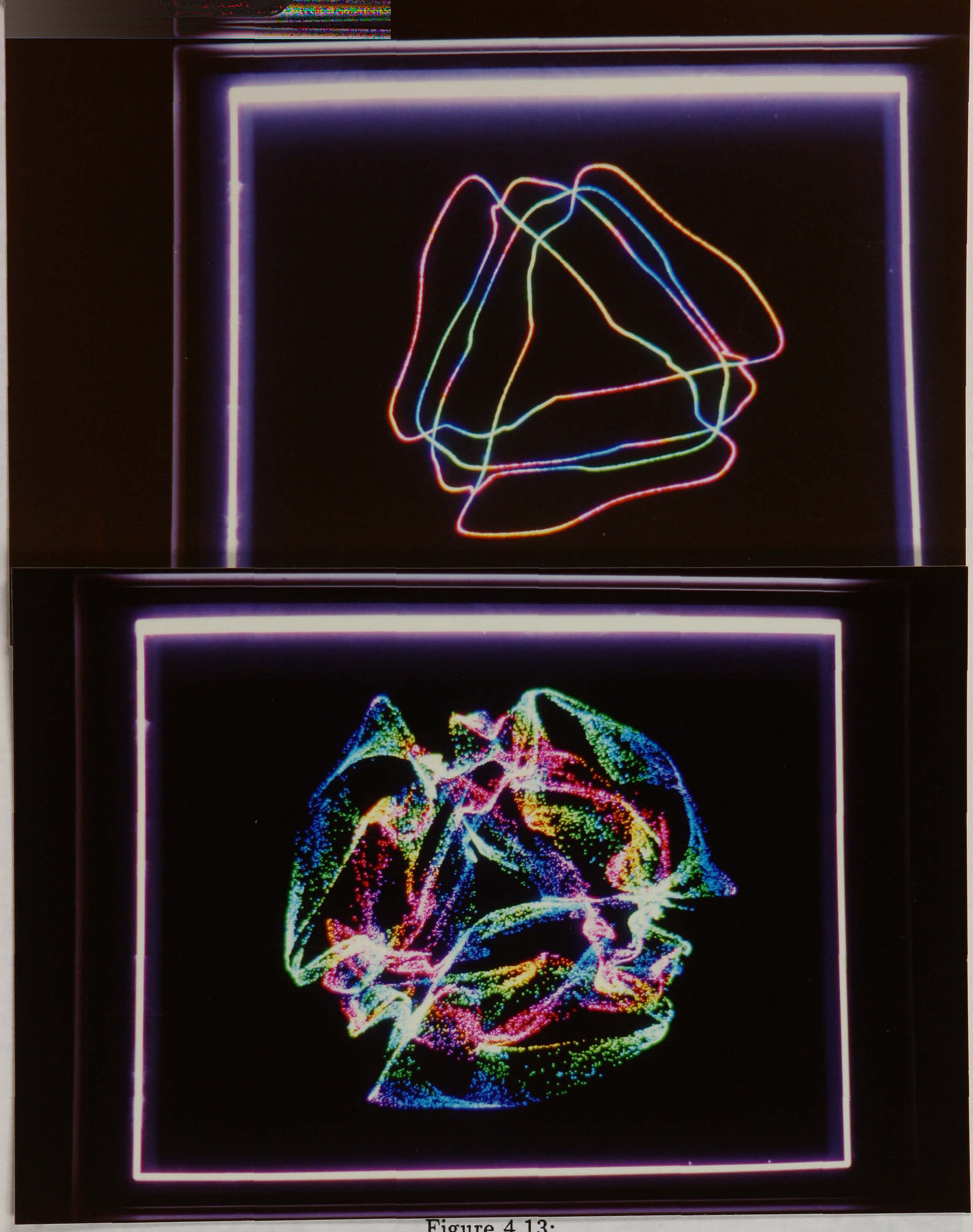

Figure 4.13:
These figures are coloured according to the distance between iterates. The addition of this extra dimension allows us to separate features that are projected to the same point without the colouring. (a) This 2-torus is hysteretic with an attracting 3-torus (not shown) over the range A=2.6 to 3.1. It is partially mode-locked to some harmonic of the oscillators. A=3.08; Iterates=16384. (b) The 2-torus thickens to form a noisy attractor with apparent dimension between 2 and 3. There is much folding of the attractor due to the presence of hyperbolic structures in the dynamics. Especially interesting is the persistence near a few selected points, close to a stable limit cycle of large period (not shown, but observed to appear via a saddle-node bifurcation at slightly higher values of A). A=5.20; Iterates=24576.

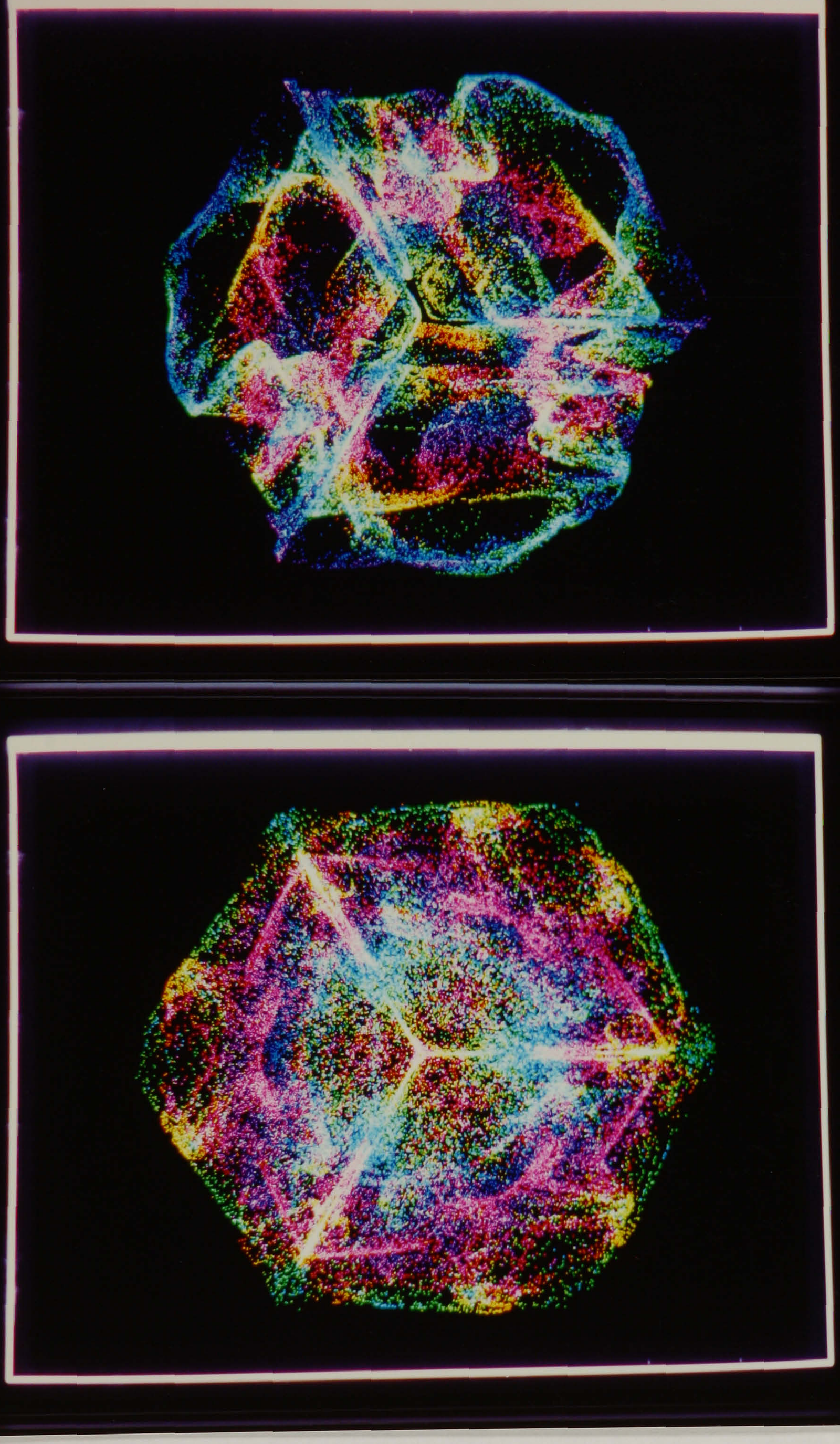

(continued from previous figure) (c) This shows the breakdown of the fine structure in e), but the attractor still shows the presence of an average $\mathbf{Z}_3$ symmetry. A=5.98; Iterates=32768. In (d) we finally arrive at $\mathbf{S}_3$-symmetric chaos through the collision of $\mathbf{Z}_3$ attractors. A=7.04; Iterates=32768.

power supply) until it selected one of the rotating waves that has $\mathbf{Z}_4$ symmetry in the projection. Then the amplitude of the forcing is increased. The transition to $\mathbf{S}_4$ chaos happens at $A \sim 6.0$V.

Other routes to $\mathbf{S}_4$ chaos are shown in [14] and can include torus doubling bifurcations.

4.3.3 Symmetric chaos; discussion

The mechanism by which fully symmetric chaos is reached in this system is a mixture of subharmonic and Hopf bifurcations to give chaotic attractors of low symmetry. In particular the results show initial breakdown of the 2-torus via saddle-node of limit cycle, Hopf and 2-torus doubling bifurcations, see [89]. The resulting chaotic attractors can collide to create ones with higher symmetry, in the way that [33] describe.

It is possible to identify tori with up to three incommensurate frequencies, circle map behaviour, and possible chaotic attractors with dimensions between 2 and 3, but there are transitions which indicate that not all of the dynamics can be embedded in a 3-torus [14]. This necessarily implies that using a map from a 2-torus to itself will not give all the transitions. Note that although the system of equations is $(2n + 1)$-dimensional with periodic forcing, the return maps generated on the oscilloscope show many of the properties of the non-invertible maps of the plane studied by Chossat and Golubitsky. One difference is that they use a small amplitude hypothesis to work with a truncated Taylor series, something which cannot be justified here.

The reason for symmetry-increasing bifurcations here can be explained thus: we start with the only stable solutions having lower symmetry than that of the system. Upon forcing the system, these solutions become chaotic and the attractors grow in size until they meet the unstable periodic orbits dividing the phase space. A crisis occurs and the trajectories on one attractor can to jump across the phase space into the basin of another conjugate attractor. Thus the average symmetry of the chaotic solution increases.

The theory of symmetric bifurcations in chaotic attractors is as yet comparatively undeveloped, and current work of Dellnitz, Golubitsky and Melbourne (pers. comm.) and Krupa and Roberts [81] indicates that a lot can be said about how symmetry constrains the bifurcations of chaotic attractors. For example, Dellnitz et al. have shown that using a suitable (strong) definition of an attractor, a chaotic attractor of a $\mathbf{D}_n$ equivariant map of the plane with full symmetry must have at one connected component for n odd and at most two connected components for n even.

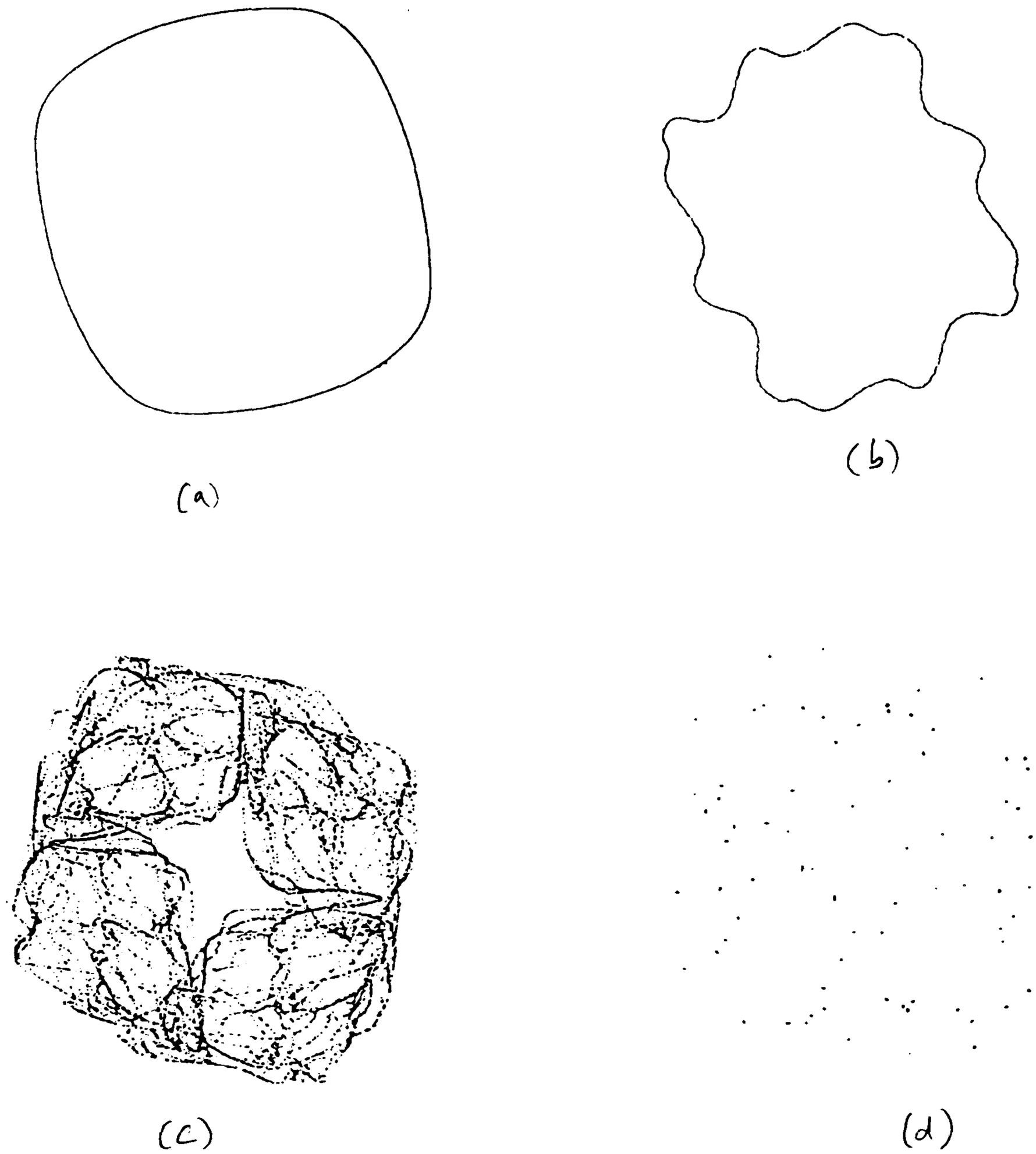

Figure 4.14:
The pictures (a) to (f) (continued on next figure) show a typical observed sequence of breakdown of a system of four identical oscillators obtained from a stable $\mathbf{Z}_4$ rotating state by forcing the system at a frequency 9.500kHz. (a) This shows one of the six possible rotating waves on four oscillators, chosen so that the projection has $\mathbf{Z}_4$ symmetry. A=0.574; Iterates=8192. (b) Resonance causes the torus to wrinkle, suggesting the presence of nearby unstable dynamics. A=3.81; Iterates=8192. (c) A hysteretic jump (b)-(c) gives rise to this attractor showing a large amount of fine structure, but still with $\mathbf{Z}_4$ rotational symmetry. A=4.51; Iterates=32768. (d) A periodic orbit of period about 75 times the forcing period appears, remaining remarkably stable (this pattern is held for a matter of minutes at about 10kHz forcing). It is interesting to note that the dots are widened by noise in the direction where the limit cycle (e) will appear. This is probably due to the noise acting most strongly in the direction of the weakest contracting eigenvalue of the linearisation about the periodic orbit. At the saddle-node (d)-(e), this eigenvalue goes through zero. A=4.91; Iterates=16384.

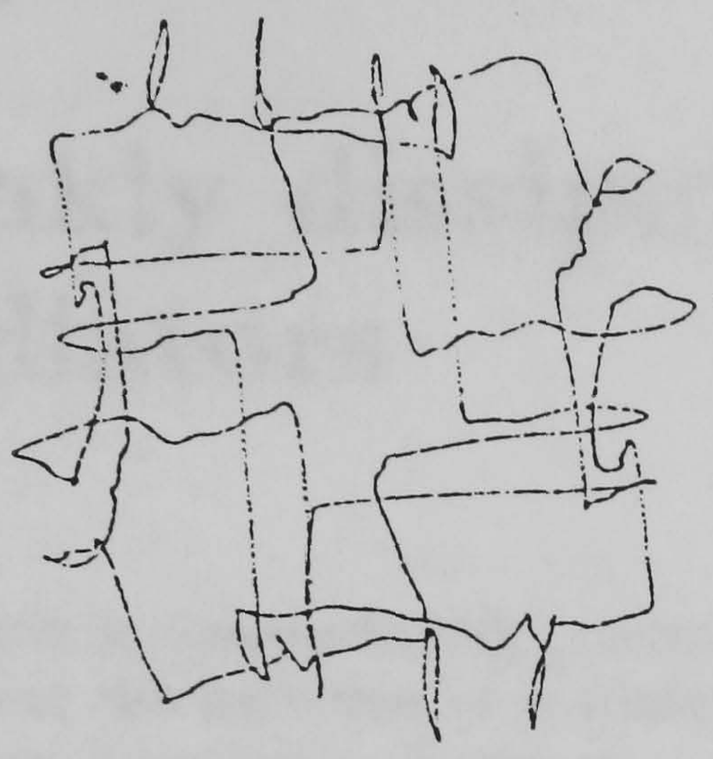

(e)

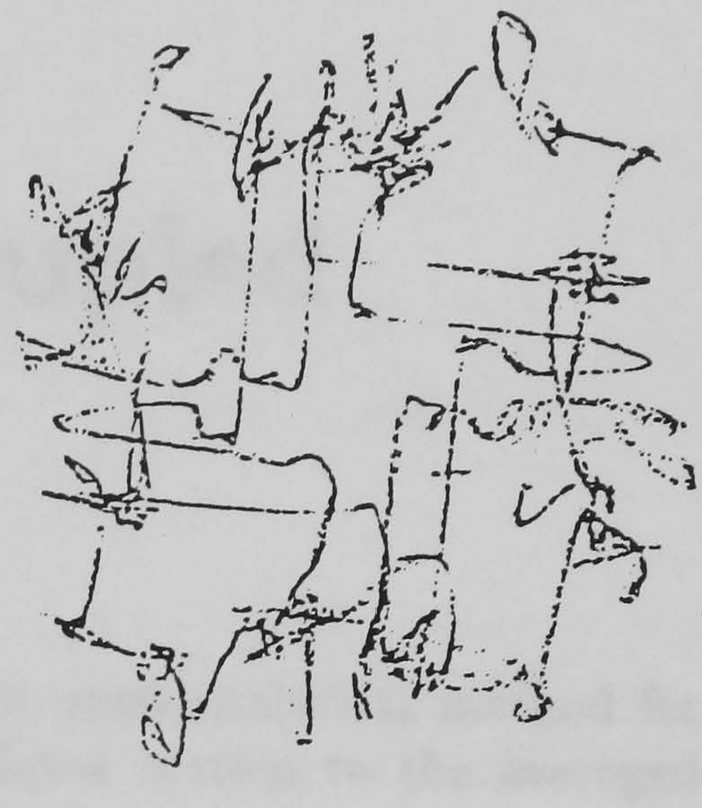

(f)

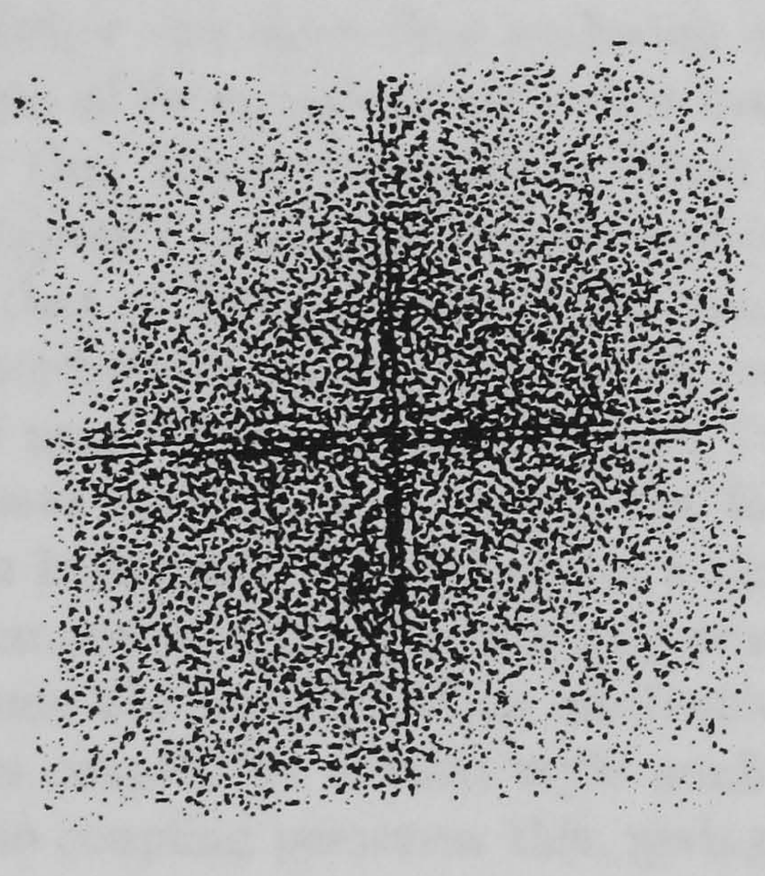

(g)

(continued from previous figure) (e) A heteroclinic bifurcation of the periodic orbit in (d) gives rise to the 2-torus shown here. Note that the $\mathbf{Z}_4$ symmetry is not perfect, but that it is identifiable. A=5.16; Iterates=8192. (f) The torus in (e) gives way to $\mathbf{Z}_4$ chaos. A=5.63; Iterates=32768. (g) The six $\mathbf{Z}_4$ symmetric attractors collide to give fully S4-symmetric chaos. The lack of structure in the pattern (apart from the folds), is probably due to the fact that six pictures like (f) are superimposed on each other (cf. figure 4.4(d)). A=6.16; Iterates=61440.

Chapter 5

Weakly dissipative coupled oscillators

This chapter is concerned with providing a semi-rigorous, semi-analytical method for carrying out the reduction of a weakly coupled n oscillator system to the averaged normal form described in chapter 2.

We develop a method for treating strongly nonlinear oscillators that are close to planar Hamiltonian systems, under the assumption of weak dissipation and weak coupling. For a group of n oscillators weakly coupled by arbitrary functions, we construct the action-angle variables explicitly and show slow evolution equations for the actions and angles, reducing to a system of $2n$ equations with slow evolution. Under a further assumption of coupling weaker that dissipation (and identical oscillators) we get a set of n equations of the form of chapter 2 which are the averaged equations on the n-torus.

The method is similar to that of Bourland and Haberman [26, 88] for single oscillators with slowly varying coefficients, and is a variation on the Melnikov method [61, 133] for periodic orbits of near integrable systems and an explicit application of averaging in a strongly nonlinear setting. It relies on the fact that the trajectories of the system deviate from the integrable trajectories on a slow timescale. Note that *singular* nonlinear oscillators cannot be treated in the way presented.

As an example, we give some observations of an electronic simulation of two van der Pol-Duffing type oscillators coupled by a cubic-style nonlinearity. The oscillators each have $\mathbf{Z}_2$ symmetry and the coupling preserves this, giving a system with $\mathbf{Z}_2 \times \mathbf{Z}_2$ symmetry.

We apply the theory to this system with assumptions on the orders of magnitude of the coupling and dissipation, and similarities and differences are noted from the experimental observations. As the Duffing oscillator can be integrated in terms of elliptic functions, it would be possible to give expressions for the slow equations in terms of these, and give analytical expressions for the loss of stability of the in-phase solution in the case of cubic coupling and a limiting set of parameter values.

Given two limit cycles on the plane coupled by dissipative linear coupling, we give a sufficient condition for the in-phase solution to be stable.

Finally we discuss the inheritance of reversibility from the Hamiltonian system to the averaged equation and suggest a way of asymptotically perturbing the integrable oscillator to break this artificial symmetry.

5.1 Groups of oscillators with weak dissipation and coupling

Many authors have studied the coupling of nonlinear oscillators using simple two degree of freedom oscillator, notably the van der Pol [109] oscillator

$$\ddot{x} + (x^2 - \mu)\dot{x} + x = 0$$

and the Duffing oscillator

$$\ddot{x} + x^3 \pm \mu x = 0.$$

Combining the nonlinear dissipation term of the van der Pol oscillator with the nonlinear response of the Duffing oscillator gives us the van der Pol-Duffing oscillator [71, 61]

$$\ddot{x} + (x^2 - \nu - x^2)\dot{x} + x^3 \pm \mu x = 0 \tag{5.1}$$

which (in the regime of weak nonlinearity) can be viewed as a generic perturbation of linear simple harmonic oscillator in a dissipative setting. A lot of work has been done to weakly couple weakly nonlinear oscillators of this form [112], and Bogoliubov's method of averaging [23, 61] has been used extensively in such systems.

5.1.1 Isochrons and oscillators

The oscillators we discuss in this chapter have in general a period which depends on the amplitude of the oscillation; this is related to the concept of isochronicity, [136, 137, 112], or 'twist' described by Ermentrout to be necessary for the formation of spiral waves (as opposed to pinwheel wave) in oscillator arrays.

Isochrons are defined by [60] to be points in the neighbourhood of an attracting limit cycle which have asymptotically the same phase as some point on the limit cycle. More precisely, Guckenheimer [60] proves that given a flow $\Phi : M \times \mathbf{R}^+ \to M$ with a stable limit cycle γ, with period T then the *isochron* for a point $g \in \gamma$ is the set

$$I_g = \{s \in M : |\Phi(s,t) - \Phi(g,t)| \to 0 \text{ as } t \to \infty\}$$

which defines, a local stable set for each point on the limit cycle. One way to see this is to consider the action of the time T map on the phase space, and consider the stable manifold of each point on the limit cycle (which is now a fixed point with one degenerate direction). Isochronous oscillators are usually referred to as those whose isochrons are straight lines, for example the simple harmonic oscillator. We do not use isochrons for the systems studied in this chapter: in the limit of no dissipation the limit cycles are neutrally stable. Instead, we use the angle variables for the Hamiltonian system. We use the word *nonisochronous* to mean that the period of the Hamiltonian system is dependent on its energy.

5.1.2 Weak coupling and dissipation; slow variables

Definition 5.1.1 *A* weakly coupled weakly dissipative (WCWD) *network of n coupled nonlinear two dimensional identical oscillators is a set of equations:*

$$\ddot{v}_i + \frac{dU}{dv_i}(v_i) = \epsilon(f(v_i, \dot{v}_i) + \sum_{j=1}^{n} g(v_i, v_j, \dot{v}_i, \dot{v}_j)) = \epsilon F_i \tag{5.2}$$

where $\epsilon \ll 1$ and i runs through $1 \ldots n$, U, f, g are C^∞ and $U(v) \to \infty$ as $|v| \to \infty$ for some M. We assume pairwise coupling with S_n symmetry of the network.

Note that the method does not depend at all on S_n symmetry or pairwise coupling, and the fact that f and U are the same for all oscillators means we have an identical oscillator network as defined in chapter 2.

The equation for each oscillator is a perturbation of a Hamiltonian oscillator with Hamiltonian:

$$H(v, \dot{v}) = \frac{\dot{v}^2}{2} + U(v) = \alpha \tag{5.3}$$

and α is constant when $\epsilon = 0$. We shall suppose that the contours of H are closed curves for all values of α except a finite set $\mathcal{E} = \{\alpha_0, \alpha_1, ..., \alpha_k\}$ where the contours are not smooth and represent heteroclinic or homoclinic orbits in equation 5.3. We shall consider an open neighbourhood of $\mathcal{E}$ removed from the range of α for convenience. As an example, consider the potential and phase portrait shown in figure 5.1.

By perturbing such a system we get a system of slow equations for the change of energy and change of phase of each oscillator. There are some delicate considerations to be made in this process, however. In particular, for defining a useful notion of phase, it is helpful to normalise the period on the level curves in the following manner:

Define $\omega(\alpha)$ such that all solutions $z(\alpha, \psi)$ of the equation

$$\frac{\omega^2}{2}\left(\frac{\partial z}{\partial \psi}\right)^2 + U(z) = \alpha \tag{5.4}$$

have period 2π in ψ for $\alpha \notin \mathcal{E}$ and such that:

$$z(\alpha, 0) \text{ is a maximum of } z.$$

Note that $2\pi/\omega$ is the *period* of the solution to equation 5.3. The curves of constant α are called the *normalised periodic orbits* and ψ the *normalise phases*. Together they are called the *action-angle coordinates*, and we shall look for solutions of equation 5.2 ($n = 1$ for simplicity) of the form:

$$v(t) = z(\alpha(t), \psi(t)) \tag{5.5}$$

with

$$\psi(t) = \int_0^t \omega(\alpha(t))dt + \phi(t).$$

We shall demonstrate that ϕ and α are slowly varying on a timescale $T = \epsilon t$. Since we have increased the number of variables to two, we are at liberty to apply a constraint relating α and ϕ implicitly:

$$\frac{dv}{dt} = \omega(\alpha)\frac{\partial z}{\partial \psi}(\alpha, \psi) \tag{5.6}$$

If we seek solutions of equation 5.2 of the form eqn 5.5 and include the constraint equation 5.6, by differentiating the former with respect to t, we get:

$$\dot{\alpha}\frac{\partial z}{\partial \alpha} + \dot{\phi}\frac{\partial z}{\partial \psi} = 0. \tag{5.7}$$

5.1.3 A property of the normalised periodic orbits

The normalised periodic orbits $z(\alpha, \psi)$ are defined such that they are differentiable in both α and ψ, and all derivatives are periodic in ψ. Assuming z is sufficiently smooth, their derivatives satisfy a *very useful relation*, as we will show. In all the below discussion, $\frac{\partial}{\partial \psi}$ is at constant α and $\frac{\partial}{\partial \alpha}$ is at constant ψ.

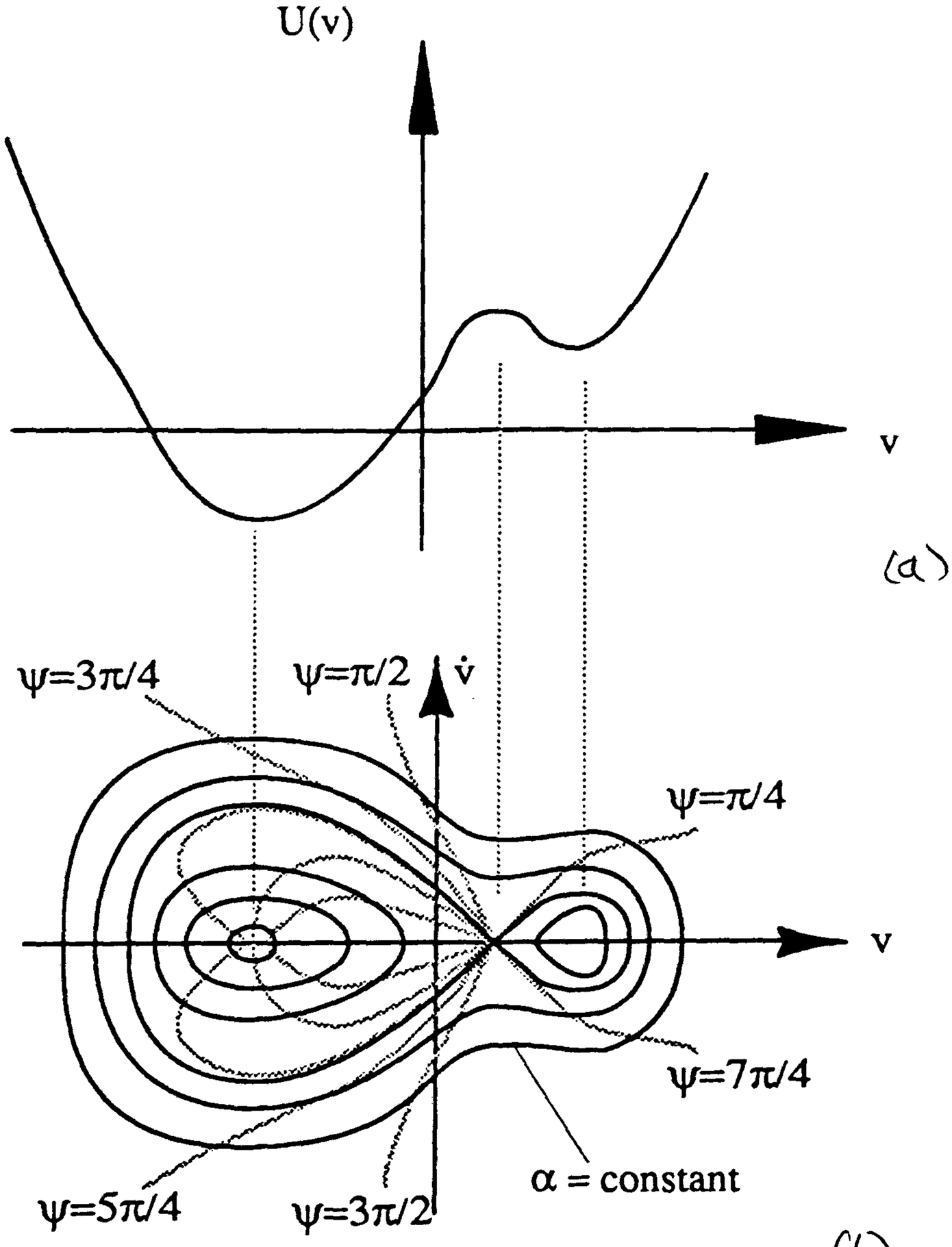

Figure 5.1: (a) shows an example potential $U(v)$, while (b) shows the phase portrait for the Hamiltonian oscillator $\ddot{v} + U'(v) = 0$ with the action-angle coordinates marked.

We write the differentials

$$\frac{\partial z}{\partial \alpha} = z_{,\alpha}$$

and

$$\frac{\partial z}{\partial \psi} = z_{,\psi}.$$

Differentiating eqn 5.4 with respect to ψ we obtain:

$$\omega^2 z_{,\psi\psi} + U'(z) = 0 \tag{5.8}$$

while differentiating eqn 5.4 with respect to α we obtain:

$$\omega \left[\omega z_{,\psi} z_{,\alpha\psi} + \omega_{,\alpha}(z_{,\psi})^2\right] + U'(z) z_{,\alpha}(z) = 1 \tag{5.9}$$

Now substituting eqn 5.8 to eliminate U', we obtain the VERY USEFUL RELATION:

$$\omega \left[\omega z_{,\psi} z_{,\alpha\psi} + \omega_{,\alpha}(z_{,\psi})^2 - \omega z_{,\psi\psi} z_{,\alpha}\right] = 1 \tag{5.10}$$

This is explicitly independent of the potential U, and reduces to the formula $\cos^2\psi + \sin^2\psi = 1$ when $U(z) = -z$ and the oscillators are simple harmonic (and isochronous).

5.1.4 The slow timescale evolution equations

Differentiating eqn 5.6 with respect to time t, we get:

$$\frac{d^2 z}{dt^2} = \dot{\alpha}\left(\omega_{,\alpha} z_{,\psi} + \omega z_{,\psi\alpha}\right) + \omega(\omega + \dot{\phi}) z_{,\psi\psi}$$

and therefore in equation 5.2 we get:

$$\omega_i^2 z_{i,\psi\psi} + \dot{\alpha}_i\left(\omega_{i,\alpha} z_{i,\psi} + \omega_i z_{i,\psi\alpha}\right) + \omega_i z_{i,\psi\psi}(\omega_i + \dot{\phi}_i) + U'(z_i) = \epsilon F_i$$

where $\omega_i = \omega(\alpha_i)$ and $F_i \equiv f(v_i, \dot{v}_i) + \sum_{j=1}^{n} g(v_j, \dot{v}_j)$. Using equation 5.8 this reduces to

$$\dot{\alpha}_i\left(\omega_{,\alpha} z_{i,\psi} + \omega_i z_{i,\psi\alpha}\right) + \dot{\phi}_i(\omega_i z_{i,\psi\psi}) = \epsilon F_i. \tag{5.11}$$

Taking the combination:

$$(5.11)\ \omega_i z_{i,\psi} - \ (5.7)\ \omega_i^2 z_{i,\psi\psi}$$

we get:

$$\dot{\alpha}_i \omega_i \left[\omega_i z_{i,\psi} z_{i,\alpha\psi} + \omega_{i,\alpha}\left(z_{i,\psi}\right)^2 - \omega_i z_{i,\psi\psi} z_{i,\alpha}\right] = \epsilon F_i \omega_i z_{i,\psi}$$

and applying eqn 5.10, we arrive at the equation for the slow variation of the actions α_i.

$$\boxed{\dot{\alpha}_i = \epsilon \omega_i z_{i,\psi} F_i.} \tag{5.12}$$

whereas taking the combination:

$$(5.11)\ \omega_i z_{i,\alpha} - \ (5.7)\ \omega_i\left(\omega_i z_{i,\psi\alpha} + \omega_{i,\alpha} z_{i,\psi}\right)$$

gives:

$$\dot{\phi}_i \omega_i \left[\omega_i z_{i,\psi} z_{i,\alpha\psi} + \omega_{i,\alpha}\left(z_{i,\psi}\right)^2 - \omega_i z_{i,\psi\psi} z_{i,\alpha}\right] = -\epsilon F_i \omega_i z_{i,\alpha}$$

and by using eqn 5.10 we get the equation for the slow variation of the angles ϕ_i

$$\boxed{\dot{\phi}_i = -\epsilon\omega_i z_{i,\alpha} F_i.} \tag{5.13}$$

The two sets of equations 5.12 and 5.13 are exact equations for the slow evolution of the system, but note that they are not autonomous; in order to make them more tractable than the original problem, it is necessary to *average* over t and separate the timescales fully; note that we have gone from n second order autonomous ODEs to $2n$ first order non-autonomous ODEs. This reduction is not dependent on the oscillators being identical or identically coupled, but also can be performed for a more general case, as long as WCWD applies.

5.1.5 Averaging the slow equations

Because we have potentially n frequencies in our system, averaging in such a context must be carried out with care, and will not always be possible. We shall consider two cases; very weak coupling, and non-resonant averaging:

Very weak coupling

It is possible to apply the results from chapter 2 to the WCWD systems, by placing a further constraint on the orders of magnitude of the system. Since we require the limit cycles to be strongly attracting in the limit of no coupling, this means that we shall make a hypothesis of *very weak coupling*, VWC, by assuming $||g|| \ll ||f||$ in the neighbourhood of interest.

It is possible that the dissipation function f will permit many stable limit cycles, but we shall assume we turn on the coupling from a state where all the oscillators are on identical hyperbolically stable limit cycles.

The averaging is defined by:

$$< X(t) >= \frac{1}{2\pi}\int_{s=0}^{2\pi} X(s)ds.$$

Assuming that all the oscillators have $\alpha_i = \alpha$, and thus $\omega_i = \omega$, we must have that

$$\dot{\alpha}_i = 0 = \epsilon < \dot{v}_i F_i >= \epsilon < \dot{v}_i\, f(v_i, \dot{v}_i) > +O(\epsilon^2)$$

(recall that $v_i = z_i$, $\dot{v}_i = \omega z_{i,\psi}$) and so this supports our assumption of VWC, through

$$< \dot{v}_i g(v_j, \dot{v}_j) >= O(\epsilon)$$

This removes all dependence on α_i in the equations once we know the roots of:

$$< \dot{v} f(v, \dot{v}) >= 0 \tag{5.14}$$

and leaves us with a set of averaged ψ_i equations of the type discussed in chapter 2. After removing the constant ωt term, we have:

$$\dot{\phi}_i = -\epsilon < \omega z_{i,\alpha} \sum_{j=0}^{n} g(v_j, \dot{v}_j) > \tag{5.15}$$

and from these we can examine the equations for the phase differences.

Non-resonant averaging

If we assume that we have 2 oscillators that have settled down to two different limit cycles α_1, α_n with different periods, to see what sort of behaviour this implies, we must look at the ratio of the periods given by $\kappa = \omega(\alpha_1)/\omega(\alpha_2)$. If $\kappa \in \mathbf{Q}$, then we can apply the reasoning above to average over some multiple of periods of ψ.

However, if not then the limit $\epsilon \to 0$ does not allow phase locking, i.e. we need to average over a 2-torus, and this will decouple all the angles by making the equations of the actions independent of ϕ_i for all i.

Thus, at least for a set of full measure of parameter values near $\epsilon = 0$ [8], we should expect to see tori. These may go through large period phase locking at any non-zero value of ϵ which could be investigated by looking for periodic orbits of a particular winding number.

Further insight could be gained by considering n oscillator systems with k *rational relations* on the frequencies of the form

$$\sum_{i=1}^{n} n_i \omega_i = m$$

for n_i and m in $\mathbf{Z}$ (see Baesens et al. [20] and [16]).

5.2 Two identical weakly coupled van der Pol-Duffing oscillators

5.2.1 Introduction

In this section we will apply the theory developed in section 5.1 to a specific problem, that of two van der Pol-Duffing oscillators, at the limit of weak dissipation and very weak coupling.

Duffing oscillators with potentials of the form $v^3 - v$ are one of the simplest oscillators that have a non-trivial phase space, and correspond to a Hamiltonian oscillator with a twin-well potential. Upon breaking the energy preserving nature by addition of a van der Pol type dissipation term, they have been extensively studied because they arise in a very general codimension two interaction between Hopf and pitchfork bifurcations [61, 30]. Alternatively, the equation can be viewed as a Hopf bifurcation interacting with a cusp creating a twin well potential.

We first discuss the construction of an electronic van der Pol-Duffing (VDPD) oscillator and note the presence of a symmetric Bogdanov-Takens point. Two VDPD oscillators are then weakly coupled through a cubic resistive load. For this case, we derive expressions for the motion on $\mathbf{T}^2$ of the coupled system, and demonstrate how these equations undergo a pitchfork bifurcation to a stable oscillating state with non-trivial phase lag. This is confirmed both analytically and experimentally. The results can also be used to find a subset of the dynamics of two interacting Bogdanov-Takens singularities, i.e. a codimension four point in parameter space with $\mathbf{Z}_2 \times \mathbf{Z}_2$ symmetry or codimension two with $\mathbf{D}_4$ symmetry. The latter case has been investigated by Armbruster et al. in [7], and they find that in the $\mathbf{D}_4$ setting, there is a wedge of parameter space where chaotic behaviour can be found, by virtue of the fact that the underlying Hamiltonian in 4-D is non-integrable. However, in this section we will not discuss the possibility of chaotic behaviour, although it may exist in other regions of parameter space.

5.2.2 An electronic VDPD oscillator

A van der Pol-Duffing oscillator can be constructed electronically using the circuit shown in figure 5.2. This has a nonlinear negative resistor (formed by a negative impedance converter [72]) and capacitor in parallel with an inductor which is in series with a resistor. Using the Kirchoff current laws, we get that the motion of the systems is given by

$$\begin{aligned} C\dot{v} + H(v) - \frac{v}{R_a} + \frac{v-u}{R_d} &= 0 \\ u + L\frac{(\dot{u}-\dot{v})}{R_d} &= 0 \end{aligned} \tag{5.16}$$

where $H(v)$ is the current through the nonlinear circuit element (assume that $H'(0) = 0$ and H an odd function. If we define a, d to be the conductances ($a = 1/R_a$ and $d = 1/R_d$) of resistors R_a and R_d (note that $a, d > 0$), we can eliminate u to give the second order ODE

$$\ddot{v} + \left[\frac{1}{Ld} - \frac{a}{C} + \frac{H'(v)}{C}\right]\dot{v} + \frac{(d-a)v + H(v)}{LCd} = 0. \tag{5.17}$$

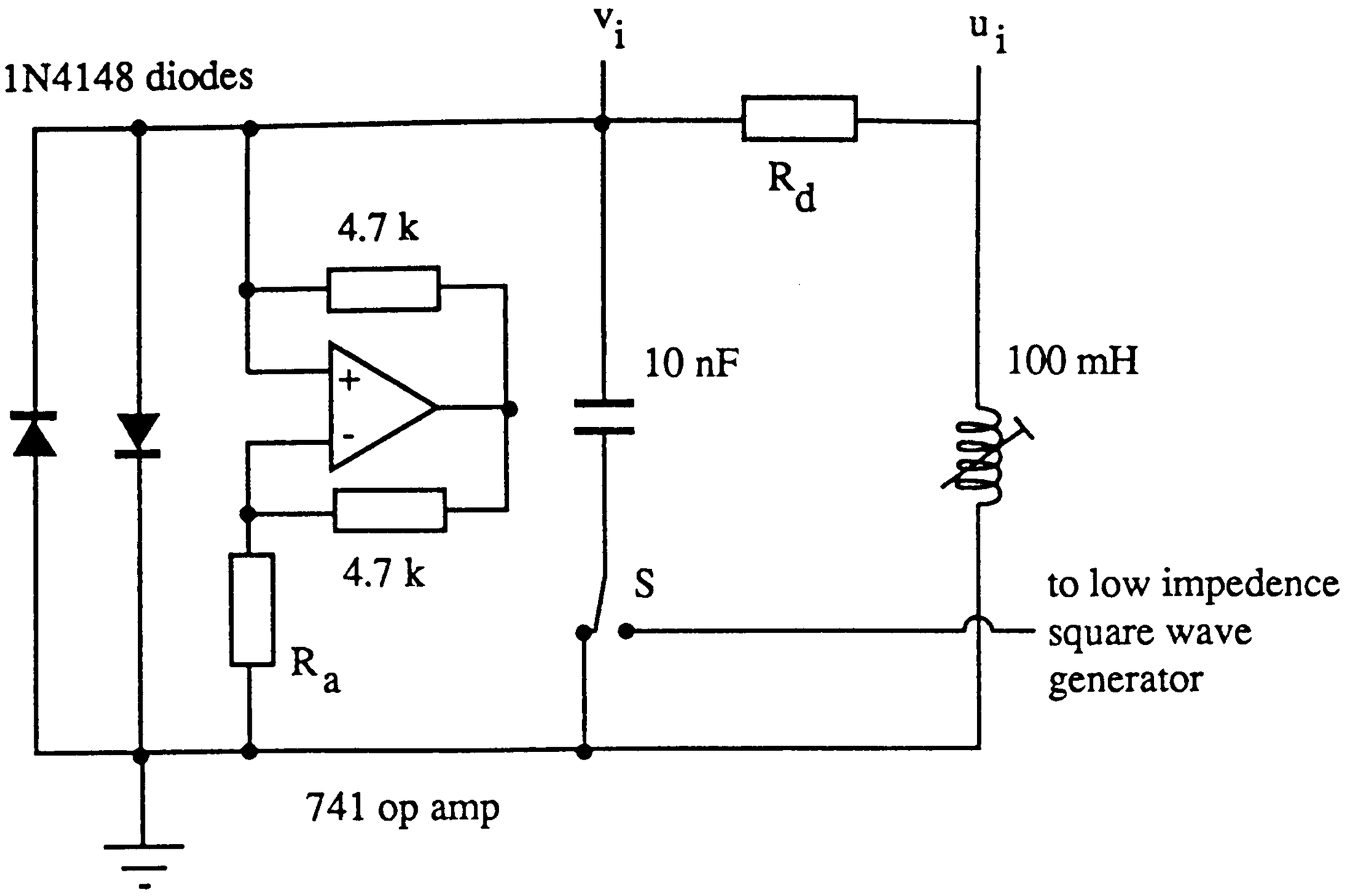

Figure 5.2: An electronic van der Pol-Duffing oscillator. The resistance is negative for small voltages but becomes positive for larger voltages. An input from a low frequency square wave generator can be connected as shown, to force the system to display transients.

Experimental details For all the experiments, the inductors used were 100mH trimmable, and the capacitors were 10nF polystyrene. A single signal diode was used in each direction to previde a positive nonlinear resistance. The nonlinear part of the V-I characteristic is an odd function which can be roughly written as

$$H(v) = H_0 v^3/3$$

giving the required results in this section. However, note that in chapter 4, a more detailed model using exponentials was required to tie experiments to quantitative predictions.

It was possible to visualise the stable dynamics not only for the stable behaviour, but also some of the transients could be recorded by exciting the oscillator with a signal generator producing low frequency square waves connected in series with the capacitor C. This has the effect of causing a sudden change in v of the amplitude of the forcing waves, every time the square wave changes sign, and will be approximated by solutions of the system forced by a train of delta functions:

$$\ddot{v} + \left[\frac{1}{Ld} - \frac{a}{C} + \frac{H'(v)}{C}\right]\dot{v} + \frac{(d-a)v + H(v)}{LCd} = K\sum_{n=-\infty}^{\infty}\delta(t+nP) \tag{5.18}$$

By adjusting the period P and amplitude A, ensuring that P was much greater than the period of any limit cycles, it was possible to lock the pattern displayed into some subharmonic of the oscillator frequency and get pictures such as those shown in figure 5.3. These pictures show the destruction of a limit cycle in a saddle node bifurcation, as predicted by a local analysis of the Bogdanov-Takens point of interaction between the Hopf and pitchfork bifurcations.

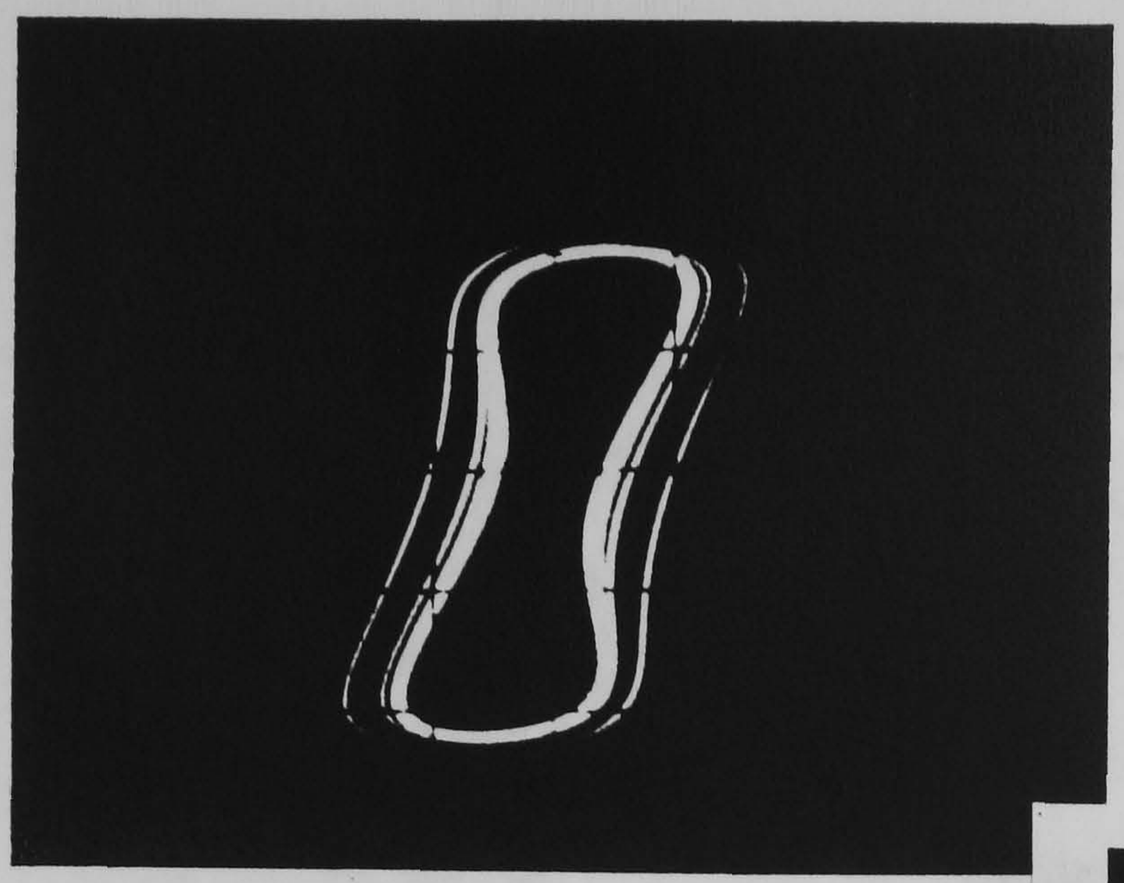

(a)

(b)

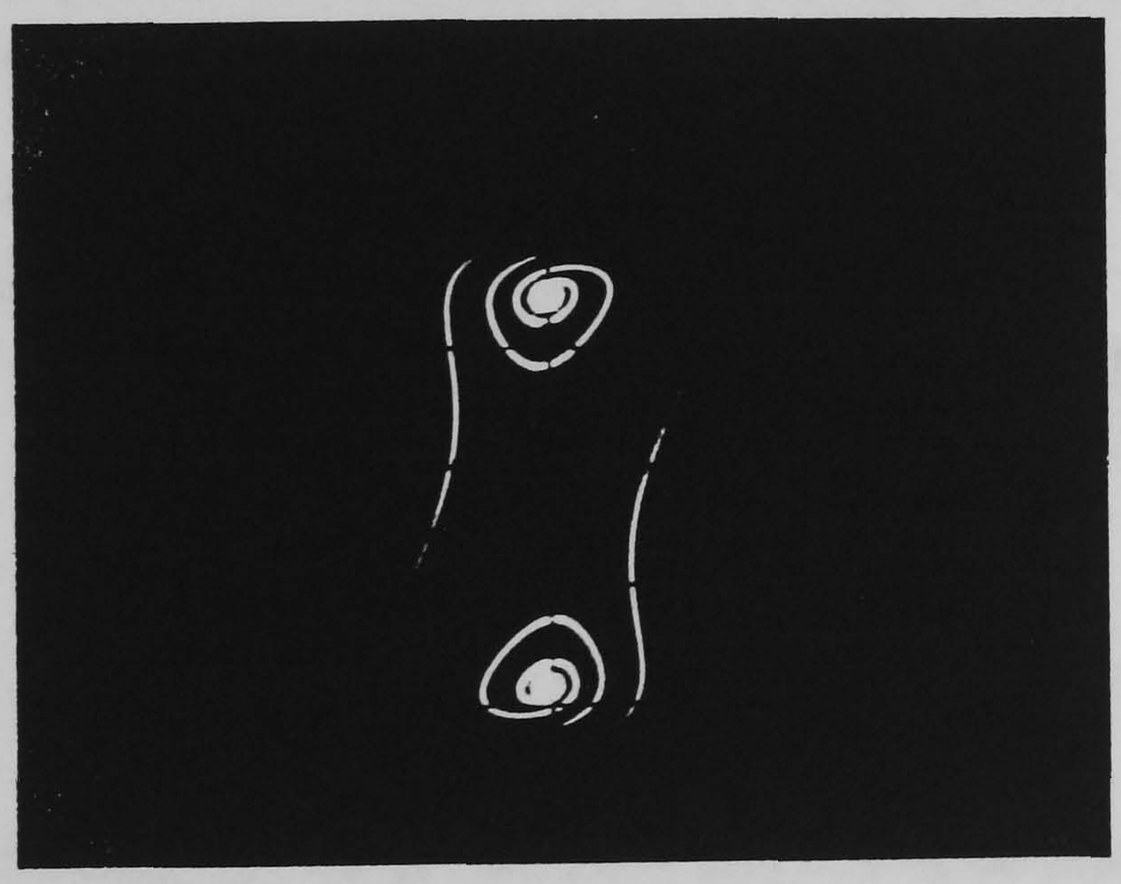

(c)

Figure 5.3: Photographs taken from the experimental system. The transients are shown going to the stable dynamics on the three cases (a)-(c) shown as points on the previous diagram of the phase space. (a) shows a transient settling down to a limit cycle about the origin, (b) shows transients going through an area where the limit cycle shown in (a) has been destroyed by an unstable limit cycle meeting it in a saddle node bifurcation. (c) shows transients to the two nontrivial stable steady states. The projection used is onto the (u, v) plane, so all fixed points lie on the vertical axis.

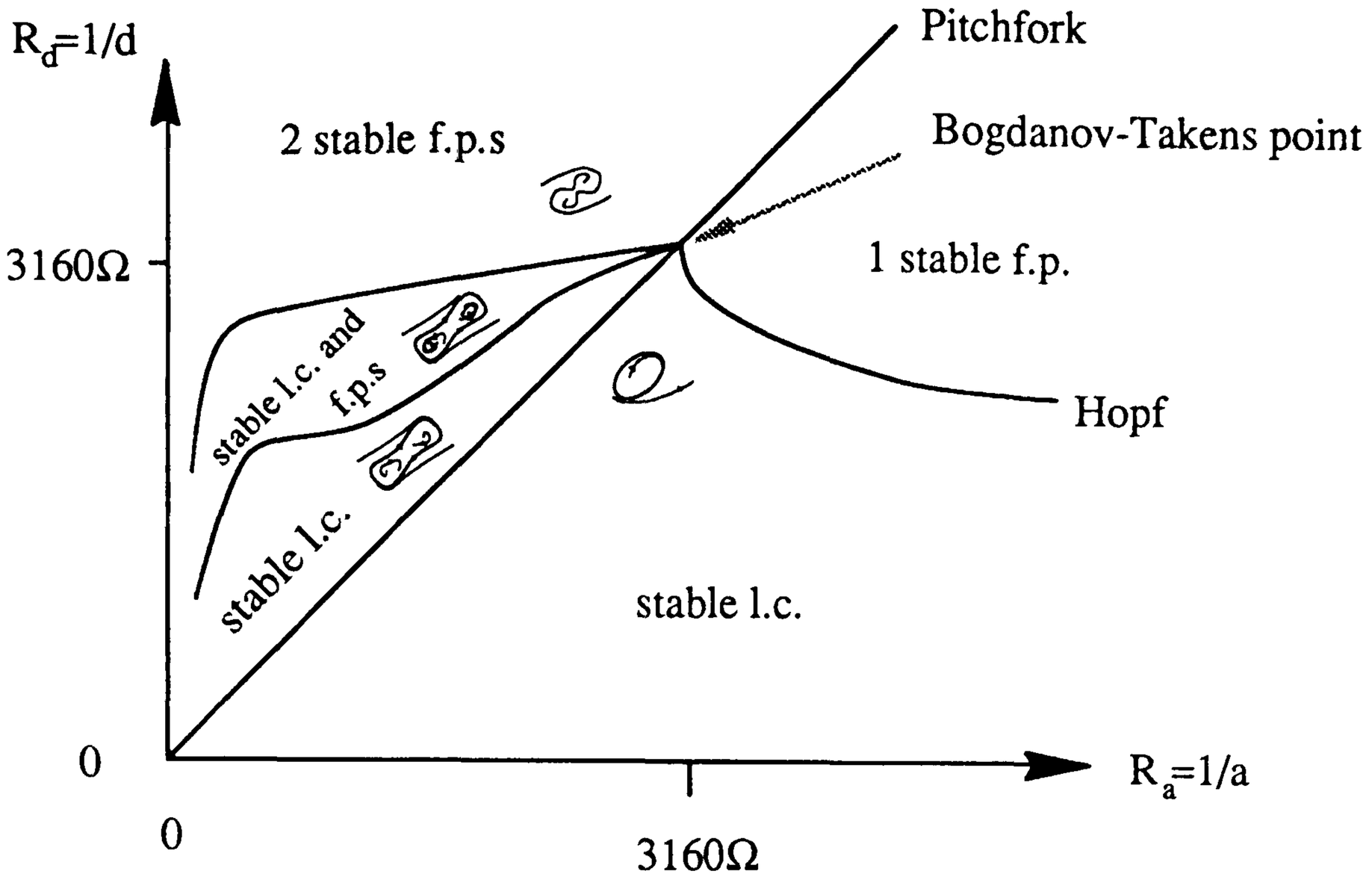

Figure 5.4: The bifurcation diagram for a van der Pol-Duffing oscillator. There is a pitchfork of steady states at $a + d = 0$ and a Hopf bifurcation at $ad = C/L = a_c^2$. At the point of intersection $(a, d) = (a_c, a_c)$, there is a Bogdanov-Takens codimension two point.

5.2.3 Bifurcations of a single VDPD oscillator

By defining:

$$\mu = -9\left(\frac{a+d}{LCd}\right),$$

$$\nu = -3\left(\frac{1}{Ld} - \frac{a}{C}\right),$$

$$v' = \frac{v}{\sqrt{H_0}},$$

$$t' = 3t$$

and dropping the primes on v' and t', it is possible to rewrite equation 5.17 in the more familiar nondimensional form:

$$\ddot{v} + (v^2 - \nu)\dot{v} + (v^2 - \mu)v = 0.$$

The codimension one local bifurcations of the steady solutions to this equation are:

- Supercritical Hopf at $\nu = 0$, $\mu > 0$
- Pitchfork at $\mu = 0$.

Where the two happen simultaneously at the origin of parameter space, we get a Bogdanov-Takens point with $\mathbf{Z}_2$ symmetry [61]. The local analysis in this reference implies existence of several extra curves of global bifurcations all emanating from this *organising centre* of the bifurcation diagram. Figure 5.4 gives shows the bifurcation diagram experimentally obtained in the parameters $(R_a = 1/a, R_d = 1/d)$ of the circuit. The parameter points where the photographs in figure 5.3 were taken are marked (a)-(c).

The Bogdanov-Takens point gives us a useful route into the weakly coupled case, using the advantage of looking at high codimension bifurcations; namely we find many branches of bifurcations coming from one point, even global ones.

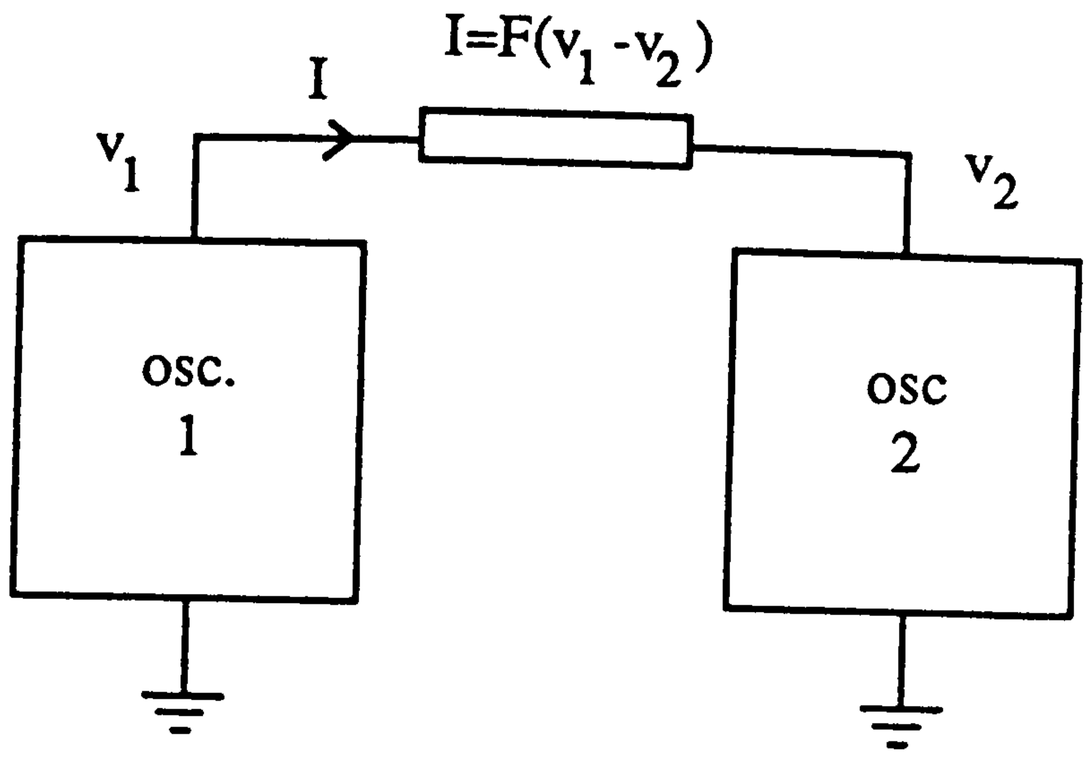

Figure 5.5: Two van der Pol-Duffing oscillators coupled through a cubic resistive load.

5.2.4 Two nonlinearly coupled VDPD oscillators: experiments

Consider two identically constructed oscillators as described in figure 5.2, coupled through a cubic nonlinear resistance connected between the non-earthed nodes of the oscillators as in figure 5.5. If we assume that *the oscillators always stay identical*, then the system will depend only on a,d and the coupling F. We now limit ourselves to looking at an F with V versus I characteristic of the form

$$I = F(V) = r(sV + V^3)$$

with s of either sign. A more general form of coupling (that preserves the degrees of freedom in the system) would include capacitive and inductive elements. The oscillators had trimmable inductors in order to make them as close as possible to identical, and the operational amplifiers were adjusted for zero offset null.

By fixing one of the parameters and varying the other two, it is possible to find stable behaviour of many types. We will discuss the symmetry breaking of in-phase oscillations to oscillations with nontrivial phase shift.

5.2.5 Results

For the two uncoupled systems in the region with a stable limit cycle and three fixed points, for purely dissipative coupling ($s > 0$) the in-phase solution was always stable. For large enough negative $s < 0$, the in-phase solution became unstable and the anti-phase solution stabilises, as might be expected from intuitive arguments. For different values of a, d the point when $s = 0$ we get loss of stability of the in-phase solution in a pitchfork bifurcation to solutions with an arbitrary phase shift. The criticality of the pitchfork is determined by the cubic form of the coupling and the dynamics on the limit cycle.

5.2.6 The equations

The two resistively coupled identical van der Pol-Duffing oscillators depicted in figure 5.5 are governed by the equation:

$$(5.19)\qquad \ddot{v}_1 + \left[\frac{1}{Ld} - \frac{a}{C} + \frac{H'(v_1)}{C}\right]\dot{v}_1 + \frac{(d-a)v_1 + H(v_1)}{LCd} = -\frac{(\dot{v}_1 - \dot{v}_2)}{C}F'(v_1 - v_2) - \frac{F(v_1 - v_2)}{LCd}$$

and that obtained by interchanging the 1 and 2 subscripts. Note the nonlinear coupling through both v and $\dot{v}$. We shall see that in the region of weak dissipation, the coupling will be mainly thorough $\dot{v}$. This is equivalent to saying that to first order, the resistive coupling comes into the equation as a dissipative term in the equations. Upon nondimensionalising we get

$$(5.20)\qquad \ddot{v}_1 = \mu v_1 + \nu\dot{v}_1 - v_1^3 - v_1^2\dot{v}_1 - \kappa\{(\dot{v}_1 - \dot{v}_2)G'(v_1 - v_2) + G(v_1 - v_2)\}$$

where

$$G(v) = v(\eta + v^2)$$

and κ gives the coupling strength and η the linear part of the coupling. We shall assume μ is greater than zero, thus putting us in the 'twin-well' regime. The case $\mu < 0$ effectively just leaves us with a Hopf bifurcation in the dynamics on passing $\nu = 0$.

Assuming the linear terms (μ, ν) and F are small, we scale the parameters thus:

$$\mu \mapsto \epsilon^2$$

$$\nu \mapsto \epsilon^2\nu$$

$$G \mapsto \epsilon^2 G$$

$$t \mapsto t/\epsilon$$

and the slow time equations are now in the form of eqns 5.2:

$$(5.21)\qquad \ddot{v}_1 + v_1^3 - v_1 = \epsilon[(\nu - v_1^2)\dot{v}_1 - \kappa G'(v_1 - v_2)(\dot{v}_1 - \dot{v}_2)] + O(\epsilon^2)$$

In the limit of $\epsilon \to 0$ and $\kappa \to 0$ with $\epsilon/\kappa \to \infty$ we get the integrable system

$$(5.22)\qquad \frac{\dot{v}_i^2}{2} + \frac{v_i^4}{4} - \frac{v_i^2}{2} = \alpha_i$$

for $i = 1, 2$. This is two decoupled Hamiltonian oscillators with energy α and potential $U(v) = v^4/4 - v^2/2$. We shall perturb this system about $\epsilon = 0$ to examine the limit of WDVWC perturbations to this Hamiltonian system.

Remark This is a subproblem of a Bogdanov-Takens type nilpotent singularity of codimension four in systems with $(\mathbf{Z}_2)^3$ symmetry, with Jordan normal form of the linear part being:

$$\begin{pmatrix} 0 & 1 & 0 & 0 \\ 0 & 0 & 0 & 0 \\ 0 & 0 & 0 & 1 \\ 0 & 0 & 0 & 0 \end{pmatrix}$$

The nonlinear terms in normal forms of this type of problem has been considered by Cushman and Sanders [41]. Here, the action of $(\mathbf{Z}_2)^3$ is through the action of $\mathbf{Z}_2$ on each oscillator (limiting us to odd powers in the nilpotent normal form) and $\mathbf{Z}_2$ permuting the two identical oscillators).

Define the normalised periodic orbits $z(\alpha, \psi)$ as in equation 5.4. Using these exact solutions of the $\epsilon = 0$ case, we introduce a slow time $T = \epsilon t$ and we shall seek solutions of the equations 5.21 of the form:

$$v_i(t) = z(\alpha_i(T), \psi_i(T)) \tag{5.23}$$

with $\psi_i = \int^t \omega(\alpha_i)dt + \phi_i$ where ϕ_i and α_i are slowly varying and subject to the constraint:

$$\frac{dv_i}{dt} = \omega(\alpha_i)z_{,\psi}(\alpha_i, \psi_i). \tag{5.24}$$

Using equations 5.12 and 5.13 we get the evolution equations for the slow system:

$$\dot{\alpha}_1 = ((\nu - z_1^2)\omega_1 z_{1,\psi} - \kappa G'(z_1 - z_2)(\dot{z}_1 - \dot{z}_2))\omega_1 z_{1,\psi} \tag{5.25}$$

$$\dot{\phi}_1 = -((\nu - z_1^2)\omega_1 z_{1,\psi} - \kappa G'(z_1 - z_2)(\dot{z}_1 - \dot{z}_2))\omega_1 z_{1,\alpha} \tag{5.26}$$

where the dot indicates differentiation with respect to $T = \epsilon t$ and with the expressions for $\dot{\alpha}_2, \dot{\phi}_2$ given by permuting the 1 and 2 suffices.

5.2.7 The averaged system

Assuming WDVWC, and that

$$\alpha_i = \alpha + O(\epsilon)$$

independent of i, we can average the previous system 5.25,5.26. Defining the sum and difference of the phases;

$$\Theta = \phi_1 + \phi_2$$

$$\theta = \phi_1 - \phi_2$$

we arrive at the averaged equations:

$$\dot{\alpha} = \langle(\nu - z^2)\omega^2 z_{,\psi}^2\rangle \tag{5.27}$$

$$\dot{\Theta} = -2\langle(\nu - z^2)\omega^2 z_{,\psi} z_{,\alpha}\rangle \tag{5.28}$$

$$\dot{\theta} = \kappa\langle G'(z_s - z)(z_{s,\psi} - z_{,\psi})\omega z_{s,\alpha} - G'(z - z_s)(z_{,\psi} - z_{s,\psi})\omega z_{,\alpha}\rangle \tag{5.29}$$

where z is evaluated at (α, ψ) and z_s is the phase shifted z;

$$z_s(\alpha, \theta; \psi) = z(\alpha, \psi + \theta).$$

We are not interested in Θ, which represents a detuning of the oscillator pair, and shall consider only the dynamics in the α, θ plane. However, there is nothing in principle that stops Θ being calculated. From the above definitions, we can see that

$$\dot{\alpha} = (\nu - R(\alpha))\left\langle z_{,\psi}^2\right\rangle$$

where R is a ratio of Abelian integrals evaluated on level curves of $U(v)$ and is, of course, dependent on the exact form of the nonlinearity in U. The particular case for the van der Pol-Duffing equation is discussed in [30].

Thus we can calculate the fixed points of the systems by finding α such that $\dot{\alpha} = 0$. This means we need to solve

$$\nu = R(\alpha) = \frac{\langle z^2 z_{,\psi}^2\rangle}{\langle z_{,\psi}^2\rangle}$$

where the integrals are over one period of ϕ, or alternatively

$$\nu = \frac{\oint z^2 z_{,\psi} dz}{\oint z_{,\psi} dz}$$

where the integrals are over the loop $z(\alpha, \psi)$. Thus we have determined the value of the action variable α.

We now consider the phase difference θ. Using the explicit form of the coupling function $G(v) = v(\nu + v^2)$ allows us to write equation 5.29 thus:

$$\dot{\theta} = \kappa\omega S(\alpha, \theta, \eta)$$

where S is defined by

$$\begin{aligned} S(\alpha,\theta,\eta) &= \langle (z_{s,\psi} - z_{,\psi})(z_s - z)^2 z_{s,\alpha} - (z_{,\psi} - z_{s,\psi})(z - z_s)^2 z_{,\alpha} \rangle + \\ &\quad \eta \langle (z_{s,\psi} - z_{,\psi}) z_{s,\alpha} - (z_{,\psi} - z_{s,\psi}) z_{,\alpha} \rangle \end{aligned}$$

5.2.8 Numerical method and results

Having reduced the problem from a flow in R^4 to calculating some integrals, a program (shown in appendix B) was written to perform the integration. This was achieved by integrating equation 5.22 to generate tables of values of $\omega(\alpha)$ and then $z(\alpha, \psi)$. These values were then used to generate approximate integrals to give the vector fields giving the asymptotic slow evolution equations for the system.

A fourth order Runge-Kutta method was used to firstly calculate the period of the level curves (and thus $\omega(\alpha)$), and then to calculate the normalised level curves. A simple trapezium rule integrator was used in conjunction with symmetric difference formulae for the derivative with respect to α.

Some typical results are displayed in figure 5.6, which shows the function $R(\alpha)$ and $S(\alpha, \theta, \eta)$ for two different values of α. The contours at the zero level represent steady states of the phase difference θ. Note how on both graphs of S, there are branches of periodic orbits connecting the in-phase and anti-phase solutions.

5.3 Synchronisation with dissipative coupling

The theory in this chapter allows us to tackle a more general problem of why two dissipative oscillators on the plane tend to synchronise with dissipative coupling, something that is often assumed to happen by starting with *averaged* equations with a dissipative coupling.

Definition 5.3.1 *A set VWCWD oscillators are* dissipatively coupled *if they can be written in the form of equation 5.2 with*

$$g(v_i, v_j, \dot{v}_i, \dot{v}_j) = \kappa h(v_i - v_j)(\dot{v}_i - \dot{v}_j)$$

with $h(v) > 0$ for v in some neighbourhood of zero and $i, j = 1, 2$ $(\kappa \to 0)$.

This is a general form of coupling when LCR oscillators are coupled through a resistive network, as the oscillator equations are second order in $v = \int^t V(s)ds$, and the coupling is dependent on V.

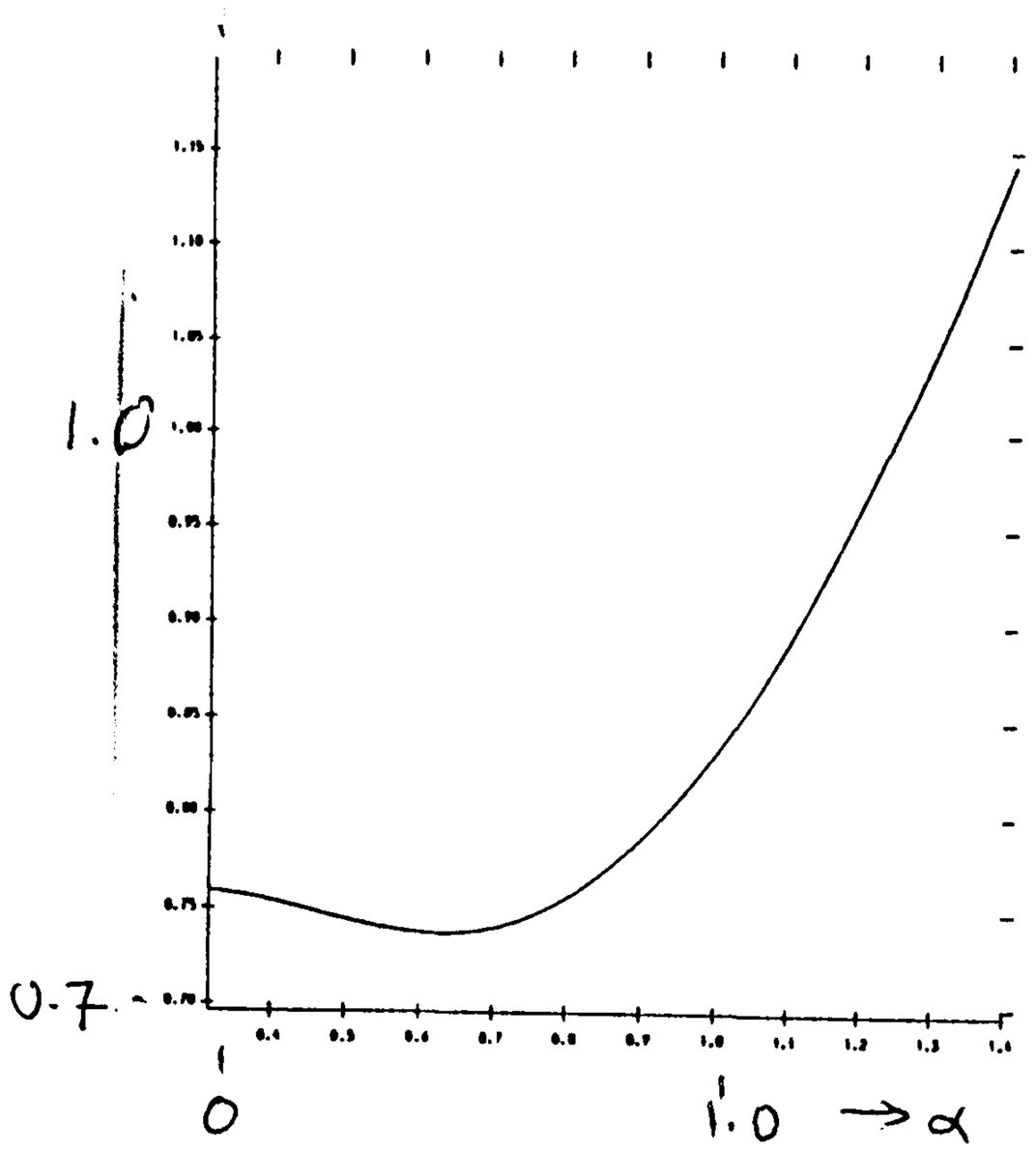

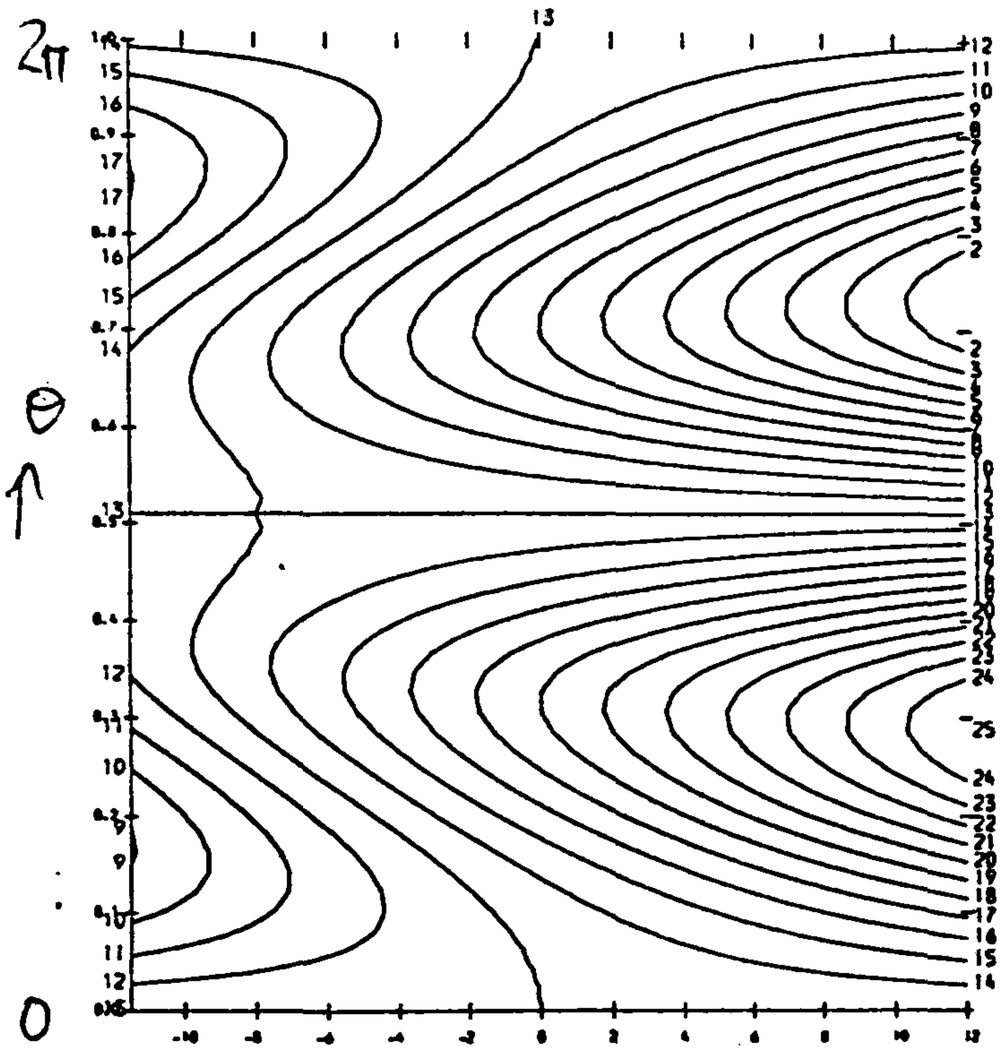

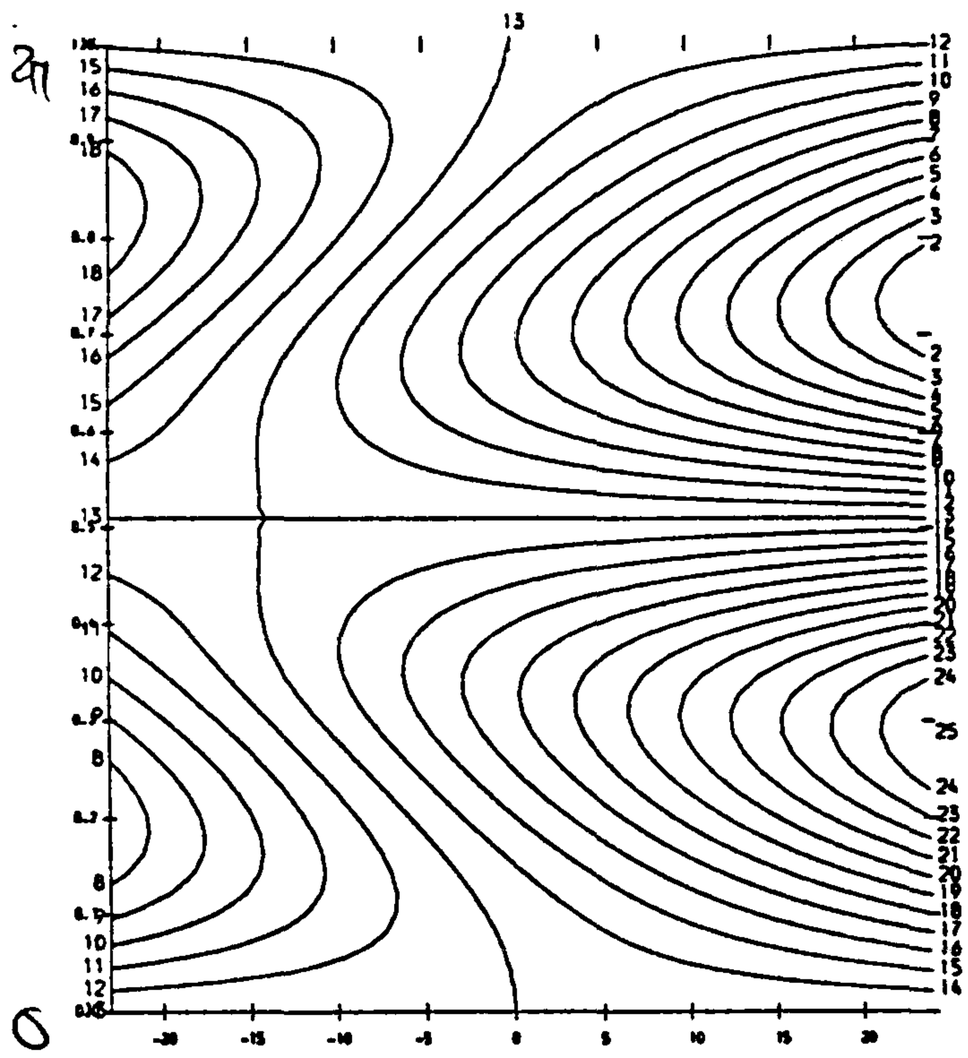

Figure 5.6: The functions (a) $R(\alpha)$ (b) $S(1.010, \theta, \eta)$ and (c) $S(1.105, \theta\eta)$ for a symmetric quartic potential. The minimum of the curve $R(\alpha)$ corresponds to a saddle node of periodic orbits. Note how, for $\eta > 0$ all phases except antiphase are attracted to the in-phase solution, and as η passes through zero a supercritical pitchfork bifurcation gives rise to stable limit cycle solutions without symmetry. These stabilise the antiphase solution by another pitchfork.

In this case, after computing the normalised periodic orbits and applying the results for the slow angles as in the previous two sections, we arrive at the following formula for the slow phase difference $\theta = \phi_1 - \phi_2$.

$$\dot{\theta} = p(\theta) = \kappa\omega\langle h(z_s - z)(z_{s,\psi} - z_{,\psi})z_{,\alpha} - h(z - z_s)(z_{,\psi} - z_{s,\psi})z_{s,\alpha}\rangle$$

The stability of the in-phase solution $\theta = 0$ is determined by $dp/d\theta$, and if we assume that z is odd in ψ, $z_{,\alpha}$ is odd in ψ (and so $z_{,\psi}$ is even in ψ), we get

$$\frac{dp}{d\theta} = 2\kappa\omega h(0)\langle z_{,\psi\psi}z_{,\alpha}\rangle$$

Using the very useful relation, equation 5.10, we have

$$\omega z_{,\psi\psi}z_{,\alpha} = -\frac{1}{\omega} + \omega z_{,\psi}z_{,\alpha\psi} + \omega_{,\alpha}(z_{,\psi})^2$$

and averaging over ψ (using integration by parts) gives

$$\omega\langle z_{,\psi\psi}z_{,\alpha}\rangle = -\frac{1}{\omega} + \omega_{,\alpha}\langle(z_{,\psi})^2\rangle - \omega\langle z_{,\psi\psi}z_{,\alpha}\rangle$$

so that

$$\frac{dp}{d\theta} = \kappa h(0)\left(-\frac{1}{\omega} + \omega_{,\alpha}\langle(z_{,\psi})^2\rangle\right).$$

Note that the last expression involves only the derivative of ω with respect to α, and not that of z; this suggests there may be another way of deriving this result.

Thus for an isochronous oscillator $\omega_{,\alpha} = 0$ we have $dp/d\theta < 0$ always, and thus the in-phase solution is stable with this type of coupling. For non-isochronous oscillators with periods that are *increasing* as action α grows ($\omega_{,\alpha} < 0$), we will also have $dp/d\theta < 0$, and more generally, the in-phase solution keeps stability if

$$\langle(z_{,\psi})^2\rangle(\omega^2)_{,\alpha} < 1.$$

We end this section by noting that if the potential energy goes like some even power of v;

$$U(v) = v^{2m},$$

with $m \in \mathbf{N}$, this implies that the in-phase solutions are stable (thanks to Mark Muldoon for suggesting the method used here).

This is because

$$\dot{v} = (2\alpha - 2v^{2m})^{1/2}$$

gives

$$\int_{v=-(\alpha)^{1/2m}}^{(\alpha)^{1/2m}} \frac{dv}{(2\alpha - 2v^{2m})^{1/2}} = \frac{\text{Period}}{2} = \frac{\pi}{\omega}$$

and changing variables to $w = v/\alpha^{1/2m}$ gives

$$\omega = \alpha^{\frac{-1}{2m}+\frac{1}{2}} I^{-1}$$

with the integral I independent of α;

$$I = \frac{\pi}{2}\int_{w=-1}^{1} \frac{dw}{(1 - w^{2m})^{1/2}}.$$

(The integral exists by comparison with square root singularities at the limits.) Thus, $d\omega/d\alpha < 0$ for all $m \in \mathbf{N}$.

5.4 Discussion

The same procedure can be used for groups of VWCWD (dissipative) Josephson junctions [62] in a manner similar to that for van der Pol-Duffing oscillators, just by using a different potential and coupling. Sanders and Cushman [116] use Abelian integrals in a problem with a single Josephson junction, and manage to find contractible limit cycles using equations with a nonlinear dissipation term. We could consider linear dissipation and nonlinear coupling in the case of two identical Josephson junctions, to find bifurcations from the in-phase solution to nontrivially phase shifted solutions. It may also be possible to use the WCWD equations unaveraged to detect bifurcations to period doubled orbits in the case of linear coupling, and this would be very interesting to test.

Something that became evident in the study of the averaged equations of the van der Pol-Duffing equation is that they introduce a 'normal form symmetry' corresponding to time reversal. This is under the involution $t \mapsto -t, x \mapsto x$ in equation 5.1, and because of the $\mathbf{Z}_2$ symmetry of the system, in phase solution is stable if and only if the antiphase solution is unstable.

In order to get a more generic picture, one possibility would be to average on a perturbed equation. For the van der Pol equation, rather than working from

$$\ddot{x} + x = 0,$$

one could start with a conservative system of the form

$$\frac{\dot{x}^2}{2} + \frac{(\epsilon\dot{x} + x)^2}{2} = \alpha$$

(which cannot be written as a second order system in one variable). This would be an interesting starting point for a future investigation into averaging in oscillator system, as it would break the time reversal $(x, \dot{x}, t) \mapsto (x, -\dot{x} - t)$ symmetry in the perturbed equation. Another interesting continuation of this chapter would be to compute the elliptic integrals necessary to evaluate the Abelian integrals in the style of [30, 116] and others.

Chapter 6

Bifurcation of flames on rectangles

6.1 Introduction

Since Sivashinsky's [120] asymptotic derivation of a nonlinear partial differential equation of a flame front, a lot of progress has been made in analysing this and more general model equations, motivated not only by flame front dynamics but also by more general dynamics in spatially extended systems [32]. The equation has also been used as a model for investigating links between finite and infinite dimensional dynamics, as with other model PDE chaos equations (Ginzberg-Landau, Swift-Hohenberg etc. [103]). However, until now, comparatively little work has been done extending the work from 1-d interfaces to 2-d sheets.

We shall review first some literature on nonlinear models of laminar flame fronts and their use in studying instabilities. We shall then concentrate on the Kuramoto-Sivashinsky and Michelson-Sivashinsky (hereafter referred to as K-S and M-S) equations [120].

We examine the nature of the K-S equation on a rectangular domain with Neumann boundary conditions at points close to primary bifurcation. Certain number-theoretic degeneracies in the linear part of equation cause the existence of multiple bifurcations (mode interactions) at certain sizes of the rectangular domain, and in chapter 7 we use an automated Liapunov-Schmidt reduction to investigate the branching of mixed-mode solutions from these points in a two-parameter setting. These high corank bifurcations are shown to be generic in a suitable setting for a wide range of commonly examined problems on square, rectangular or even rhombic domains.

6.2 Nonlinear PDEs and the problem of flame fronts

Much of this section is from the review by Clavin [36], Williams' monograph [134] and the review in Harper's thesis [66], and is not original. Flame fronts are localised regions of reaction in reacting flows. The problems of mathematically describing a flame typical of a highly exothermic process are great for a variety of reasons. All the problems of turbulent flow are present, and many more, even though there can sometimes be elegant simplifications, for example the laminar flame approximation. Even without including the spatially extended nature of most combustion problems, well-stirred reactors can undergo complex dynamical behaviour owing to the nature of autocatalytic reactions (for example the Belousov-Zhabotinsky reaction [64], experimentally shown to display

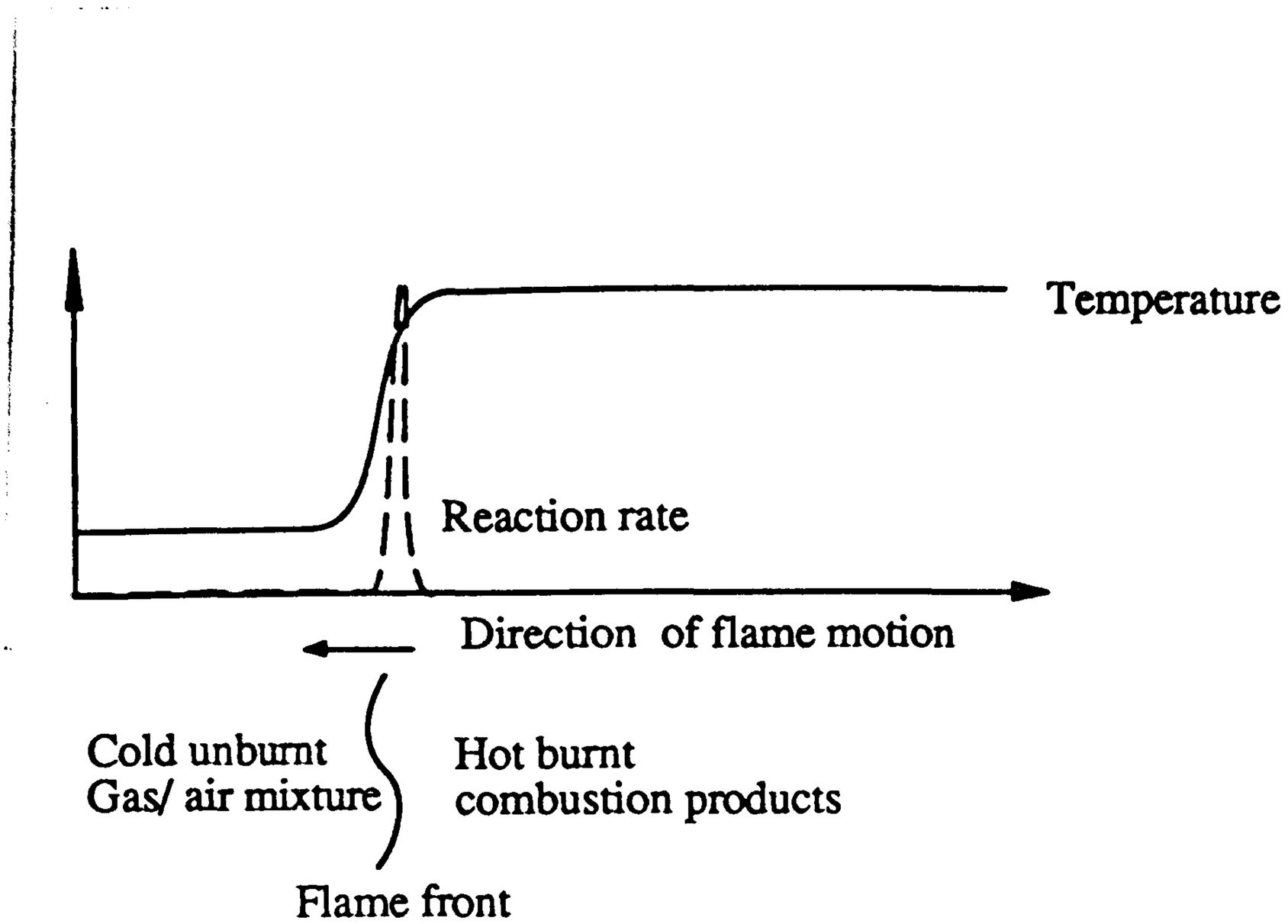

Figure 6.1: A schematic picture of a flame front. To the left are cold unburnt gases, and to the right are hot burnt gases. In the frame of reference of the flame front, there is a net flow of gas from left to right. The extreme sensitivity of the reaction rate to temperature ensures that the flame front is near two dimensional.

many phenomena associated with low dimensional chaos).

With the addition of space variation to the system, one can only hope to find an accurate description for turbulent burning using a statistical theory based on a knowledge of internal structure of the system. In this sense, it is important to have a good understanding of how laminar flames can interact and behave.

Laminar flames exist as two-dimensional structures in a three dimensional flow if the reaction is of asymptotically high non-dimensional activation energy (Zeldovich number $\beta \gg 0$). Their very existence provides a silver lining in the cloud of general combustion theory, as they allow us in certain circumstances to reduce the problem to a locally two dimensional problem described by the movement of an interface separating cold unburnt gas from hot burnt gas (see figure 6.1).

6.2.1 The problem of flame stability

It is possible to obtain laminar flames in reality by using low burning rates and careful controls on conditions. By increasing the flow rate in a burner, we might expect to see a cascade of bifurcations in the qualitative behaviour of the flame until the flame is totally turbulent. Some of the destabilising mechanisms can be explained in purely fluid dynamical terms (e.g. shear flow or boundary layer, such as Kelvin-Helmholtz) whereas other are associated with double-diffusive or convective instabilities.

6.2.2 Flame fronts as dynamical systems

In mathematical terms, we describe a flame as a two dimensional surface moving in three dimensions, and as such, we wish to use the language of parabolic PDEs to describe the motion as a semiflow, if this can be done. This is not possible if, for example, singularities develop in the flame surface after finite time. This has been discussed in

[25] which derives a wave equation on the flame front that is second order in time, and suggests singularities may occur.

6.2.3 Linear stability theory

A laminar flame can be shown to exist by virtue of the Galilean symmetries (invariance to uniform propagation) of the fundamental equations in $\mathbf{R}^3$ assuming a uniform motion in the x direction, say. Assume we have unburnt reactants for $x < 0$ and burnt combustion products for $x > 0$, as in figure 6.1. Near $x = 0$, we can show the existence of a steadily propagating flat flame by symmetry arguments. It is possible to show the same for e.g. spherical symmetries assuming a point source of reactants [28, 27] or cylindrical symmetries with a line source of reactants [22]. This sort of simple laminar flame is usually taken as a starting point for examining the behaviour of the flame under its own and external influences.

It is possible to find the response of the flame to perturbations and see if these grow or die away. In order to do this we look at the linear stability of the 2-d flame to perturbations of the form $\exp(\omega t + i\mathbf{k}.\mathbf{x})$ where $\mathbf{x}$ are the coordinates on the 2-d surface, and derive a curve in $(\mathbf{k}, \omega)$ space; the dispersion relation. If the projection of this curve into ω space lies totally in the left half plane of the complex numbers, this indicates that the flame is linearly stable. If moreover, the projection is bounded away from the $Re(\omega) = 0$ axis, then the flame is asymptotically stable ([69, 93, 30]).

In the limit of small gas expansion, the dispersion relation looks like a quartic in $k = |\mathbf{k}|$ and linear in ω, owing to the double-diffusive effects in space. Much work has been done by Clavin and others [36] in uncovering the nature of this dispersion relation and the effects of the various physical processes involved. We shall limit ourselves to the dispersion relation of Sivashinsky, which includes only thermal-diffusive and asymptotically small hydrodynamic effects (the former was first investigated by Zeldovich [139] and the latter by Landau and Darrieus [86]). In real flames, these assumptions are dubious, and better but more complex models are now available. However [36] indicates that, ignoring the effect of gravity, the M-S equation agrees qualitatively with a more accurate model, only with different coefficients.

Under assumptions of a one-step reaction in a dilute mixture with high activation energy and high heat release, Sivashinsky [120] derives the asymptotic ($\sigma \to 1, N \to \infty$ and $N(1-\sigma) < \infty$) relation

$$\omega + 4k^4 + \left[\frac{1}{2}N(1-\sigma)(1-L) - 1\right]k^2 - \frac{1}{2}(1-\sigma)k = 0 \tag{6.1}$$

where

N is the dimensionless activation energy

σ is the density ratio of the burnt to unburnt gases (which is more often of order unity).

L is the Lewis number, $\kappa_b/\rho_b D_b c_p$ the ratio of molecular diffusion to thermal diffusion.

The quartic and quadratic terms in k represent double-diffusion and the linear term in k represents a non-local hydrodynamic (Landau) instability. This equation has two natural simplifying limits, that of low thermal expansion ($\sigma = 1$) leading to the relation

$$\omega + 4k^4 + \left[\frac{1}{2}N(1-L) - 1\right]k^2 = 0 \tag{6.2}$$

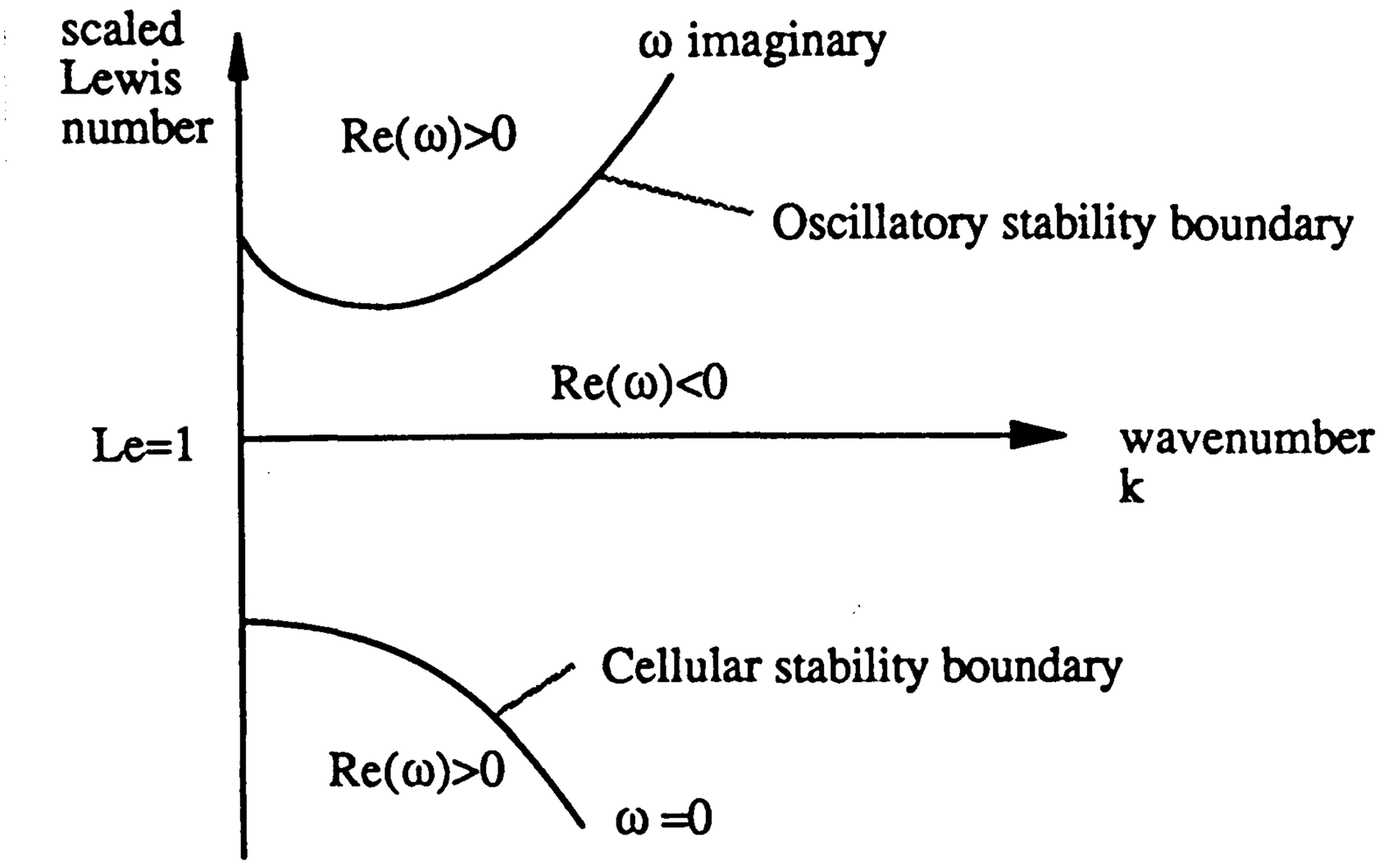

Figure 6.2:
(β, k) plot for zero gas expansion, large activation energy N and near-unity Lewis number $L = 1 + \beta/N$. (from Matkowsky and Sivashinsky [95])

and that of $L > L_0$, Lewis number greater than critical, leading to the relation

$$\omega + k^2 - \frac{1}{2}(1 - \sigma)k = 0. \tag{6.3}$$

There are two types of instability that can develop from a linearly stable flame. Upon changing one of the parameters (N, σ, L) in the dispersion relation, generically either one solution to $\omega = 0$ (steady-state bifurcation) or a complex conjugate pair with $Re(\omega) = 0$ (Hopf or oscillatory bifurcation) will be created. Both of these possibilities can occur, as we record below ([120]).

Restricting ourselves to finite domains, the problem reduces to a countable number of admissible wavenumbers, which are bounded below by the maximum size of the domain. The same statement holds whether we choose no-flux (Neumann) boundary conditions or periodic boundary conditions. This restriction is necessary to enable us to use the tools of finite dimensional bifurcation theory, as otherwise we get a continuum of eigenvalues passing through $Re(\omega) = 0$, and we cannot apply reduction techniques such as Liapunov-Schmidt or Centre Manifold [51, 30, 67].

Examining the (ω, k) plots (figure 6.2) for the above dispersion relations [25], we see that on limiting to a finite domain, we get spectra such as those represented by the points in figure 6.2, with smaller wavenumbers permissible as we move to larger domain sizes. These relations agree with those of McIntosh [96] (except that he defines the Lewis number to be the reciprocal of that defined above).

Cellular instability

We get a value $\omega = 0$ in the dispersion relation. For K-S on a line with periodic boundary conditions, this will correspond to a two dimensional centre manifold to the trivial solution; one corresponding to left travelling waves, and the other corresponding to right travelling waves. For K-S on a plane, things are more complicated; there can be many eigenfunctions corresponding to any particular wavenumber k. Exactly

how many is an interesting problem depending on the exact shape of the domain on which we work; for an infinite flame sheet, we have an infinite number of eigenfunctions parametrised by elements in $O(2)$, the symmetries of a circle. In section 6.3, we shall investigate how rectangular domains affect this result.

Oscillatory instability

This can occur as an effect of double diffusion in the case of $\sigma = 1$, and has been extensively investigated by Matkowsky and his co-workers starting from a model of Matkowsky and Sivashinsky [95]. In a series of papers, they have examined supercritical and subcritical bifurcations and mode-interactions in a variety of geometries, for example cylindrical [94, 24, 25] or rectangular [91] domains with lean burn one-step reactions and no thermal expansion. This has been extended to more realistic models by Margolis et al. [92], and more recently [22] examines such a transition numerically, using a large but finite non-dimensional activation energy.

6.2.4 Nonlinear models

Upon instability of any eigenfunction of the linearised problem the asymptotic dynamics is no longer determined by the linear terms and we must turn to the nonlinear effects in the equation, which up until now we have ignored. In particular, we need nonlinear models to talk about the bifurcations of the system, in particular the asymptotic behaviour upon loss of stability. In general, there will be several symmetrically related patterns all going through a loss of stability at the same time, and it is the *nonlinear terms* that select which will be stable, if any. This is referred to as *pattern selection* or *formation* [103]. More crudely, the nonlinear terms can provide us with information about whether the loss of stability is *soft* (with nearby stable solutions) or *hard* (no local stable solutions) upon bifurcation, using the terminology of [8, 9]. This problem is one of considerable mathematical difficulty, and requires order asymptotic expansions and reduction of the problem to finite dimensions. We concentrate on the K-S equation, which includes a nonlinear term of the form $(\nabla u)^2$.

More recently, a model has been derived by Frankel and Sivashinsky in [48], which generalises the Kuramoto-Sivashinsky equation to a coordinate free form on a curved surface.

6.3 The Kuramoto-Sivashinsky equation: theory

The equation can be, and has been, written in many forms, so we will start with that of Sivashisky [120], and then provide our own form:

$$(6.4) F_t + 4(1+\epsilon)^2\nabla^4 F + \epsilon\nabla^2 F + \frac{1}{2}(\nabla F)^2 = \frac{(1-\sigma)}{8\pi^2}\int_{-\infty}^{\infty} |\mathbf{k}| e^{i\mathbf{k}.(\mathbf{x}-\mathbf{z})} F(\mathbf{z},t) d\mathbf{k} d\mathbf{z},$$

with $F(\mathbf{x},t)$ the dimensionless perturbation of the flame front surface in units of the width l_T of thermal structure of the flame, and $\epsilon = (L_0 - L)/(1 - L_0)$ where L_0 (which satisfies $\frac{1}{2}N(1-\sigma)(1-L_0) = 1$) being the critical Lewis number. We shall consider the two limits already considered in the dispersion relations discussed above. The first of these is a constant-density model obtained for $\epsilon > 0$ and $\sigma = 1$, and is (up to rescaling) referred to as the *Kuramoto-Sivashinsky* equation by [32, 19, 73, 97, 49, 7]. A slight modification to ensure that $\oint F$ is independent of time (i.e. there are no secular terms in the solution) is given in [59], and many others using the K-S equation include this modification later to get better behaved solutions.

$$u_t + \nabla^4 u + \nabla^2 u + (\nabla u)^2 = 0 \tag{6.5}$$

As noted by Aston [19], this equation has some very convenient scaling properties. Namely, by rescaling time, space and the variable u, we can assign any values to the coefficient outside the three terms with spatial derivatives, the only restriction being that we must preserve their signs. It also admits a multiple-timescale decomposition related to its Galilean equivariance to give steady states for large systems [49], and is amenable to inertial manifold techniques to give rigorous reductions of all dynamics (not just locally) to finite dimensional systems. Nicolaenko et al. [105] prove lower and upper bounds for the dimension of the global attractor [38, 126] in the case of the K-S equation on a line, while Manneville [90] demonstrates spatio-temporal chaos in the equation on a line.

The Kuramoto-Sivashinsky equation has also been applied to other instabilities, for example travelling waves on fluid interfaces [31] or chemical waves [82, 84, 83]

Some work has been done in trying to construct this finite dimensional attractor by Armbruster et al. [7]. They investigate a four mode centre-unstable manifold to the trivial solution, and find reasonable agreement where one would expect to see an inertial manifold of dimension less than or equal to four. Kevrekedis et al. [77] have done an exhaustive study of the one dimensional case for periodic boundary conditions of small size, both computationally and theoretically, stressing that this equation has some atypical (non-generic) properties even in the way the nonlinear terms divide the function space into invariant regions. They find, amongst other things, bifurcation to travelling waves and structurally stable heteroclinic cycles in the dynamics, the latter being from nongeneric internal symmetries of the equation. However, very little work has been done on extending this to two-dimensional domains, which should be an interesting problem since a variety of different geometries are available.

Another limiting case ($\epsilon < 0$ and $\sigma > 1$) of equation 6.4, called the Michelson-Sivashinsky equation by Joulin [76], and has been studied there and in [98, 49].

$$u_t + \frac{1}{2}(\nabla u)^2 = \mu \nabla^2 u + \frac{1}{8\pi^2} \int_{-\infty}^{\infty} |\mathbf{k}| e^{i\mathbf{k}(\mathbf{x}-\mathbf{z})} u(\mathbf{z}, t) d\mathbf{k} d\mathbf{z} \tag{6.6}$$

Because this admits a pole decomposed solution (at least in one dimension) to describe the dynamics, it is possible to investigate the formation and stability of cusp-like solutions using the dynamics of the poles, an n body problem on the complex plane [76].

6.3.1 K-S on a rectangular domain

We shall concentrate on equation 6.5 on a domain whose boundary is a rectangle of sides $(a\pi, b\pi)$. The ratio a/b is referred to as the *aspect ratio* of the system in comparison to other spatially extended systems, and to tie in with the theory of Armbruster and Dangelmayr [5, 6], Crawford et al. [39] and Gomes [55] on mode interactions in rectangular domains with Neumann-type boundary conditions. They have calculated the possible Taylor series by using singularity theoretic techniques. The system is equivariant [54] under the symmetry group of the rectangle, $\mathbf{D}_2$, generated by the two isometries

$$\begin{aligned} (x, y) &\mapsto (-x, y) \\ (x, y) &\mapsto (x, -y) \end{aligned}$$

If the domain has unit aspect ratio and is thus a square, the symmetry is $\mathbf{D}_4$, the group generated by one of the above reflections and

$$(x, y) \quad \mapsto \quad (y, x).$$

The domain and boundary conditions are as follows;

$$\begin{aligned} u &= u(\mathbf{x}, t) \\ \mathbf{x} &\in [0, a\pi] \times [0, b\pi] \equiv \Omega \\ u_n &= (\nabla^2 u)_n = 0 \quad \text{for} \quad \mathbf{x} \in \partial\Omega. \end{aligned}$$

Defining:

$$e(k,l) = \cos\left(\frac{kx}{a}\right)\cos\left(\frac{ly}{b}\right) \tag{6.7}$$

with $(k, l) \in \mathbf{N}^2$, we note that $\{e(k,l)\}$ forms a basis of eigenvectors of the linear part of the equation, this being self-adjoint (diagonalisable). Thus

$$\nabla e(k,l) = \left(-\frac{k}{a}\sin\left(\frac{kx}{a}\right)\cos\left(\frac{ly}{b}\right), -\frac{l}{b}\cos\left(\frac{kx}{a}\right)\sin\left(\frac{ly}{b}\right)\right)$$

and therefore

$$\begin{aligned} \nabla e(k,l).\nabla e(i,j) \;=\; & \left\{\frac{-ik}{4a^2} + \frac{-lj}{4b^2}\right\} e(k+i, l+j) \\ & + \left\{\frac{ik}{4a^2} + \frac{-lj}{4b^2}\right\} e(k-i, l+j) \\ & + \left\{\frac{-ik}{4a^2} + \frac{lj}{4b^2}\right\} e(k+i, l-j) \\ & + \left\{\frac{ik}{4a^2} + \frac{lj}{4b^2}\right\} e(k-i, l-j). \end{aligned}$$

By substituting

$$u = \sum_{k=0}^{\infty}\sum_{l=0}^{\infty} y_{k,l}\, e(k,l)$$

into equation 6.5, multiplying by $e(k,l)$ and integrating over all space, we get a weak form of the equation;

$$\int\int \{u_t + \nabla^4 u + \nabla^2 u + (\nabla u)^2\}\, e(k,l)\, dx\, dy = 0 \tag{6.8}$$

which implies that:

$$\begin{aligned} y_t(k,l) \;=\; & \left(\frac{k^2}{a^2} + \frac{l^2}{b^2}\right)\left(\left(\frac{k^2}{a^2} + \frac{l^2}{b^2}\right) - 1\right) y(k,l) \\ & -\frac{1}{4}\sum_{i=0}^{\infty}\sum_{j=0}^{\infty}\sum_{m=0}^{\infty}\sum_{n=0}^{\infty} \\ & \left\{\left\{\frac{-im}{4a^2} + \frac{-jn}{4b^2}\right\}\delta_{i+m,k}\,\delta_{j+n,l}\right. \\ & + \left\{\frac{-im}{4a^2} + \frac{jn}{4b^2}\right\}\delta_{i+m,k}\,\delta_{|j-n|,l} \\ & + \left\{\frac{im}{4a^2} + \frac{-jn}{4b^2}\right\}\delta_{|i-m|,k}\,\delta_{j+n,l} \\ & \left. + \left\{\frac{im}{4a^2} + \frac{jn}{4b^2}\right\}\delta_{|i-m|,k}\,\delta_{|j-n|,l}\right\} y(i,j)\, y(m,n) \end{aligned}$$

with steady solutions obeying $y_t(k,l) = 0$ for all (k,l). We use this weak form of the equation in the numerical experiments.

6.3.2 Linear theory: steady-state bifurcations from the flat flame

With these 'Neumann-type' boundary conditions, the eigenfunctions of the linearisation about the trivial solution are given by the $e(k,l)$ mode with eigenvalue:

$$\omega = \left(\frac{k^2}{a^2} + \frac{l^2}{b^2}\right)\left(\left(\frac{k^2}{a^2} + \frac{l^2}{b^2}\right) - 1\right), \tag{6.9}$$

(incidentally, $\mathrm{Re}(\omega) = 0$ has only real roots, preventing any Hopf bifurcation), and thus we get a steady-state bifurcation whenever

$$\left(\frac{k^2}{a^2} + \frac{l^2}{b^2}\right) = 1. \tag{6.10}$$

We regard the two numbers $(a,b) \in \mathbf{R}^2$ as bifurcation parameters. Varying a and keeping the ratio a/b constant is equivalent to the parametrisation used by many other authors.

The set of bifurcation points in the (a,b) plane is shown in figure 6.3 for $(a,b) \in [0,20]^2$. At a constant value of (k,l). the curves can be parametrised by $(a,b) = (k\csc(\theta), l\sec(\theta))$ for $\theta \in (0,2\pi)$.

6.4 Mode interactions on a rectangle

The algebraic form of the equation 6.10 means that there can be multiple bifurcations caused by *number-theoretic degeneracies* in the equation, and these appear as multiple intersections of bifurcation lines in figure 6.3.

Armbruster and Danglmayr developed a theory of mode interactions on a one dimensional domain with $O(2)$ symmetry [5, 6] and this has been extended to a rectangle by Gomes [55] and Crawford *et al.* [39]. They calculated the restrictions placed on the Taylor series of the bifurcation equations using singularity and group theory techniques.

6.4.1 Number theoretic degeneracies

Examining the problem of PDEs that are equivariant under the Euclidean group on $\mathbf{R}^2$, but restricted to rectangular domains with Neumann, Dirichlet or periodic boundary conditions, generic bifurcations problems with higher dimensional kernels than those predicted by the rectangular symmetry can appear. Traces of the Euclidean symmetry remain and cause multiple eigenvalues. Whether a problem has such exceptional kernels depends on the ratio of the side lengths. The results generalise to higher dimensional rectangular domains.

Golubitsky et al. [51, 54] develop a method for applying the tools of symmetric bifurcation theory to PDE with compact symmetries; the Liapunov-Schmidt reduction can be used in an equivariant setting giving reduced equations that have essentially the same bifurcation structure as that for ODEs with the same symmetry group. However, that this is often not the whole story for the *nonlinear terms.* For example, on a rectangular domain using just $\mathbf{D}_2$ singularity theory, we get terms that are shown not to appear in the Liapunov-Schmidt reduced bifurcation equations by Gomes [55] and also found by [5, 6] in one dimensional PDEs with Neumann boundary conditions.

This section is concerned just with *linear degeneracy* on multi-dimensional domains, a problem that seems to be part of the folklore: for example it is mentioned in Kuttler and Sigillito [85]. In the following sections, we examine exactly where these 'number theoretic degeneracies' come from and what effects the have in terms of genericity.

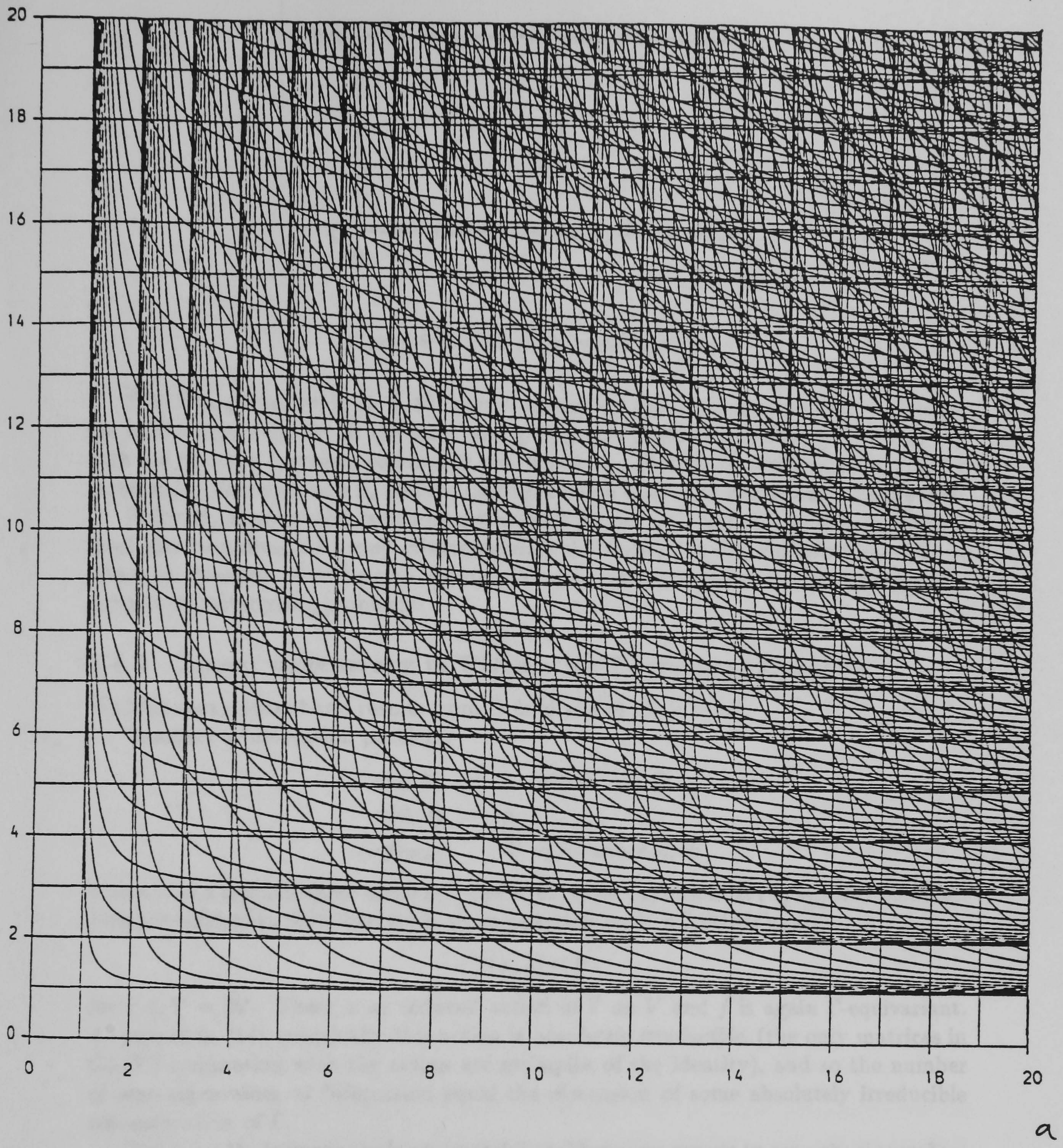

Figure 6.3: The locations of the bifurcations in the (a, b) plane for $(a, b) \in [0, 20]^2$. Note the crossings of the primary mode bifurcations, causing mode interactions.

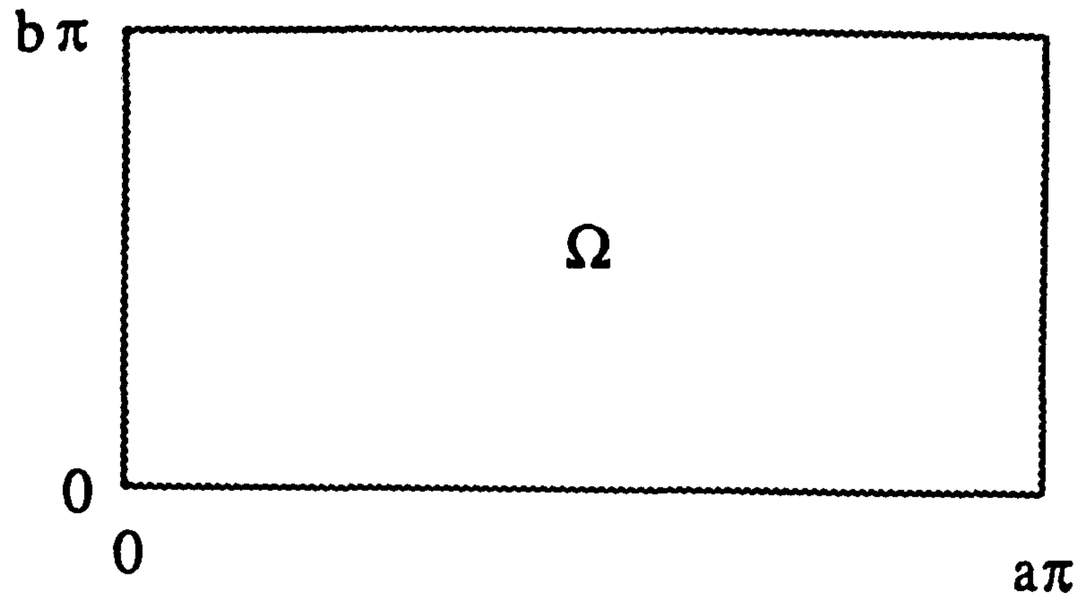

Figure 6.4: The rectangular domain

The ideas presented in [5, 6, 55] involve extending the problem to an infinite domain ($\mathbf{R}$ in the first two, $\mathbf{R}^2$ in the last) and giving this problem periodic symmetry. We then see that the *boundary conditions are symmetry constraints*, as discussed in [39] for rectangular domains, and in [46] for more general domains, in particular hemispheres.

However, many of the examples discussed have not only periodic symmetry (which gives rise to a compact group of symmetries; the torus) but full *Euclidean symmetry*, which in domains of dimension greater than one leads to linear degeneracies in the context of rectangular problems.

6.4.2 Linear degeneracy in PDEs with Euclidean symmetry

We first recap some basic results from Golubitsky et al. [51, 54].

Consider a bifurcation problem:

$$\begin{aligned} g(x,\lambda) &= 0 \quad x \in X \; \lambda \in \mathbf{R} \\ g(0,0) &= 0 \\ (dg)_{(0,0)} & \quad \text{is of corank } r < \infty \end{aligned}$$

where X is a Banach space and g is Γ-equivariant. In the case that $(dg)_{(0,0)}$ is Fredholm, Liapunov-Schmidt reduction leads to an equation on $V = ker((dg)_{(0,0)})$:

$$f(x,\lambda) = 0$$

for $x \in V = \mathbf{R}^r$. There is an induced action of Γ on V and f is again Γ-equivariant. As proved in [54], generically this action is *absolutely irreducible*, (the only matrices in $GL(V)$ commuting with the action are multiples of the identity), and so the number of zero eigenvalues at bifurcation equal the dimension of some absolutely irreducible representation of Γ.

Thus, for $\mathbf{D}_2$ (rectangularly symmetric) problems, we expect to see only eigenvalues with multiplicity one or two, corresponding to the only two irreducible representations of $\mathbf{D}_2$, the trivial and the standard. Now consider a PDE on a rectangle, with the equation having rectangular symmetry and the boundary conditions respecting that symmetry (figure 6.4). Write this in the form:

$$\begin{aligned} G(f) &= 0 \\ f|_{\partial\Omega} &= 0 \\ f &\in X \\ \Omega &= (0, a\pi) \times (0, b\pi). \end{aligned}$$

with X some suitable Banach space. Suppose $\mathbf{D}_2$ is generated by

$$\begin{aligned}(x,y) &\mapsto (a\pi - x, y)\\ (x,y) &\mapsto (x, b\pi - y)\end{aligned}$$

and that G is equivariant under $\mathbf{D}_2$ and $\partial\Omega$ is invariant under $\mathbf{D}_2$. If we adopt the position that 'there must be a symmetry group setting in which our equations are generic' and there are no other symmetries in the problem (e.g. oddness of G), we would expect that the only multiplicities of zero eigenvalues possible are one or two.

However, consider the same example when G is $E(2)$-equivariant, where $E(2)$ is the Euclidean group of all translations and rotations in the plane. Extending to an infinite domain and looking at dG on the plane $\mathbf{R}^2$, from Ian Melbourne (pers. comm.);

For a linear operator L on a suitable Banach space X (isomorphic to $L^1(\mathbf{R}^2)$), then L is $E(2)$-equivariant if and only if

$$L\exp(i\mathbf{k}.\mathbf{x}) = P(|\mathbf{k}|)\exp(i\mathbf{k}.\mathbf{x}),$$

where $P : [0,\infty) \to \mathbf{R}$ is the dispersion relation for $u_t = Lu$. This implies that:

- The spectrum $\{\lambda : (L - \lambda I)$ is not of full rank $\} \equiv \text{spec}(L) = P([0,\infty))$
- L generates an analytic semigroup $\Leftrightarrow spec(L) < R < \infty$
- L is a PDE of order $m \Leftrightarrow P$ is an even polynomial of degree m
- $\omega = P(|k|)$ is the dispersion relation of the PDE $u_t = Lu$.

.

By noting that the functions $\exp(i(k.x + \phi))$ are eigenfunctions for the unbounded problem, we can see that combinations of these which respect the boundary conditions must be eigenfunctions for the bounded problem. The bifurcation problem then becomes a problem of calculating all admissible wavevectors k that satisfy both the boundary conditions and $P(|k|) = 0$.

If we examine Neumann (N) or Dirichlet (D) boundary conditions, the admissibility conditions are just $(k_1, k_2) = (k/a, l/b)$ with $(k,l) \in \mathbf{Z}$, and the eigenfunctions are

$$\cos(k_1 x)\cos(k_2 y) \quad \text{(N)}$$

or

$$\sin(k_1 x)\sin(k_2 y) \quad \text{(D)}.$$

Periodic boundary conditions lead to combinations of the same expressions on the domain $(0, 2a\pi)\times(0, 2b\pi)$. The same holds if in all directions one of the above boundary conditions holds, e.g. Neumann at $x = 0, a\pi$, Dirichlet at $y = 0, b\pi$. To find the wavevectors of bifurcating modes, we need to find the solutions of:

$$\frac{k^2}{a^2} + \frac{l^2}{b^2} = |\mathbf{k}|^2 = (P^{-1}(0))^2 \tag{6.11}$$

for $(k,l) \in \mathbf{Z}^2$

Solutions of this depend on the rationality of a with respect to b. We consider each case in turn.

6.4.3 The square, $a = b$

Here, equation 6.11 becomes:

$$k^2 + l^2 = k_0^2 a^2 = n$$

and the number of solution of this in $\mathbf{N}^2$ is given by

Theorem [65, 85] Let $r(n)$ be the number of solutions $(k, l) \in \mathbf{Z}^2$ with $k > 0, l \geq 0$ to $k^2 + l^2 = n$. For any $\epsilon > 0$:

$$r(n) \quad < \quad O(n^{\epsilon})$$
$$r(n) \quad \not< \quad O((log(n))^{\epsilon}).$$

□

There is an explicit formula going back to Legendre [129, 74] for $r(n)$:

$$r(n) = \sum_{d|n} (-1)^{\frac{(d-1)}{2}},$$

with the sum over all odd d, from which it is possible to see that $r(n)$ is unbounded by choosing wavenumbers with large numbers of factors $\cong 1 \bmod 4$. For example, $r(5^k) = k + 1$ or $r(13.5^k) = 2k + 2$.

6.4.4 Rectangles with $a^2/b^2 \in \mathbf{Q}$

This includes the square, and also permits arbitrarily large numbers of bifurcating modes:

Writing $a/b = p/(q\sqrt{d})$ with integers p, q and some square-free integer $d > 0$, means we can rewrite equation 6.11 as:

$$q^2 k^2 + dp^2 l^2 = n.$$

Therefore the number of solutions is at least $R(n/(pq)^2)$ for any n such that $pq|\sqrt(n)$, where $R(n)$ is the number of solutions of the equation

$$x^2 + dy^2 = n$$

with $d > 0$ square-free and $(x, y) \in \mathbf{Z}^2$. For all d, $R(n)$ can be shown to be unbounded using the following theorem (thanks to M. Harrison and C. Matthews for discussions leading to this).

Theorem 6.4.1 $S(n) = sup_{r \leq n} R(r) > O((\log n)^{1/2})$. *In particular, it is unbounded in* n.

Proof For any $k \in \mathbf{N}$, define

$$\alpha = 2kd + i\sqrt{d}.$$

then $\arg(\alpha) < \tan(\arg(\alpha)) < 2k$, and so the set of numbers

$$\mathcal{S} = \{\alpha^l \bar{\alpha}^{2k-l}; 0 \leq l < k\}$$

has k distinct element in $\mathbf{Z}(\sqrt{-d})$, with $\beta \in \mathcal{S}$ implies $\beta\bar{\beta} = \alpha^k\bar{\alpha}^k = n \in \mathbf{N}$. Thus we have shown that for any k, d there exists an n with at least k solutions to $x^2 + dy^2 = n$. Now $(\alpha\bar{\alpha})^k = n$ imples that

$$k \log k > O(\log n)$$

and therefore

$$S(n) > O((\log n)^\epsilon)$$

for $0 < \epsilon < 1$. □

This is not a sharp estimate, and by comparison with the case $d = 1$, it may be true for all $\epsilon > 0$. One consequence of this theorem is that for large $R(n)$, the arguments of the critical wavevectors fill the interval $[0, 2\pi)$. We define

$$\mathcal{R}(n) = \{x + iy\sqrt{d} : x^2 + dy^2 = n, (x, y) \in \mathbf{Z}^2\}$$

(so $R(n) = |\mathcal{R}(n)|$).

Lemma 6.4.1 *For any $\epsilon > 0$, there exists an infinite sequence $\{n_i\}$ with $n_i \to \infty$ such that the ϵ-neighbourhood of $\{\arg z : z \in \mathcal{R}(n_i)\}$ covers $[0, 2\pi)$.*

Proof This follows from the definition of the sets $\mathcal{S}$ in lemma 6.4.1□

6.4.5 Rectangles with $a^2/b^2 \notin \mathbf{Q}$

These cannot have arbitrarily large null spaces; a result (mentioned by [104]) is:

Proposition If $\{a^2, b^2\}$ are independent over the rationals and a solution of

$$b^2k^2 + a^2l^2 = n$$

exists with $(k, l) \in \mathbf{Z}_+^2$, then it is unique.

Proof The set of accessible n lie within a vector space over $\mathbf{Q}$ of dimension 2.□

6.4.6 Generalisations

We sum up the results above and generalise to d-dimensional rectangles in the following theorem. Here $E(d)$ is the d-dimensional Euclidean group.

Theorem 6.4.2 *Let $F(u, \lambda) = 0$ (with $F(0, \lambda) = 0\ \forall\lambda$) be an $E(d)$ equivariant bifurcation problem with bounded solutions on $\mathbf{R}^d$, restricted to a rectangle R with sides of length $\{a_i\pi : i = 1..d\}$ and Neumann, Dirichlet or periodic boundary conditions imposed on each pair of parallel faces of Ω. Assume that the dispersion relation associated with F has bifurcating wavenumbers $k \to \infty$ as $\lambda \to \infty$ and is continuous in λ. Then there can exist arbitrarily large null spaces at bifurcation if and only if there exist $i \neq j$ such that a_i^2/a_j^2 is rational. This happens precisely when the vector space generated by $\{a_i^2 : i = 1..d\}$ over $\mathbf{Q}$ is of dimension less than d.*

Comments This result shows that in the case of restrictions of $E(d)$-equivariant problems to d-dimensional rectangles with certain boundary conditions, it is generic in certain cases to have *hidden symmetries* in the problem which enlarge the null space.

This effect is a linear effect, rather than the nonlinear effects noticed by [39, 5, 55], and the eigenvalues can be split up only by:

- Perturbating the equation to break the $E(d)$ symmetry, e.g. discretizing with a finite difference method.
- Breaking the rectangular shape of the domain, e.g. to trapezoid.
- Imposing more general (but still homogeneous) boundary conditions, for example of the form $\partial u/\partial x + f(u) = 0$.

Rhombic and hexagonal lattices As pointed out by Ian Melbourne (pers. comm.), the arguments above also apply to the case of periodic boundary conditions on a rhombus, triangle or hexagon, as by considering an $E(2)$ equivariant problem with periodicity on a rhombic lattice with generating vectors $v_1 = (1, 0)$ and $v_2 = (a, b)$ $(b \neq 0)$, we have eigenfunctions of the form

$$\exp(ikx)\exp(il(ax + by))$$

with eigenvalues

$$\lambda = (k + al)^2 + b^2 l^2.$$

The number of solutions of this can be unbounded in the same way as for the rectangle if $(a/b)^2$ is rational and a is rational. Thus for a hexagonal lattice where $a = 1/2, b = \sqrt{3}/2$ the corank at bifurcation is generically unbounded. It may be possible to use this to advantage, in the investigation of structurally stable heteroclinic cycles in oscillatory convection; it has been found that there are regimes where on a hexagonal lattice where rolls in the three possible directions are connected by a heteroclinic connection (related to the Kuppers-Lortz instability [29, 122]). In fact, this behaviour is shown to occur most naturally between rolls at angles separated by about 58 degrees (Ian Melbourne and Mary Silber, pers. comm.). Using these multiple mode interactions may present a way of analytically investigating heteroclinic connections at angles other than 60 degrees, by use of lemma 6.4.1.

Chapter 7

Mode interactions in the Kuramoto Sivashinsky equation

In this chapter, we discuss application of Liapunov-Schmidt reduction to the K-S equation at the mode interactions predicted to exist in chapter 6. Briefly moving on to examine the equation on a disk and on a sphere, the bifurcation structure will be very different. In the final section, we briefly mention some numerical experiments carried out with the K-S equation on a rectangular domain.

7.1 Liapunov-Schmidt reduction

Looking closer at the multiple bifurcations described in the previous chapter (note that the same things apply for the Michelson-Sivashinsky and many model PDEs on a rectangle), we can investigate analytically the creation of branches of mixed-mode steady solutions from the trivial solution, even though these may be unstable. The method used is in Golubitsky and Schaeffer [51], but benefits from the fact that the nonlinearity is merely quadratic. The idea is to project the full equations onto the null space at bifurcation, and thus reduce the bifurcation problem from infinite dimensions to the dimension of the null space. Consider the equation for steady solutions:

$$\Phi(u,\lambda) = 0$$

with $\lambda = (a,b) \in \mathbf{R}^2$ and

$$\begin{aligned} \Phi &: C^{4,\alpha}(\Omega) \times \mathbf{R}^2 \to C^{0,\alpha}(\Omega) \\ \Phi(u,\lambda) &\equiv \nabla^4 u + \nabla^2 u + (\nabla u)^2 \; (= -u_t) \end{aligned}$$

where $\Omega = [0, a\pi] \times [0, b\pi]$ and $C^{k,\alpha}(\Omega)$ is the space of k times continuously differentiable functions $\overline{\Omega} \to \mathbf{R}$ with Neumann-type boundary conditions (i.e. $u_n = (\nabla^2 u)_n = 0$) satisfying a Hölder condition with exponent α. Given that $(0,\lambda)$ is always a solution, when $\mathrm{d}\Phi_{(0,0)}$ has non-trivial null space we can perform a bifurcation analysis by projecting onto that null space. By the inverse function theorem (which lies at the core of Liapunov-Schmidt reduction), there exists a smooth branch of solutions. It is that we aim to find. Due to the lengthy calculations required, computer algebra is used, as in [114]. Assume that the bifurcation takes place at $\lambda = 0$.

$$\begin{aligned} \mathrm{d}\Phi_{(0,0)} &: C^{4,\alpha}(\Omega) \times \mathbf{R}^2 \to C^{0,\alpha}(\Omega) \\ \mathrm{d}\Phi_{(0,0)}(u,\lambda) &\equiv \nabla^4 u + \nabla^2 u \\ \Phi &\equiv \mathrm{d}\Phi_{(0,0)} + \phi \end{aligned}$$

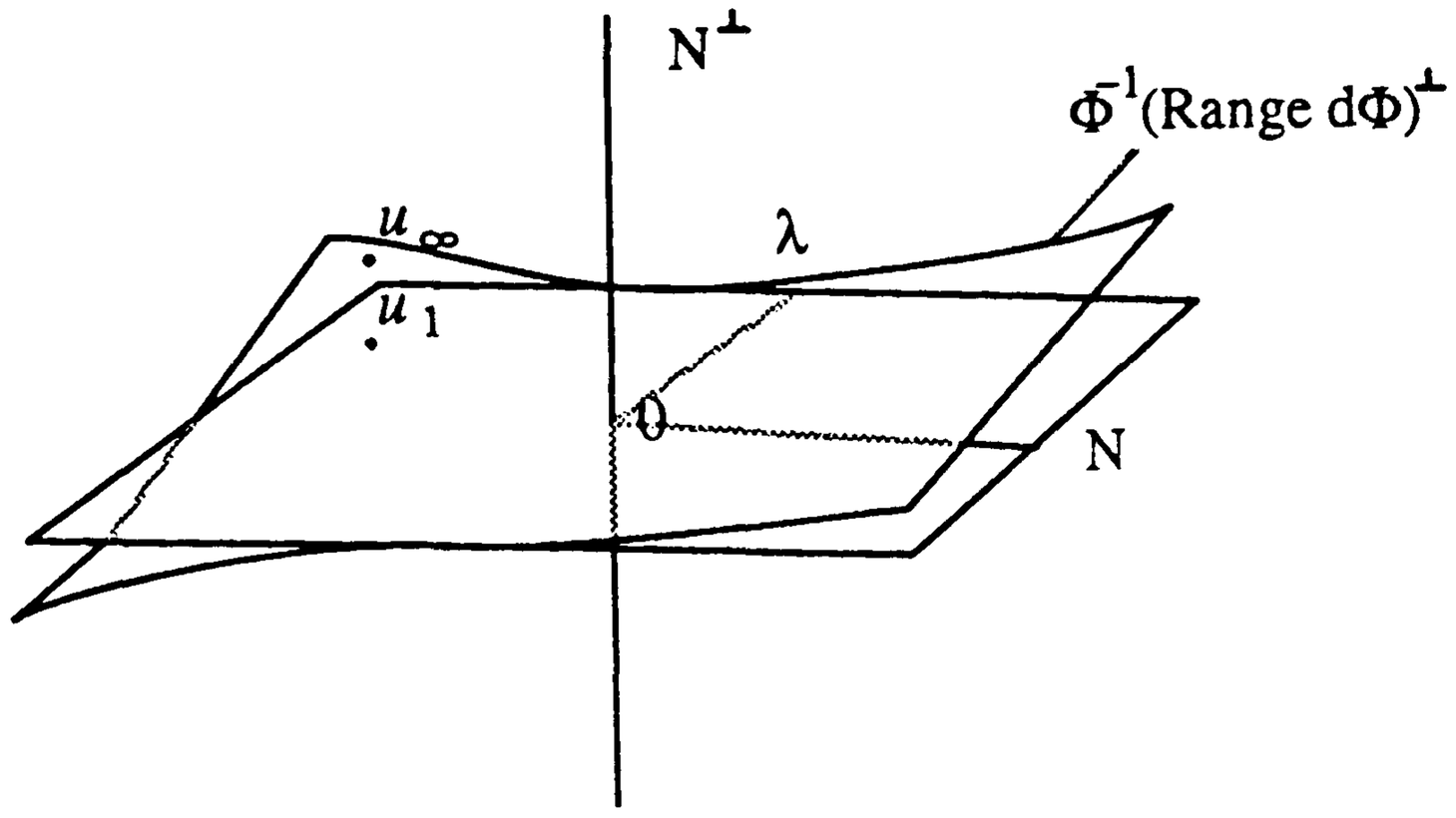

Figure 7.1:
A schematic diagram showing the method of Liapunov-Schmidt reduction. The solution set of $\Phi = 0$ passes through the origin tangent to the null space of $d\Phi_{(0,0)}$. By picking a point in the null space, u_1, we generate a series u_i that converges to u_∞, where $\Phi(u_\infty)$ is in $\text{Range}(d\Phi)^{\perp}$, and the projection onto the null space is u_1.

Let N be the *null space* of $d\Phi|_{C^{4,\alpha}(\Omega)}$ at $\lambda = 0$, i.e. the largest subspace of $C^{4,\alpha}(\Omega)$ such that

$$d\Phi_{(0,0)}(N, 0) = 0.$$

Now $d\Phi$ is a Fredholm linear operator [138], so N is a finite dimensional space. Note that $(N, 0) \oplus (0, \mathbf{R}^2)$ is the null space of the operator $d\Phi_{(0,0)}$ because of its trivial action on λ. Using the Fredholm condition, we construct a splitting of $C^{4,\alpha}(\Omega)$ into $N \oplus N^{\perp}$. All the nonlinear terms are in the expression ϕ, which has linear part zero at $(0, 0)$.

Define the inverse of the linear part from the range of $d\Phi$ to $N^{\perp}$:

$$(d\Phi_{(0,0)})^{-1} : \text{Range}(d\Phi)^{\perp} \to N^{\perp}.$$

Invert the projection shown in figure 7.1 by considering

$$u_1 \in N, \ \lambda \in \mathbf{R}^2 \tag{7.1}$$

The Liapunov-Schmidt technique will find a value of u with projection u_1 on to N, but also with $\Phi(u, \lambda) \in \text{Range}(d\Phi)^{\perp}$. Define successive approximations, suppressing the dependence on λ (which comes into the nonlinear term ϕ) by:

$$u_i = (d\Phi_{(0,0)})^{-1}(-\phi(u_{i-1})) + u_1 \tag{7.2}$$

and at each stage, approximate E by;

$$E_i = d\Phi_{(0,0)}\, u_{i-1} + \phi(u_{i-1}) = \Phi(u_{i-1}). \tag{7.3}$$

Note that at each stage, by construction the projection onto the null space of u_i is u_1. The projection of E_∞ onto $\text{Range}(d\Phi)^{\perp}$ will be the reduced bifurcation equations.

Theorem 7.1.1 *For the iteration defined by equations 7.2, 7.3, there exist positive constants* R, K_1, K_2, K_3 *such that:*

$$\begin{aligned} ||u_n - u_{n-1}|| &< (K_1\,\epsilon)^n \\ ||u_n|| &< K_2\,\epsilon \\ ||E_n - E_{n-1}|| &< (K_3\,\epsilon)^n. \end{aligned}$$

for $||u_1, \lambda|| < \epsilon < R$. *The iterations* $u_i \to u_\infty$ *and* $E_i \to E_\infty$ *converge.*

Proof of first two estimates Because $(\mathrm{d}\Phi)^{-1}$ is bounded and ϕ is differentiable (it is a polynomial) in some neighbourhood of 0, we can pick M_1 and M_2 such that

$$\begin{aligned} ||(\mathrm{d}\Phi_{(0,0)})^{-1} u|| &< M_1\,||u|| \\ ||\mathrm{d}\phi_{(u,\lambda)}\,v|| &< M_2\,||v|| \text{ for } ||u, \lambda|| < R. \end{aligned}$$

Assume that the estimates hold for $n = 1, \cdots, k-1$.

$$\begin{aligned} ||u_k - u_{k-1}|| &= ||(\mathrm{d}\Phi_{(0,0)})^{-1}(-\phi(u_{k-1})) - (\mathrm{d}\Phi_{(0,0)})^{-1}(-\phi(u_{k-2}))|| \\ &< M_1||\phi(u_{k-2}) - \phi(u_{k-1})|| \\ &< M_1 \sup_{t\in[0,1]} \{||t u_{k-1} + (1-t)u_{k-2}||\}\,||u_{k-1} - u_{k-2}|| \\ &< 2M_1\,M_2\,K_2\,(K_1\,\epsilon)^k \end{aligned}$$

and so $2M_1\,M_2\,K_2 < K_1$, and

$$\begin{aligned} ||u_k|| &< \sum_{n=2}^{k} ||u_n - u_{n-1}|| + ||u_1|| \\ &< \epsilon/(1 - K_2\epsilon) \\ &< 2\epsilon \end{aligned}$$

for $\epsilon < 1/K_2$, and the inductive step is complete. □

Thus, for some neighbourhood U of the origin in $N \times \mathbf{R}^2$, the sequence (u_i, E_i) converges to some (u_∞, E_∞). If $E_\infty = 0$, then u_∞ is the required solution with projection u_1 onto the null space N.

Apply this to the K-S equation in its weak form, keeping a matrix of the coefficients $y(k,l)$ of the Fourier modes. The nature of the nonlinearity ϕ means that at each stage in the iteration, each pair of non-zero modes excites at most four other modes corresponding to sums and differences in the x and y directions. In order to move the parameter dependence on domain size to a dependence in the equations, set $\Omega = [0, 2\pi]^2$, and the linearised equation at parameters (a_0, b_0) becomes:

$$\mathrm{d}\Phi_{(0.0)} = \frac{u_{xxxx}}{a_0^4} + 2\frac{u_{xxyy}}{a_0^2 b_0^2} + \frac{u_{yyyy}}{b_0^4} + \frac{u_{xx}}{a_0^2} + \frac{u_{yy}}{b_0^2}.$$

The nonlinear terms at $(a_0/\sqrt{1-\tilde{a}}, b_0/\sqrt{1-\tilde{b}})$ are polynomial functions of u, its spatial derivatives up to fourth order, and the perturbations of the parameters $\tilde{a}$ and $\tilde{b}$. We truncate all equations at first order in the parameters and at a specified order in the null space coordinates. The iteration was performed using the computer algebra package MAPLE produced by WATCOM at the University of Waterloo.

Theoretically, the most efficient way of calculating the equations E_i to any order i, is to identify possible non-zero coefficients by the singularity theory of [6, 55], and simultaneously work backwards from these coefficents and forward from the null space, calculating all the nonlinear modes that fan out from it at each order. In practise, we truncate all coefficients at $i+1$st order and accept a large level of redundancy in the calculations.

Performing the above iteration to a specified order m is a matter of repeatedly applying equation 7.2, each time truncating all the answers to order $m+1$ in ϵ. Finally, truncating E_m to this order will give us a set of algebraic equations of order at most m involving the coordinates in the null space and the parameters. These equations must be satisfied in order to find a solution for the original system. Since we now have the set of algebraic equations, as long as they are non-degenerate to their highest order, we can set $\epsilon = 1$ and hypothesise that $(u, v, w, ...)$ are of order $\epsilon \ll 1$.

Below, we discuss Liapunov-Schmidt reduction for a specific example, the $(1,2)$: $(2,1)$ mode interaction on the square, and then list some examples of higher order mode interactions allowed by the theorem above.

7.1.1 A reduction by hand: $(1,2):(2,1)$

We shall start by setting

$$\begin{aligned} u_0 &= ue(2,1) + ve(1,2) \\ a &= \sqrt{5}/(1-A) \\ b &= \sqrt{5}/(1-B) \end{aligned}$$

assuming (u, v, A, B) are all order ϵ, and ignoring terms which are not linear in (A, B) or (uA, vB, vA, vB). Then E_1 is given by;

$$E_1 = v\left(-\frac{A}{5} - \frac{4B}{5}\right)e(1,2) + u\left(-\frac{4A}{5} - \frac{B}{5}\right)e(2,1).$$

Defining u_1 as above, we get

$$\begin{aligned} u_1 &= u_0 + \frac{15}{16}u^2e(0,2) + \frac{15}{704}v^2e(0,4) \\ &\quad + \frac{5}{3}vue(1,1) + \frac{15}{16}v^2e(2,0) + \frac{1}{48}v^2e(2,4) \\ &\quad + \frac{5}{117}vue(3,3) + \frac{15}{704}u^2e(4,2). \end{aligned}$$

Going to the second stage of approximation, E_2 is

$$\begin{aligned} E_2 &= v\left(-\frac{A}{5} - \frac{4B}{5} + \frac{227}{528}u^2 + \frac{8}{39}v^2\right)e(1,2) \\ &\quad + u\left(-\frac{4A}{5} - \frac{B}{5} + \frac{227}{528}v^2 + \frac{8}{39}u^2\right)e(2,1) \end{aligned}$$

which is three determined (i.e. as a germ at the origin, it is strongly equivalent [51] to its truncation at third order) and provides the bifurcation equation we seek. We can also calculate the manifold $\Phi = 0$ to third order, u_2.

7.1.2 Examples of reduced bifurcation equations and unfoldings

In order to simplify the Liapunov-Schmidt reduction, perturb the point (a_0, b_0) in parameter space to $(a_0/\sqrt{1-\tilde{a}}, b_0/\sqrt{1-\tilde{b}})$ (so that the linear part $\mathrm{d}\Phi_{(0,0)}$ has polynomial dependence upon the perturbed parameters, rather than polynomial or infinite power series). Linearising in the perturbations of the parameters, this corresponds to perturbing (a_0, b_0) to $(a_0(1+\tilde{a}/2), b_0(1+\tilde{b}/2))$, and thus the orientation of increasing a and b is preserved. The following sections give the bifurcation equations, viewed as being unfolded by these new parameters $(\tilde{a}, \tilde{b})$.

(k,0):(0,l) for (k,l) in $\mathbf{N}^2$

The interaction between two 1-d modes in different directions is essentially very simple. The projection of the bifurcation equation is just two decoupled ones; note that this is an effect described in the section on 1-d solutions of the 2-d equation. For example, the $(1,0),(0,1)$ mode interaction which happens at $(a,b) = (1,1)$, defining $(a,b) = (1/\sqrt{1-\tilde{a}}, 1/\sqrt{1-\tilde{b}})$ has bifurcation equation

$$\begin{aligned} 0 &= -\tilde{b}u + \frac{u^3}{12} \\ 0 &= -\tilde{a}v + \frac{v^3}{12} \end{aligned}$$

with the coordinate in the null space being $u\,e(0,1) + v\,e(1,0)$.

There are several solutions near this bifurcation, but note that the decoupling of the x and y equations makes this a trivial problem with a double-pitchfork bifurcation: The possible solutions are:

$u = 0, v = 0$	trivial
$u = \pm\sqrt{12\tilde{b}}, v = 0$	pure u mode
$u = 0, v = \pm\sqrt{12\tilde{a}}$	pure v mode
$u = \pm\sqrt{12\tilde{b}}, v = \pm\sqrt{12\tilde{a}}$	mixed mode

See figure 7.2 for the associated bifurcation diagram.

(1,1):(2,0)

This mode interaction happens at $(a,b) = (2, 2/\sqrt{3})$ and gives rise to a 1-d like mode interaction between 1 and 2 in the x-direction [6]. If the null space coordinates are $u\,e(1,1) + v\,e(2,0)$ and $(a,b) = (2/\sqrt{1-\tilde{a}}, 2/(\sqrt{1-\tilde{b}}\sqrt{3}))$, then the resulting bifurcation equations are

$$\begin{aligned} 0 &= -\frac{u(\tilde{a}+3\tilde{b})}{4} + \frac{uv}{2} + \frac{5u^2}{96} + \frac{v^2}{8} \\ 0 &= -\tilde{a}v + \frac{u^2}{8} + \frac{u^2 v}{16} + \frac{v^3}{12} \end{aligned}$$

It it noticeable that any $\mathbf{Z}_2$ symmetry (inherited from linearisation) is broken by nonlinear terms, in this case by the presence of the quadratic terms uv and u^2, as predicted in [6], a phenomenon sometimes called *strong resonance.*

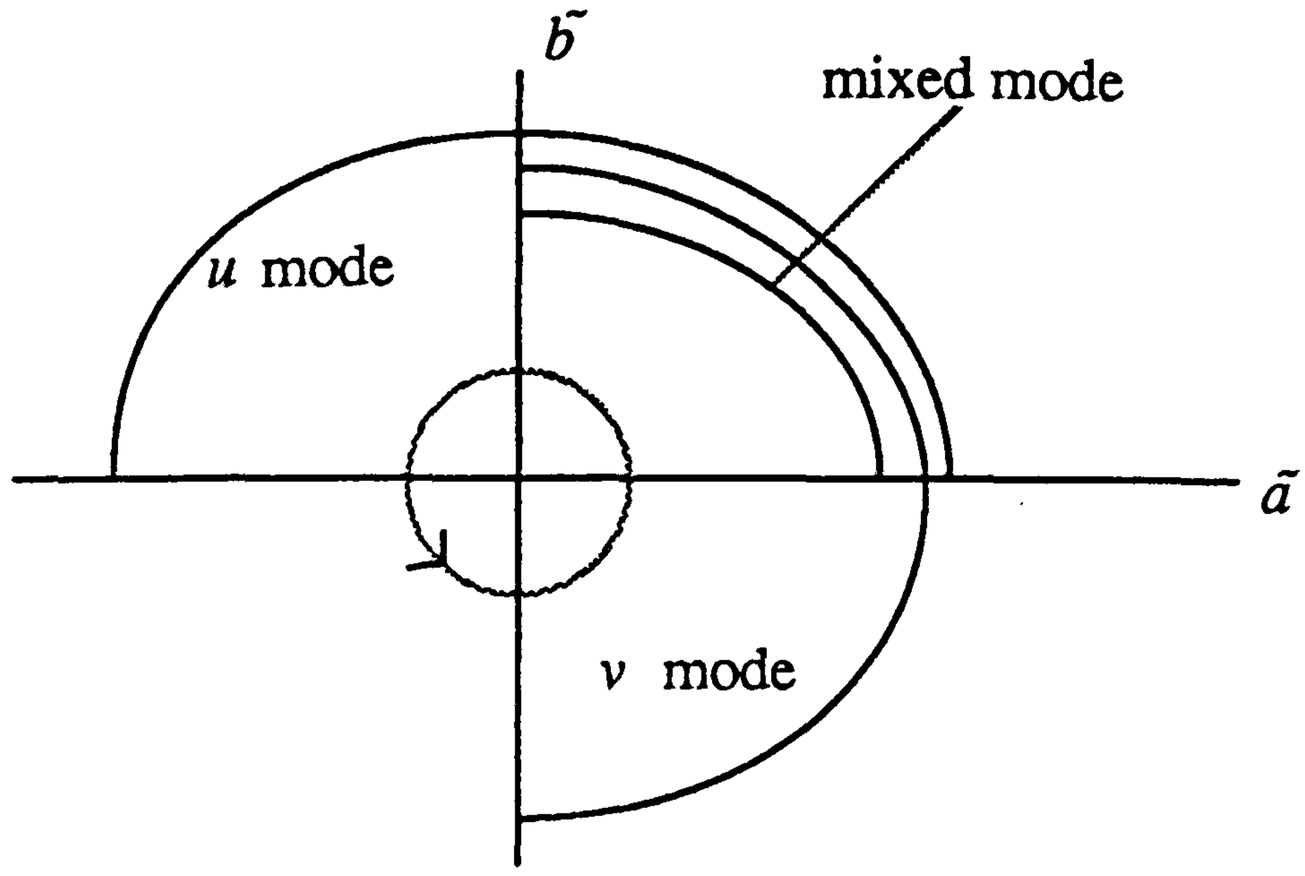

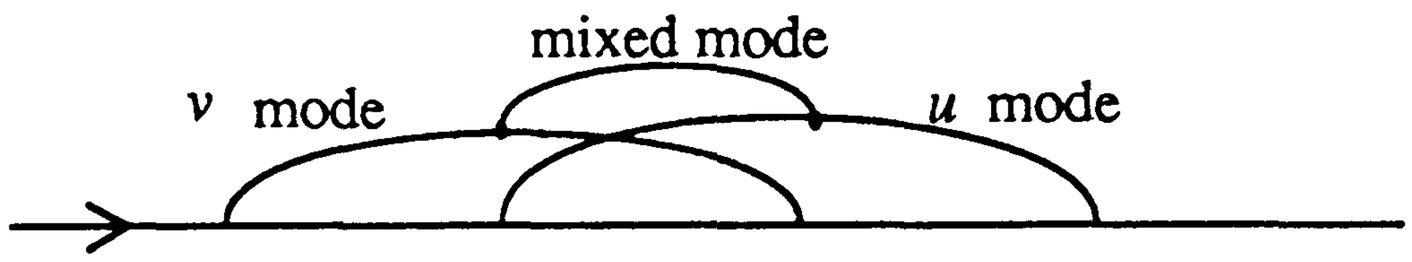

Figure 7.2: The interaction between pure $(k,0)$ and $(0,l)$ modes. Each of the modes is one dimensional, and the resulting bifurcation diagram factors into a product of two pitchforks. (a) shows the interaction in the $(\tilde{a},\tilde{b})$ plane, and (b) shows the bifurcation diagram to be obtained by making an asymptotically small circuit about the origin of (a).

In order to put this bifurcation equation into a more pleasant form, use the transformation of [6] for a 1-d mode interaction between modes 1 and 2, setting

$$\begin{aligned} x &= u + \frac{8uv}{24} \\ y &= v + \frac{10u^2}{96} \\ \alpha &= \tilde{a} \\ \beta &= \frac{(\tilde{a}+3\tilde{b})}{4} \end{aligned}$$

and so we get the equations

$$\begin{aligned} 0 &= x(-\beta + y/2) \\ 0 &= y(\frac{y^2}{12} - \alpha) + x^2 \end{aligned}$$

with the possible solutions being

$x=0, y=0$	trivial
$x=0, y=\pm\sqrt{12\alpha}$	pure v mode
$x=\pm\sqrt{2\beta(\frac{\beta^2}{3}-\alpha)}, y=2\beta$	mixed mode

(see figure 7.3 for bifurcation diagrams).

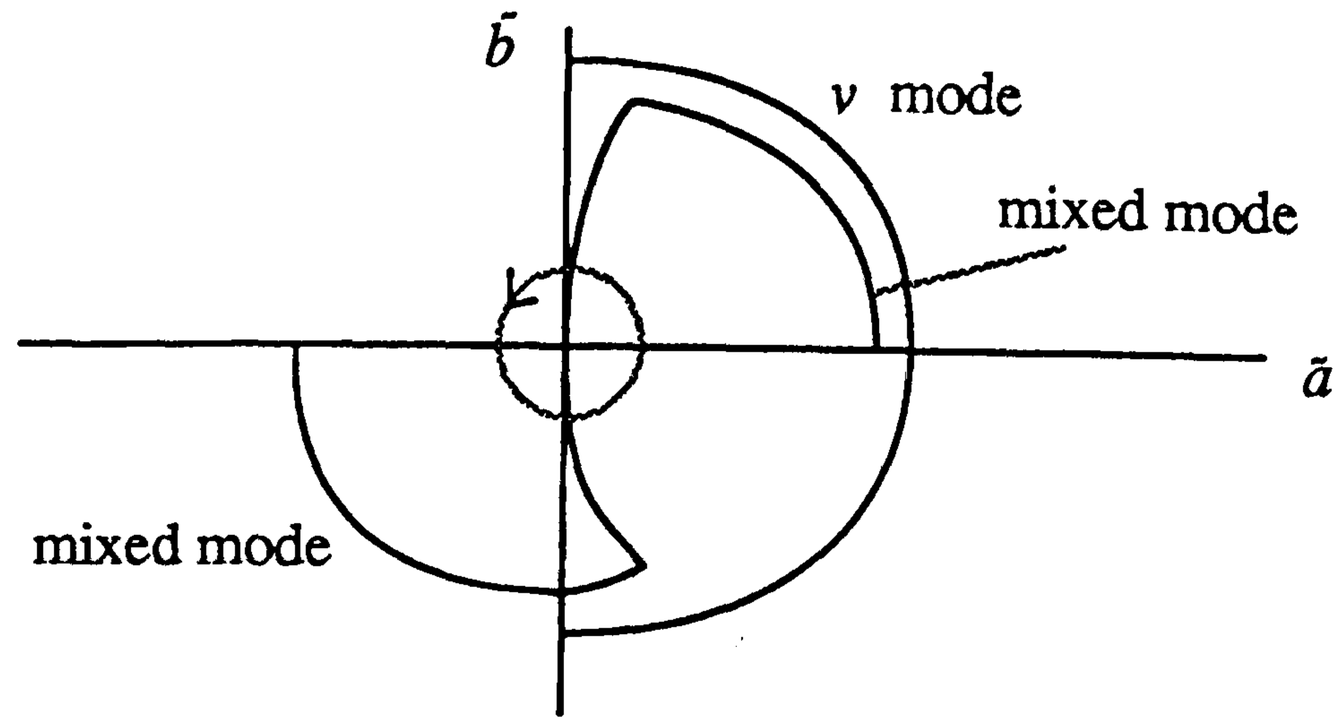

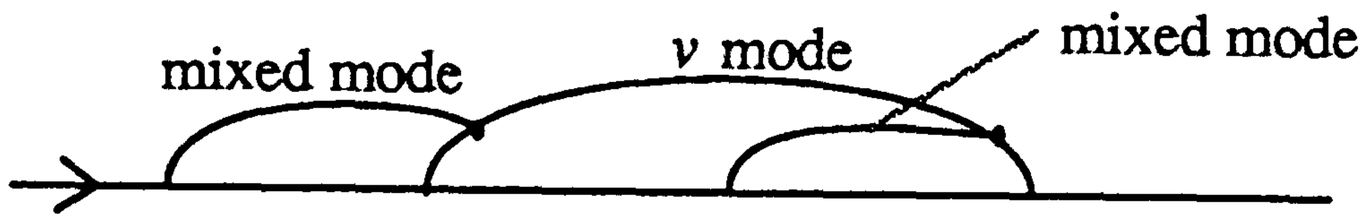

Figure 7.3: The interaction between the $(1,1)$ and $(2,0)$ modes. There are two regions of existence of a mixed-mode solution that is a pure $(1,1)$ mode near its bifurcation from the trivial solution, and meets the $(2,0)$ mode as a mixed mode.

(1,2):(2,1)

This fully two-dimensional mode interaction on the square at $(a,b) = (\sqrt{5},\sqrt{5})$ has been derived by hand in subsection 7.1.1. The equations are determined at cubic order, and displays $\mathbf{D}_4$ square symmetry. If the null space coordinates are $u\,e(2,1) + v\,e(1,2)$ and $(a,b) = (2/\sqrt{1-\tilde{a}}, 2/(\sqrt{3}\sqrt{1-\tilde{b}})$, then the resulting bifurcation equations are

$$\begin{aligned} 0 &= -\frac{u(4\tilde{a}+\tilde{b})}{5} + \frac{227u^3}{528} + \frac{8v^2u}{39} \\ 0 &= -\frac{v(\tilde{a}+4\tilde{b})}{5} + \frac{227v^3}{528} + \frac{8u^2v}{39}. \end{aligned} \tag{7.4}$$

This cubic determined mode interaction has solutions like that for the $(k,0) : (0,l)$ interactions above. The solutions are:

$u = 0, v = 0$	trivial
$u = \pm\sqrt{0.98\tilde{a} + 3.90\tilde{b}}, v = 0$	pure u mode
$u = 0, v = \pm\sqrt{+3.90\tilde{a} + 0.98\tilde{b}}$	pure v mode
$u = \pm\sqrt{-0.55\tilde{a} + 2.12\tilde{b}}, v = \pm\sqrt{2.12\tilde{a} - 0.55\tilde{b}}$	mixed mode

Note that in fact all the coefficients given here to two decimal places are in fact rational numbers coming from solving equations 7.4. See figure 7.4 for the bifurcation diagram.

(1,3):(4,2):(5,1)

This three mode interaction occurs at $(a,b) = (2\sqrt{7}, 2\sqrt{7/3})$. If the null space coordinates are $u\,e(5,1) + v\,e(1,3) + w\,e(4,2)$ and $(a,b) = (2\sqrt{7}/\sqrt{1-\tilde{a}}, 2\sqrt{7/3}/\sqrt{1-\tilde{b}})$, then the resulting bifurcation equations are:

$$0 = -\frac{u(25\tilde{a}+3\tilde{b})}{28} + \frac{vw}{4} + \frac{133u^3}{576} + \frac{199w^2u}{960} + \frac{29v^2u}{1440}$$

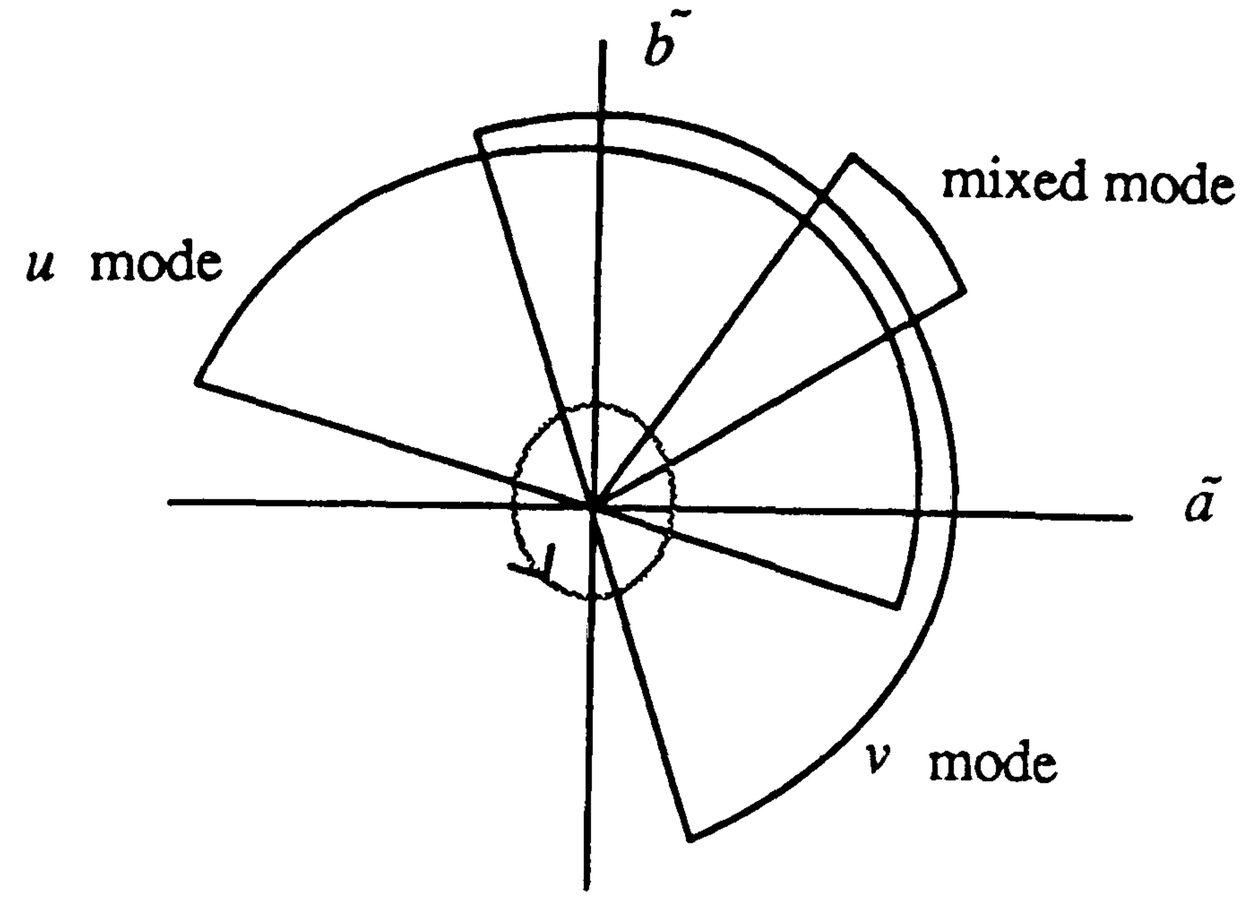

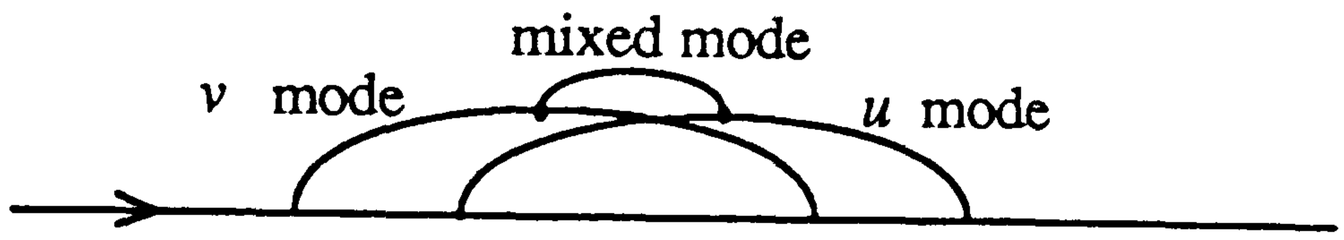

Figure 7.4: The interaction of the $(2,1)$ and $(1,2)$ modes. This behaves very much like the superposition of two pitchfork bifurcations.

$$0 = -\frac{v(\tilde{a}+27\tilde{b})}{28}+\frac{wu}{4}+\frac{63v^3}{320}+\frac{139w^2v}{576}+\frac{29u^2v}{1440}$$
$$0 = -\frac{w(4\tilde{a}+3\tilde{b})}{7}+\frac{vu}{4}+\frac{7w^3}{720}+\frac{199u^2w}{960}+\frac{139v^2w}{576}.$$

As with the 2, 1 mode interaction on a line, the presence of quadratic terms breaks the symmetry, unlike in the following section. In fact there are no two-mode interactions, but there is a three-mode one. The solution set (up to cubic order) looks like:

$u=0, v=0, w=0$	trivial
$u=\pm\sqrt{3.87\tilde{a}+0.46\tilde{b}}, v=0, w=0$	pure u mode
$u=0, v=\pm\sqrt{0.18\tilde{a}+4.72\tilde{b}}, w=0$	pure v mode
$u=0, v=0, w=\pm\sqrt{14.7\tilde{a}+11.0\tilde{b}}$	pure w mode
$u=\pm\sqrt{(0.04\tilde{a}+0.96\tilde{b})(0.57\tilde{a}+0.43\tilde{b})}$ $v=\pm\sqrt{(0.89\tilde{a}+0.11\tilde{b})(0.57\tilde{a}+0.43\tilde{b})}$ $w=\pm\sqrt{(0.04\tilde{a}+0.96\tilde{b})(0.89\tilde{a}+0.11\tilde{b})}$	mixed mode

The bifurcation diagram is shown in figure 7.5.

(9,2):(7,4):(5,5)

If the null space coordinates are $u\,e(9,2)+v\,e(7,4)+w\,e(5,5)$ and

$$(a,b)=(1\sqrt{11/3}/\sqrt{1-\tilde{a}}, 2.5\sqrt{11/3}/\sqrt{1-\tilde{b}}),$$

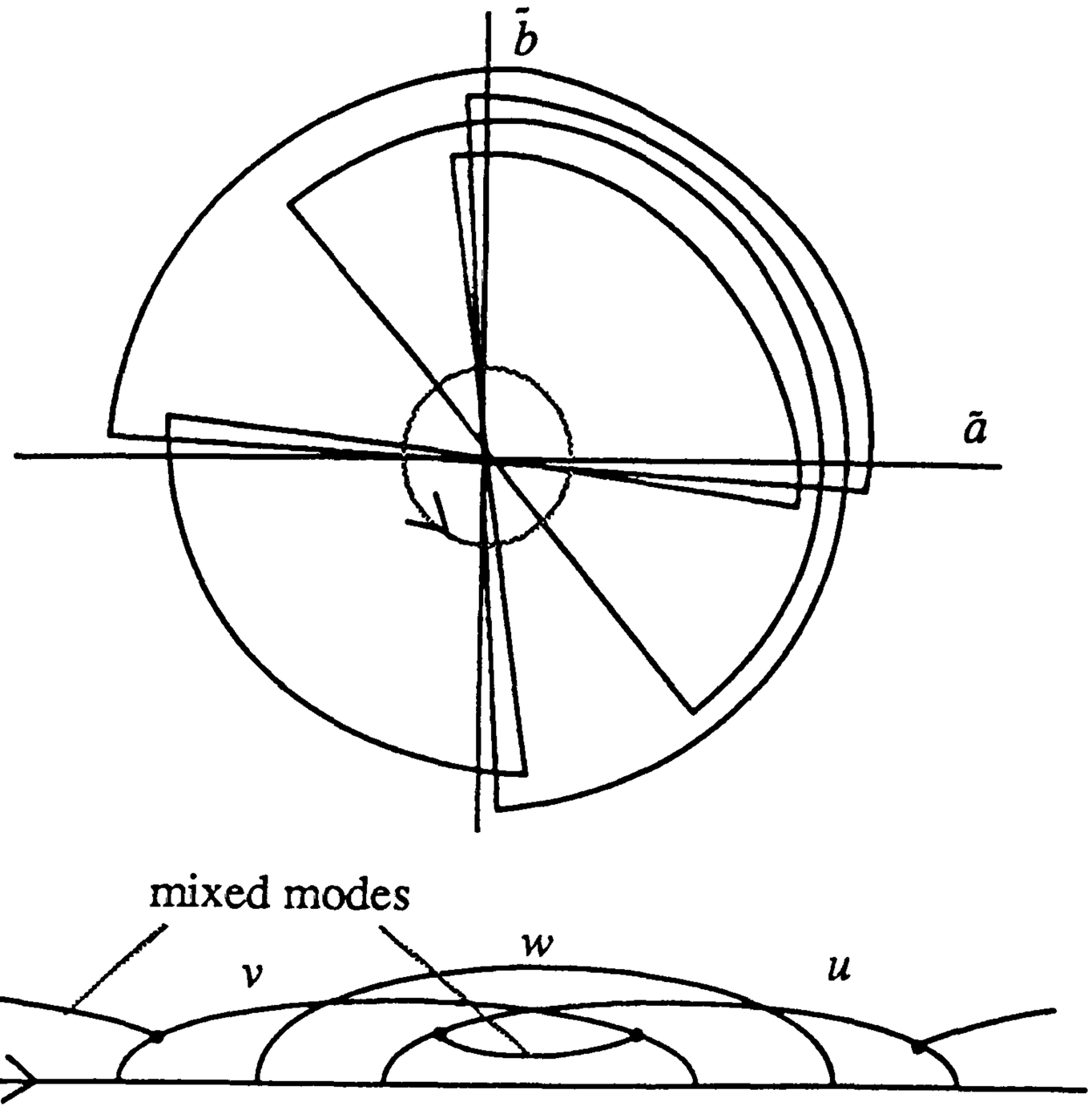

Figure 7.5: The three mode interaction of modes $(1,3),(4,2),(5,1)$. The pure $(5,1)$ and $(1,3)$ modes are joined by a mixed mode that also has a $(4,2)$ component of the same order.

then the resulting bifurcation equations are

$$\begin{aligned}
0 &= -\frac{u(243\tilde{a}+32\tilde{b})}{275}+\frac{130107u^3}{546448}-\frac{89v^2u}{213}+\frac{5743w^2u}{30597}\\
0 &= -\frac{v(147\tilde{a}+128\tilde{b})}{275}+\frac{21839v^3}{1186896}+\frac{403w^2v}{2737}-\frac{89vu^2}{213}\\
0 &= -\frac{w(3\tilde{a}+8\tilde{b})}{11}-\frac{193w^3}{336}+\frac{403wv^2}{2737}+\frac{5743wu^2}{30597}.
\end{aligned}$$

(8,1):(1,8):(7,4):(4,7)

Finally, an example of a four-mode interaction on a square domain. Note that the extra symmetry a square has over a rectangle causes the modes to come in pairs unless they are of the form (k,k). This interaction comes at $(\tilde{a},\tilde{b})=(0,0)$ where $(a,b)=(\sqrt{65}/\sqrt{1-\tilde{a}},\sqrt{65}/\sqrt{1-\tilde{b}})$, and if the null space coordinates are $u\,e(8,1)+v\,e(1,8)+w\,e(7,4)+x\,e(4,7)$, then the equations are:

$$\begin{aligned}
0 &= -\frac{u(64\tilde{a}-\tilde{b})}{65}+\frac{106907u^3}{559248}+\frac{6064w^2u}{15873}-\frac{128v^2u}{3201}+\frac{173x^2u}{759}\\
0 &= -\frac{v(\tilde{a}+64\tilde{b})}{65}+\frac{106907v^3}{559248}+\frac{6064x^2v}{15873}-\frac{128u^2v}{3201}+\frac{173w^2v}{759}\\
0 &= -\frac{w(49\tilde{a}+16\tilde{b})}{65}+\frac{26276w^3}{6288}+\frac{6064u^2w}{15873}+\frac{173v^2w}{759}+\frac{1568x^2w}{8319}\\
0 &= -\frac{x(16\tilde{a}+49\tilde{b})}{65}+\frac{26276x^3}{6288}+\frac{6064v^2x}{15873}+\frac{173u^2x}{759}+\frac{1568w^2x}{8319}.
\end{aligned}$$

Upon solving these truncated equations, it was found that there are pure, two-mode and three-mode branches of solutions, but no four-mode. We do not list them all (up to reflection, there are 41 possible branches counting all permutations of + and − signs, of which only 24 are real). As examples, here are some examples of representative branches with (u,v,w,x) equal to:

$(0,0,0,0)$	trivial
$(\pm\sqrt{5.15\tilde{a}+0.08\tilde{b}},0,0,0)$	pure u mode
$(\pm\sqrt{5.40\tilde{a}+1.21\tilde{b}},\pm\sqrt{1.21\tilde{a}+5.40\tilde{b}},0,0)$	mixed u-v mode
$(\pm\sqrt{6.2\tilde{a}+.3\tilde{b}},0,\pm\sqrt{-.4\tilde{a}+.1\tilde{b}},\pm\sqrt{.3\tilde{a}+.2\tilde{b}})$	mixed u-w-x mode

The only three mode solutions that occur are v-w-x and u-w-x, and figure 7.6 shows how these modes fit together in a small circuit about the mode interaction. Of course, these interactions are degenerate in that they are of codimension higher than the two parameters (a,b), but there is persistence of branches of steady solutions to small perturbations in the equations.

7.1.3 1-d solutions and multiple steady states in 2-d

The K-S equation has another interesting (but atypical) property: a superposition of an x-independent steady solution and a y-independent steady solution (called 1-d steady solutions) is a steady solution on the rectangle. Moreover if both of the 1-d solutions are asymptotically stable, then so is their superposition. In this way, it is possible to find a lot of possible stable dynamics, for example using the 1-d stable solutions found by Frisch et al. [49] to find 2-d superpositions thereof. The multistability of the 1-d states that they find also goes across to give lots of multistability on the rectangle (subject to the proviso that the linear parts are as described below). The following argument also holds for periodic boundary conditions.

Suppose one 1-d solution is $U(x)$, and the other is $V(y)$, satisfying

$$U_{xxxx}+U_{xx}+(U_x)^2=0$$

and

$$V_{yyyy}+V_{yy}+(V_y)^2=0.$$

with $x\in[0,a\pi]$ and $y\in[0,b\pi]$ respectively, and Neumann-type boundary conditions. Define

$$u(x,y)=U(x)+V(y).$$

Then this satisfies the 2-d equation as well, since $u_{xxyy}=0$.

Now suppose that each of the solutions is stable in the 1-d equation (with respect to time), in other words suppose that the linear operators

$$\begin{aligned} L_x\delta u &\equiv -\delta u_{xxxx}-\delta u_{xx}-2U_x\delta u_x \\ L_y\delta v &\equiv -\delta v_{yyyy}-\delta v_{yy}-2V_y\delta v_y \end{aligned}$$

both have contracting time-1 maps; their exponentials are contracting (we do not allow non-semisimple linear parts). The stability of the composite solution is determined by the the stability or otherwise of

$$\begin{aligned} L\delta u &\equiv -\delta u_{xxxx}-2\delta u_{xxyy}-\delta u_{yyyy}-\delta u_{xx}-\delta u_{xxyy}-2U_x\delta u_x-2U_y\delta u_y \\ &= L_x\delta u+L_y\delta u-2\delta u_{xxyy}. \end{aligned}$$

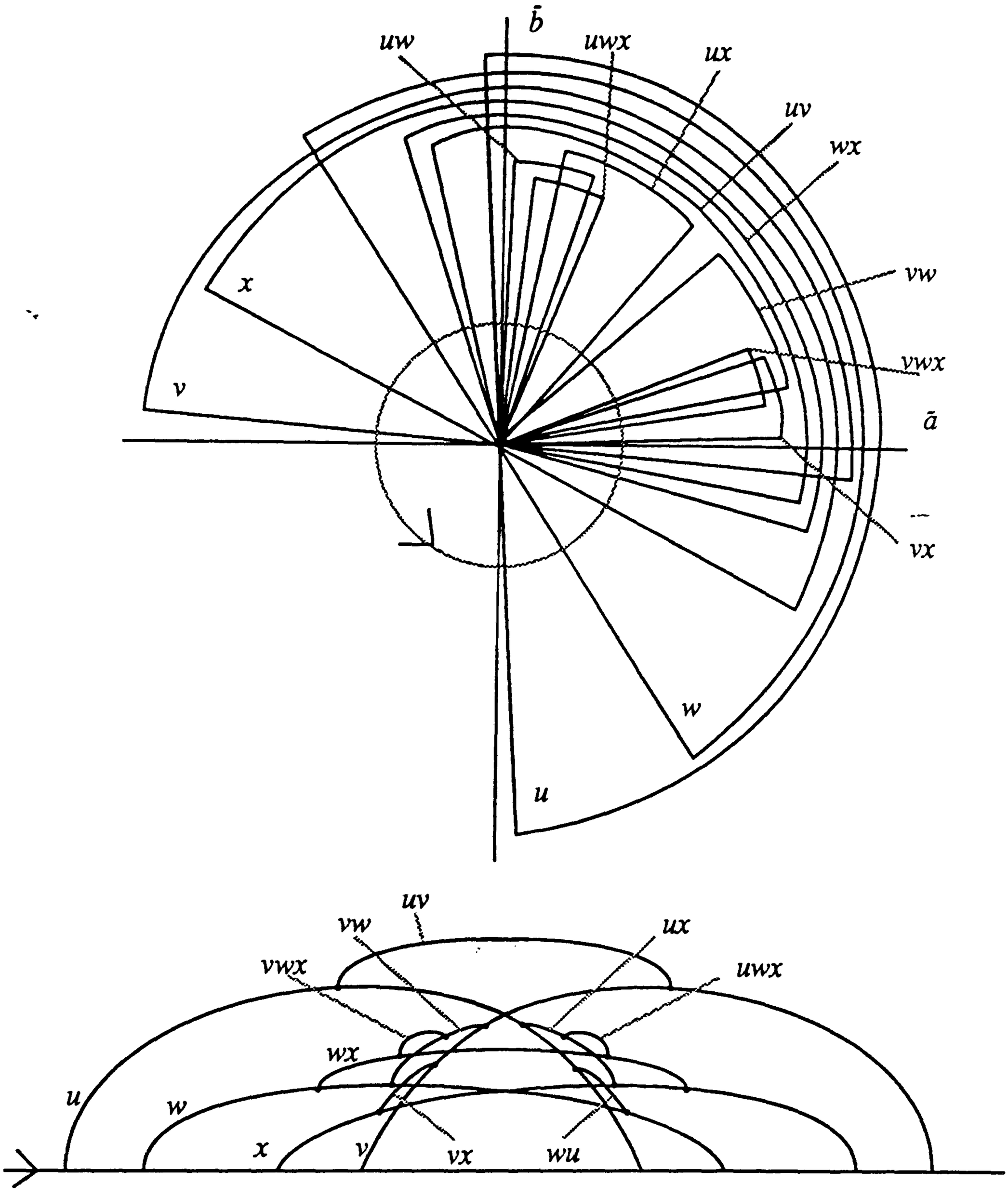

Figure 7.6: The four mode interaction between $(8,1):(1,8):(7,4):(4,7)$. Note there are pure modes, two mode and three mode branches in any neighbourhood of the origin of the perturbed parameter plane $(\tilde{a},\tilde{b})$.

However, the spectrum of the $-2\delta u_{xxyy}$ term is stable, as it has eigenfunctions

$$\cos(kx/a)\cos(ly/b)$$

with eigenvalues $-2(kl/ab)^2$. Thus the exponential of this is also contracting and the composition of the three operators is thus stable. (Alternatively, if we assume that L_x and L_y have a Hilbert basis of eigenvectors and real or complex conjugate pairs of eigenvalues (ϕ_n, λ_n) and (ψ_n, μ_n) respectively, is is simple to demonstrate that $L_x + L_y$ has a basis of eigenvectors $(\phi_n(x)\psi_m(y))$ with eigenvalues $\lambda_n + \mu_m$).

7.1.4 K-S on a disk

As an example to show how important the shape of the domain is in the previous example, we shall describe the linear theory for the K-S equation on a disk with Dirichlet-type boundary conditions. Note that on a rectangle, there is essentially no difference between Dirichlet and Neumann boundary conditions in the K-S equation, except that one-dimensional solutions like the $(0, k)$ modes are not permitted.

Changing to plane polar coordinates, the K-S equation becomes:

$$\begin{aligned} 0 &= u_t + \left(\frac{\partial^4}{\partial r^4} + \frac{2}{r}\frac{\partial^3}{\partial r^3} + \frac{1}{r^3}\frac{\partial}{\partial r} + \frac{2}{r^2}\frac{\partial^4}{\partial r^2 \partial\theta^2} + \frac{4}{r^4}\frac{\partial^2}{\partial\theta^2} + \frac{1}{r^4}\frac{\partial^4}{\partial\theta^4}\right) u \\ &\quad + \left(\frac{\partial^2}{\partial r^2} + \frac{1}{r}\frac{\partial}{\partial r} + \frac{1}{r^2}\frac{\partial^2}{\partial\theta^2}\right) u \\ &\quad + \left(\frac{\partial u}{\partial r}\right)^2 + \frac{1}{r^2}\left(\frac{\partial u}{\partial\theta}\right)^2 \end{aligned}$$

Looking at

$$\begin{aligned} u &= u(\mathbf{x}, t) \\ \mathbf{x} &\in D \equiv \{(r,\theta) : 0 \le r < a, \theta \in [0, 2\pi)\} \end{aligned}$$

with boundary conditions

$$\left.\begin{aligned} u &= 0 \\ \nabla^2 u &= 0 \end{aligned}\right\} \text{for } \mathbf{x} \in \partial D$$

with $D(a)$ being a disk of radius a centred at the origin. For the eigenfunctions, try:

$$e(m,n) = \exp(in\theta) J_n\left(\frac{k_{n,m}\, r}{a}\right)$$

where J_n is the nth order (cylindrical) Bessel function [1], and $k_{n,m}$ is the mth zero of $J_n(x)$). (With Neumann type boundary conditions, the only difference is that $k_{n,m}$ needs to be the mth zero of $J_n'(x)$. Note that the zeros of the derivative must interlace with the zeros of the function itself, but this only guarantees there are no mode interactions between modes with adjacent n.) Thus the dispersion relation becomes:

$$\omega + \frac{k_{n,m}^4}{a^4} - \frac{k_{n,m}^2}{a^2} = 0$$

and at bifurcation ($\omega = 0$), this implies that

$$k_{n,m}^2 = a^2.$$

Table 7.1 lists the first few modes (to 4 significant figures) in the order in which they become unstable. By examining the zeros of the Bessel functions, there are no number theoretic degeneracies up to (8,1), and it seems reasonable to expect there are none after that. It would be good, however, to have an analytical proof of this, or a counter-example.

mode	$k_{n,m}$	mode	$k_{n,m}$
(0,1)	2.4048	(5,1)	8.7715
(1,1)	3.8317	(3,2)	9.7610
(2,1)	5.1356	(6,1)	9.9361
(0,2)	5.5200	(1,3)	10.173
(3,1)	6.3801	(4,2)	11.064
(1,2)	7.0156	(7,1)	11.086
(4,1)	7.5883	(2,3)	11.619
(2,2)	8.4172	(0,4)	11.791
(0,3)	8.6537	(8,1)	12.225

Table 7.1:
The wavenumbers corresponding to the first 18 modes to bifurcate from the origin for the K-S equation on a disk with Dirichlet boundary conditions.

7.1.5 K-S on a sphere

If we pose the Kuramoto- Sivashinsky equation on a sphere of radius a, one of the most noticeable things is that there are no boundary conditions. The eigenfunctions are the spherical harmonics:

$$u(\theta,\phi) = P_m^l(\cos\theta)\left\{ \begin{array}{c} \sin \\ \cos \end{array} \right\}\phi$$

and the eigenvalues are proportional to l and not m. Thus, as higher and higher order modes bifurcate, we will get null spaces of size $2(2l+1)$. This is because for each l there are $2l+1$ spherical harmonics with $|m| \leq l$. As we increase a, we will get bifurcations from the spherical solution with null spaces of size 2,6,10,14.. corresponding to the irreducible representations of O(3) as given in [54, 34].

7.2 Mode interactions in the Michelson-Sivashinsky equation

It is possible to apply the above methods to mode interactions in the Michelson-Sivashinsky equation with $u_n = 0$ (Neumann boundary conditions). The only difference being that the dispersion relation is of the form:

$$\omega = \left(\frac{k^2}{a^2} + \frac{l^2}{b^2}\right)\left(1 - \sqrt{\frac{k^2}{a^2} + \frac{l^2}{b^2}}\right). \tag{7.5}$$

The square root prevents the reduced bifurcation equation from having rational coefficients. This means that it is necessary to either use the program to find the coefficients in surd form, or to work with floating point numbers. As an example the above technique can be applied to a four mode interaction on the square:

7.2.1 (1,8):(8,1):(4,7):(7,4) for the M-S equation

The MAPLE program yields the following bifurcation equations (to 3 decimal places):

$$\begin{aligned} 0 &= u(-.985\tilde{a} - .0154\tilde{b} + .409u^2 - .081v^2 + .693w^2 + .438x^2) \\ 0 &= v(-.0154\tilde{a} - .985\tilde{b} - .081u^2 + .409v^2 + .438w^2 + .693x^2) \end{aligned}$$

$$
\begin{aligned}
0 &= w(-.753\tilde{a} - .246\tilde{b} + .693u^2 + .438v^2 + 8.43w^2 + .343x^2) \\
0 &= x(-.246\tilde{a} - .753\tilde{b} + .438u^2 + .693v^2 + .343w^2 + 8.43x^2)
\end{aligned}
$$

Solving these equations in the $(\tilde{a}, \tilde{b})$ plane gives a bifurcation diagram that is essentially identical to that shown in figure 7.6.

7.3 Numerical experiments

7.3.1 Numerical method used

In order to check out the various effects and predictions described in the previous section, some numerical experiments on the K-S equation in a rectangle were performed. The Fourier decomposition in section 6.3.1 was used (Galerkin projection) to reduce the infinite dimensional problem to a finite dimensional one, and the resulting equations (being rather stiff due to the k^4 terms) were integrated using the variable step variable order Gears method [131] DO2QBF provided in the NAG library. The tolerance used was 10^{-6} for a 8 by 8 grid of 64 Fourier modes for two dimensions, and a 64 mode truncation for one mode. Only a small region in parameter space could be investigated with so few modes, and the results were tested to higher tolerances and more modes to assure that convergence was taking place.

The derivative dF for the equation $u_t + F(u) = 0$ was calculated explicitly for the root finding algorithm in the Gears method routine. With hindsight, it would have been more efficient to calculate the nonlinear terms using a FFT method [77].

The $(0,0)$ mode of the truncation decouples from all the others, being merely driven by them [7], and for this reason, we set this mode to zero for all time. This is equivalent to the formulation used by [59] for the K-S equation.

7.3.2 Results

We start with a set of initial conditions with an amplitude of 1 in the (1,1) mode and amplitudes of 10^{-5} in all other modes, to ensure that the integrator is not trapped in an isotropy subspace of the equation, that is respected exactly by the Galerkin method (see [77]). It was found in the region investigated there are many 1-d stable solutions, and it was difficult to find to any non-trivial (genuine 2-d modes).

7.4 Conclusions

As we have seen, Liapunov-Schmidt reduction has found a rich structure of branches bifurcating from the trivial solution, and the approach of reducing the problem to one for smooth germs works well, even though it is necessary to modify the concept of genericity with symmetry to take account of the structure of the problem, and not just the symmetry of the domain. All of the results depend quite strongly on the Euclidean invariance and the simple form of the nonlinearity, but with care, many of the results found could be seen as being generic for flame front equations.

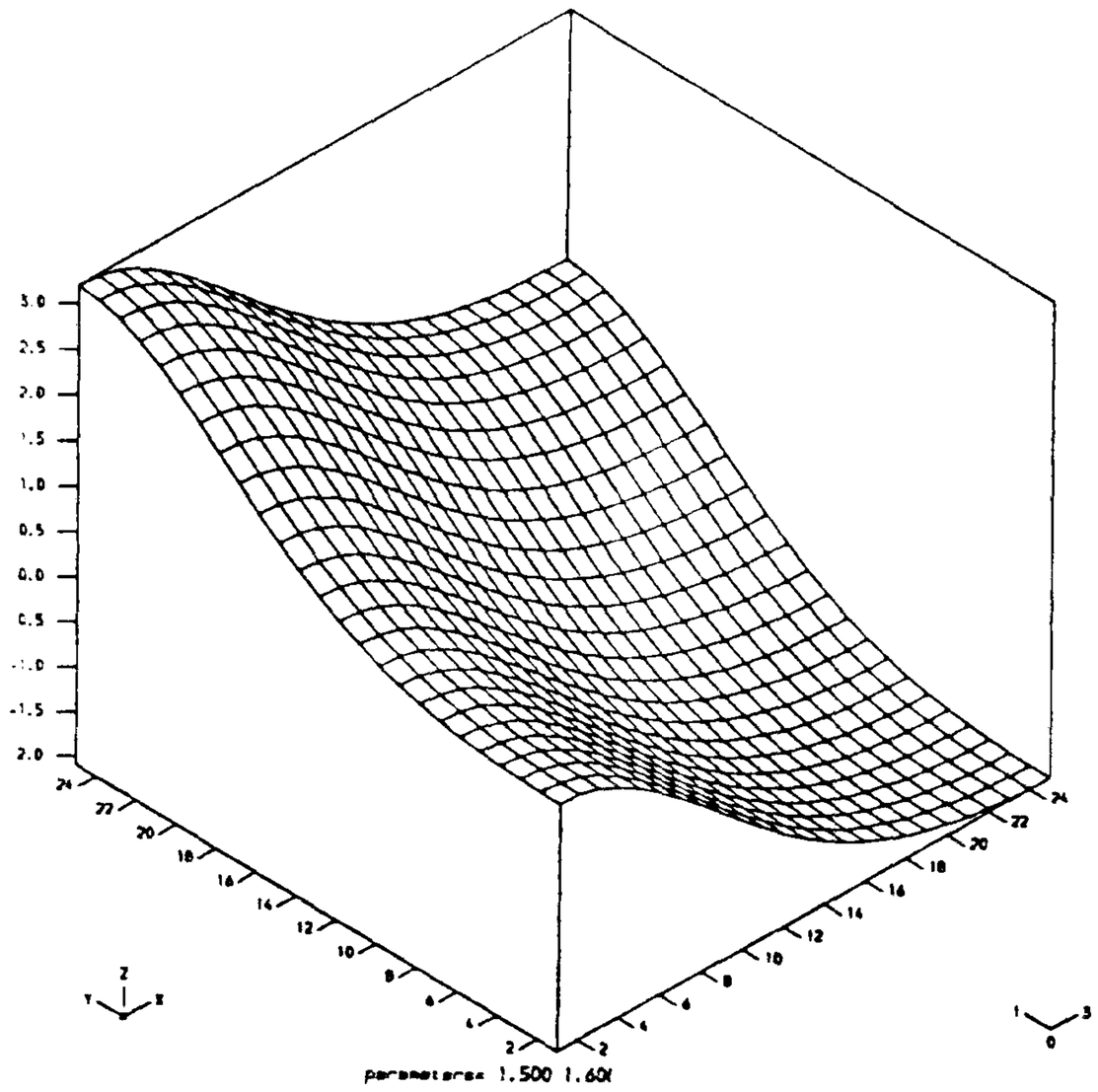

(1.5, 1.6)

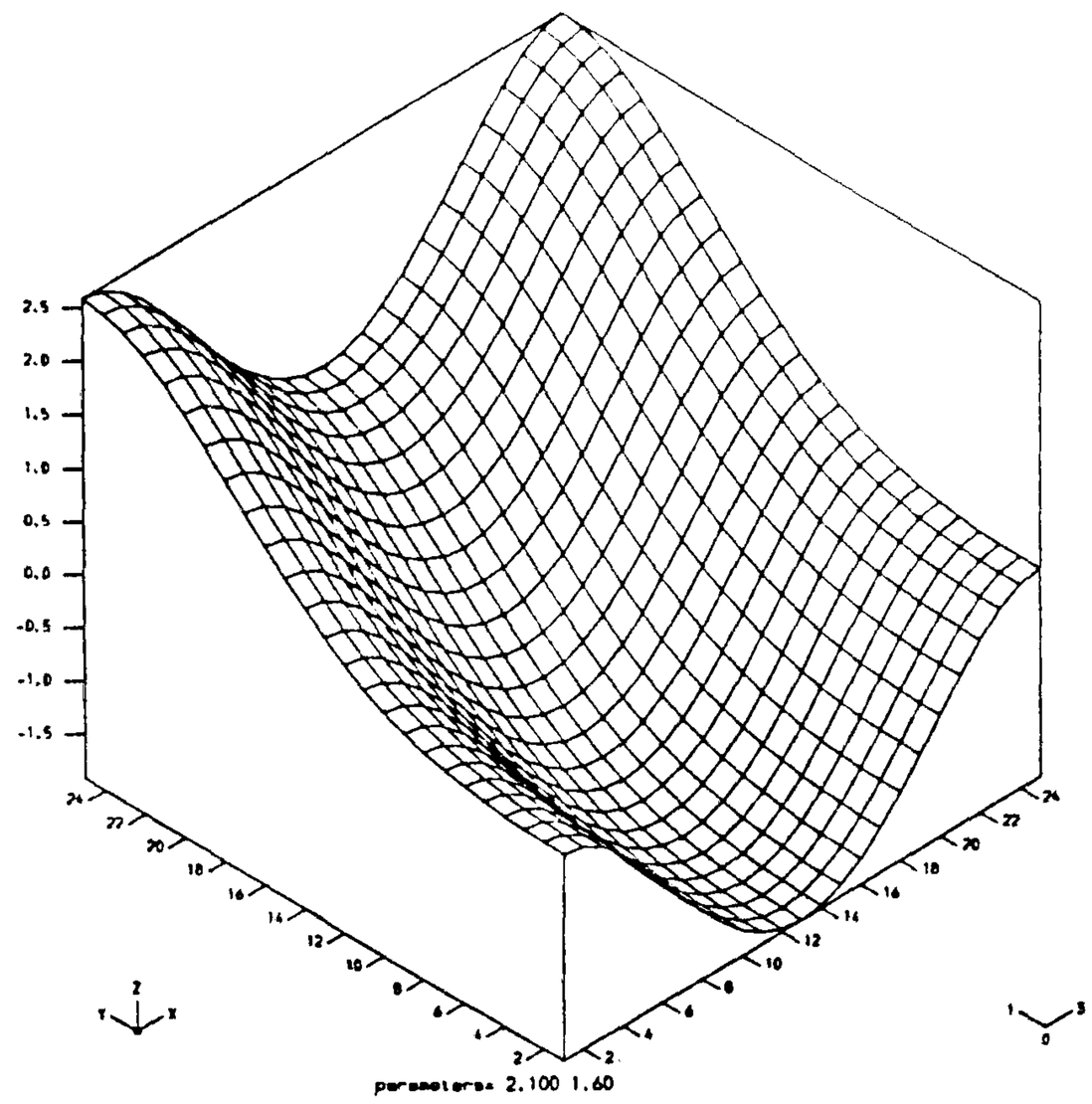

(2.1, 1.6)

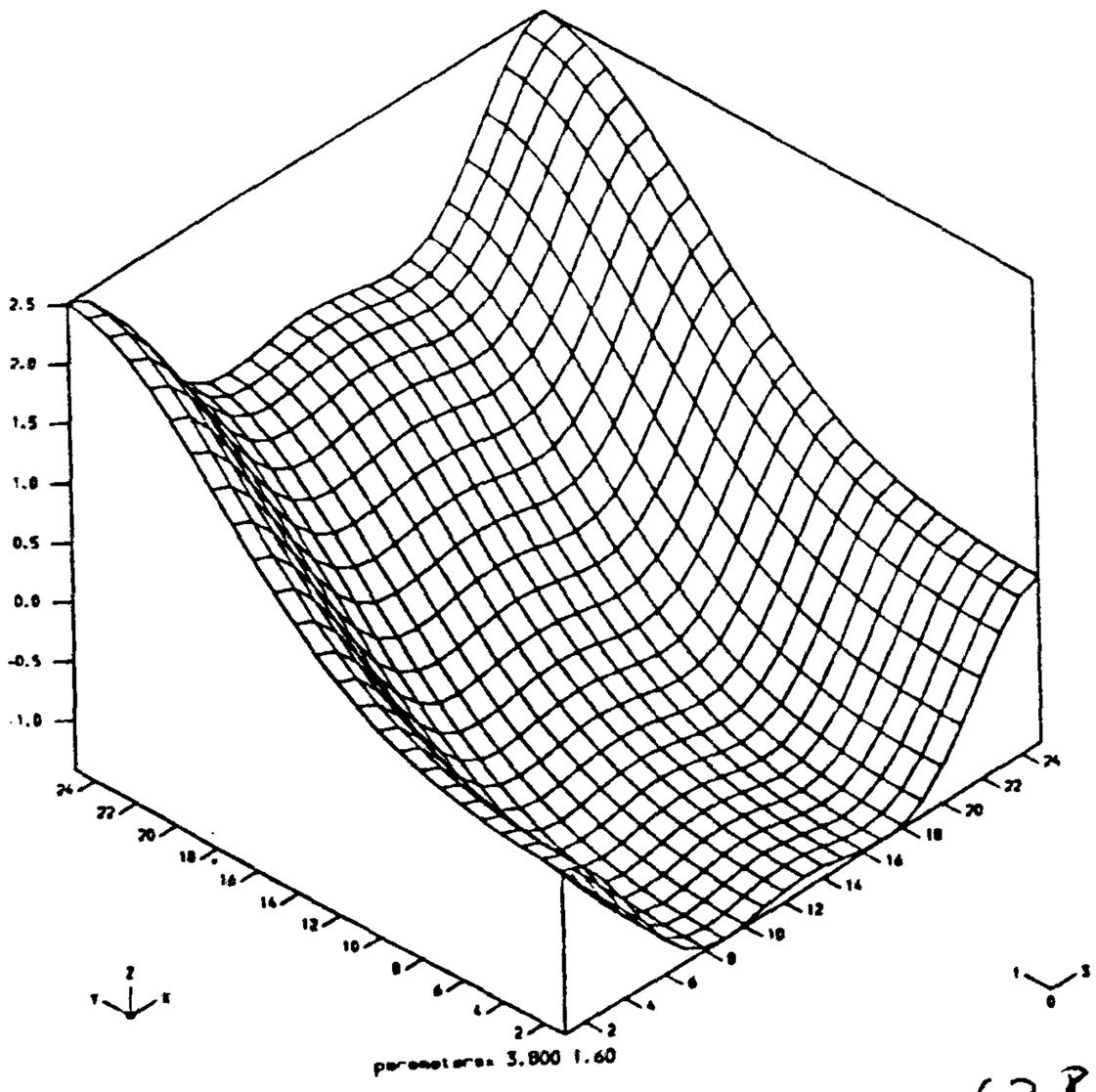

(3.8, 1.6)

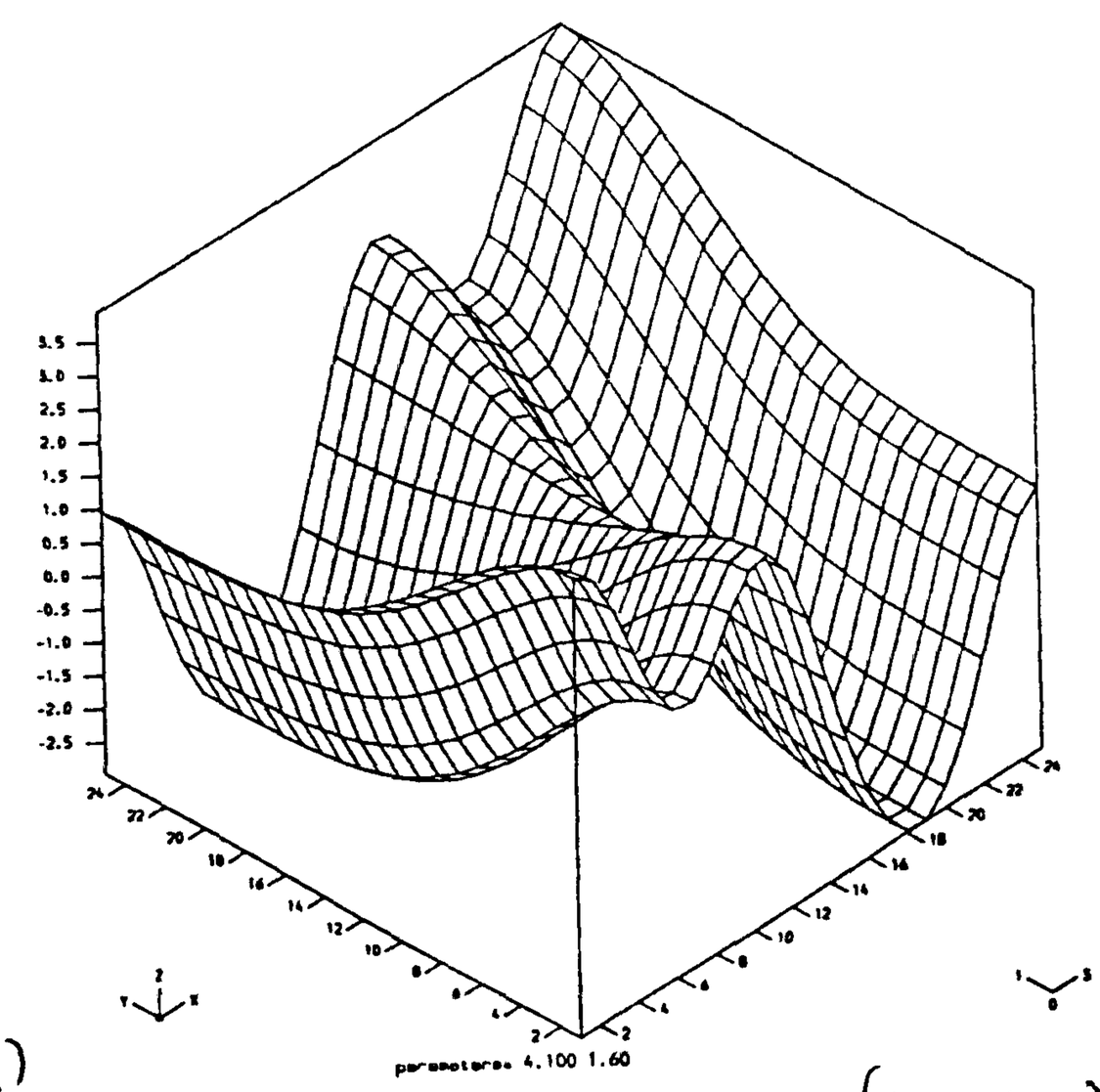

(4.1, 1.6)

Figure 7.7: The numerical results; Steady solutions on a rectangle at a few different values of (a, b). Three are superpositions of pure 1-d modes in the x and y directions, whereas the fourth is a fully 2-d mode.

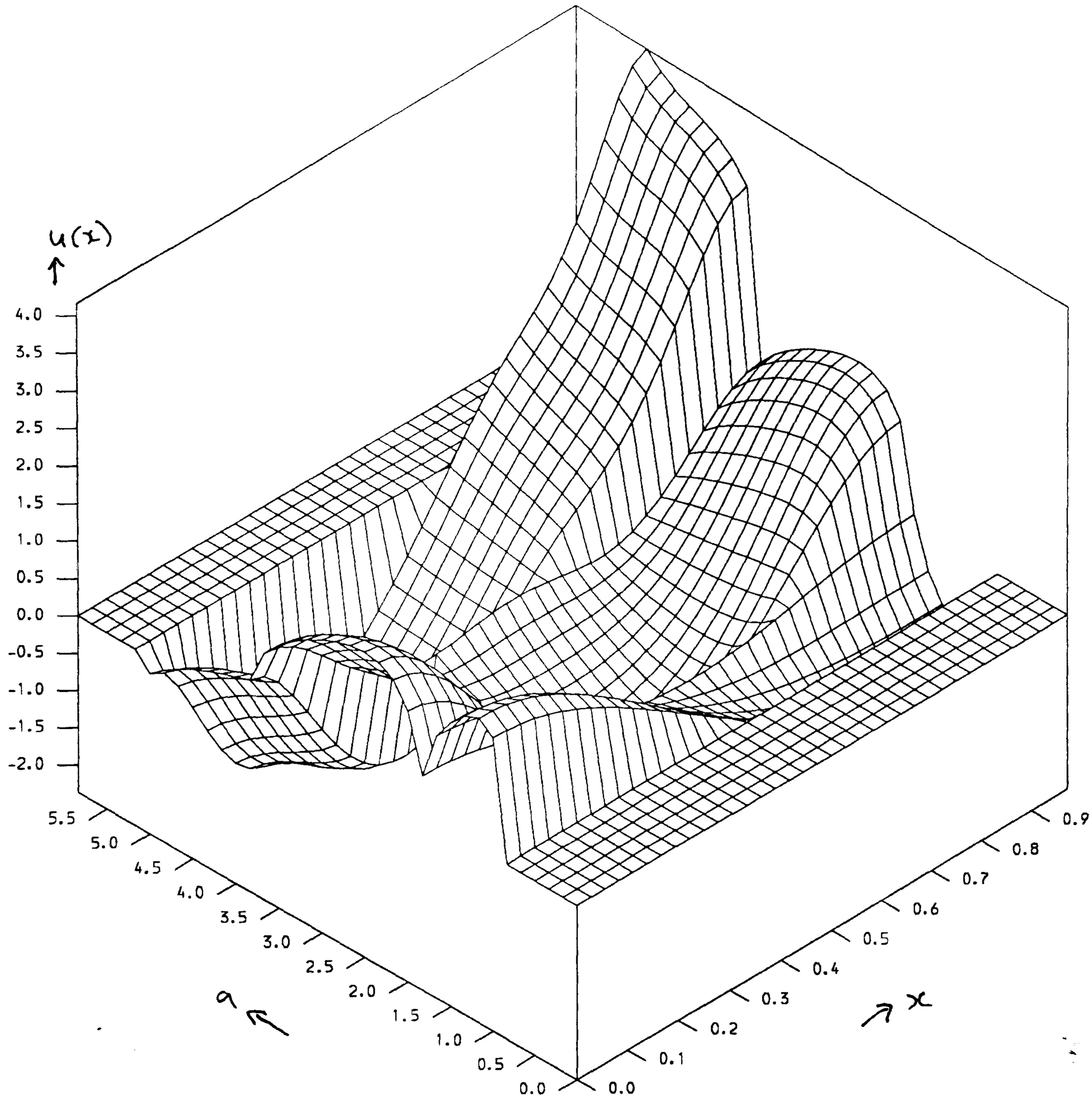

Figure 7.8: Steady solutions of the K-S equation on the line as the length of domain a varies. At each value of a, the diagram shows the solution u against x. Solutions equal to zero mean that the trivial solution is stable ($a < 1$) or that the residual after ever 30 timesteps had not died away to less than 10^{-14} after 500 time steps. At each parameter value, the previous final conditions are used as initial conditions.

Appendix A

Notation

n is the number of oscillators in the system in chapter 2

ω is the primitive n^{th} root of unit $e^{i2\pi/n}$.

$\mathbf{T}^1$ is the circle group (the 1-torus!) written as either $(\mathbf{R}/2\pi\mathbf{Z}, +)$ or $(\{z \in \mathbf{C} : |z| = 1\}, \times)$.

$\mathbf{T}^n$ is the n-torus, $\mathbf{T}^1 \times \cdots \times \mathbf{T}^1$.

$\mathbf{1}$ is the point $(1, \cdots, 1) \in \mathbf{T^n}$.

$\mathbf{T}^{n-1}$ is the torus $\mathbf{T}^n/\mathbf{T}^1\mathbf{1}$.

$G \times H$ is the direct (Cartesian) product of the groups G and H.

$G \otimes H$ is the semidirect product of the groups G and H.

$G \leq H$ with G and H groups means that G is a subgroup of H.

$\mathbf{S}_n$ is the symmetric group on n objects.

$\mathbf{D}_n$ is the dihedral group of symmetries of an n-sided polygon.

$\mathbf{Z}_n$ is the cyclic group of order n.

$\mathbf{O}(n)$ is the orthogonal group of all area preserving linear maps on $\mathbf{R}^n$.

$\mathbf{E}(n)$ is the Euclidéan group of all orthogonal transformations and affine translations in $\mathbf{R}^n$.

fix(G) is the fixed point space of all points invariant under the action of the representation of the group G.

e is the identity element in the group $\mathbf{S}_n$.

Appendix B

Computer program listings

(1) The program used to integrate the van der Pol-Duffing oscillators for the results in chapter 5.

(2) The MAPLE program for performing Liapunov-Schmidt reduction at the interaction of the $(0,1)$ and $(1,0)$ modes of the K-S equation. The same program with slight alterations is used for all the mode interaction calculations in chapter 7.

```
C
C       phaseav.f
C
C       Program to calculate level curves in vdpd system;
C       display on TEK4014 screen using ghost graphics.
C
C       P. Ashwin
C       Started 9-8-91
C       Latest revision 16-9-91
C
C       Compile using f77 -lghost -lg4014
C
        integer          numlev,numpha
        parameter        (numlev=50,numpha=50)
        double precision        xmax,xmin,lstep
        parameter        (xmax=1.5d0,xmin=.1d0,lstep=1.0d0)
C
C       numlev is number of energy levels to be calculated
C       numpha is number of phase " " "
C
C
        integer nout
        parameter        (nout=6)
        double precision        x,xstep,maxstep
        parameter        (maxstep=0.1)
        double precision        per(numlev),z(numlev,numpha)
        real    dphidt(numlev,numpha,2),dp(numlev,numpha),levs(25),maxdp
        real    uavx(numlev),uavy(numlev),minuav,maxuav
        integer          i,j,ii,jj
        character *60    txt
        double precision        y(2),yy,p,tstep
        double precision        ivalue,zval,dzdt,dzda
        external         ivalue,zval,dzdt,dzda
        external         contra,paper,axes,grend
        external         fcn,period,dsolve,corr
        intrinsic        dble
        common /zzz/ z(numlev,numpha)
        common /zph/ dphidt(numlev,numpha,2),uavx(numlev),uavy(numlev)
C
C       Main routine
C
C       Calculate period along 'i'th level
C
        do 20 i=1,numlev
          yy=ivalue(i)
          call period(yy,p,maxstep)
          per(i)=p
20      continue
C
C       calculate scaled integral curves
C
        do 50 i=1,numlev
          y(1)=0
          y(2)=ivalue(i)
          x=0
          xstep=per(i)/dble(numpha)
          ii=int(xstep/maxstep)+1
          xstep=xstep/ii
          do 40 j=1,numpha
            z(i,j)=y(1)
            do 30 jj=1,ii
              call dsolve(x,xstep,y)
              x=x+xstep
30          continue
40        continue
50      continue
```

```
      minuav=10e9
      maxuav=-10e9
C
C     Draw graph of R(alpha) against alpha
C
      do 70 i=1,numlev
        tstep=per(i)/dble(numpha)
        uavx(i)=sqrt(real(ivalue(i)))
        call corr(i,tstep)
        if (uavy(i).lt.minuav) minuav=uavy(i)
        if (uavy(i).gt.maxuav) maxuav=uavy(i)
70    continue
      du=(maxuav-minuav)/10.0
      call paper(1)
      call map(sqrt(real(ivalue(2))),sqrt(real(ivalue(numlev-1))),
     +   minuav-du,maxuav+du)
      call pspace(0.2,0.8,0.2,0.9)
      write (txt,'(A)') 'R(alpha) vs alpha for vdpd'
      call pcscen(0.0,-0.1,txt)
      call scales
      call curveo(uavx,uavy,2,numlev-1)
      call grend
C
C     Draw contours of dphi/dt vs. theta and nu for two values of alpha
C     with coupling function (nu+z^2)dzdt
C
      do 110 il=numlev/2,numlev/2+5,5
        call frame
        do 100 k=1,numlev
          do 80 j=1,numpha
            dp(k,j)=dphidt(il,j,1)*dble(k-(numlev/2))*lstep+dphidt(il,j,2)
80        continue
100     continue
        maxdp=0
        do 107 i=2,numlev-1
          do 106 j=1,numpha
            if (abs(dp(i,j)).gt.maxdp) maxdp=abs(dp(i,j))
106     continue
107     continue
        do 105 i=1,25
          levs(i)=maxdp*(-1.0+(real(i)-1.0)/12.0)
105     continue
        call paper(1)
        call map(real(dble(2-numlev/2)*lstep),
     +     real(dble(numlev/2-1)*lstep),0.0,1.0)
        call pspace(0.2,0.8,0.2,0.9)
        write (txt,'(A,f6.3)') 'dphidt for cubic coupled vdpd;
     +     alpha=',sqrt(ivalue(il))
        call pcscen(0.0,-0.1,txt)
        call scales
        call contra(dp,2,numlev-1,numlev,1,numpha,numpha,levs,1,25)
        call grend
110   continue
      stop
      end
C                                   SUBROUTINES
C
C
C
      subroutine      period(yy,p,xstep)
      double precision yy,p,xstep
C
C     Calculate p = period of contour starting at (0,yy)
C
      double precision maxx
      parameter       (maxx=1000)
      integer n,nout
```

```
      parameter          (n=2,nout=6)
      double precision x,y(n),ny(n)
      external           fcn,dsolve
      intrinsic          dble
      x=0
      y(1)=0
      y(2)=yy
5     continue
      ny(1)=y(1)
      ny(2)=y(2)
      call dsolve(x,xstep,y)
      x=x+xstep
      if (x.gt.maxx) then
        print *,'period overflow'
        stop
      endif
      if ((ny(1).ge.0).or.(y(1).le.0)) goto 5
      if ((ny(1)-y(1)).ne.0) then
        p=x-xstep*(y(1)/(y(1)-ny(1)))
      else
        p=x
      endif
      return
      end
C
C
C
      subroutine       dsolve(x,step,y)
      double precision          x,step,xstep,y(2),k(2,4),ty(2),f(2),oy(2)
      external         fcn
      intrinsic        dble
C
C     Fourth order Runge-Kutta in two variables; three steps
C
      xstep=step/3.0d0
      do 10 i=1,3
        oy(1)=y(1)
        oy(2)=y(2)
        call fcn(x,oy,f)
        k(1,1)=xstep*f(1)
        k(2,1)=xstep*f(2)
        ty(1)=oy(1)+.5d0*k(1,1)
        ty(2)=oy(2)+.5d0*k(2,1)
        call fcn(x,ty,f)
        k(1,2)=xstep*f(1)
        k(2,2)=xstep*f(2)
        ty(1)=oy(1)+.5d0*k(1,2)
        ty(2)=oy(2)+.5d0*k(2,2)
        call fcn(x,ty,f)
        k(1,3)=xstep*f(1)
        k(2,3)=xstep*f(2)
        ty(1)=oy(1)+k(1,3)
        ty(2)=oy(2)+k(2,3)
        call fcn(x,ty,f)
        k(1,4)=xstep*f(1)
        k(2,4)=xstep*f(2)
        y(1)=oy(1)+(k(1,1)+k(1,4)+2d0*(k(1,2)+k(1,3)))/6d0
        y(2)=oy(2)+(k(2,1)+k(2,4)+2d0*(k(2,2)+k(2,3)))/6d0
10    continue
      return
      end
C
C
C
      subroutine fcn(t,y,f)
      double precision         t,f(2),y(2)
```

```
      intrinsic dble
      f(1)=y(2)
      f(2)=y(1)-y(1)**3
      return
      end
C                       dUdv = -y(1)+y(1)**3
C                       U = -y(1)**2/2+(y(1)**4)/4
C
      subroutine corr(i,tstep)
C
C     Calculate dphi/dt for linear coupling dphidt(,,1)
C                           and cubic coupling dphidt(,,2)
C
      integer i
      integer numlev,numpha,nout
      double precision tstep
      parameter(nout=6,numlev=50,numpha=50)
      double precision z(numlev,numpha),stp,a0,a1,a2,a3
      real    dphidt(numlev,numpha,2),uavx(numlev),uavy(numlev)
      double precision ans2(numpha),ans3(numpha)
      integer j,k,jj

      double precision zval,dzda,dzdt
      external zval,dzda,dzdt

      intrinsic dble

      common /zzz/ z(numlev,numpha)
      common /zph/ dphidt(numlev,numpha,2),uavx(numlev),uavy(numlev)

      stp=1.0d0/dble(numpha)
      a0=0.0d0
      a1=0.0d0
      do 60 k=1,numpha
        a0=a0+stp*(dzdt(i,k)/tstep)**2
        a1=a1+stp*(zval(i,k)*dzdt(i,k)/tstep)**2
        a2=0.0d0
        a3=0.0d0
        do 50 j=1,numpha
          jj=j+k-1
          if (jj.gt.numpha) jj=jj-numpha
          a2=a2+stp*(dzda(i,jj)*(dzdt(i,j)-dzdt(i,jj))-
     +          dzda(i,j)*(dzdt(i,jj)-dzdt(i,j)))/tstep
          a3=a3+stp*(dzda(i,jj)*(dzdt(i,j)-dzdt(i,jj))*
     +          (zval(i,j)-zval(i,jj))**2-
     +          dzda(i,j)*(dzdt(i,jj)-dzdt(i,j))*
     +          (zval(i,jj)-zval(i,j))**2)/(tstep**2)
50      continue
        ans2(k)=a2
        ans3(k)=a3
        dphidt(i,k,1)=float(ans2(k))
        dphidt(i,k,2)=float(ans3(k))
60      continue
        uavy(i)=real(a1/a0)
        write (nout,'(A F10.5)') 'R(alpha)=',uavy(i)
        return
        end
C
C     Initial value for 'i'th level
C
      double precision function ivalue(i)
      integer i
      double precision mina,astep,alpha
      parameter(mina=0.02d0,astep=0.04d0)
      intrinsic       dble
      alpha=mina+dble(i)*astep
```

```
      ivalue=alpha
      return
      end
C
C     Extend z() to zval() periodically in phases
C
      double precision function zval(i,j)
      integer i,j
      integer numlev,numpha,ii,jj
      parameter(numlev=50,numpha=50)
      double precision z(numlev,numpha)
      intrinsic dble
      common /zzz/ z(numlev,numpha)
      ii=i
      jj=j
      if (ii.gt.numlev) ii=ii-numlev
      if (ii.lt.1) ii=ii+numlev
      if (jj.gt.numpha) jj=jj-numpha
      if (jj.gt.numpha) jj=jj-numpha
      if (jj.lt.1) jj=jj+numpha
      zval=z(ii,jj)
      return
      end
C
C     Finite difference dz/dt
C
      double precision function dzdt(i,j)
      integer i,j
      integer numlev,numpha
      parameter(numlev=50,numpha=50)
      double precision z(numlev,numpha),u
      common /zzz/ z(numlev,numpha)
      double precision zval
      external zval,fcn
      u=(zval(i,j+1)-zval(i,j-1))/2.0d0
      dzdt=u
      return
      end
C
C     Finite difference dz/dalpha
C
      double precision function dzda(i,j)
      integer i,j
      integer numlev,numpha,i1,i2
      parameter(numlev=50,numpha=50)
      double precision z(numlev,numpha),u
      common /zzz/ z(numlev,numpha)
      double precision zval
      external zval
      intrinsic dble
      i1=i+1
      i2=i-1
      u=(zval(i1,j)-zval(i2,j))/2.0d0
      dzda=u
      return
      end
```

```
#
# ks0110.maple
#

trun:=proc(A,om):convert(taylor(A,eps,om),polynom):end:

s:=16:

# max size of mode

A:=array(0..s,0..s,[]);

for i from 0 to s do:
for j from 0 to s do:
A[i,j]:=0:
od:
od:

Empty:=copy(A):

a:=a0/sqrt(1+eps*a1):
b:=b0/sqrt(1+eps*b1):

# modes are bifurcating from
#
a0:=1;
b0:=1;

# null space coordinates
#
A[0,1]:=eps*u;
A[1,0]:=eps*v;
AA:=copy(A):

maxord:=4;

for oeps from 1 to maxord do:

 tord:=oeps+4:
 B:=copy(Empty):
 for i from 0 to s do:
 for j from 0 to s do:
  if A[i,j]<>0 then:
   for k from 0 to s do:
   for l from 0 to s do:
    mul:=A[i,j]*A[k,l]:
    if (mul<>0) then:
         i1:=abs(i+k):i2:=abs(i-k):
     j1:=abs(j+l):j2:=abs(j-l):
     mm:=i*k/(4*a^2):
     nn:=j*l/(4*b^2):
         if i1<=s and j1<=s then:B[i1,j1]:=trun(B[i1,j1]+(-mm-nn)*mul,tord):fi:
         if i1<=s and j2<=s then:B[i1,j2]:=trun(B[i1,j2]+(nn-mm)*mul,tord):fi:
         if i2<=s and j1<=s then:B[i2,j1]:=trun(B[i2,j1]+(mm-nn)*mul,tord):fi:
         if i2<=s and j2<=s then:B[i2,j2]:=trun(B[i2,j2]+(mm+nn)*mul,tord):fi:
    fi:
   od:od:
  fi:
 od:od:
 DASQ:=copy(B):
 A:=copy(AA):
 print(order=oeps);

 for i from 0 to s do:
 for j from 0 to s do:
  pp:=i*i/(a^2)+j*j/(b^2):
```

```
  pq:=pp*(pp-1):

  if (pp<>0) then:
   if ((i<>0 or j<>1) and (i<>1 or j<>0)) then:
    A[i,j]:=trun(A[i,j]-DASQ[i,j]/pq,tord+1):
   fi:
  fi:

  EQN:=trun(A[i,j]*pq+DASQ[i,j],oeps+1):
  if (EQN<>0) then:
   print([i,j]=EQN);
  fi:

 od:od:

od:
```

```
quit;
```

Bibliography

[1] M. Abramowitz and I.A. Stegun. *Handbook of Mathematical Functions.* New York, Dover, 1965.

[2] J.C. Alexander and G. Auchmuty. Global bifurcations of phase-locked oscillators. *Arch. Rat. Mech. Anal.*, 93:253–270, 1986.

[3] J.C. Alexander and B. Fiedler. Global bifurcations of coupled symmetric oscillators. In Ladas Dafermos and Papanicolaou, editors, *Proceedings of the equadiff conference.*, volume 118 of *lecture notes in pure an applied mathematics (differential equations)*, pages 7–. AMS, Providence, RI, 1987.

[4] A.A. Andronov, A.A. Vitt, and S.E. Chaikin. *Theory of oscillators.* Pergamon, Oxford, 1966.

[5] D. Armbruster and G. Danglmayr. Corank-two bifurcations for the brusselator with non-flux boundary conditions. *Dyn. and Stab. Systems*, 1:187–200, 1986.

[6] D. Armbruster and G. Danglmayr. Coupled stationary bifurcations in non-flux boundary value problems. *Math. Proc. Camb. Phil. Soc.*, 101:167–192, 1987.

[7] D. Armbruster, J. Guckenheimer, and P. Holmes. Kuramoto-Sivashinsky dynamics on the center-unstable manifold. *SIAM .J. App. Math.*, 49:676–691, 1989.

[8] V.I. Arnold. *Geometrical methods in the theory of ODEs*, volume 250 of *Grundlehren der mathematischen Wissenschaft.* Springer, Berlin, 1983.

[9] V.I. Arnold. *E.M.S. 5*, volume 5 of *Encyclopaedia of mathematical sciences.* Springer, Berlin, 1991.

[10] D.G. Aronson, E.J. Doedel, and H.G. Othmer. An analytical and numerical study of the bifurcations in a system of linearly coupled oscillators. *Physica D*, 25:20–104, 1987.

[11] D.G. Aronson, E.J. Doedel, and H.G. Othmer. The dynamics of coupled current-biased Josephson junctions-part ii. *International Journal of Bifurcation and Chaos*, 1:51–66, 1991.

[12] D.G. Aronson, M. Golubitsky, and M. Krupa. Coupled arrays of Josephson junctions and bifurcations of maps with S(n) symmetry. Preprint, Dept of Mathematics, University of Minnesota, 1989.

[13] D.K. Arrowsmith and C.M. Place. *An introduction to dynamical systems.* C.U.P., Cambridge, 1990.

[14] P. Ashwin. Symmetric chaos in systems of three and four coupled oscillators. *Nonlinearity*, 3:604–618, 1990.

[15] P. Ashwin. Identical oscillators with symmetry. In *Proceedings of Coupled Oscillating Neurons, King's College, London, 13-15 Dec. 1990.* Springer, Berlin, 1991. (to appear).

[16] P. Ashwin, J. Guaschi, and G.P. King. Rotation sets and mode locking in a three oscillator system. Preprint, University of Warwick, Mathematics Institute, 1991.

[17] P. Ashwin, G.P King, and J.W. Swift. Three identical oscillators with symmetric coupling. *Nonlinearity*, 3:585–603, 1990.

[18] P. Ashwin and J.W. Swift. The dynamics of n identical oscillators with symmetric coupling. *Journal of Nonlinear Science*, 1992. (to appear).

[19] P.J. Aston. Scaling laws and bifurcation. In *Singularity theory and its applications, Warwick 1989*, volume 1463 of *LNM*, pages 1–21. Springer, 1991.

[20] C. Baesens, J. Guckenheimer, S. Kim, and R.S. MacKay. Three coupled oscillators: mode-locking, global bifurcations and toroidal chaos. *Physica D*, 24:387–475, 1991.

[21] J.S. Bay and H. Hemami. Modelling of a neural pattern generator with coupled nonlinear oscillators. *IEEE Trans BME*, 34:297–306, 1987.

[22] A. Bayliss, B.J. Matkowsky, and M. Minkoff. Bifurcation and pattern formation in combustion. In B.D. Sleeman and R.J. Jarvis, editors, *Proc. 10th Dundee conference on differential equations (1988).* Longman Scientific and Technical, Harlow, UK, 1989.

[23] N.N. Bogoliubov. *Asymptotic methods in nonlinear oscillations.* Hindustan Pub. Corp., Delhi, 1961.

[24] M.R. Booty, S.B. Margolis, and B.J. Matkowsky. Interaction of pulsating and spinning waves in nonadiabatic flame propagation. *SIAM J. App. Math.*, 47:1241–1286, 1987.

[25] M.R. Booty, M. Matalon, and B.J. Matkowsky. A nonlinear wave equation in nonadiabatic flame propagation. *SIAM J. App. Math.*, 48:519–535, 1988.

[26] F.J. Bourland and R. Haberman. The modulated phase shift for stronly nonlinear, slowly varying and weakly damped oscillators. *SIAM J. Appl. Math.*, 48:737–748, 1988.

[27] J.D. Buckmaster and G.S.S. Ludford. *Lectures on mathematical combustion*, volume 43 of *SIAM CBMS-NSF.* SIAM, 1982.

[28] J.D. Buckmaster and G.S.S. Ludford. *Theory of laminar flames.* Cambridge monographs on mechanics and applied mathematics. Cambridge University Press, Cambridge, UK, 1982.

[29] F.H. Busse and K.E. Heikes. Convection in a rotating layer: a simple case of turbulence. *Science*, 208:173–175, 1980.

[30] J. Carr. *Applications of centre manifold theory.* Springer, New York, 1981.

[31] H.C. Chang. Travelling waves on fluid interfaces: Normal form analysis of the Kuramoto-Sivashinsky equation. *Phys. Fluids*, 10:3142–3147, 1986.

[32] H. Chaté and P. Manneville. Transition to turbulence via spatio-temporal intermittency. *Phys. Rev. Letters*, 58:423–436, 1987.

[33] P. Chossat and M. Golubitsky. Symmetry-increasing bifurcation of chaotic attractors. *Physica D*, 32:423–436, 1988.

[34] P. Chossat, R. Lauterbach, and Ian Melbourne. Steady-state bifurcation with O(3) symmetry. University of Houston research report UH/MD-69, 1990.

[35] G. Cicogna. Symmetry breakdown from bifurcation. *Lett. Nuovo Cimento*, 31:600–602, 1981.

[36] P. Clavin. Dynamic behaviour of premixed flame fronts in laminar and turbulent flows. *Prog. Energy and Combustion Sci.*, 11:1–59, 1985.

[37] J.J. Collins and I.N. Stewart. Coupled nonlinear oscillators and the symmetries of animal gaits. Preprint, University of Warwick, Mathematics Institute, 1990.

[38] P. Constantin, C. Foias, and R. Temam. *Attractors representing turbulent flows*, volume 314 of *Memoirs of the AMS*. AMS, Providence, RI, 1985.

[39] J.D. Crawford, M. Golubitsky, M.G.M. Gomes, E. Knobloch, and I.N. Stewart. Boundary conditions as symmetry constraints. In *Proceedings of symposium on singularities and their applications, Warwick, 1989*. Springer, New York, 1991.

[40] A. Cumming and P.S. Linsay. Quasiperiodicity and chaos in a system with three competing frequencies. *Phys Rev Lett*, 60:2719–2722, 1988.

[41] R. Cushman and J.A. Sanders. Nilpotent normal forms and representation theory of SL(2,R). In *Multiparameter bifurcation theory*, volume 56 of *Contemporary Maths*, pages 31–51. AMS, Providence, RI, 1985.

[42] T. Endo and S. Mori. Mode analysis of a ring of a large number of mutually coupled van der Pol oscillators. *IEEE CAS*, 25:7–18, 1978.

[43] G.B. Ermentrout. The behavior of rings of coupled oscillators. *J. Math. Biol.*, 23:55–74, 1985.

[44] G.B. Ermentrout and N. Kopell. Frequency plateaus in a chain of weakly coupled oscillators. *SIAM J. Math. Anal.*, 15:215–237, 1984.

[45] B. Fiedler. *Global bifurcations of periodic solutions with symmetry*, volume 1309 of *Springer lecture notes in mathematics*. Springer, Berlin, 1988.

[46] M. Field, M. Golubitsky, and I.N. Stewart. Bifurcations on hemispheres. *J. Nonlin. Sci.*, 1:201–223, 1991.

[47] M.J. Field and R.W. Richardson. Symmetry breaking and the maximal isotropy subgroup conjecture for reflection groups. *Arch. Rat. Mech. Anal.*, 105:61–94, 1989.

[48] M.L. Frankel and G.I. Sivashisky. On the equation of a curved flame front. *Physica D*, 30:28–42, 1988.

[49] U. Frisch. Z.S. She, and O. Thual. Viscoelastic behaviour of cellular solutions to the Kuramoto-Sivashinsky model. *J. Fluid Mech.*, 168:221–240, 1986.

[50] P. Glendinning. Global bifurcations in flows. In T. Bedford and J. Swift, editors, *New directions in dynamical systems*, volume 127 of *LMS Lecture notes in Maths.* Cambridge University Press, 1988.

[51] M. Golubitsky and D. Schaeffer. *Groups and singularities in bifurcation theory volume 1*, volume 51 of *App. Math. Sci.* Springer, New York, 1986.

[52] M. Golubitsky and I.N. Stewart. Hopf bifurcation in the presence of symmetry. *Arch. Rat. Mech. Anal.*, 87:107–165, 1985.

[53] M. Golubitsky and I.N. Stewart. Hopf bifurcation with dihedral group symmetry. In *Multiparameter bifurcation theory*, volume 56 of *Contemporary Maths*, pages 131–173. AMS, Providence, RI, 1985.

[54] M. Golubitsky, I.N. Stewart, and D. Schaeffer. *Groups and singularities in bifurcation theory volume 2.* App. Math. Sci. 69. Springer, New York, 1988.

[55] M.G.M. Gomes. Steady-state mode interactions in rectangular domains. MSc thesis, Maths Dept., University of Warwick, 1989.

[56] J. Grasman. *Asymptotic methods for relaxation oscillations and applications*, volume 63 of *Appl. Math. Sci.* Springer, New York, 1987.

[57] J. Grasman and M.J.W. Jansen. Mutually synchronised relaxation oscillators as prototypes of oscillating systems in biology. *J. Math. Biol.*, 7:171–197, 1988.

[58] C. Grebogi, E. Ott, and J.A Yorke. Crises, sudden changes in chaotic attractors and transient chaos. *Physica D*, 7:181–200, 1983.

[59] J.M. Greene and J.-S. Kim. The steady states of the Kuramoto-Sivashinsky equation. *Physica D*, 33:99–120, 1988.

[60] J. Guckenheimer. Isochrons and phaseless sets. *J. Math. Biol.*, 1:259–273, 1975.

[61] J. Guckenheimer and P. Holmes. *Nonlinear oscillations, dynamical systems and bifurcations of vector fields.* App. Math. Sci. 42. Springer, New York, 1983.

[62] P. Hadley. *Dynamics of Josephson junction arrays.* PhD thesis, Dept of Applied Physics, Stanford University, 1989.

[63] P. Hadley. M.R. Beasley, and K. Wiesenfeld. Phase locking of Josephson junction series arrays. *Phys Rev B*, 38:8712–8719, 1988.

[64] H. Haken. *Synergetics.* Springer, Heidelberg, 1978.

[65] G.H. Hardy and Wright. *An introduction to the theory of numbers.* Cambridge University Press, 1956.

[66] C.M. Harper. *Turbulence and combustion instabilities in engines.* PhD thesis, Dept. of Mech. Engineering, Leeds University, 1989.

[67] B.D. Hassard, N.D. Kazarinoff, and Y-H. Wan. *Theory and applications of Hopf bifurcation*, volume 41 of *LMS lecture notes.* Cambridge University Press, 1981.

[68] C. Hayashi. *Nonlinear oscillations in physical systems.* McGraw Hill, 1964. Reprinted 1985 by Princeton University Press.

[69] D. Henry. *Semilinear parabolic equations*, volume 840 of *LNM.* Springer, Berlin, 1978.

[70] M. Hirsch, C. Pugh, and M. Shub. *Invariant Manifolds*, volume 583 of *LNM.* Springer, Berlin, 1977.

[71] P. Holmes and D. Rand. Phase portraits and bifurcations of a non-linear oscillator. *Int. J. Non-linear Mech.*, 15:449–458, 1980.

[72] P. Horowitz and W. Hill. *The Art of Electronics.* Cambridge University Press, 1980.

[73] J.M. Hyman and B. Nicolaenko. The Kuramoto-Sivashisky equation: a bridge between PDEs and dynamical systems. *Physica D*, 18:113–126, 1986.

[74] K. Ireland and M. Rosen. *A classical introduction to modern number theory.* Graduate texts in maths. Springer, New York, 1980.

[75] D.W. Jordan and P. Smith. *Nonlinear ordinary differential equations.* Oxford applied mathematics and computing science series. Clarendon Press, Oxford, 1977.

[76] G. Joulin. On the hydrodynamic stability of curved premixed flames. *J. Phys. France*, 50:1069–1082, 1989.

[77] I.G. Kevrekedis, B. Nicolaenko, and J.C. Scovel. Back in the saddle again: a computer assisted study of the Kuramoto-Sivashinsky equation. *SIAM J. App. Math.*, 50:760–790, 1990.

[78] G.P. King and I.N. Stewart. Symmetric chaos. In Ames W. and Rogers C., editors, *Nonlinear Equations in the Applied Sciences.* Academic press, 1991.

[79] M. Kitano, T. Yabuzaki, and T. Ogawa. Symmetry-recovering crises of chaos in polarization-related optical bistability. *Phys. Rev. A*, 29:1288–1296, 1984.

[80] N. Kopell and G.B. Ermentrout. Symmetry and phase locking in chains of weakly coupled oscillators. *Comm. Pure App. Math.*, 39:623–660, 1986.

[81] M. Krupa and R.M. Roberts. Symmetry breaking in equivariant circle maps. Preprint, Maths Institute, University of Warwick, 1991.

[82] Y. Kuramoto. Diffusion-induced chaos in reaction systems. *Supp. of Prog. of Theor. Physics*, 64:346–367, 1978.

[83] Y. Kuramoto. *Chemical oscillations, waves and turbulence*, volume 19 of *Synergetics.* Springer, Berlin, 1984.

[84] Y. Kuramoto. Phase dynamics of weakly unstable periodic structures. *Prog. of Theor. Physics*, 71:1182–1196, 1984.

[85] J.R. Kuttler and V.G. Sigillito. Eigenvalues of the Laplacian in two dimensions. *SIAM Review*, 26:163–193, 1984.

[86] L.D. Landau. On the theory of slow combustion. *J. Exp. Theor. Phys.*, 6:240–245, 1944. (in Russian).

[87] D. Linkens. Nonlinear circuit mode analysis. *IEEE proc*, 130A:69–87, 1983.

[88] J.C. Luke. A perturbation method for nonlinear dispersive wave problems. *Proc. R. Soc. London A*, 292:403–412, 1965.

[89] R.S. MacKay and C. Tresser. Transition to topological chaos for circle maps. *Physica D*, 19:206–237, 1986.

[90] P. Manneville. Liapounov exponents for the Kuramoto-Sivashisky model. In O. Pirronneau, editor, *Macroscopic modelling of turbulent flows and fluid mixtures*. Springer, Berlin, 1984.

[91] S.B. Margolis and B.J Matkowsky. Flame propagation in channels: secondary bifurcation to quasi-periodic pulsation. *SIAM J. App. Math.*, 45:45–, 1985.

[92] S.B. Margolis, G.I. Sivashinsky, and J.K. Bechtold. Secondary infinite-period bifurcation of spinning combustion waves near a hydrodynamic cellular stability boundary. Sandia Report 89-8660, Sandia National Labs, New Mexico, 1989.

[93] J. Marsden and S. McCraken. *The Hopf bifurcation and its applications*, volume 19 of *App. Math. Sci.* Springer, New York, 1976.

[94] B.J. Matkowsky and D.O. Olagunju. Spinning waves in gaseous combustion. *SIAM J. Appl. Math.*, 42:1138–1156, 1982.

[95] B.J. Matkowsky and G.I. Sivashinsky. An asymptotic derivation of two models in flame theory associated with the constant density approximation. *SIAM J. Appl. Math.*, 37:686–699, 1979.

[96] A.C. McIntosh. On the cellular instability of flames near porous-plug burners. *J. Fluid Mech.*, 161:43–73, 1985.

[97] D.M. Michelson. Steady solutions of the Kuramoto-Sivashinsky equation. *Physica D*, 19:89–111, 1986.

[98] D.M. Michelson and G.I. Sivashinsky. Nonlinear analysis of hydrodynamic instability in flames- II. numerical experiments. *Acta Astronautica*, 4:1206–1221, 1977.

[99] R.E. Mirollo and S.H. Strogatz. Synchronisation of pulse-coupled biological oscillators. *SIAM J. App. Math.*, 50:1645–1662, 1990.

[100] R.E. Mirollo and S.H. Strogatz. Existence of splay states for Josephson junction arrays. Pers. comm, 1991.

[101] F. Moss and P.V.E. McClintock. *Noise in nonlinear dynamical systems, vols 1-3.* C.U.P, Cambridge, 1989.

[102] J.D. Murray. *Mathematical Biology*, volume 13 of *Biomathematics*. Springer, Berlin, 1989.

[103] A.C. Newell. Dynamics and analysis of patterns. In D. Stein, editor, *Complex systems*, SFI studies in the sciences of complexity. Addison-Wesley Longman, London, 1989.

[104] W-M. Ni and I. Takagi. On the neumann problem for some semilinear elliptic equations and systems of activator-inhibitor type. *Trans AMS*, 297:351–368, 1986.

[105] B. Nicolaenko, B. Scheurer, and R. Temam. Some global dynamical properties of the Kuramoto-Sivashinsky equations: nonlinear stability and attractors. *Physica D*, 16:155–183, 1984.

[106] I. Ohta and T. Kaneko. Parallel running system of three oscillators coupled through a six-port magic junction. *IEEE Trans MTT*, 37:1699–1707, 1989.

[107] H.G. Othmer and L.E. Scriven. Instability and dynamic pattern formation in cellular networks. *J. Theor. Biology*, 32:507–537, 1971.

[108] J. Palis and W. de Melo. *Geometric theory of dynamical systems.* Springer, New York, 1982.

[109] B. van der Pol. On relaxation oscillations. *Phil. Mag.*, 7-2:978–992, 1926.

[110] B. van der Pol. Forced oscillations in a circuit with nonlinear resistance. *Phil. Mag.*, 7-3:18–38, 1927.

[111] B. van der Pol and J. van der Mark. The heartbeat considered as a relaxation oscillator and an electrical model of the heart. *Phil. Mag. Suppl.*, 6:763–765, 1928.

[112] M. Poliashenko, S.R. McKay, and C.W. Smith. Chaos and nonisochronism in weakly coupled oscillators. *Phys. Rev. A*, 1991. (to appear).

[113] A.A. Putnam. *Combustion driven oscillations in industry.* Elsevier, New York, 1971.

[114] R.H. Rand and D. Armbruster. *Perturbation methods, bifurcation theory and computer algebra*, volume 65 of *Applied Math. Sciences.* Springer, New York, 1987.

[115] Lord Rayleigh. *The theory of sound, vol. 2.* Dover, New York, 1945. 2nd edition.

[116] J.A. Sanders and R. Cushman. Limit cycles in the Josephson equation. preprint, Free University of Amsterdam, 1984.

[117] J.A. Sanders and F. Verhulst. *Averaging methods in nonlinear dynamical systems.* App. Math. Sci. 59. Springer, New York, 1985.

[118] D.H. Sattinger. *Group theoretic methods in bifurcation theory*, volume 762 of *Lecture notes in math.* Springer, New York, 1979.

[119] G. Schwarz. Smooth functions invariant under the action of a compact Lie group. *Topology*, 14:63–68. 1975.

[120] G.I. Sivashinsky. Nonlinear analysis of hydrodynamic instability in flames- I. derivation of the basic equations. *Acta Astronautica*, 4:1177–1206, 1977.

[121] S.H. Strogatz, C.M. Marcus, R.M. Westervelt, and R.E. Mirollo. Collective dynamics of coupled oscillators with random pinning. *Physica D*, 36:23–50, 1990.

[122] J.W. Swift. Convection in a rotating fluid layer. In J.E. Marsden, editor, *Fluids and plasmas, geometry and dynamics*, volume 28 of *Comtemp. Math.*, pages 435–448. AMS, Providence RI, 1984.

[123] J.W. Swift. Hopf bifurcation with the symmetry of the square. *Nonlinearity*, 1:333–377, 1988.

[124] J.W. Swift and K. Wiesenfeld. Suppression of period doubling in symmetric systems. *Phys. Rev. Lett.*, 59:705–708, 1984.

[125] K.G. Szabó and T. Tél. On the symmetry-breaking bifurcation of chaotic attractors. *J. Stat. Phys.*, 54:925–948, 1989.

[126] R. Temam. *Navier-Stokes equations, theory and numerical analysis*, volume 2 of *Studies in mathematics and its applications*. North-Holland, Amsterdam, 1979.

[127] K.Y. Tsang, R.E. Mirollo, S.H. Strogatz, and K. Wiesenfeld. Slow dynamics in a globally coupled oscillator array. Submitted to Physica D, 1990.

[128] A.M. Turing. The chemical basis of morphogenesis. *Phil. Trans. Roy. Soc. Lond. B*, 237:37–72, 1952.

[129] J.V. Uspensky and M.A. Heaslet. *Elementary number theory*. McGraw-Hill, New York, 1939.

[130] R. van Buskirk and C. Jeffries. Observation of chaotic dynamics of coupled nonlinear oscillators. *Phys. Rev. A*, 31:3332–3357, 1985.

[131] R.E. White. *An introduction to the finite element method with applications to nonlinear problems*. Wiley-Interscience, 1985.

[132] K. Wiesenfeld and P. Hadley. Attractor crowding in oscillator arrays. Preprint, Dept. of Physics, Georgia Tech., 1988.

[133] S. Wiggins. *Global bifurcations and chaos*, volume 73 of *App. Math. Sci.* Springer, New York, 1988.

[134] F.A. Williams. *Combustion Theory*. Benjamin Cummings, California, USA, 1985. Second edition.

[135] A.T. Winfree. Biological rhythms and the behaviour of populations of coupled oscillators. *Theoretical biology*, 16:15–42, 1967.

[136] A.T. Winfree. Patterns of phase compromise in biological cycles. *J. Math. Biol.*, 1:73–95, 1974.

[137] A.T. Winfree. *The geometry of biological time*, volume 8 of *Texts in biomathematics*. Springer, New York, 1980. Reprinted 1990, Springer study editions.

[138] J. Wloka. *Partial differential equations*. McGraw Hill, 1987.

[139] Ya. B. Zeldovich. *Theory of combustion and detonation of gases*. Acad. Sc. USSR Moscow, 1944.